

Identification and Characterization of autophagic and non-autophagic Interaction Partners of Atg18

DISSERTATION

for the award of the degree

“Doctor rerum naturalium“

of the Georg-August University Göttingen

within the doctoral program „Molecular Medicine“ of the
Georg-August University School of Science (GAUSS)

submitted by

Lisa Marquardt

from

Stuttgart

Göttingen, 2021

Members of the thesis committee and examination board

Prof. Dr. Michael Thumm (Supervisor and first referee)	Department of Cellular Biochemistry University Medical Center Göttingen
Prof. Dr. Blanche Schwappach-Pignataro (second referee)	Dean of the Faculty of Medicine University Medical Center Hamburg- Eppendorf
former	Department of Molecular Biology University Medical Center Göttingen
Dr. Dieter Schmitt	Department of Neurobiology Max Planck Institute for Biophysical Chemistry, Göttingen

Further members of the examination board

Prof. Dr. Ralph Kehlenbach	Department of Molecular Biology University Medical Center Göttingen
Prof. Dr. Silvio Rizzoli	Department of Neuro- and Sensory Physiology University Medical Center Göttingen
Prof. Dr. Stefan Jakobs	Department of NanoBiophotonics Max Planck Institute for Biophysical Chemistry, Göttingen

Date of oral examination: 21.05.2021

I hereby declare that the thesis entitled "Identification and Characterization of autophagic and non-autophagic Interaction Partners of Atg18" has been written independently and with no other sources and aids than quoted.

Lisa Marquardt
Göttingen, March 2021

Table of Contents

LIST OF FIGURES.....	V
LIST OF TABLES.....	VII
LIST OF ABBREVIATIONS.....	VIII
1. SUMMARY.....	1
2. INTRODUCTION.....	3
2.1. THE MODEL ORGANISM <i>S. CEREVISIAE</i>.....	3
2.2. TRANSPORT IN CELL.....	4
2.2.1. GOLGI TO VACUOLE.....	4
2.2.2. GOLGI TO PLASMA MEMBRANE.....	5
2.3. AUTOPHAGY.....	5
2.3.1. MACROAUTOPHAGY.....	7
2.3.2. SELECTIVE AUTOPHAGY.....	8
2.3.3. MICROAUTOPHAGY.....	9
2.3.4. CHAPERONE MEDIATED AUTOPHAGY.....	10
2.3.5. MECHANISM.....	11
2.3.5.1. Atg1 kinase and scaffolding complex.....	11
2.3.5.2. PI3 Kinase Complex.....	12
2.3.5.3. Atg9 vesicles and the role of Atg9.....	13
2.3.5.4. Origin of membrane lipids.....	15
2.3.5.5. Ubiquitin like conjugation system and Atg8.....	16
2.3.5.6. Fusion and Degradation.....	18
2.3.5.6.1. Closure of the autophagosome.....	18
2.3.5.6.2. Fusion with the vacuole.....	20
2.3.5.6.3. Degradation of the cargo.....	22
2.3.5.7. Regulation.....	22
2.4. ATG18.....	24
2.4.1. STRUCTURE.....	24
2.4.2. FUNCTION IN AUTOPHAGY.....	27
2.4.3. FUNCTION AT THE VACUOLAR MEMBRANE.....	28
2.5. AIM OF THIS STUDY.....	31

Table of Contents

3. MATERIAL AND METHODS	32
3.1. MATERIAL	32
3.1.1. SOFTWARE	32
3.1.2. EQUIPMENT	32
3.1.3. CHEMICALS AND CONSUMABLES	34
3.1.4. COMMERCIALY AVAILABLE KITS	36
3.1.5. ANTIBODIES	36
3.1.6. ENZYMES	37
3.1.7. MEDIUM	37
3.1.8. BUFFER	38
3.1.9. STRAINS	40
3.1.10. PLASMIDS	43
3.1.11. OLIGONUCLEOTIDES	44
3.2. METHODS	47
3.2.1. CULTIVATION CONDITIONS	47
3.2.1.1. Cultivation of <i>S. cerevisiae</i>	47
3.2.1.2. Cultivation of <i>E. coli</i>	47
3.2.1.3. Nitrogen starvation	47
3.2.2. MOLECULAR BIOLOGICAL METHODS	48
3.2.2.1. DNA Isolation	48
3.2.2.1.1. Isolation of chromosomal DNA from Yeast	48
3.2.2.1.2. Isolation of plasmid DNA from <i>E. coli</i>	48
3.2.2.1.3. Purification of DNA fragments	48
3.2.2.2. Agarose gel electrophoresis	48
3.2.2.3. Determination of DNA concentration	49
3.2.2.4. Molecular Cloning	49
3.2.2.4.1. Polymerase Chain Reaction (PCR)	49
3.2.2.4.2. Restriction	50
3.2.2.4.3. Ligation	50
3.2.2.4.4. Site-Directed Mutagenesis	50
3.2.2.4.5. BuilderKit	51
3.2.2.5. Genome engineering based on homologous recombination	51
3.2.2.6. Transformation	51
3.2.2.6.1. Transformation of <i>E. coli</i>	51
3.2.2.6.1. Transformation of <i>S. cerevisiae</i>	52

Table of Contents

3.2.2.7. PCR to verify size of gene / plasmid.....	52
3.2.2.8. Sequencing of DNA.....	53
3.2.3. BIOCHEMICAL METHODS.....	53
3.2.3.1. Alkaline lysis of yeast cells.....	53
3.2.3.2. Co-IP.....	53
3.2.3.3. SDS-PAGE.....	54
3.2.3.4. Immunoblotting.....	55
3.2.3.5. Coomassie brilliant blue staining.....	55
3.2.4. DELTAVISION.....	56
3.2.5. BIOID ASSAY.....	56
3.2.5.1. Small scale.....	57
3.2.5.2. BioID with SILAC approach.....	58
3.2.5.3. Isolation of biotinylated proteins.....	59
3.2.6. MASS SPECTROMETRY.....	59
3.2.6.1. Sample preparation.....	59
3.2.6.2. LC-MS analysis.....	60
3.2.7. STATISTICAL ANALYSES.....	60
<u>4. RESULTS.....</u>	61
4.1. <i>BioID</i>.....	61
4.1.1. PRELIMINARY EXPERIMENTS.....	62
4.1.2. BIOID RESULTS.....	65
4.1.3. AUTOPHAGIC AND ENDOSOMAL INTERACTIONS.....	68
4.1.4. VALIDATION OF BIOID CANDIDATES.....	70
4.1.4.1. GFP-Traps with endogenous promotor.....	72
4.1.4.2. GFP-Traps with overexpressed Atg18.....	73
4.1.4.3. Effect of nitrogen starvation on binding.....	75
4.1.1. AUTOPHAGIC ACTIVITY.....	77
4.1.2. VPS35 COLOCALIZES WITH ATG18.....	81
4.2. <i>Vps35</i>.....	83
4.2.1. VPS35 BINDS TO ALL PROPPINS.....	83
4.2.2. ATG18 COMPETES WITH VPS17/Vps5.....	85
4.2.3. ATG18 IS NOT NECESSARY FOR TYPICAL RETROMER ACTIVITY.....	89
4.2.4. INTERACTION DEPENDS PARTIALLY ON MEMBRANE ASSOCIATION OF ATG18.....	91
4.2.5. ATG18 IS MISLOCALIZED IN <i>vps35Δ</i>	92

Table of Contents

4.2.6.	ATG18 COLOCALIZES WITH FM4-64.....	94
4.2.7.	ATG18 ACCUMULATES AT THE AUTOPHAGOSOME/PAS IN <i>VPS35</i> Δ CELLS.....	97
4.2.8.	VPS35 IS RECRUITED TO THE PAS.....	100
4.2.9.	BINDING SITE OF VPS35 AT ATG18.....	101
4.2.10.	INTERACTION OF VPS35 WITH ATG2 AND ATG9.....	103
4.2.1.	LOCALIZATION OF ATG2 AND ATG9 IN <i>VPS35</i> Δ CELLS.....	105
5.	<u>DISCUSSION.....</u>	108
5.1.	<i>Bioid</i>.....	108
5.1.1.	PROXIMITY-BASED LABELING ASSAYS.....	108
5.1.2.	OPTIMIZATION OF THE BIOID ASSAY.....	109
5.1.3.	ATG18 INTERACTOME.....	110
5.1.4.	SAP155 AND THE PHOSPHATASE SIT4.....	113
5.1.5.	YCK3 REGULATES VACUOLAR FUSION EVENTS.....	114
5.1.6.	SNF7 COULD BE INVOLVED IN AUTOPHAGOSOME CLOSURE.....	115
5.1.7.	FUSION WITH VACUOLE REQUIRES YKT6.....	116
5.2.	<i>Vps35 AND SNX3</i>.....	118
5.2.1.	ATG18 FORMS COMPLEX WITH RETROMER.....	118
5.2.2.	FUNCTION OF ATG18 IN RETROMER ACTIVITY.....	121
5.2.3.	CONNECTION BETWEEN VPS35 AND AUTOPHAGY.....	122
5.2.4.	ATG9 LOCALIZATION IS MEDIATED BY RETROMER.....	123
5.2.5.	VPS35 AFFECTS ATG18 LOCALIZATION.....	125
5.2.6.	ATG18 IS CARGO OF RETROMER.....	126
5.2.7.	REPLACING ATG2 WITH VPS35.....	128
5.2.8.	ATG18 AND RETROMER INVOLVED IN FUSION OF AUTOPHAGOSOME WITH THE VACUOLE?.....	130
	<i>CONCLUSION AND OUTLOOK</i>.....	132
6.	<u>BIBLIOGRAPHY.....</u>	133
7.	<u>SUPPLEMENT.....</u>	159
	<u>ACKNOWLEDGEMENT.....</u>	161
	<u>CURRICULUM VITAE.....</u>	162

List of Figures

FIGURE 2-1: MODEL OF A FEW INTRACELLULAR TRAFFICKING PATHWAYS	4
FIGURE 2-2: MODEL OF DIFFERENT AUTOPHAGIC PATHWAYS.	7
FIGURE 2-3: OVERVIEW OF THE DIFFERENT STEPS INVOLVED IN AUTOPHAGY.	11
FIGURE 2-4: MODEL FOR ATG9 RECRUITMENT TO THE PAS AND ITS RECYCLING.....	14
FIGURE 2-5: ATG9 IS AN INTEGRAL MEMBRANE PROTEIN AND ACTS AS A SCRAMBLASE IN A HOMOTRIMERIC COMPLEX.	15
FIGURE 2-6: THE UBIQUITIN-LIKE SYSTEMS TO CONJUGATE ATG8 TO PE.	17
FIGURE 2-7: MECHANISTIC MODEL FOR ATG8 DECONJUGATION DURING AP MATURATION.....	20
FIGURE 2-8: MODEL OF AUTOPHAGOSOME-VACUOLE FUSION.....	21
FIGURE 2-9: REGULATION OF AUTOPHAGY BY TORC1 AND PKA.	23
FIGURE 2-10: SEQUENCE AND STRUCTURAL FEATURES OF WD40 DOMAINS.....	25
FIGURE 2-11: CRYSTAL STRUCTURE FOR SCATG18 AND KLHsv2.....	27
FIGURE 2-12: MODEL OF FUNCTIONAL CONTACT SITE BETWEEN THE GROWING IM AND ER EXIT SITES.	28
FIGURE 2-13: MODEL OF THE FAB1 COMPLEX.	30
FIGURE 3-1: WORKFLOW FOR THE BIOID ASSAY	57
FIGURE 4-1: SCHEMA FOR A PROXIMITY-BASED LABELING ASSAY.....	62
FIGURE 4-2: PRELIMINARY EXPERIMENTS FOR BIOID.....	64
FIGURE 4-3: RESULTS OF THE BIOID PERFORMED TO IDENTIFY ADDITIONAL INTERACTION PARTNERS OF ATG18.....	66
FIGURE 4-4: MEMBRANE RECRUITMENT OF ATG18 DEPENDS ON TWO PTDINS 3-KINASE COMPLEXES.	69
FIGURE 4-5: BIOID TO DISTINGUISH BETWEEN ENDOSOMAL AND AUTOPHAGIC INTERACTION PARTNERS.....	70
FIGURE 4-6: EXPRESSION LEVEL AND PROTEIN SIZE OF HA TAGGED BIOID CANDIDATES-.....	71
FIGURE 4-7: BOTH Vps35 AND SAP155 CO-PRECIPIRATE WITH ATG18 AT ENDOGENOUS LEVELS.....	73
FIGURE 4-8: OVEREXPRESSION OF ATG18 WITH A <i>MET25</i> PROMOTOR IMPROVES CO-IMMUNOPRECIPITATION.	74
FIGURE 4-9: EFFECT OF NITROGEN STARVATION ON BINDING TO ATG18.....	76
FIGURE 4-10: AUTOPHAGIC ACTIVITY IN BIOID CANDIDATE KNOCKOUT STRAINS.....	79
FIGURE 4-11: CO-LOCALIZATION OF ATG18 WITH Vps35 AND SAP155.....	82
FIGURE 4-12: MODEL OF Vps10 TRAFFICKING IN YEAST.	83
FIGURE 4-13: Vps35 INTERACTS WITH ALL THREE PROPPINS.....	84
FIGURE 4-14: CRYSTAL STRUCTURE OF <i>C. THERMOPHILUM</i> RETROMER IN COMPLEX WITH Vps5.	85
FIGURE 4-15: ATG18 COMPETES WITH THE SNX-BAR-PART OF THE RETROMER COMPLEX.	86
FIGURE 4-16: INTERACTION OF ATG18 AND Vps26 IS MEDIATED BY Vps35.....	87
FIGURE 4-17: ATG18 DOES NOT FUNCTION IN EAR1 AND Kex2 RECYCLING MEDIATED BY RETROMER.....	90
FIGURE 4-18: INTERACTION BETWEEN Vps35 AND CYTOSOLIC ATG18 ^{FTTG} IS REDUCED.	91
FIGURE 4-19: LOCALIZATION OF ATG18 IS DEPENDENT ON Vps35.	93
FIGURE 4-20: ATG18 LOCALIZES PARTIALLY WITH THE ENDOSOMAL AND VACUOLAR MEMBRANE.	95
FIGURE 4-21: ATG18 IS ENRICHED AT AUTOPHAGOSOMES IN <i>vps35Δ</i> CELLS.	98
FIGURE 4-22: ATG18 POSITIVE STRUCTURES COLOCALIZE WITH Ape1.....	99
FIGURE 4-23: Vps35 CO-LOCALIZES WITH THE PAS MARKER ATG8.....	101

List of Figures

FIGURE 4-24: CRYSTAL STRUCTURE OF SCATG18 WITH INDICATED ATG2 BINDING SITES.	102
FIGURE 4-25: Vps35 DOES NOT BIND ATG18 VIA KNOWN ATG2 BINDING SITES.	103
FIGURE 4-26: Vps35 COPURIFIES WITH ATG9 AND ATG2 INDEPENDENT OF ATG18.	104
FIGURE 4-27: RECYCLING OF ATG9 FROM THE MATURE AUTOPHAGOSOME IS NOT DEPENDENT ON Vps35.	106
FIGURE 5-1: MAP OF INTERACTIONS BETWEEN ATG18 AND OTHER PROTEINS.	112
FIGURE 5-2: MODEL OF RETROMER IN COMPLEX WITH ATG18.	118
FIGURE 5-3: MODEL OF SNX3 IN COMPLEX WITH RETROMER BASED ON AN ALIGNMENT OF THE CRYSTAL STRUCTURE OF HUMAN SNX3 BOUND TO Vps35 AND Vps26 FROM <i>C. THERMOPHILUM</i>	120
FIGURE 5-4: MODEL FOR ATG18 LOCALIZATION IN THE ABSENCE OF Vps35.	127
FIGURE 5-5: PROPOSED MODEL FOR RETROMER RECRUITMENT TO THE AUTOPHAGOSOME.	131
FIGURE 7-1: FUNCTIONALITY OF TAGGED Vps35 IN AUTOPHAGY.	159
FIGURE 7-2: PTDIns3P AT THE VACUOLAR MEMBRANE IS SIMILAR TO WILDTYPE AND CAN ALSO BE FOUND AT THE VESICLE LIKE STRUCTURES.	160

List of Tables

TABLE 3-1: SOFTWARE AND DATABASES USED IN THIS THESIS.....	32
TABLE 3-2: EQUIPMENT USED IN THIS THESIS.....	32
TABLE 3-3: CHEMICALS USED IN THIS THESIS.....	34
TABLE 3-4: KITS USED IN THIS THESIS	36
TABLE 3-5: ANTIBODIES USED IN THIS THESIS	36
TABLE 3-6: ENZYMES USED IN THIS THESIS	37
TABLE 3-7: MEDIA USED IN THIS THESIS	37
TABLE 3-8: BUFFER USED IN THIS THESIS.....	38
TABLE 3-9: BACKGROUND OF STRAINS USED IN THIS STUDY.....	40
TABLE 3-10: STRAINS OF BY4741 BACKGROUND USED IN THIS THESIS	40
TABLE 3-11: STRAINS OF WCG BACKGROUND USED IN THIS STUDY	41
TABLE 3-12: <i>E. COLI</i> STRAINS USED IN THIS THESIS	43
TABLE 3-13: PLASMIDS USED IN THIS THESIS	43
TABLE 3-14: FILTER SETS FOR LIVE-CELL FLUORESCENCE MICROSCOPY USED IN THIS THESIS.....	56
TABLE 4-1: LIST OF THE MOST INTERESTING BIOID HITS.....	67

List of Abbreviations

Φ	Hydrophobic amino acid
β-ME	β-mercaptoethanol
(v/v)	(volume/volume)
(w/v)	(weight/volume)
11-BR	Atg11-binding region
AIM	Atg8-interacting motif
AP	autophagosome
Ape1	aminopeptidase 1
APS	Amoniumpersulfate
atg	autophagy related gene
BAR	bin/amphiphysin/Rvs161
CIP	Calf intestinal alkaline phosphatase
CM	complete minimal
COP	coat protein complex
CPY	carboxypeptidase Y
CRC or CSC	cargo recognition or selection complex
cvt	cytosolic to vacuolar
ddH ₂ O	double-distilled water
DIC	Differential interference contrast
DMSO	Dimethylsulfoxide
e.g.	exempli gratia; for example
EDTA	ethylenediamintetraacetic acid
ERES	ER exit site
ESCRT	endosomal sorting complex required for transport
et al.:	<i>et alii</i> , and others
EtOH	ethanol
FFAc	free fatty acid
fig.	figure
FYVE	Fab1, YOTB, Vac1 and EEA1
GEF	guanine nucleotide exchange factor

List of Abbreviations

GFP	green fluorescent protein
HOPS	homotypic fusion and vacuole protein sorting
HRP	horseradish peroxidase
Hygro	Hygromycin
ILV	intraluminal vesicles
IM	isolation membrane
IMP	intramembrane particle
KD	kinase domain
LB	lysogeny broth
LIR	LC3-interacting motif
mCherry	monomeric Cherry
MS	mass spectrometry
MVB	multivesicular body
N-or C-terminal	amino or carboxy terminal
Nrs	Nourseothricin
o/n	over night
PAS	phagophore assembly site
PBS	phosphate buffered saline
PCR	polymerase chain reaction
PMSF	phenylmethylsulfonylfluoride
PROPPIN	β -propeller that binds phosphoinositides
PtdIns 3-kinase	phosphoinositide 3-kinase
PtdIns(3,5) <i>P</i> ₂	phosphatidylinositol 3,5-bisphosphate
PtdIns3 <i>P</i>	phosphatidylinositol 3-phosphate
PX	phox homology
RFP	red fluorescent protein
rpm	rounds per minute
RT	room temperature (20-25°C)
SD-N	synthetic minimal medium w/o nitrogen
SDS	sodium dodecyl sulfate
SDS-PAGE	SDS polyacrylamide gel electrophoresis
SEM	standard error of the mean

List of Abbreviations

SNARE	soluble N-ethylmaleimide-sensitive-factor attachment receptor
SNX	sorting nexin
SOC	super optimal broth containing glucose
tab.	table
TAE	tris acetate EDTA buffer
TBST	tris buffered saline with Tween
TCA	trichloroacetic acid
TEMED	N,N,N',N'-Tetramethylethylenediamine
TGN	trans Golgi network
ubl	ubiquitin-like
VPS	vacuolar protein sorting
WIPI	WD repeat domain PI-interacting motif
wt	wildtype
YPD	yeast peptone dextrose

Units

°C	degree(s) celsius
%	per cent
x g	times gravity
A	Ampere
bp	basepair
Da	Dalton
g	gram
h	hour
L	liter
M	mole per liter
min	minute
OD ₆₀₀	optical density /absorbance at 600 nm wavelength
rpm	revolution per minute
s	second

1. Summary

The PROPPIN Atg18 belongs to the WD40 repeat containing family and folds into a typical seven-bladed β -propeller. Conserved regions at blade 5 and 6 allow for binding to phosphatidylinositolphosphates and mediate the association with the membrane. WD40 repeat proteins often act as platform for protein-protein interactions, which turns Atg18 into an efficient PtdIns P effector.

In yeast the protein fulfills two distinct functions: it is essential for the process of autophagy but also regulates membrane fission events at the vacuole. Autophagy is a physiological process to degrade cellular components, either cytosolic proteins or whole organelles. This is necessary in normal cellular homeostasis to regulate protein turnover but also helps the cell in adapting to extracellular stress such as nutrient scarcity by mobilizing metabolic precursors. During the process cargo is engulfed in a double-membraned sphere that fuses at the edges to form an autophagosome. Fusion with the vacuole releases the cargo enveloped by a single-membrane into the vacuolar lumen to be degraded. Atg18 is essential for membrane expansion during the early stages of autophagosome formation.

The second function of Atg18 is at the vacuolar membrane: Atg18 forms a complex with the vacuolar PtdIns 5-kinase and its regulators Vac7 and Vac14 as well as the phosphatase Fig4. Here, it regulates the synthesis of PtdIns(3,5) P_2 by providing negative feedback to the kinase. It is also thought to promote fission events by inducing membrane curvature with its hydrophobic loop inserted into the membrane.

Not much is known about the mechanisms behind the regulation of vacuolar morphology mediated by Atg18. Therefore, a proximity-dependent labeling assay combined with SILAC was performed to identify potential interaction partners of Atg18. Several new proteins potentially in a complex with Atg18 were identified and three of them could be validated by independent experiments. One of them was chosen for further analyses.

Vps35 is a component of the retromer complex, which mediates retrograde transport from the endosome and the vacuole of Golgi-resident membrane proteins. Another protein identified in the BioID approach was the sorting nexin Snx3, which forms a complex with retromer and mediates contact with the membrane. Atg18 was shown to be a cargo of this trafficking pathway, as a defect in retromer – deletion of VPS35 -

1. Summary

caused mislocalization of the PROPPIN to the vacuolar and autophagosomal membrane. This indicates involvement of the retromer complex in the recycling of autophagosomal proteins, or at least Atg18, after autophagy. This could occur either at the autophagosomal membrane or at the vacuolar membrane after autophagosome-vacuole fusion.

Interestingly, the only known integral membrane protein located to the PAS, Atg9, was also observed to interact with Vps35. Most likely, recycling of Atg9 is not mediated directly by the retromer complex, as deletion of Vps35 does not cause Atg9 mislocalization to the vacuolar membrane.

However, it was shown that retrograde trafficking mediated by the retromer complex is involved in recycling proteins of the autophagic machinery.

2. Introduction

2.1. The model organism *S. cerevisiae*

Until the late 18th Century the term “yeast” mostly described a substance necessary for fermentation of alcoholic beverages such as beer. That this was caused by a living organism was first discovered by Louis Pasteur (Pasteur, 1879), although it was already described in 1837 by a medical doctor and botanist Franz Meyen (Feyder et al., 2015). The scientific name of this fungi (-*myces*) is derived from its high affinity to sugar (*saccharo-*) and its famous use in brewing beer (*cerevisiae*). Since then it was extensively studied and was the first organism with a fully sequenced genome (Goffeau et al., 1996). A haploid cell contains 16 chromosomes with a total of about 12,000 kb DNA and around 6,000 open reading frames have been predicted. An extensive set of molecular tools has been developed, allowing for simple and easy genetic manipulations with homologous recombination of exogenous DNA fragments to change promoters, tag or delete proteins (Guldener, 1996; Janke et al., 2004; Longtine et al., 1998). There are also well-established and ever growing plasmid collections, which can be introduced into a similarly large strain collection (Sikorski & Hieter, 1989).

S. cerevisiae is a single celled eukaryote and member of the Fungi kingdom. It has a haploid and a diploid form and proliferates by mitotic (budding) or meiotic (sporulation) division with a doubling time of 90 min under optimal conditions (Sherman, 2002). Meiotic reproduction occurs when cells of different mating types (*Mata* or *Mat α*) mate to form a diploid cell. Sporulation is induced by stress signals such as nutrient shortage and leads to the formation of asci containing four haploid ascospores (Neiman, 2005).

Another advantage of *S. cerevisiae* as a model organism is the high level of sequence and functional conservation between yeast and more complex eukaryotic species (Duina et al., 2014; Gavin et al., 2002; Sikorski & Hieter, 1989). This allows for a sometimes direct transfer of findings from one organism to another.

2. Introduction

2.2. Transport in cell

S. cerevisiae has a complex intracellular organization into different organelles, which are connected via a multitude of different trafficking pathways (reviewed in (Feyder et al., 2015)). Proteins destined to one of these compartments are translocated to the Endoplasmic Reticulum (ER) and transported to the Golgi.

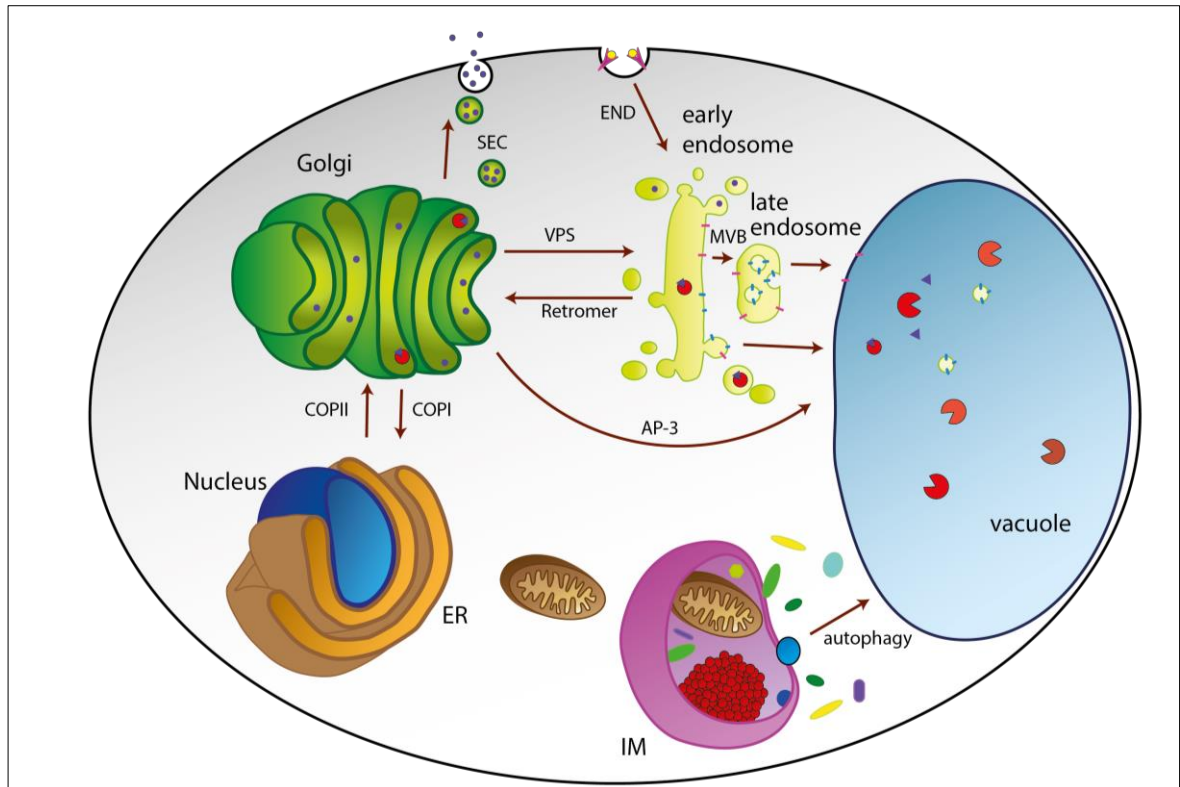


Figure 2-1: Model of some of the intracellular trafficking pathways

2.2.1. Golgi to vacuole

Proteins are sorted according to their final destination: proteins targeted to the vacuole are either trafficked directly - for example via the adaptor protein-3 (AP-3) pathway - or through the endosome via the vacuolar protein sorting (VPS) pathway. Proteins for the AP-3 pathway such as the alkaline phosphatase (ALP) are sorted into AP-3 clathrin covered vesicles at the trans Golgi network (TGN) and delivered to the vacuole (Cowles, 1997; Cowles et al., 1997; Stepp et al., 1997). The VPS pathway sorts cargo to the endosome and then the vacuole. Several different effector proteins have been identified (Bowers & Stevens, 2005; Raymond et al., 1992). Cargo proteins such as the vacuolar carboxyl peptidase (CPY) are concentrated by specific receptors (in this case Vps10) and sorted into vesicles targeted to the endosome. Soluble proteins like

2. Introduction

CPY are released into the endosomal lumen, while membrane proteins such as the vacuolar ATPase are now associated with the endosomal membrane. The fusion of the late endosome with the vacuole delivers both to their final destination. Cargo receptors like Vps10 are recycled to the Golgi mediated by the retromer complex.

Membrane proteins targeted to the vacuolar lumen require an additional sorting step at the endosome. The cargo is marked by ubiquitination and concentrated into invaginations. Inward protrusion of the limiting membrane of early endosomes leads to the formation of intraluminal vesicles (ILVs) and multivesicular bodies (MVB) orchestrated by the ESCRT machinery (reviewed in (Katzmann et al., 2002; Piper & Katzmann, 2010)).

2.2.2. Golgi to plasma membrane

The secretory (SEC) pathway for proteins targeted to the plasma membrane (PM) was extensively researched by the group of Randy Schekman: the cargo is loaded at the TGN into vesicles which are then delivered to the PM (Novick et al., 1980, 1981). Internalization of these proteins or extracellular medium occurs via endocytosis (END pathway).

2.3. Autophagy

Autophagy is another pathway to the vacuole or lysosome in eukaryotes. Autophagy literally translates as “self-eating” from the Greek words for “self” – *auto* - and “to eat” – *phagein* and describes a physiological process to degrade cellular components. Most of the proteolytic activity, with the exception of proteasome-mediated protein degradation, is located at the vacuole in yeast or lysosome in mammals. In order to be degraded, redundant or damaged proteins and organelles are sequestered within double-membrane structures and transported to the vacuole (Reggiori & Klionsky, 2002). This provides the cell with much needed biosynthetic precursors and energy sources during starvation. Rapid changes in the proteome help the cell to adapt to changes in the environment. It is also an important mechanism for quality control, as damaged or incorrectly synthesized or folded proteins are removed before they can aggregate and disturb cellular homeostasis (Goldberg, 2003). Autophagy can also function in regulating the size of different compartments by adding or removing lipids from the membrane.

2. Introduction

Autophagy was first discovered in the sixties with electron microscopy of rat liver cells: perfusion with glucagon led to the formation of lysosomes containing partially digested mitochondria (Ashford & Porter, 1962; de Duve, 1963; Novikoff & Essner, 1962). Depletion of amino acids induced the same morphological changes (Mitchener et al., 1976; Mortimore & Schworer, 1977). Since then autophagy has also been described in yeast cells and more than 40 autophagy related (Atg) proteins have been identified through genetic screenings (Takeshige et al., 1992; Thumm et al., 1994; Tsukada & Ohsumi, 1993). Between 16 to 20 of these are essential for autophagy, depending on the organism.

One of the functions of autophagy is the removal of superfluous or aggregated proteins or organelles which can become dangerous to the cell or organism. Protein aggregations caused by impaired autophagy are associated with neurodegeneration, cancer, cardiovascular disorders and ageing (Mizushima & Komatsu, 2011). Autophagic activity can be detrimental under certain circumstances or it can help prevent severe illnesses (reviewed in (Levine & Kroemer, 2019)). Autophagy has also been described in immunological processes such as the elimination of intracellular pathogens, control of inflammation, antigen presentation and secretion of immune mediators (Cadwell & Debnath, 2018; Deretic et al., 2013). It was identified as a factor in several inflammatory autoimmune diseases such as Crohn's disease. Furthermore, autophagy has been shown to be essential for lifespan extension, while a decline in activity correlates with age progression (Ichimiya et al., 2020).

Autophagy can be divided into two main types: macroautophagy and microautophagy, as depicted in Figure 2-2. A third type was described in mammalian cells as chaperone mediated autophagy (CMA). Although morphological different all three share a common goal: the delivery of cargo to the vacuole/lysosome for degradation (Parzych & Klionsky, 2014). Both macro- and microautophagy can occur as unselective, e.g. bulk autophagy, or selective, e.g. cvt pathway or pexophagy.

The core autophagic machinery is highly conserved among all eukaryotes and most ATGs found in mammals have counterparts in yeast or plant cells (Reggiori & Klionsky, 2002).

2. Introduction

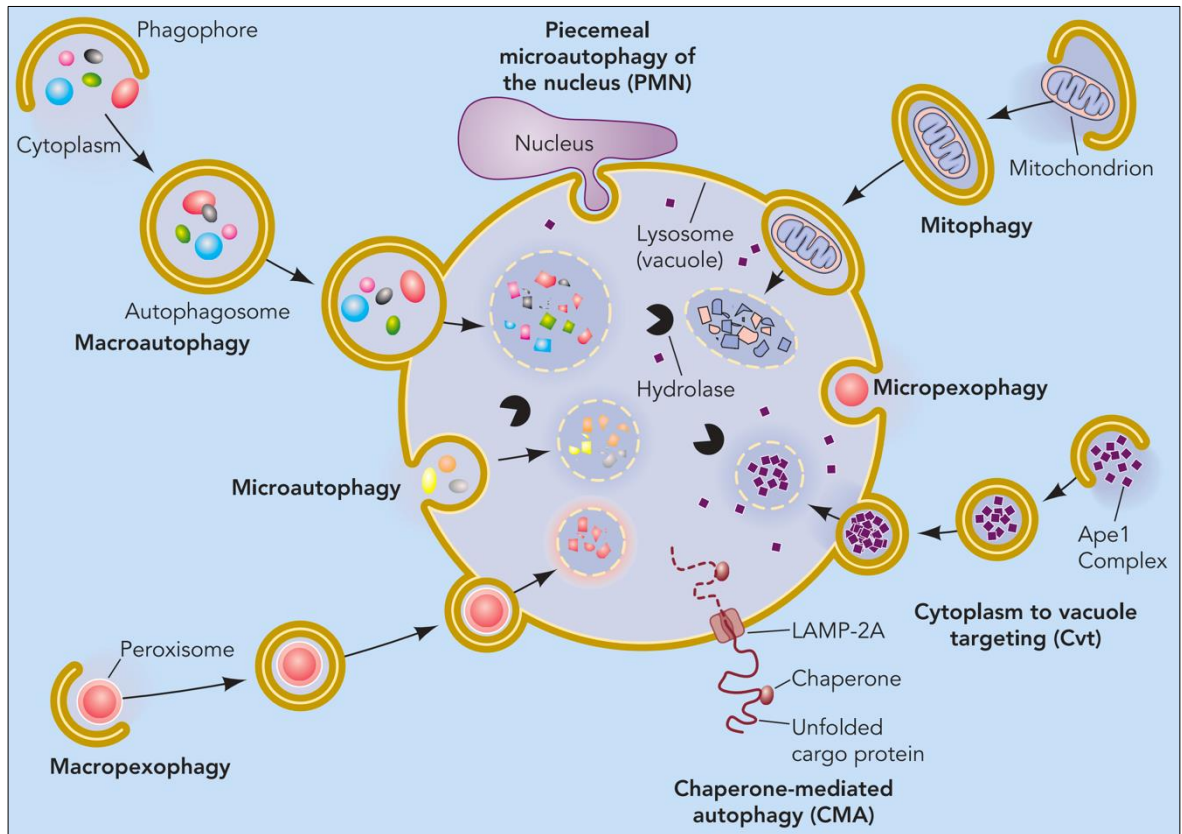


Figure 2-2: Model of different autophagic pathways.

Autophagy can be divided into three different groups: during macroautophagy cargo is engulfed in a de novo formed double-membrane and delivered to the lysosome/vacuole. Cargo is directly taken up by the lysosome/vacuole during microautophagy. CMA describes the translocation of selective proteins from the cytosol into the lumen of the lysosome/vacuole. Both macro- and microautophagy can be selective (e.g. Cvt or micropexophagy) or non-selective. (Yen & Klionsky, 2008)

2.3.1. Macroautophagy

Macroautophagy, from now on simply referred to as autophagy, is the best described autophagy pathway. It is constitutively active at a low level, constantly and non-selectively degrading random portions of the cytosol. External and internal stress factors including nutrient scarcity (starvation), hypoxia and cellular damage can increase activity substantially.

Autophagy can be broken down into five distinctive steps (Parzych & Klionsky, 2014; Wen & Klionsky, 2016): Nucleation of the phagophore or isolation membrane (IM) is initiated at the preautophagosomal structure or phagophore assembly site (PAS). The IM forms *de novo* and expands around the cargo, engulfing it in a spherical or cup-shaped structure. After fully surrounding its cargo the edges fuse together to form a double membraned autophagosome (AP) with a diameter between 0.4 and 0.9 μm in yeast (Baba et al., 1994; Takeshige et al., 1992). Once its contents are completely

2. Introduction

separated from the cytosol the outer membrane of the autophagosome fuses with the vacuolar membrane. This results in the release of a single membraned autophagic body into the vacuolar lumen. The limiting membrane of the autophagic bodies is then broken down by vacuolar lipases and the cargo is eventually degraded by hydrolases. Metabolic precursors such as amino acids are then transported into the cytosol. The whole process of initiation, phagophore formation and expansion, closure and fusion with the vacuole takes approximately 7-10 min (Geng et al., 2008; Xie et al., 2008).

2.3.2. Selective autophagy

Autophagy was initially thought to be the non-selective degradation of random portions of the cytosol (Wen & Klionsky, 2016). Since then mechanisms selective for specific cargo such as organelles or proteins have been described. Unlike nonselective autophagy, where the phagophore engulfs huge portions of the cytosol, during selective autophagy the sequestering membrane tightly forms around the cargo to exclude other cytosolic components (Reggiori & Klionsky, 2013).

Selective autophagy requires the same core machinery as non-selective autophagy in addition to specific cargo receptors also named SARs (selective autophagy receptors) (Farré & Subramani, 2016). SARs can be divided into soluble receptors, such as Atg19 and Atg34, and membrane associated receptors such as Atg32 and Atg36. In addition to cargo recruiting, they can also bind to the core autophagic protein Atg8. Atg8 and its mammalian counterpart LC3 are membrane associated proteins involved in IM expansion and localize to the inner and the outer leaflet of the IM. Interaction with the SARs occurs through one or more Atg8 interacting motifs (AIM) or LC3-interacting motifs (LIR) in mammals. Most AIMs are defined by a conserved (W/F/Y)xx(L/I/V) motif, surrounded by at least one proximal acidic residue (Farré & Subramani, 2016; Noda et al., 2008). Hydrophobic residues of the AIM bind to hydrophobic pockets of Atg8 while the negatively charged acidic residues stabilize the interaction (Noda et al., 2010). An additional interaction is seen between many different SARs and the scaffold protein Atg11 (for a more detailed description of the autophagic machinery see chapter 2.3.5), which is facilitated by Atg11-binding regions (A11BR) in SARs.

Several different cargos of selective autophagy and their respective receptor have been identified: autophagy of the mitochondria (mitophagy) is mediated by the receptor Atg32 (Kanki et al., 2009; Liu & Okamoto, 2021), while degradation of peroxisomes

2. Introduction

(pexophagy) relies on Atg36 in *S. cerevisiae* (Motley et al., 2012). Selective autophagic pathways have also been identified for ribosomes (Kraft et al., 2008), the ER and the nucleus (Mochida et al., 2015).

One particularly well described mechanism for constitutive non-induced selective autophagy is the cytosol-to-vacuole targeting (cvt) pathway, which mediates transport of vacuolar hydrolases such as the vacuolar aminopeptidase 1 (Ape1), the aspartyl aminopeptidase 4 (Ape4) and the α -mannosidase 1 (Ams1) from the cytosol to the vacuole (Hutchins & Klionsky, 2001; Yuga et al., 2011). Although several different cargos have been identified, only Ape1 can function as a template or scaffold for the autophagic machinery (Shintani & Klionsky, 2004).

A precursor form of Ape1 containing a 45 amino acid propeptide at the N-terminus is synthesized in the cytosol (Klionsky et al., 1992) and rapidly oligomerizes into a dodecameric complex (Kim et al., 1997). The formation of a higher order structure termed the Ape1 complex is dependent on the propeptide (Shintani & Klionsky, 2004). The complex is then recognized through the coiled-coil (CC) domain of the autophagic receptor Atg19 (Leber et al., 2001; Scott et al., 2001). Atg19 binds to Atg8 via AIM and Atg11 through the A11BR to form the Cvt complex, which mediates the recruitment of the autophagic core machinery (reviewed in (Yamasaki & Noda, 2017)). A double membrane completely engulfs the cargo to form a so called Cvt vesicle, which fuses with the vacuolar membrane to release its cargo into the vacuolar lumen. Here, the precursor Ape1 is processed by cleaving off its propeptide to form mature Ape1. The shift in size can be detected by immunoblotting and is often used as a measure for autophagic activity.

2.3.3. Microautophagy

Microautophagy is defined as the uptake of cargo at the vacuolar surface through direct invagination of the limiting membrane and subsequent budding of vesicles into the vacuolar lumen. It is also thought to play a role in the regulation of vacuolar size. To date many different macroautophagic processes have been discovered, including microautophagy of the nucleus, peroxisomes, cytosol, mitochondria, lipid droplets, ER, and vacuole membrane proteins (reviewed in (Schuck, 2020)). The size of the structure can vary greatly, as whole organelles can be engulfed and transported into the vacuole, but can be up to 350 nm during starvation (Oku et al., 2017).

2. Introduction

Microautophagy or the uptake of soluble components (Kunz et al., 2004) is induced upon starvation or treatment with the TOR (target of rapamycin) complex inhibitor rapamycin. Microautophagy occurs in five steps (reviewed in (Li et al., 2012)). First, the limiting membrane protrudes into the vacuolar lumen under the exclusion of transmembrane proteins. High lipid density in combination with the autophagic machinery results in vesicle formation, expansion and ultimately scission through homotypic fusion. The released vesicle is then broken down in an Atg15 dependent manner.

Selective microautophagy has been described for the degradation of entire peroxisomes (micropexophagy), piecemeal microautophagy of the nucleus (PMN) and micromitophagy (Kiššová et al., 2007; Krick, Muehe, et al., 2008; Kvam & Goldfarb, 2007; Otto & Thumm, 2020; Sakai et al., 2006).

2.3.4. Chaperone mediated Autophagy

CMA has mainly been described in mammalian cells and is a unique and highly selective form of autophagy. It is constitutively active but can be further activated under stress conditions (Cuervo, 2010). Unlike other types of autophagy, no formation of membrane-enclosed intermediates is involved. Cargos of CMA have a common pentapeptide targeting motif consisting of Lys-Phe-Glu-Arg-Gln (KFERQ) or biochemically similar amino acid residues (Chiang & Dice, 1988). This tag is often hidden in a properly folded protein, but accessible if it is misfolded or damaged (Orenstein & Cuervo, 2010). It is therefore an efficient tool in quality control. The KFERQ motif is recognized by chaperones in the cytosol, notably the heat shock cognate protein 70-kDa (HSC70) (Chiang et al., 1989). The chaperone binds the CMA cargo and targets it to the lysosomal membrane. Here the lysosomal-associated membrane protein type 2a (LAMP2A) oligomerizes upon binding the substrate and forms the translocation complex. Together with a multi-molecular chaperone complex, it mediates cargo unfolding and translocation into the lysosomal lumen (Agarraberes & Dice, 2001; Cuervo & Dice, 1996; Salvador et al., 2000). The translocation complex is then disassembled and the substrate is degraded by lysosomal hydrolases.

2. Introduction

2.3.5. Mechanism

The basic mechanism of autophagy is highly conserved among all eukaryotes and will be described in detail for the well-researched organism *S. cerevisiae*. In yeast, 18 of the 42 identified proteins involved in autophagy (Atgs) are essential for autophagosome formation and degradation of cargo and are classified as the core autophagic machinery (Mizushima et al., 2011; Parzych et al., 2018). They can be divided into six functional complexes, as shown in Figure 2-3, which will be further described in the following chapters.

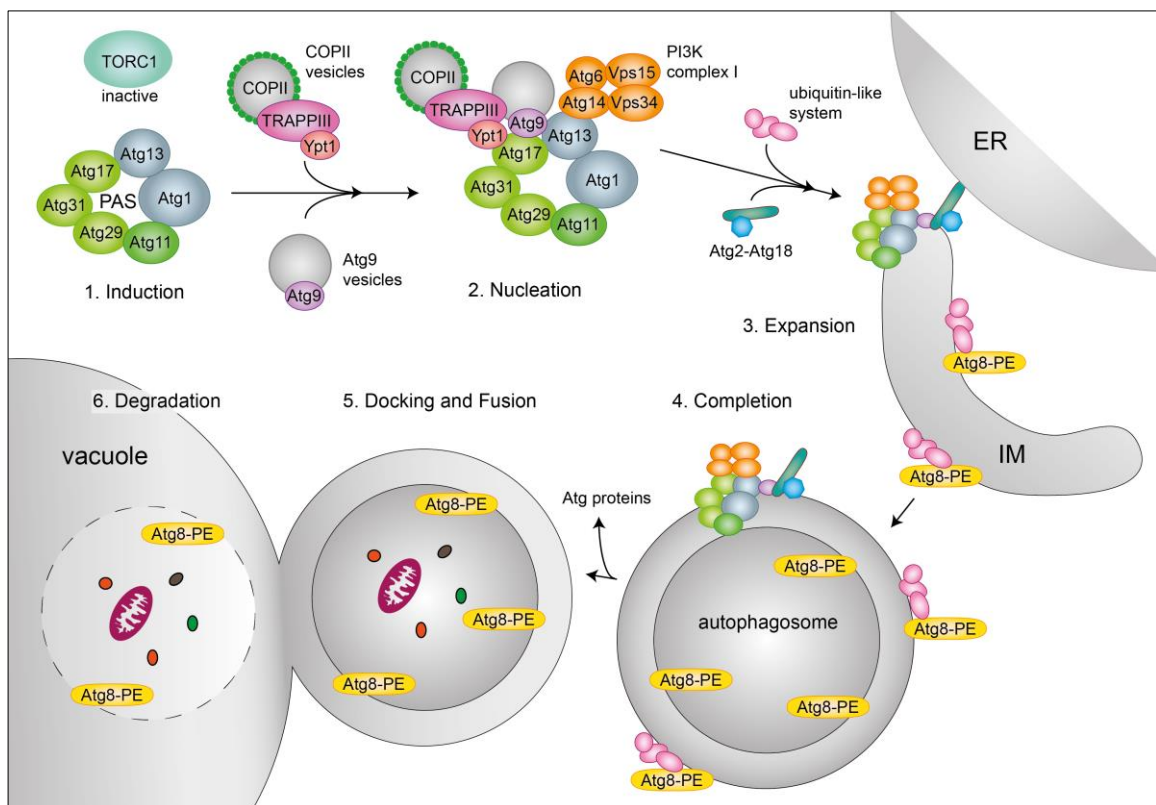


Figure 2-3: Overview of the different steps involved in autophagy.

Starvation or treatment with rapamycin inactivates the TORC1 complex, which activates autophagy (step 1). Atg13 is hypophosphorylated and interacts with Atg1 and Atg17. The core machinery is assembled at the PAS, organized by the scaffold components Atg11 and Atg17-Atg29-Atg31 subcomplex (step 2) during selective and non-selective autophagy, respectively. Atg9 and COPII vesicles are thought to contribute membrane lipids to initiate expansion (step 3) together with the PI3-kinase complex (Atg14, Atg6, Vps34, Vps15), the Atg18-Atg2 complex and the ubiquitin-like conjugation system (Atg5-Atg12-Atg16 depicted as pink molecules) with Atg8-PE. Cargo is engulfed into the double-membraned autophagosome (step 4), which fuses with the vacuolar membrane (step 5). The autophagic body is then released into the vacuolar lumen and degraded (step 6).

2.3.5.1. Atg1 kinase and scaffolding complex

Atg1 is a Ser/Thr protein kinase (Matsuura et al., 1997), it forms a platform with Atg13 and the Atg17-Atg31-Atg29 scaffolding complex and is essential for the organization of the PAS.

2. Introduction

Atg1 contains an N-terminal kinase domain (KD) connected to an intrinsically disordered region (IDR). The kinase activity of Atg1 is not necessary to recruit the autophagic machinery but is involved in Atg components disassembly after completion of the membrane (Cheong et al., 2008). Both Atg2 and Atg9 have been identified as substrates of the KD of Atg1 as well as Atg1 itself (Papinski et al., 2014). Two microtubule-interacting and transport (MIT) domains are located at the C-terminus of Atg1 and thought to interact with MIT-interacting motifs (MIMs) found at the C-terminal region of Atg13 (Fujioka et al., 2014). This is necessary for Atg1 activation and PAS assembly. Atg13 contains a HORMA (Hop1p, Rev1p, Mad2p) domain at its N-terminus, which is able to bind both Atg9 and Atg14 (Jao et al., 2013). The C-terminal region of Atg13 is predicted to be an intrinsically disordered region (IDR) strongly phosphorylated under nutrient rich conditions (Kamada et al., 2000). Dephosphorylation during starvation enables interaction with Atg17 through two functionally relevant Atg17 binding regions (17-BR) within the IDR of Atg13 as well as with Atg1 (Fujioka et al., 2014; Yamamoto et al., 2016). Atg17 is comprised of four α -helices forming a crescent shaped structure with a radius of 1 nm. It self-assembles into S-shaped homodimers, each homodimer binding two Atg31-Atg20 heterodimers. The hexameric complex further oligomerizes by interconnection mediated by Atg13 (Kabeya et al., 2005; Mao et al., 2013; Ragusa et al., 2012).

2.3.5.2. PI3 Kinase Complex

Phosphoinositides (PtdIns) represent about 1% of total cellular phospholipids (reviewed in (De Craene et al., 2017)) and are generated by the phosphorylation of phosphatidylinositol on its inositol ring. Phosphorylation at position D3 of inositol results in the production of PtdIns3P and is catalyzed by the lipid kinase Vps34 (vacuolar protein sorting 34) (Schu et al., 1993). Deletion of VPS34 results in severe protein sorting as well as vacuolar biogenesis defects, although the vacuolar morphology seemed normal (Herman & Emr, 1990).

Vps34 forms a complex with the protein kinase Vps15, which is required for the activation of Vps34 and stable association to the membrane (Stack et al., 1993, 1995). Vps15 is myristoylated at the N-terminus which facilitates its association with the membrane (Herman, Stack, DeModena, et al., 1991). However, additional factors have

2. Introduction

to be involved, since non-myristoylated Vps15 is still associated with the membrane (Herman, Stack, & Emr, 1991).

Another subunit of the PI3 kinase complex was identified as Vps30 (or Atg6) (Kihara et al., 2001), a protein known to interact with Atg14 and essential for autophagy (Kametaka et al., 1998). An involvement of PtdIns3P in autophagy was first suggested by (Kiel et al., 1999) in *H. polymorpha*. The deletion of the functional homologue to ScVps34 led to a complete block in peroxisome degradation. Published data suggest at least two different PI3 kinase complexes with Vps34, Vps17 and Vps30 as core machinery and additional subunits to regulate function (Kihara et al., 2001). Complex I contains Atg14 and Atg38 (Araki et al., 2013; Ohashi et al., 2016) and is essential for autophagy, while Vps38 is part of complex II and required for endosomal protein transport. Co-IP experiments suggest that both Atg14 and Vps38 act as connectors between Vps30 and the Vps34-Vps15 subcomplex (Kihara et al., 2001).

Recruitment of the PI3-kinase complex I to the PAS is mediated by Atg14 (Obara, Noda, et al., 2008). The N-terminal region of Atg13 contains a HORMA (Hop1p, Rev1p, Mad2p) domain, which is necessary for autophagic activity as well as recruitment of Atg14 (Jao et al., 2013). Atg14 also failed to localize to the PAS in *atg17Δ* and *atg9Δ* cells (Suzuki et al., 2007). PtdIns3P is highly enriched at the isolation membrane and recruits the Atg18-Atg2 complex (Obara & Ohsumi, 2008).

2.3.5.3. Atg9 vesicles and the role of Atg9

Atg9 is the only transmembrane protein essential for autophagy. It localizes to single-membraned vesicles of 30-60 nm diameter (Yamamoto et al., 2012) forming peripheral tubulovesicular clusters derived from the Golgi, which is depicted in Figure 2-4 (Mari et al., 2010; Ohashi & Munro, 2010). The formation of these structures is dependent on the peripheral single-pass membrane proteins Atg23 and Atg27 (Backues et al., 2015; Tucker et al., 2003; Yamamoto et al., 2012; Yen et al., 2007).

Autophagy induction recruits Atg9 vesicles to the PAS, where interaction with the Atg1 kinase complex is mediated by the Rab GTPase Ypt1 and its guanidine exchange factor (GEF) transport protein particle III (TRAPP III) complex (J. Wang et al., 2013). Recruitment to the PAS is dependent on interaction with Atg17 (Sekito et al., 2009) and Atg13 (Suzuki et al., 2015) or Atg11 and Atg19 during the Cvt pathway.

2. Introduction

It is thought that the initial IM is formed out of three Atg9 vesicles tethered together by the Atg1 kinase complex, as depicted in Figure 2-4 (Rao et al., 2016; Yamamoto et al., 2012). Atg9 is then phosphorylated by Atg1 (Papinski et al., 2014).

Recognition of PtdIns3P by Atg18 recruits the Atg2-Atg18 complex to the IM (Obara, Sekito, et al., 2008) and the interaction between Atg2 and Atg9 restricts localization of the complex to the edge of the IM (Gómez-Sánchez et al., 2018). Electron microscopy of mammalian Atg2 reveals a rod-like structure of about 20 nm, with the mammalian homologue to Atg18 bound to one end of it (Chowdhury et al., 2018; Zheng et al., 2017). Overall, this structure is very similar to membrane tethering complexes and the experiments demonstrated the ability of Atg2 to tether liposomes. A function for Atg2 in connecting the PAS to the ER was suggested, with each membrane bound to one side of the rod, while Atg18 is located at the IM side (Kotani et al., 2018). Additionally, it was discovered that Atg2 also mediates lipid transfer between membranes. Structural analysis revealed a hydrophobic groove connecting both sides of the rod-like structure of Atg2, through which lipids could be transported directly from the ER to the IM (Osawa et al., 2019; Osawa & Noda, 2019; Valverde et al., 2019).

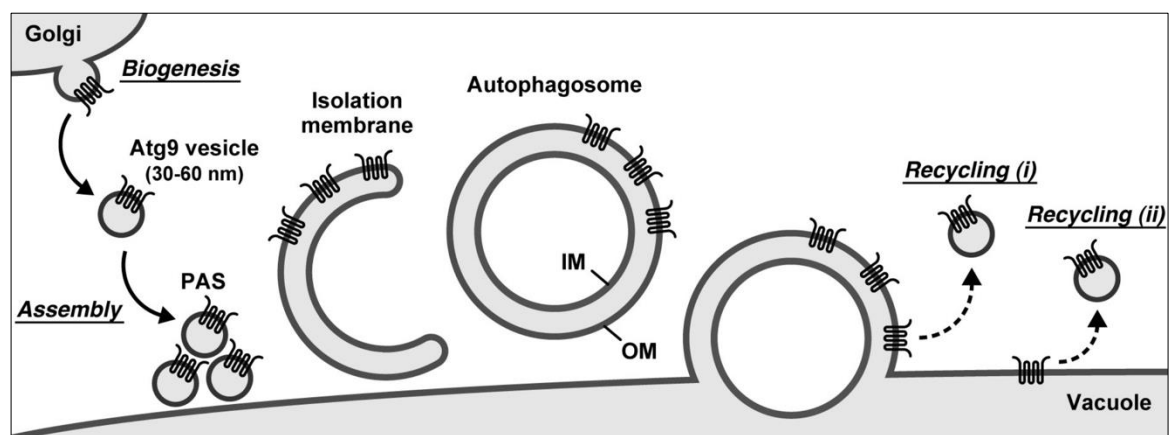


Figure 2-4: Model for Atg9 recruitment to the PAS and its recycling.

Atg9 is localized to perivacuolar pools and recruited to the PAS upon starvation. About three Atg9 containing vesicles fuse to initiate IM formation. Atg9 is localized to the outer membrane (OM) of the expanding phagophore and recycled either from the closed autophagosome before or during fusion with the vacuolar membrane (i) or shortly afterwards (ii). (Yamamoto et al., 2012)

Atg9 was predicted to contain six to eight membrane domains (Lang et al., 2000; T. Noda et al., 2000). However, recent cryo-EM studies show only four transmembrane helices (Matoba et al., 2020), with two additional helices peripherally associated with the membrane (see Figure 2-5A). The membrane protein forms multimers, which were found to be essential during phagophore expansion (He et al., 2008). Recent studies have shown that Atg9 forms a trimer in a lipid bilayer membrane (Figure 2-5B), which

2. Introduction

results in the formation of a large pore at the center of the complex, vertical to the membrane (vertical pore – VP) (Matoba et al., 2020). Each Atg9 molecule also contains a lateral amphipathic pore (lateral pore – LP), which together could facilitate phospholipid translocation from one side of the lipid bilayer to the other. Further experiments suggest a direct role in IM expansion mediated by the LP and VP of Atg9 in the homotrimeric complex. Atg9 could act as a lipid scramblase translocating incoming phospholipids from the cytoplasmic leaflet of the IM to the luminal side, following the actions of Atg2 (Figure 2-5C).

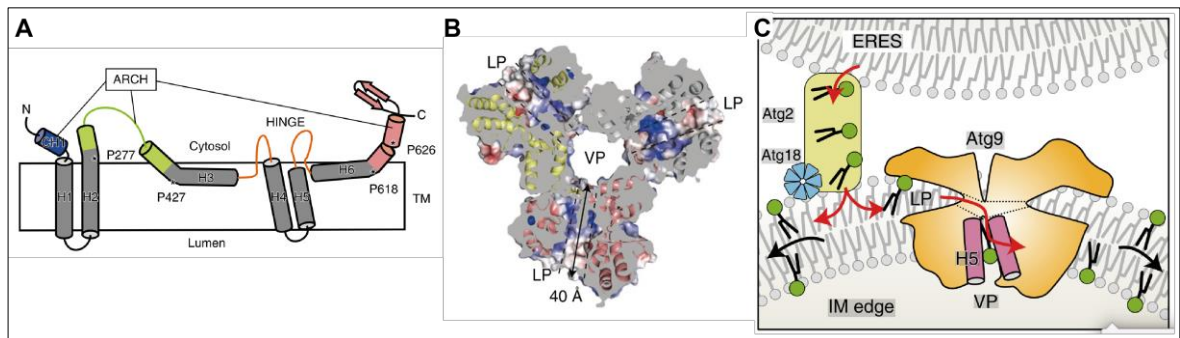


Figure 2-5: Atg9 is an integral membrane protein and acts as a scramblase in a homotrimeric complex

(A) Topology of the membrane-buried region of Atg9, grey – regions in membrane, orange – HINGE domain, blue, green and pink – ARCH domain. **(B)** structural model for Atg9 trimer, colored as in (A). **(C)** Proposed model for Atg9-mediated lipid transfer. Atg2 transfers lipids from the ERES to the cytosolic leaflet of the IM, Atg9 translocates them to the luminal side. Adapted from (Matoba et al., 2020)

2.3.5.4. Origin of membrane lipids

The double membrane expands around the cargo and completely engulfs it in minutes. The origin of the involved lipids is still under discussion. Several studies proposed the contribution of already formed membrane lipids from different source organelles such as lipid droplets (Dupont et al., 2014), mitochondria (Hailey et al., 2010), the plasma membrane (Ravikumar et al., 2010), endosomes (Puri et al., 2013), the Golgi or Golgi-endosome intermediates (Geng et al., 2010; van der Vaart et al., 2010) as well as the ER (Axe et al., 2008).

COPII vesicles mediate transport from the ER exit sites to the Golgi with the help of a set of highly conserved components (Barlowe, 1994; Jensen & Schekman, 2011; Lee et al., 2004). The inner coat is formed by a heterodimer of Sec23 and Sec24, while the outer coat contains heterotetramers Sec13 and Sec32, two of each. A small GTPase, Sar1, is activated by the ER resident guanine nucleotide exchange factor (GEF) Sec12, anchors in the membrane and recruits the other components. Budding occurs at the ER exit sites (ERES), which is closely associated with the IM (Graef et al., 2013). An

2. Introduction

involvement of COPII vesicles in IM expansion was long suspected and a study by (Ishihara et al., 2001) found several mutants deficient for COPII vesicle formation also caused defects in autophagy. Both inner coat components Sec23 and Sec24 as well as the GTPase Sec12 were shown to be necessary for efficient autophagosome formation. The transmembrane protein Axl2 is transported to the autophagosomal membrane if it is previously loaded into COPII vesicles (Shima et al., 2019). This observation further demonstrates the direct participation of COPII vesicles in membrane delivery to the growing IM, but the exact mechanism of recruitment and fusion is still unknown. Atg9 is able to interact with the COPII subunit Sec24 under autophagy inducing conditions (Davis et al., 2016). Additionally, the TRAPP III complex, which is involved in mediating the interaction between the Atg1 kinase complex and Atg9 containing vesicles, also binds the Sec23 subunit of the COPII complex (Tan et al., 2013). Tethering both Atg9 vesicles and COPII vesicles to the PAS is hypothesized to induce heterotypic fusion between the vesicles to form the IM (Davis & Ferro-Novick, 2015; Ge et al., 2014)

Another recently discussed mechanism to expand the IM is the *de novo* synthesis of phospholipids combined with the phospholipid transfer from the ER to the phagophore mediated by Atg2-Atg18 (see chapter 2.3.5.3). The ER is the organelle responsible for *de novo* lipid synthesis. Recently, the conserved acyl-CoA synthetase Faa1 was discovered at the phagophore nucleation site. It is thought to activate fatty acids (FAs) with coenzyme A (CoA) and channel them into phospholipid synthesis within the ER (Schütter et al., 2020). Afterwards they are transported to the expanding IM mediated by the Atg2-Atg18 complex and distributed on both the inner and outer membrane via the scramblase function of Atg9 (see chapter 2.3.5.3). The direct lipid flow from the ER to the growing phagophore could well be the largest source of phospholipids during autophagy and is comparable to mammalian cells. Here, an intermediate structure named the omegasome emerges from a PtdIns3P enriched subdomain of the ER. It is thought to act as scaffold and lipid source for phagophore expansion and links the ER to the phagophore (Axe et al., 2008; Otomo et al., 2018).

2.3.5.5. Ubiquitin like conjugation system and Atg8

Expansion of the IM is largely dependent on Atg8 and the ubiquitin-like (ubl) lipidation machinery. Furthermore, it is required for autophagosome closure and cargo selectivity during selective autophagy (Slobodkin & Elazar, 2013). The amount of Atg8

2. Introduction

present at the expanding IM correlates directly with the size of the AP (Xie et al., 2008) and is distributed at the inner and outer membrane. It is thought to act as a scaffold for either cargo receptors at the inner membrane or the autophagic machinery at the outer membrane (Kaufmann et al., 2014).

Atg8 is covalently linked to phosphatidylethanolamine (PE) at the autophagosomal membrane which is mediated by two ubl systems as shown in Figure 2-6. The first system activates and transfers the ubiquitin-like Atg8 to PE, while the second system involves the formation of the Atg5-Atg12 complex and is essential for the last step of Atg8-PE conjugation (Hanada et al., 2007; Ichimura et al., 2000; Mizushima et al., 1998).

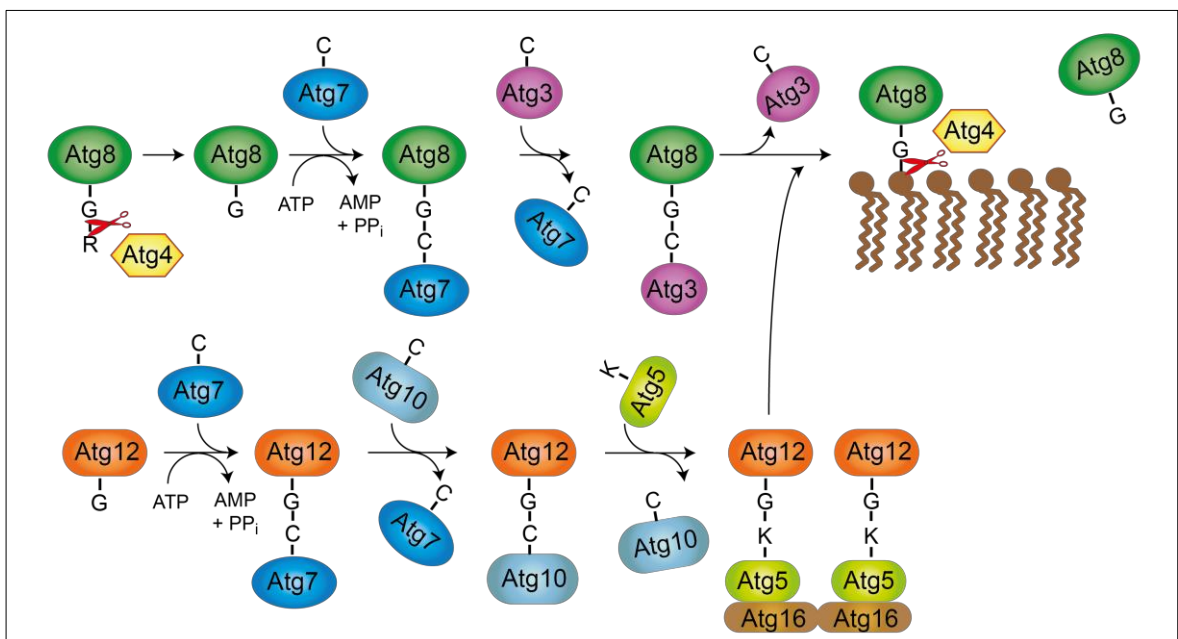


Figure 2-6: The ubiquitin-like systems to conjugate Atg8 to PE.

The C-terminal arginine of Atg8 is removed by Atg4 to reveal a glycine. Both Atg8 and Atg12 are then activated by the E1-like Atg7 and transferred to the E2-like Atg3 or Atg10, for Atg8 and Atg12 respectively. Atg12 is then linked to the lysine residue of Atg5 and oligomerized mediated by non-covalent interactions of Atg5 with Atg16. This forms an E3-like complex necessary for transferring Atg8 from Atg3 to a PE group at the membrane. Atg4 also catalyzes the release of Atg8 from PE.

Newly synthesized Atg8 is a hydrophilic protein of 117 amino acids. It is bound by the cysteine protease Atg4, which removes the C-terminal arginine to reveal a glycine. It is then transferred in an ATP dependent reaction to the E1-like Atg7 under the formation of a thioester bond between the glycine of Atg8 and the catalytic cysteine of Atg7 (Ichimura et al., 2000; Kirisako et al., 2000). Atg7 also catalyzes the activation and formation of a thioester bond between itself and Atg12 (Tanida et al., 1999). It forms a homodimer with two functional catalytic centers and is able to recognize two different

2. Introduction

ubiquitin-like proteins, Atg8 and Atg12, as well as two different E2s, Atg3 and Atg10 (Komatsu et al., 2001; N. N. Noda et al., 2011). The Atg7 homodimer binds to Atg8 with one subunit and Atg3 with the other and catalyzes the transfer of Atg8 to the catalytic cysteine residue of Atg3. The transfer of Atg12 to its E2-like protein Atg10 is processed in a similar manner (Shintani et al., 1999). Atg10 recognizes the E3-like Atg5 and transfers Atg12 to a lysine residue of Atg5. The Atg5-Atg12 conjugate is able to transfer Atg8 to PE in an *in vitro* assay using SUVs (Hanada et al., 2007), but needs to form a non-covalently linked complex with Atg16 *in vivo* (Kuma et al., 2002; Mizushima et al., 1999; Suzuki et al., 2001).

Atg5-Atg12/Atg16 oligomerizes and forms a multimeric complex which is recruited to the membrane (Fujita et al., 2008; Romanov et al., 2012). This complex then interacts with the Atg3-Atg8 conjugate as an E3-like enzyme to promote the transfer of Atg8 to PE. Interaction between Atg12 and Atg3 causes the catalytic center of Atg3 to rearrange and enables the transfer of Atg8 to the amine moiety of PE (Hanada et al., 2007; Kabeya et al., 2000; Sakoh-Nakatogawa et al., 2013).

A recent study observed recruitment of the Atg5-Atg12/Atg16 complex mediated by Atg21 and the Atg2-Atg18 complex, with Atg21 binding to Atg16 while Atg2 and Atg18 required Atg5 and Atg12, respectively (Juris et al., 2015; Munzel et al., 2020; Sawa-Makarska et al., 2020). The PtdIns effectors contribute probably together with the Atg1 kinase complex to the localization of the Atg5-Atg12/Atg16 complex to the PAS and deletion of Atg2, Atg21 and Atg18 affects IM expansion during the Cvt pathway (Sawa-Makarska et al., 2020).

Atg8 anchors the multimeric Atg5-Atg12/Atg16 complex to the membrane of the IM and forms a scaffold that is counteracted by the presence of cargo adaptors such as the mitophagy receptor Atg32 (Kaufmann et al., 2014). This indicates a role of Atg8 as receptor contact at the inner (concave) side of the membrane to connect autophagic activity with selective cargo (Farré & Subramani, 2016). The cargo adaptors or receptors contain AIMs to bind to Atg8, as described in chapter 2.3.2.

2.3.5.6. Fusion and Degradation

2.3.5.6.1. Closure of the autophagosome

After the cargo is completely enveloped by the double-membraned IM the edges have to undergo scission and fusion events in order to seal the autophagic content from the

2. Introduction

cytosol. This step is important, since the fusion of the vacuole with an unsealed autophagosome could potentially expose the vacuolar lumen to the cytosol. Most of the Atgs involved in autophagosome formation are still present at the autophagosomal membrane after closure and have to be recycled. The removal of Atgs from the sealed autophagosome is termed maturation and this event may regulate the recruitment and/or activation of the fusion machinery (Reggiori & Ungermann, 2017). The exact mechanism is still unknown, but several hypotheses have been formulated (reviewed in (Carlsson & Simonsen, 2015)).

The PtdIns3P-specific phosphatase Ymr1 (yeast myotubularin-related PI3P phosphatase) is recruited to the PAS and is required for Atg disassembly after AP closure (Cebollero et al., 2012; Parrish et al., 2004). In *YMR1* deletion mutants closed autophagosomes accumulate at the vacuole, still decorated with Atg18 and most Atg proteins (Reggiori & Ungermann, 2017). Elevating levels of PtdIns3P with the use of a hyperactive mutant Vps34 causes a block in later steps of autophagy, partly by delaying the disassembly of Atg proteins from the AP (Steinfeld et al., 2021). Therefore, the regulation of PtdIns turnover could regulate the different steps necessary for AP closure and fusion with the vacuole. Atg18 is a well-known PtdInsP effector and localizes in complex with Atg2 and Atg9 to the edges of the expanding IM (Graef et al., 2013; Suzuki et al., 2013). Deletion of *ATG2* inhibits autophagosome closure in mammalian cells (Velikkakath et al., 2012). The presence or absence of the Atg2-Atg18 complex could function as a signal to progress to the next step.

The ESCRT machinery involved in the budding and subsequent fission of intraluminal vesicles during the MVB pathway shares topological similarities with AP closure (Hurley & Hanson, 2010). A connection between several ESCRT components and autophagy has long been discussed (Filimonenko et al., 2007; Rusten et al., 2007). Several of the ESCRT subunits also bind PtdIns3P and could thereby be recruited to the phagophore before closure (Carlsson & Simonsen, 2015).

Autophagosome maturation requires an additional mechanism to PtdIns turnover, which is depicted in Figure 2-7: Atg8 is conjugated to PE during IM expansion by the ubiquitin-like conjugation machinery described in chapter 2.3.5.5 and is localized to both the outer and the inner membrane of the expanding IM. The cysteine protease Atg4 cleaves Atg8-PE and recycles the protein (Kirisako et al., 2000). Deletion of *ATG4* results in erroneously lipidated Atg8 on various intracellular membranes and an

2. Introduction

impaired autophagic process, probably caused by constitutively and non-selective PE conjugation to Atg8. Recycling of Atg8 mediated by Atg4 is essential to mobilize sufficient amounts for autophagy (Nair et al., 2012; Nakatogawa et al., 2012). A second role for Atg4 emerges at a later stage of autophagy, as deletion of ATG4 causes accumulation of Atg8 positive structures in the cytosol (Yu et al., 2012).

Atg4 has conserved AIM motifs, which facilitate the constitutive binding and cleaving of Atg8-PE (Abreu et al., 2017). The deconjugating activity is blocked exclusively at the PAS by specific phosphorylation with the Atg1 kinase (Sánchez-Wandelmer et al., 2017). Inactivation and dissociation of Atg1 after completion of the autophagosome enables active Atg4 to bind to Atg8-PE and catalyze the cleavage of PE and Atg8. This releases Atg8 from the AP and could signal either autophagosome closure or fusion with the vacuole.

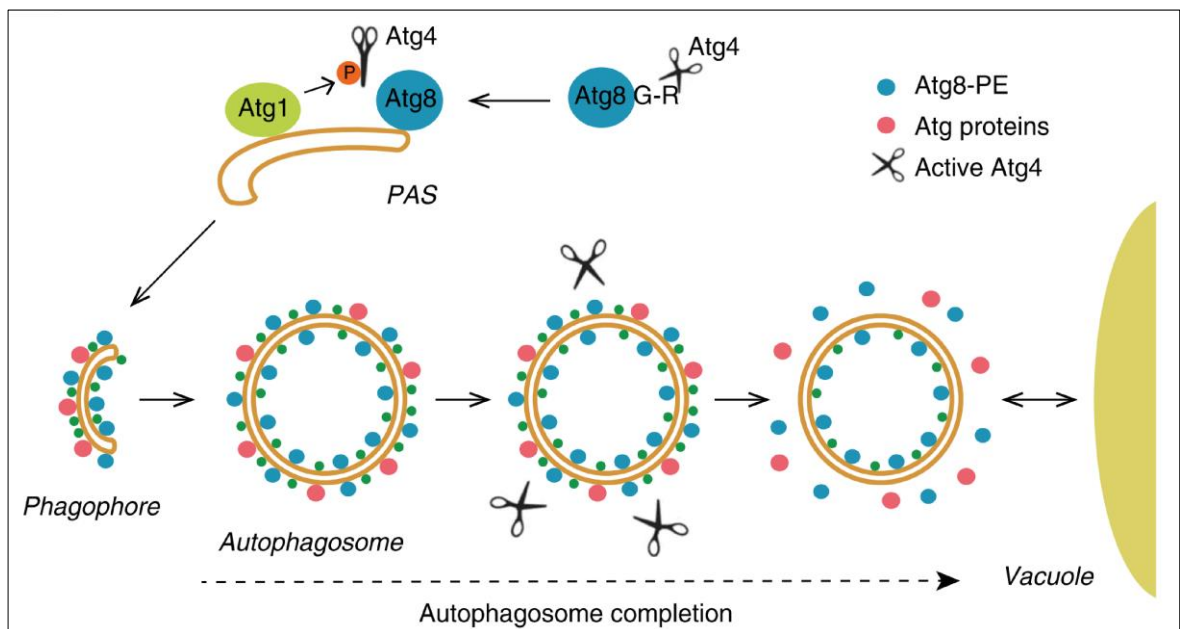


Figure 2-7: Mechanistic model for Atg8 deconjugation during AP maturation.

Newly synthesized Atg8-PE is constitutively processed by Atg4 in the cytoplasm. Atg1 mediated phosphorylation inhibits Atg4 at the PAS and the expanding IM. Upon AP completion Atg1 is released from the AP and active Atg4 can cleave Atg8-PE. This releases Atg8 from the outer membrane of the AP, which could signal the disassembly of other Atg proteins from the autophagosomal membrane. (Sánchez-Wandelmer et al., 2017)

2.3.5.6.2. Fusion with the vacuole

Autophagosome fusion with the vacuole requires the Rab7 like GTPase Ypt7, the homotypic vacuole fusion and protein sorting (HOPS) tethering complex and the guanidine nucleotide exchange factor of Ypt7, the Mon1-Ccz1 complex (Reggiori & Ungermann, 2017). Rab like GTPases have very specific functions during fusion events: bound to GDP they are inactive and cytosolic. A Rab specific GEF converts them into

2. Introduction

their active form at the membrane (Barr, 2013), which can then recruit tethering factors such as the HOPS complex. The Mon1-Ccz1 complex was identified as a GEF of Ypt7 (Nordmann et al., 2010; C.-W. Wang et al., 2003) and is also essential for vacuolar fusion of the AP (Hegedűs et al., 2016; Meiling-Wesse et al., 2002; C.-W. Wang et al., 2002). Ccz1 binds to Atg8-PE through AIM motifs at its C-terminus, which localizes the GEF complex to the IM (Gao, Langemeyer, et al., 2018). It is then able to recruit and activate Ypt7, although this also depends on the presence of PtdIns3P (Bas, Papinski, Licheva, et al., 2018). Ypt7 in turn recruits the HOPS tethering complex (Hickey & Wickner, 2010; Ho & Stroupe, 2015; Krämer & Ungermann, 2011). The HOPS complex tethers two Ypt7 positive membranes together and triggers the assembly of SNAREs.

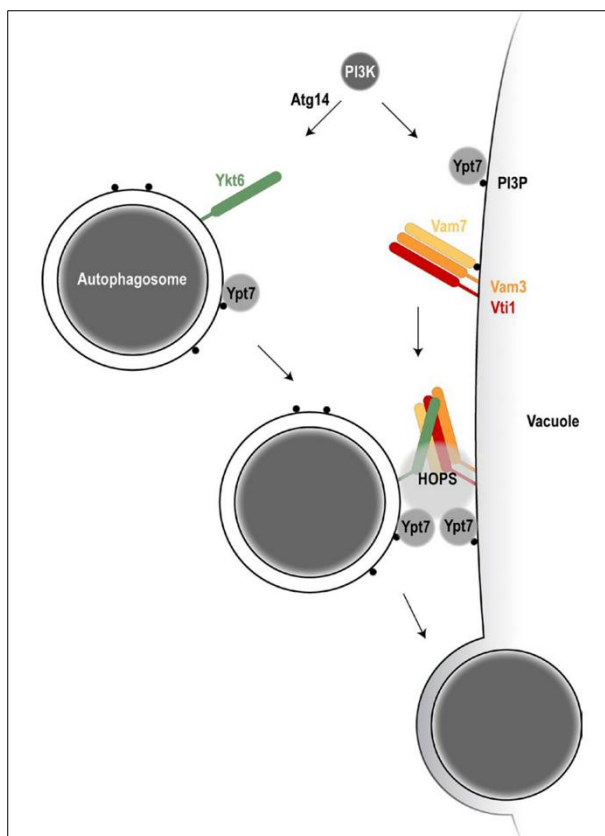


Figure 2-8: Model of autophagosome-vacuole fusion.

Ypt7 is recruited to the autophagosomal membrane by PtdIns3P and Mon1-Ccz1. The GTPase recruits the HOPS complex, which in turn mediates the assembly of the trans-SNARE bundle. The R-SNARE Ykt6 is localized at the autophagosomal membrane, while the Q-SNAREs Vam3, Vti1 and Vam7 are at the vacuolar membrane. (Bas, Papinski, & Kraft, 2018)

Several SNAREs essential for autophagy have been discovered, which are recruited by the HOPS complex and induce membrane fusion (Kriegenburg et al., 2019; Wickner & Rizo, 2017). Deletion of the vacuolar Q-SNAREs Vam3, Vam7 and Vti1 as well as the R-SNARE Ykt6 causes the accumulation of sealed APs in the cytosol but does not interfere with IM expansion (Darsow et al., 1997; Dilcher et al., 2001; Fader et al., 2009; Ishihara et al., 2001; von Mollard & Stevens, 1999). Vam7 has previously been reported to interact with Atg17 of the Atg17-Atg31-Atg29 complex associated with the Atg1 kinase (Liu et al., 2016) and could potentially function to block premature fusion with the vacuole (Bas, Papinski, & Kraft, 2018). Ykt6 is recruited to the

PAS early on mediated by COPII vesicles and the ER-resident Dsl1 complex (Gao et al., 2020). Direct phosphorylation by Atg1 kinase inactivates the SNARE and regulates vacuolar fusion (Barz et al., 2020).

2. Introduction

2.3.5.6.3. Degradation of the cargo

After fusion of the outer autophagosomal membrane with the vacuole, the cargo enveloped in the inner membrane is released into the vacuolar lumen. Breakdown of the autophagic bodies requires the vacuolar lipase Atg15 (Epple et al., 2001; Teter et al., 2001). The integral membrane protein is essential for autophagy and transported to the vacuole via the MVB pathway (Epple et al., 2003). Recent studies observe two functionally distinct domains, with the lipase domain at the C-terminus (Hirata et al., 2021).

Other vacuolar proteases necessary for efficient degradation are the aspartyl endoprotease (proteinase A) Pep4 and the proteinase B (Prb1) (Takeshige et al., 1992). In addition to directly degrading cargo, they also process and activate many zymogens present in the vacuole. Recently, proteinase C (Prc1) and its functional homologue Atg42 have been shown to play a role in the degradation of autophagic bodies (Parzych et al., 2018)

2.3.5.7. Regulation

Autophagy is induced as a response to extracellular stress such as nutrient scarcity, which can be detected and signaled by different cellular pathways. The first step in autophagy induction is the formation and activation of the Atg1 kinase complex. Target of rapamycin complex 1 (TORC1) is a phosphatidylinositol kinase-related kinase upstream of the Atg1 kinase complex and the main integrator of nutrient derived signals (T. Noda & Ohsumi, 1998). In addition to the rapamycin sensitive Tor1, it also contains the components Kog1, Tco89 and Lst8 (Cebollero & Reggiori, 2009). It is active under nutrient rich conditions and phosphorylates Atg13. This reduces the affinity of Atg13 to Atg1 and inhibits autophagy (Kamada et al., 2000). Starvation or treatment with the immune suppressive rapamycin inactivates TORC1 and causes its dissociation from the membrane. Atg13 is dephosphorylated under these circumstances and is able to form a complex with Atg1 and Atg17-Atg31-At29, as shown in Figure 2-9 (Kabeya et al., 2005; Kamada et al., 2010).

2. Introduction

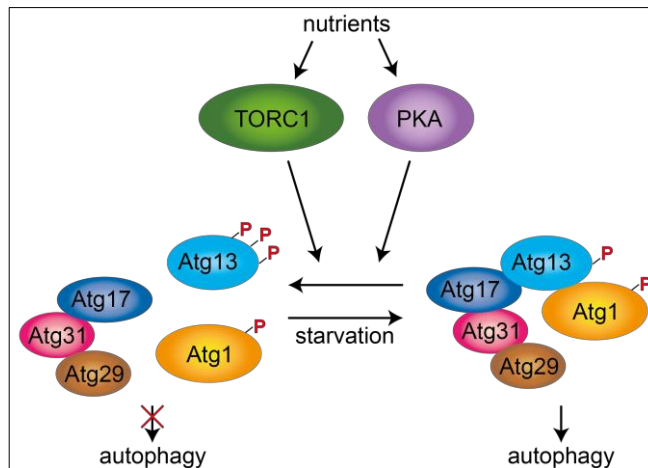


Figure 2-9: Regulation of autophagy by TORC1 and PKA.

TORC1 and PKA are active under nutrient rich conditions and phosphorylate Atg13 (and Atg1 for PKA). Starvation inactivates both, which causes dephosphorylation of Atg13 (and Atg1). They are then able to form the Atg1 kinase complex and induce autophagy.

A second mechanism to regulate Atg1 kinase activity in *S. cerevisiae* is the Ras/cyclic adenosine monophosphate (cAMP)-dependent protein kinase A (PKA). Inhibition of PKA induces autophagy independent of TORC1, while increased PKA activity blocks the process (Budovskaya et al., 2004; Stephan et al., 2009). Unlike TORC1 PKA is able to directly phosphorylate Atg1, which does not affect kinase

activity but the cellular location of the protein (Budovskaya et al., 2005). Interestingly, PKA phosphorylation sites have also been found on Atg13 and Atg18, although the functionality of the latter is not yet known.

Furthermore, autophagy is regulated at the transcriptional level (Cebollero & Reggiori, 2009). Nutrient deprivation elevates expression levels of several Atg proteins such as ATG8 and ATG14 and to a lower content also ATG1, ATG3, ATG4, ATG5, ATG7, ATG12 and ATG13 (Hardwick et al., 1999).

2. Introduction

2.4. Atg18

Atg18 was first discovered as an essential component of the core autophagic machinery in 2001, as both the constitutively active Cvt pathway as well as the starvation induced macroautophagy are completely blocked in an ATG18 deletion strain (Barth et al., 2001; Guan et al., 2001). An additional function in the recycling of vacuolar membrane proteins and maintaining vacuolar morphology under osmotic stress was described later (Dove et al., 2004).

Atg18 belongs to the PROPPINs (β -propellers that bind phosphoinositides), WD40-domain containing proteins highly conserved among eukaryotes (Michell & Dove, 2009; Thumm et al., 2013). There are two known homologues to Atg18 in yeast: Atg21 which is essential for selective autophagic pathways, and Hsv2 (homologue to Syp1) whose function is still unknown.

The mammalian homologues to PROPPINs are named WIPI (WD40-repeat protein interacting with phosphoinositides) and four WIPIs have been identified in humans. WIPI1 and 2 seem to have similar functions to Atg18 in autophagy, with WIPI2 thought to be involved in Atg9A cycling and recruiting the ATG12-ATG5-ATG16L1 complex to the PAS (Dooley et al., 2014; Proikas-Cezanne et al., 2015). However, both WIPI1 and WIPI4 are also essential for autophagy in human cells. WIPI4/WDR4 has been associated with BPAN (beta-propeller protein-associated neurodegeneration), as *de novo* mutations in WIPI4 are linked to developing static encephalopathy of childhood with neurodegeneration in adulthood (SENDA). The mutations destabilize the propeller and cause the accumulation of abnormal autophagic structures and membranes in these patients (Mollereau & Walter, 2019; Proikas-Cezanne et al., 2015; Saitsu et al., 2013).

2.4.1. Structure

The WD40 domain is one of the most abundant domains in eukaryotes as well as a few prokaryotes and mostly acts as a platform for protein-protein interactions (PPIs). Proteins containing the domain often play a role in growth, cell cycle and development as well as signal transduction, intracellular transport and cytoskeletal organization in higher organisms (Jain & Pandey, 2018). WD40 repeat is a repetitive motif of about 40 to 60 amino acids with a highly conserved tryptophan and aspartic acid (WD) dipeptide

2. Introduction

at its C-terminus as well as a conserved glycine and histidine (GH) dipeptide 11-24 residues from its N-terminus (see Figure 2-10A). Each domain forms a four-stranded antiparallel β -sheet, which then forms the blades of a propeller, as shown in Figure 2-10B. The conserved residues stabilize the propeller structure by the formation of hydrogen bonds (C. Xu & Min, 2011). In most WD40 proteins one blade is formed by strand D of the previous WD40 repeat together with strand A, B and C of the following (Figure 2-10B(iii)). This leads to an overlap of the N- and C-terminal regions at the seventh blade, which creates a 'velcro snap' to provide stability (Jain & Pandey, 2018).

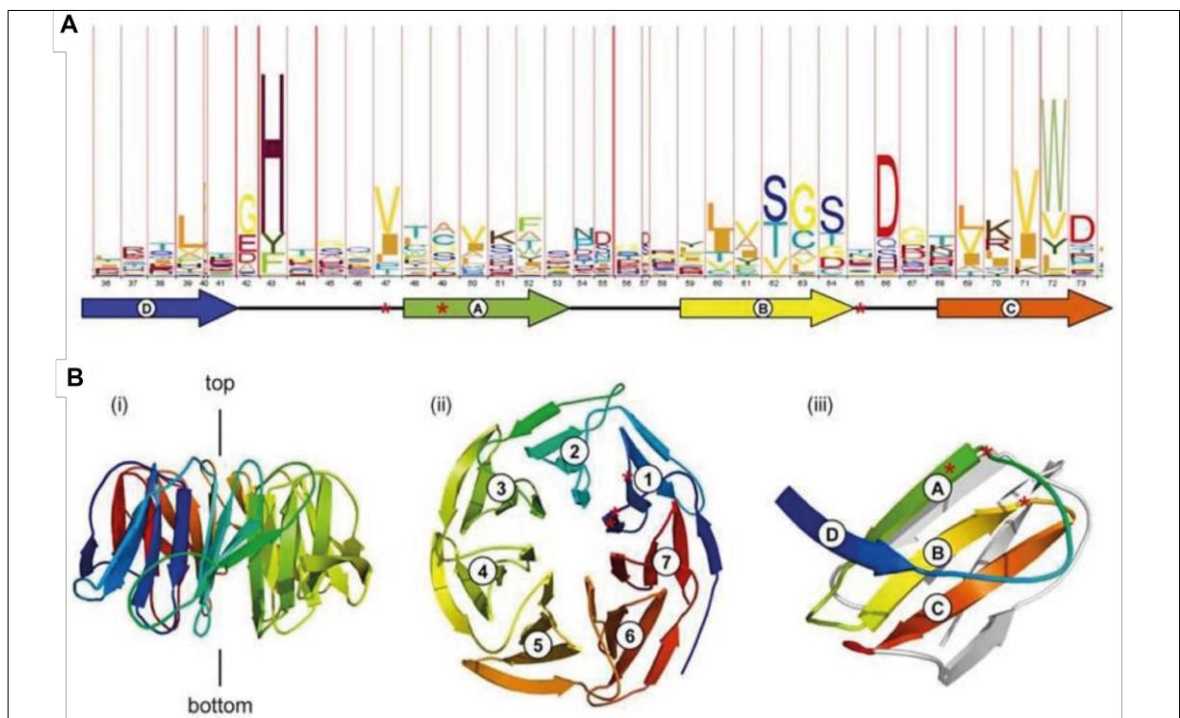


Figure 2-10: Sequence and structural features of WD40 domains.

(A) Sequence logo for WD40 repeats. The letter plot represents amino acid conservation at each position. Depicted below is the corresponding position at the propeller blades. **(B)** Model for a typical seven-bladed β -propeller, the top is defined as the narrower part containing the DA and BC loops (i). The WD40 sequence corresponds to strand D of one blade followed by strand A, B and C of the next blade. Residues often involved in PPI on the surface are highlighted with red asterisks. (Jain & Pandey, 2018; Stirnimann et al., 2010)

Proteins with as many as 16 WD repeats have been identified, although the highest number of blades discovered in a propeller is eight (Smith et al., 1999). The optimal number seems to be a seven-bladed propeller, as shown in Figure 2-10B(ii) (Jain & Pandey, 2018; Stirnimann et al., 2010). WD40 proteins can interact with several different proteins, using the whole of their surface (Stirnimann et al., 2010). It is therefore an excellent platform for protein-protein interactions and the coordinated assembly of different complexes.

2. Introduction

The yeast β -propeller Atg18 is a 500 amino acids protein with a proposed molecular weight of 55 kDa (Barth et al., 2001; Guan et al., 2001). It contains seven WD40 repeats, which were predicted to fold into a seven-bladed propeller (Dove et al., 2004). While the β -strands of the propeller blades are highly similar between Atg18, Atg21 and Hsv2, the loops connecting the blades differ between the PROPPINs. Crystal structures of Hsv2 from *Kluyveromyces lactis* and *marxianus*, as well as Atg18 from *Pichia angusta* and *Saccharomyces cerevisiae*, have been solved and used to identify conserved structures, as is shown in Figure 2-11A (Baskaran et al., 2012; Krick et al., 2012; Lei et al., 2020; Scacioc et al., 2017; Watanabe et al., 2012). As predicted Atg18 and its homologues form a seven-bladed propeller, with each blade containing four antiparallel β -strands. The blades are denoted from one to seven starting at the N-terminus as is customary, while the strands are termed A to D from the inner to the outer β -strand. Blade 7 of the PROPPINs is entirely formed by the C-terminus and lacks the Velcro-like topology observed in most other WD40 repeat proteins. The strands are connected by short loop regions, with loops BC and AD oriented towards the top, narrow side of the propeller (see Figure 2-10B for overall structure). The bottom is formed by the loops linking strand C and D or A and B, respectively. The loop connecting strand 6C and 6D is noticeably longer with 24 amino acids.

Atg18 binds to PtdIns3P and PtdIns(3,5)P₂ with high affinity, but not to either PtdIns4P, PtdIns(3,4)P₂ or PtdIns(4,5)P₂ (Dove et al., 2004). This interaction occurs independently of previously observed PtdIns binding domains such as FYVE (conserved in Fab1, YOTB, Vac1 and EEA1) (Axe et al., 2008; Gillooly, 2000; Stenmark et al., 2002). A conserved FRRG motif has been identified, which is necessary for membrane association (Dove et al., 2004; Jeffries et al., 2004). Both Atg21 and Atg18 with a mutated FTTG motif showed reduced affinity towards PtdIns3P and a defect in the Cvt pathway. Interestingly, macroautophagy was only partially affected (Krick et al., 2006, 2012).

The FRRG motif is localized at a highly conserved and positively charged region at the end of blade 5D and the loop between 5D and 6A (see Figure 2-11C). The arginine residues are oriented towards two distinct conserved basic pockets at the outer rim of the propeller which can fit PtdIns3P or PtdIns(3,5)P₂. Both binding pockets are necessary for efficient membrane association of the PROPPINs. Interaction with phospholipids within the membrane would orient the propeller perpendicular or

2. Introduction

slightly tilted towards the membrane, with hydrophobic residues of the loop between strands 6C and 6D inserted into the membrane (see Figure 2-11B) (Baskaran et al., 2012; Busse et al., 2015; Krick et al., 2012; Watanabe et al., 2012).

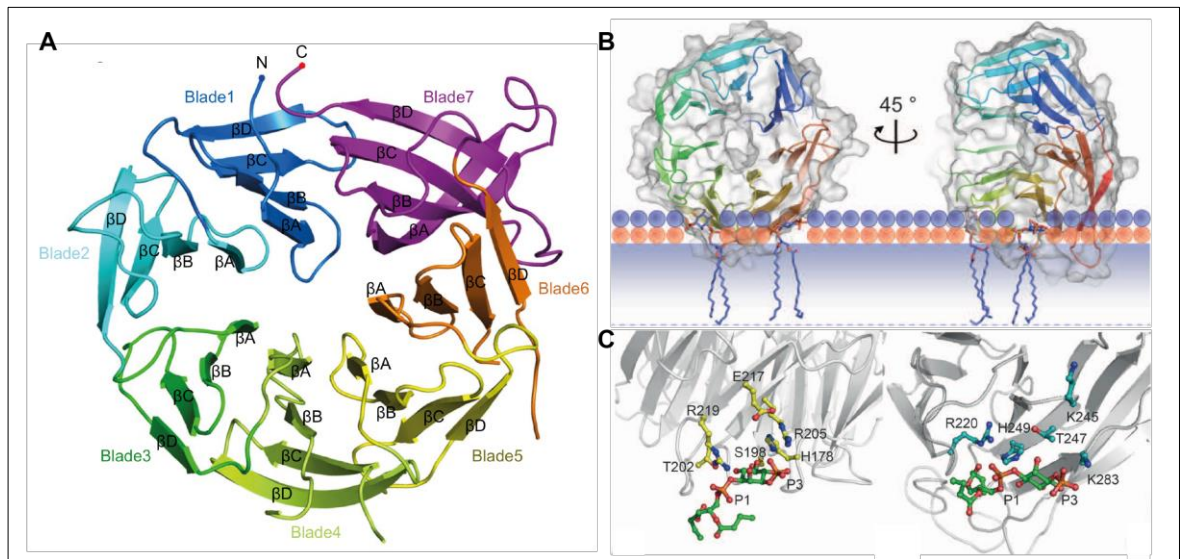


Figure 2-11: Crystal structure for ScAtg18 and KIHsv2.

(A) Overall structure of ScAtg18 shown as a cartoon with the blades displayed in different colors. Adapted from (Lei et al., 2020) **(B)** PROPPINs are thought to bind perpendicular to the membrane, with Blade 5 and 6 in contact with the membrane. One hydrophobic loop has been identified, which is inserted into the membrane. **(C)** FRRG motif at Blade 5 and 6 at the crystal structure of *K. lactis* Hsv2. (B) and (C) adapted from (Thumm et al., 2013)

2.4.2. Function in autophagy

Atg18 is essential for autophagic activity and therefore part of the core autophagic machinery (Barth et al., 2001; Guan et al., 2001). Early studies observed a function of Atg18 in the recycling of the transmembrane protein Atg9 from the autophagosome (Reggiori et al., 2004). Atg18 is recruited to the PAS during the early steps of autophagy but after assembly of the PI3-kinase complex I (Suzuki et al., 2007, 2013). Association with the PAS is dependent on its affinity towards PtdIns3P (Krick, Henke, et al., 2008; Obara, Sekito, et al., 2008).

WD40 repeat proteins often act as scaffold or platform for protein-protein interaction and Atg18 interacts with the autophagic protein Atg2. This is independent of association with PtdIns3P or the membrane (Obara, Sekito, et al., 2008). Complex formation and localization to the PAS is essential for autophagic progression. While Atg2 is recruited to the PAS in the absence of Atg18, the association of the PROPPIN with PtdIns3P at the autophagosomal membrane is mediated by Atg2 (Rieter et al., 2013). The binding of Atg2 and Atg18 involves the connecting loops of blade 2 of the PROPPIN, opposite to the conserved FRRG motif (Rieter et al., 2013; Watanabe et al.,

2. Introduction

2012). A recently published crystal structure of ScAtg18 revealed an unusually extended loop between strands 7A and 7B unique for Atg18. Deletion of this loop seemed to affect the interaction between Atg2 and Atg18 as well as the localization of Atg2 in the cell (Lei et al., 2020).

The location of autophagosome biogenesis is linked to ER exit sites (ERES), which function in COPII vesicle formation (Graef et al., 2013). Studies with enlarged phagophores have mapped the location of Atg18-Atg2 to the edges of the growing IM, as depicted in Figure 2-12 (Suzuki et al., 2013). This is mediated by the interaction between Atg2 and the integral membrane protein Atg9, which preferentially locates to tightly curved membranes (Gómez-Sánchez et al., 2018). Atg2 folds to a rod-shaped protein with a membrane binding domain at each tip and is thought to tether the edges of the phagophore to the ER (Chowdhury et al., 2018; Kotani et al., 2018). Atg18 is bound to its C-terminal end, which is closely associated with the phagophore. The

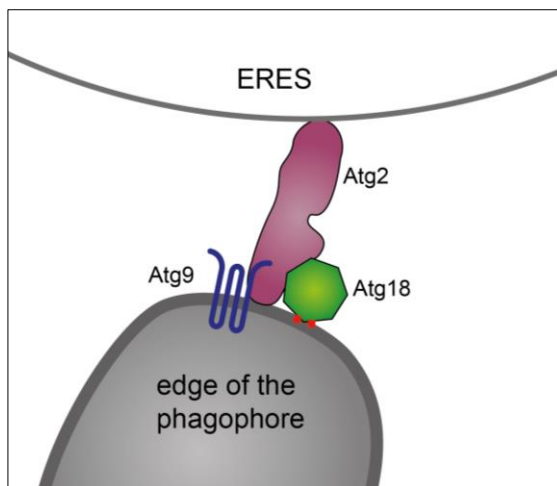


Figure 2-12: Model of functional contact site between the growing IM and ER exit sites.

The Atg2-Atg18 complex is recruited to the edges of the IM mediated by Atg9. Atg2 interacts with both the autophagosomal membrane associated with Atg18 and the ERES.

complex containing Atg9, Atg2 and Atg18 is thought to mediate direct phospholipid transfer between the ER and the growing phagophore (Maeda et al., 2019; Osawa et al., 2019, 2020; Valverde et al., 2019). This was already discussed in chapter 2.3.5.4.

Recent studies observed an additional role for PROPPINs during autophagy, specifically for Atg21. The β -propeller is not part of the core autophagic machinery, but necessary for the Cvt pathway (Barth et al., 2002). It interacts with Atg16, a

component of the Atg8 lipidation machinery (Juris et al., 2015; Munzel et al., 2020). Atg21 is sufficient to recruit the Atg5-Atg12/Atg16 complex to the membrane *in vitro*, which is accelerated in the presence of Atg2-Atg18 (Sawa-Makarska et al., 2020).

2.4.3. Function at the vacuolar membrane

Atg18 functions in a second process unrelated to autophagy, as deletion of *ATG18* causes abnormally large vacuoles, defects in vacuolar membrane recycling and accumulation of PtdIns(3,5) P_2 (Dove et al., 2004). The yeast vacuole is involved in more

2. Introduction

than waste disposal, it is also a valuable storage compartment to reserve compounds such as amino acids, polyphosphates and ions (Kane, 2007; Thumm, 2000). Fusion and fission events are used to alter the surface-to-volume ratio in a response to osmotic stress. Vacuole fragmentation helps the cell to adapt to a loss of water caused by high extracellular salt concentrations. Vacuolar fission occurs in two steps: first, invaginations lead to the formation of tubular structures, which are then pinched off in the second step (Zieger & Mayer, 2012). The invagination is thought to be caused by the proton gradient together with the dynamin like GTPase Vps1 (Peters et al., 2004) and stabilized by PtdIns3P. The PI3-kinase complex II phosphorylates phosphatidylinositol at the vacuolar and the endosomal membrane, as described in chapter 2.3.5.2. Osmotic stress upregulates the synthesis of PtdIns(3,5)P₂, which accumulates at the vacuolar membrane (Dove et al., 1997; Takatori et al., 2016). The formation of vesicles at the tubular structures is dependent on the generation of PtdIns(3,5)P₂ mediated by Fab1.

The PtdIns3P 5-kinase Fab1 contains an N-terminal FYVE domain and a C-terminal lipid kinase (Efe et al., 2005; Michell et al., 2006). It associates with the membrane of the vacuole and endosomes (Efe et al., 2007). The kinase phosphorylates PtdIns3P at position D5 to generate PtdIns(3,5)P₂ (Cooke et al., 1998; Gary et al., 1998). Fab1 is positively regulated by Vac14 and Vac7 (Bonangelino et al., 2002; Dove et al., 2002; Gomes de Mesquita et al., 1996). The phosphatase Fig4 is also involved in PtdIns(3,5)P₂ synthesis, its phosphatase activity is necessary to activate Fab1 while it is also able to directly dephosphorylate PtdIns(3,5)P₂ to PtdIns3P (Duex et al., 2006; Gary et al., 2002; Rudge et al., 2004).

Atg18 is a known PtdIns(3,5)P₂ effector and deletion of *ATG18* causes a phenotype similar to the deletion of *FAB1* (Dove et al., 2004). It colocalizes with Fab1, although the interaction is mediated by Vac7 and Vac14 (Botelho et al., 2008; Efe et al., 2007; Jin et al., 2008). However, deletion of *ATG18* causes a massive increase in PtdIns(3,5)P₂ concentration as opposed to the deletion of *FAB1*. Atg18, therefore, acts downstream of Fab1 and is involved in negative feedback regulation of the kinase (Efe et al., 2007). Two-hybrid and Co-IP studies have mapped a complex containing Fab1 as well as all of its regulators with Vac14 as a scaffold (Figure 2-13). Vac14 and Fig4 form a subcomplex in the cytosol, which is recruited by the membrane associated Fab1 (Botelho et al., 2008). Vac7 was also shown to coprecipitate with Vac14 and is part of

2. Introduction

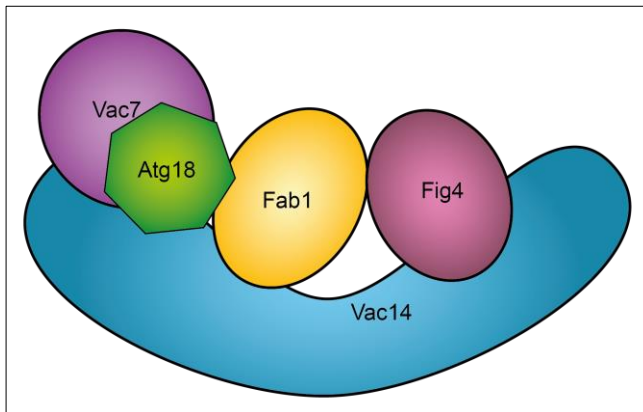


Figure 2-13: Model of the Fab1 complex.

Fig4 binds to the C-terminal part of the scaffold Vac14, while Fab1, Atg18 and Vac7 interact with overlapping regions at the N-terminal. Fab1 and Fig4 are not thought to directly interact, but Fig4 activates Fab1 probably through dephosphorylation. Atg18 deactivates Fab1 dependent on $\text{PtdIns}(3,5)P_2$ concentrations.

the complex. Although coprecipitation of Atg18 with either of the components could not be observed, additional evidence suggests that a portion of Atg18 is part of the Vac14-Fab1 complex (Jin et al., 2008).

Observations of membrane lipid distribution at the vacuolar membrane during hyperosmotic stress using quick-freeze and freeze-fracture replica labeling (QF-FRL)

electron microscopy (EM) revealed the accumulation of $\text{PtdIns}(3,5)P_2$ at intramembrane particle (IMP)-deficient regions of the membrane. In cells lacking either $\text{PtdIns}(3,5)P_2$ or Atg18, these membranes were folded into abnormal tubular structures, indicating a defect in pinching off of vesicles (Takatori et al., 2016). Atg18 contains a hydrophobic loop at Blade 6, which folds into an amphipathic α -helix upon membrane association. This loop is then inserted into the membrane and can induce curvature (Gopaldass et al., 2017). Furthermore, although Atg18 is monomeric in the cytosol, it oligomerizes bound to the membrane (Scacioc et al., 2017). This is sufficient to induce membrane scission, which could be another function of Atg18 in complex with Fab1.

2. Introduction

2.5. Aim of this study

Atg18 is a component of the core autophagic machinery, as a deletion blocks the autophagic process. Additionally, it is also involved in regulating PtdIns(3,5) P_2 concentrations at the vacuolar membrane, retrograde transport of vacuolar membrane proteins and maintaining vacuolar morphology. The molecular mechanisms behind these functions are still discussed or largely unknown.

WD40 repeat proteins such as the β -propeller Atg18 often act as platforms to promote and coordinate protein-protein interactions and Atg18 is a known PtdIns P effector, which often regulates cellular processes. It is possible that Atg18 fulfills its varying functions by interacting with different downstream proteins. Some of those interactions could be dynamic and transient, not detectable for conventional biochemical methods.

Therefore, a proximity-dependent labeling assay was performed to discover potential interaction partners *in vivo*. The goal was the identification of Atg18 containing complexes at either the endosomal or vacuolar membrane or at the autophagosome as well as determining their functions.

3. Material and Methods

3.1. Material

3.1.1. Software

Table 3-1: Software and databases used in this thesis

Software / database	Reference
Adobe® Creative Suite® 6	Adobe Systems (San Jose, California, USA)
Fiji	(Schindelin et al., 2012)
Microsoft® Office for Mac	Microsoft (Redmond, Washington, USA)
Prism 7.0d for MAC OS X	GraphPad Software (San Diego, California, USA)
SnapGene® 4.0.8	GSL Biotech LLC (Chicago, Illinois, USA)
softWoRx®	Applied Precision (Issaquah, Washington, USA)
Keynote 9.1	Apple Inc (Cupertino, California, USA)
Mendeley Desktop 1.19.4	Mendeley Ltd

3.1.2. Equipment

Table 3-2: Equipment used in this thesis

Equipment	Manufacturer
Agarose gel chamber Mini-Sub® cell GT	Bio-Rad Laboratories GmbH (München, Germany)
Agarose gel chamber wide Mini-Sub® cell GT	Bio-Rad Laboratories GmbH (München, Germany)
Amersham™ Hybond™ PVDF blotting membrane	GE Healthcare GmbH (Solingen, Germany)
Amersham™ ImageQuant™ 800	GE Healthcare GmbH (Solingen, Germany)
Autoclave Systec DX-200	Systec GmbH (Linden, Germany)
BioPhotometer 6132 spectrophotometer	Eppendorf AG (Hamburg, Germany)
Blot Shaker GFL® 3019	GFL Gesellschaft für Labortechnik mbH (Burgwedel, Germany)
Centrifuge 5415D	Eppendorf AG (Hamburg, Germany)
Centrifuge 5415R	Eppendorf AG (Hamburg, Germany)
Centrifuge 5417C	Eppendorf AG (Hamburg, Germany)

3. Materials and Methods

Centrifuge 5804	Eppendorf AG (Hamburg, Germany)
Centrifuge 5804R	Eppendorf AG (Hamburg, Germany)
Clean Bench	BDK Luft- und Reinraumtechnik GmbH (Sonnenbühl-Genkingen, Germany)
DeltaVision® Core fluorescence microscope microscope setup	Applied Precision (Issaquah, Washington, USA)
Diaphragm vacuum pump	Vacuubrand GmbH & Co. KG
Dispensette® 25 mL	BRAND GmbH & Co. KG (Wertheim, Germany)
Eppendorf Safe-Lock tubes, 1.5 mL	Eppendorf AG (Hamburg, Germany)
Eppendorf Safe-Lock tubes, 2 mL	Eppendorf AG (Hamburg, Germany)
Epson Perfection V850 Pro Scanner	Meerbusch, Germany
Freezer (-20°C)	Liebherr (Bulle, Switzerland)
Freezer (-80°C)	Heraeus Holding GmbH (Hanau, Germany)
Gasprofi 1 SCS micro	WLD-TEC GmbH (Arenshausen, Germany)
Glass beads, acid washed (425 – 600 µm)	Merck KGaA (Darmstadt, Germany)
Innova 4200 Incubator-Shaker (37°C)	New Brunswick Scientific GmbH (Nürtingen, Germany)
JULABO MA-4 heating circulator	Julabo GmbH (Seelbach, Germany)
Lab pH meter inoLab® pH 7110	Xylem Analytics Germany Sales GmbH & Co. KG (Weilheim, Germany)
Lab Shaker LS-X	Kühner Shaker GmbH (Herzogenrath, Germany)
Lab Shaker SBM/SS-X (Rack-Shaker)	Kühner Shaker GmbH (Herzogenrath, Germany)
LAS-3000 Intelligent Dark Box	FUJIFILM Europe GmbH (Düsseldorf, Germany)
Magnetic Stirrer MR 2002	Heidolph Elektro GmbH & Co. KG (Kelheim, Germany)
Magnetic Stirrer MR 3001	Heidolph Elektro GmbH & Co. KG (Kelheim, Germany)
Microwave R-939	Sharp Electronics GmbH (Hamburg, Germany)
Mini Trans-Blot® cell	Bio-Rad Laboratories GmbH (München, Germany)
Mini-PROTEAN® Tetra Vertical electrophoresis cell	Bio-Rad Laboratories GmbH (München, Germany)
Minisart® filters (pore size 0.2 µm)	Sartorius AG (Göttingen, Germany)

3. Materials and Methods

Nalgene [®] Rapid-Flow [™] 75 mm bottle top filter, 500 mL	Thermo Fisher Scientific GmbH (Bremen, Germany)
NanoVue [™] UV/Visible spectrophotometer	GE Healthcare GmbH (Solingen, Germany)
Nano-Drop One ^c Microvolume UV-Vis Spectrophotometer	Thermo Fisher Scientific GmbH (Bremen, Germany)
PCR Mastercycler [®] gradient	Eppendorf AG (Hamburg, Germany)
Pipette controllers accu-jet [®] pro	Brand GmbH & Co. KG (Wertheim, Germany)
Pipettes Eppendorf research [®] Plus	Eppendorf AG (Hamburg, Germany)
PowerPac [™] Basic Power Supply	Bio-Rad Laboratories GmbH (München, Germany)
PowerPac [™] HC Power Supply	Bio-Rad Laboratories GmbH (München, Germany)
Refrigerator (4°C)	Liebherr (Bulle, Switzerland)
Roto Shake Genie	Scientific Industries Inc. (Bohemia, New York, USA)
Sartorius Handy H51-D lab balance	Sartorius AG (Göttingen, Germany)
Sartorius Universal U4100 lab balance	Sartorius AG (Göttingen, Germany)
Shaking Water Bath SWB25	Thermo Haake GmbH (Karlsruhe, Germany)
Thermo Mixer [®] comfort	Eppendorf AG (Hamburg, Germany)

3.1.3. Chemicals and consumables

Chemicals were used in analytical grade quality and obtained from Carl Roth GmbH & Co. KG (Karlsruhe, Germany), Merck KGaA (Darmstadt, Germany), AppliChem GmbH (Darmstadt, Germany) and Serva Electrophoresis GmbH (Heidelberg, Germany) unless stated otherwise.

Table 3-3: Chemicals used in this thesis

Chemical	Manufacturer
¹³ C ₆ -L-Arginine HCl (Arg-6:HCl)	Silantes (München, Germany)
¹³ C ₆ , ¹⁵ N ₂ -L-Lysine HCl (Lys6:HCl)	Silantes (München, Germany)
¹³ C ₆ , ¹⁵ N ₄ -L-Arginine HCl (Arg-10:HCl)	Silantes (München, Germany)
4,4,5,5-D ₄ -L-Lysine 2HCl (Lys-4D:2HCl)	Silantes (München, Germany)
Agarose NEEO Ultra-Qualität	Roth (Karlsruhe, Germany)

3. Materials and Methods

Ampicillin sodium salt	ThermoFisher Scientific
Bacto™ agar	Becton Dickinson (Heidelberg, Germany)
Bacto™ peptone	Becton Dickinson (Heidelberg, Germany)
Bacto™ tryptone	Becton Dickinson (Heidelberg, Germany)
Bacto™ yeast extract	Becton Dickinson (Heidelberg, Germany)
Biotin	Sigma-Aldrich (München, Germany)
BufferW (10x) (Strep-Tactin® / Strep-Tactin®XT Wash Buffer)	iba Lifesciences (Göttingen, Germany)
cOplete™, EDTA-free	Roche (Mannheim, Germany)
Coomassie® Brilliant Blue G 250	Serva (Heidelberg, Germany)
DeltaVision Immersion Oil (N=1.520)	GE Healthcare
Difco™ Yeast nitrogen base w/o amino acids	Becton Dickinson (Heidelberg, Germany)
Difco™ Yeast nitrogen base w/o amino acids and ammonium sulfate	Becton Dickinson (Heidelberg, Germany)
Drop-Out Mix Synthetic, minus Ade, Arg, His, Leu, Lys, Met, Trp, Ura w/o Yeast Nitrogen Base	USBiological (Salem, USA)
Ethidium bromide solution (0.025%)	Roth (Karlsruhe, Germany)
Frema Reform Instant Skim Milk Powder	Granovita (Heimertingen, Germany)
Gravity flow Strep-Tactin® Sepharose® Column (0.2 ml)	iba Lifesciences (Göttingen, Germany)
Gravity flow Strep-Tactin® Sepharose® Column (1 ml)	iba Lifesciences (Göttingen, Germany)
Herring Sperm DNA	Promega (Mannheim, Germany)
Hygromycin B solution	Roth (Karlsruhe, Germany)
Invitrogen™ Molecular Probes™ FM 4-64 Dye	ThermoFisher Scientific (Bremen, Germany)
Nourseothricin-dihydrogen sulfate/clonNAT powder	Werner BioAgents (Jena, Germany)
Precision Plus Protein™ All Blue Prestained Protein Standard	Bio-Rad (München, Germany)

3. Materials and Methods

Purple Gel Loading Dye (6x)	New England Biolabs (Frankfurt, Germany)
Strep-Tactin® Spin Column	iba Lifesciences (Göttingen, Germany)
TriDye 100 b DNA Ladder	
TriDye™ 1 kb DNA Ladder	New England Biolabs (Frankfurt, Germany)

3.1.4. Commercially available kits

Table 3-4: Kits used in this thesis

Kit	Manufacturer
Amersham™ ECL™ Western-Blotting Detection Reagents	GE Healthcare GmbH (Solingen, Germany)
DreamTaq Green PCR MasterMix (2x)	ThermoFisher Scientific (Bremen, Germany)
NucleoSpin® Microbial DNA	Macherey-Nagel (Düren, Germany)
Pierce™ ECL Plus Western Blotting Substrate	ThermoFisher Scientific (Bremen, Germany)
QIAquick® Gel Extraction Kit	Qiagen (Hilden, Germany)
QIAquick® PCR Purification Kit	Qiagen (Hilden, Germany)
Wizard® Plus SV Miniprep System	Promega (Mannheim, Germany)
µMACS GFP Isolation Kit	Miltenyi Biotec (Bergisch Gladbach, Germany)

3.1.5. Antibodies

Table 3-5: Antibodies used in this thesis

antibody	dilution	manufacturer
primary		
Anti-GFP (mouse IgG1κ)	1:1000	Roche (Mannheim)
Rabbit IgG anti-Ape1	1:5000	Eurogentec (Seraing, Belgium)
HA-probe antibody (F-7) (mouse monoclonal IgG _{2a})	1:10000	Santa Cruz Biotechnology (Dallas, USA)
Mouse IgG anti-Myc	1:500	Gift from the group of Prof. P. Rehling (Dept. Cellular Biochemistry, University Göttingen)

3. Materials and Methods

secondary			
Goat anti-Mouse (H+L)-HRPO	IgG 1:10000		Dianova (Hamburg)
Goat anti-Rabbit IgG (H+L) cross-Adsorbed Secondary Antibody, HRP	1:5000		ThermoFisher Scientific (Bremen)
Strep-tag HRP conjugate	1:50000		Iba (Göttingen)

3.1.6. Enzymes

Enzymes were obtained from New England Biolabs (Frankfurt, Germany) unless stated otherwise.

Table 3-6: Enzymes used in this thesis

enzyme	manufacturer
KOD Hot Start DNA Polymerase	Merck (Darmstadt, Germany)
KOD XL Polymerase	Merck
Zymolyase 100T	Seikagaku Biobusiness (Tokyo, Japan)

3.1.7. Medium

Table 3-7: Media used in this thesis

medium	composition	reference
YPD (pH 5.5)	1% (w/v)	Bacto™ yeast extract
	2% (w/v)	Bacto™ peptone
	2% (w/v)	D-glucose
CM (pH 5.6)	0.67% (w/v)	Yeast nitrogen base w/o amino acids
	2% (w/v)	D-glucose
	0.2% (w/v)	dropout mix
CM w/o met (pH 5.6)	0.67% (w/v)	Yeast nitrogen base w/o amino acids
	2% (w/v)	D-glucose
	0.2% (w/v)	dropout mix w/o methionine
SD-N	0.67% (w/v)	Yeast nitrogen base w/o amino acids and w/o ammonium sulfate
	2% (w/v)	D-glucose

3. Materials and Methods

LB (pH 7.5)	1% (w/v)	Bacto™ tryptone	Bertani 1951
	0.5% (w/v)	Bacto™ yeast extract	
	0.5% (w/v)	sodium chloride	
SOC	2% (w/v)	Bacto™ tryptone	Hanahan 1983
	0.5% (w/v)	Bacto™ yeast extract	
	0.4% (w/v)	D-glucose	
	10 mM	sodium chloride	
	10 mM	magnesium sulfate	
	10 mM	magnesium chloride	
	2.5 mM	potassium chloride	

All necessary amino acids were added to a final concentration of 0.0117% (w/v), with the exception of p-aminobenzoic acid (0.00117%).

3.1.8. Buffer

Table 3-8: Buffer used in this thesis

medium	composition	
PEG in LiTE buffer (pH 8)	100 mM	Lithium acetate
	10 mM	Tris / acetic acid
	1 mM	EDTA
	40% (w/v)	PEG 3350
LiOAc-Sorb buffer (pH 8)	100 mM	Lithium acetate
	10 mM	Tris / acetic acid
	1 mM	EDTA
	1 M	Sorbitol
SDS running buffer	25 mM	Tris
	200 mM	Glycine
	0.1% (w/v)	SDS
2x Lämmli buffer	117 mM	Tris
	3.4% (w/v)	SDS
	12% (w/v)	Glycerol
	0.004% (w/v)	Bromophenol blue
	0.016% (v/v)	β-mercaptoethanol
Blotting buffer	200 mM	Glycine
	25 mM	Tris

3. Materials and Methods

	20% (v/v)	Ethanol
TBST buffer (pH 7.6)	20 mM	Tris
	140 mM	Sodium chloride
	0.1% (w/v)	Tween-20
TAE buffer (pH 7,5)	40 mM	Tris
	20 mM	Acetic acid
	2 mM	EDTA
BioID Lysis buffer	10 mM	HEPES pH 7.9
	10 mM	KCl
	1.5 mM	MgCl ₂
	1 mM	PMSF
	1x	25x cOmplete
	0.5 mM	DTT
Co-IP Lysis buffer	50 mM	Tris HCl pH 7.5
	1 mM	EDTA
	0.5% (w/v)	Tween-20
	1 mM	PMSF
	1x	1000x Inhibitor Mix
	1x	25x cOmplete
Co-IP Wash buffer I	50 mM	Tris HCl pH 7.5
	0.25% (w/v)	SDS
CBB fixation buffer I	10% (v/v)	Phosphoric acid
	10% (v/v)	methanol
	40% (v/v)	ethanol
CBB fixation buffer II	1% (v/v)	Phosphoric acid
	10% (v/v)	Ammonium sulfate
CBB staining solution	10% (v/v)	Phosphoric acid
	45% (v/v)	Ethanol
	0.125% (w/v)	Coomassie Brilliant Blue
CBB destaining solution	5% (v/v)	Phosphoric acid
	40% (v/v)	Ethanol
	0.1% (w/v)	Antipain

3. Materials and Methods

Protease Inhibitor Mix (1000x)	0.1% (w/v)	Aprotinin
	0.1% (w/v)	Pepstatin
	0.1% (w/v)	Leupeptin
	0.1% (w/v)	Chymostatin

3.1.9. Strains

Table 3-9: Background of strains used In this study

strain	genotype	reference
BY4741	MAT α ; <i>his3Δ1, leu2Δ0, met15Δ0, ura3Δ0</i>	Euroscarf
WCG	WCG4 MAT α <i>his3-11,15 leu2-3,112 ura3</i>	W. Heinemeyer, Stuttgart

Table 3-10: Strains of BY4741 background used in this thesis

strain	genotype	reference
<i>atg1Δ</i>	<i>atg1Δ::KAN</i>	Euroscarf
<i>atg18Δ vps17Δ Vps35-6xHA</i>	<i>atg18Δ::hphNT1 vps17Δ::KAN VPS35-6xHA::NatNT2</i>	This study
<i>atg18Δ vps26Δ Vps35-6xHA</i>	<i>atg18Δ::hphNT1 vps26Δ::KAN VPS35-6xHA::NatNT2</i>	This study
<i>atg18Δ vps29Δ Vps35-6xHA</i>	<i>atg18Δ::hphNT1 vps29Δ::KAN VPS35-6xHA::NatNT2</i>	This study
<i>atg18Δ Vps35-6xHA</i>	<i>atg18Δ::hphNT1 VPS35-6xHA::NatNT2</i>	This study
<i>atg18Δ vps5Δ Vps35-6xHA</i>	<i>atg18Δ::hphNT1 vps5Δ::KAN VPS35-6xHA::NatNT2</i>	This study
<i>pib2Δ</i>	<i>pib2Δ::KAN</i>	Euroscarf
<i>sap155Δ</i>	<i>sap155Δ::KAN</i>	Euroscarf
<i>snf7Δ</i>	<i>snf7Δ::KAN</i>	Euroscarf
<i>snx3Δ</i>	<i>snx3Δ::KAN</i>	Euroscarf
<i>vac14Δ</i>	<i>vac14Δ::KAN</i>	Euroscarf
<i>vps35Δ</i>	<i>vps35Δ::KAN</i>	Euroscarf
<i>yck3Δ</i>	<i>yck3Δ::KAN</i>	Euroscarf

3. Materials and Methods

Table 3-11: Strains of WCG background used in this study

strain	genotype	reference
<i>atg18Δ</i>	<i>atg18Δ::KAN</i>	Euroscarf
<i>atg18Δ</i> 3xtagBFP-Pho8	<i>atg18Δ::hphNT1</i> 3xtagBFP-Pho8::LEU2	This study
<i>atg18Δ arg4Δ lys1Δ</i>	<i>atg18Δ::KAN arg4Δ::hphNT1</i> <i>lys1Δ::natNT2</i>	This study
<i>atg18Δ arg4Δ lys1Δ</i> <i>atg14Δ</i>	<i>atg18Δ::KAN arg4Δ::hphNT1</i> <i>lys1Δ::natNT2 atg14Δ::HIS3</i>	This study
<i>atg18Δ arg4Δ lys1Δ</i> <i>vps38Δ</i>	<i>atg18Δ::KAN arg4Δ::hphNT1</i> <i>lys1Δ::natNT2 vps38Δ::HIS3</i>	This study
<i>atg18Δ</i> Atg2-3xHA	<i>atg18Δ::KAN</i> ATG2-3xHA::hphNT1	This study
<i>atg18Δ atg21Δ</i> Ear1-yeGFP	<i>atg18Δ::KAN atg21Δ::natNT2</i> EAR1-yeGFP::hphNT1	This study
<i>atg18Δ atg21Δ hsv2Δ</i> Ear1-yeGFP	<i>atg18Δ::KAN atg21Δ::natNT2</i> <i>hsv2Δ::His3MX6</i> EAR1-yeGFP::hphNT1	This study
<i>atg18Δ atg21Δ hsv2Δ</i> Kex2-yeGFP	<i>atg18Δ::KAN atg21Δ::natNT2</i> <i>hsv2Δ::His3MX6</i> KEX2-yeGFP::hphNT1	This study
<i>atg18Δ atg21Δ hsv2Δ</i> Vps35-6xHA	<i>atg18Δ::KAN atg21Δ::natNT2</i> <i>hsv2Δ::hphNT1</i> Vps35-6xHA::His3MX6	This study
<i>atg18Δ atg21Δ</i> Kex2-yeGFP	<i>atg18Δ::KAN atg21Δ::natNT2</i> KEX2-yeGFP::hphNT1	This study
<i>atg18Δ</i> Cdc48-6xHA	<i>atg18Δ::KAN</i> CDC48-6xHA::NatNT2	This study
<i>atg18Δ</i> Lsb6-6xHA	<i>atg18Δ::KAN</i> LSB6-6xHA::NatNT2	This study
<i>atg18Δ</i> Pib2-6xHA	<i>atg18Δ::KAN</i> PIB2-6xHA::NatNT2	This study
<i>atg18Δ</i> Sap155-6xHA	<i>atg18Δ::KAN</i> SAP155-6xHA::NatNT2	This study
<i>atg18Δ</i> Sap155-mCherry	<i>atg18Δ::KAN</i> SAP155-mCherry::hphNT1	This study
<i>atg18Δ</i> Snf7-6xHA	<i>atg18Δ::KAN</i> SNF7-6xHA::NatNT2	This study
<i>atg18Δ</i> Snx3-6xHA	<i>atg18Δ::KAN</i> SNX3-6xHA::NatNT2	This study
<i>atg18Δ</i> Vac14-6xHA	<i>atg18Δ::KAN</i> VAC14-6xHA::NatNT2	This study
<i>atg18Δ</i> Vps26-6xHA	<i>atg18Δ::KAN</i> VPS26-6xHA::hphNT1	This study
<i>atg18Δ</i> Vps29-6xHA	<i>atg18Δ::KAN</i> VPS29-6xHA::hphNT1	This study

3. Materials and Methods

<i>atg18Δ</i> Vps35-6xHA	<i>atg18Δ::KAN VPS35-6xHA::NatNT2</i>	This study
<i>atg18Δ</i> Vps35-mCherry	<i>atg18Δ::KAN VPS35-mCherry::hphNT1</i>	This study
<i>atg18Δ vps35Δ</i>	<i>atg18Δ::KAN vps35Δ::hphNT1</i>	This study
<i>atg18Δ vps35Δ</i> 3xtagBFP-Pho8	<i>atg18Δ::hphNT1 vps35Δ::natNT2 3xtagBFP-Pho8::LEU2</i>	This study
<i>atg18Δ vps35Δ</i> Atg2-3xHA	<i>atg18Δ::KAN vps35Δ::His3MX6 Atg2-3xHA::hphNT1</i>	This study
<i>atg18Δ vps35Δ</i> Atg2-yeGFP	<i>atg18Δ::KAN vps35Δ::natNT2 Atg2-yeGFP::hphNT1</i>	This study
<i>atg18Δ vps35Δ</i> Atg9-yeGFP	<i>atg18Δ::KAN vps35Δ::His3MX6 Atg9-yeGFP::hphNT1</i>	This study
<i>atg18Δ vps35Δ</i> Vps26-6xHA	<i>atg18Δ::KAN vps35Δ::his3MX6 VPS26-6xHA::hphNT1</i>	This study
<i>atg18Δ</i> Vtc3-6xHA	<i>atg18Δ::KAN VTC3-6xHA::NatNT2</i>	This study
<i>atg18Δ</i> Yck3-6xHA	<i>atg18Δ::KAN YCK3-6xHA::NatNT2</i>	This study
<i>atg2Δ atg18Δ</i> Vps35-6xHA	<i>atg2Δ::hphNT1 atg18Δ::KAN VPS35-6xHA::His3MX6</i>	This study
<i>atg2Δ atg9Δ atg18Δ</i> Vps35-6xHA	<i>atg2Δ::hphNT1 atg9Δ::natNT2 atg18Δ::KAN VPS35-6xHA::His3MX6</i>	This study
<i>atg2Δ</i> Vps35-6xHA	<i>atg2Δ::hphNT1 Vps35-6xHA::natNT2</i>	This study
<i>atg9Δ</i> Vps35-6xHA	<i>atg9Δ::hphNT1 VPS35-6xHA::natNT2</i>	This study
Ear1-yeGFP	<i>EAR1-yeGFP::hphNT1</i>	This study
Kex2-yeGFP	<i>KEX2-yeGFP::hphNT1</i>	This study
<i>vps35Δ</i>	<i>vps35Δ::hphNT1</i>	This study
<i>vps35Δ</i> Atg2-yeGFP	<i>vps35Δ::His3MX6 Atg2-yeGFP::hphNT1</i>	This study
<i>vps35Δ</i> Atg9-yeGFP	<i>vps35Δ::His3MX6 Atg9-yeGFP::hphNT1</i>	This study
<i>vps35Δ</i> Ear1-yeGFP	<i>vps35Δ::His3MX6 EAR1-yeGFP::hphNT1</i>	This study
<i>vps35Δ</i> Kex2-yeGFP	<i>vps35Δ::His3MX6 KEX2-yeGFP::hphNT1</i>	This study

3. Materials and Methods

3.1.10. Plasmids

Table 3-12: *E. coli* strains used in this thesis

strain	genotype	reference
XL1-Blue	recA1 endA1 gyrA96 thi-1 hsdR17 supE44 relA1 lac [F' proAB lacI ^q ΔM15 Tn10 (Tet ^r)]	Agilent (Santa Clara, USA)
XL10-Gold	Tet ^r Δ(mcrA)183 Δ(mcrCB-hsdSMR-mrr)173 recA1 endA1 gyrA96 thi-1 supE44 relA1 lac Hte [F' proAB lacI ^q ΔM15 Tn10 (Tet ^r) Amy Cam ^r]	Agilent (Santa Clara, USA)

Table 3-13: Plasmids used in this thesis

name	genotype	reference
6xHA-Sec4	pRS313 P _{SEC4} -6xHA-Sec4-T _{SEC4}	This study
6xHA-Ykt6	pRS313 P _{YKT6} -6xHA-Ykt6-T _{YKT6}	This study
Ape1-RFP	pRS316 P _{APE1} -Ape1-RFP-T _{RFP}	R. Krick (AG Thumm)
Atg18-yeGFP	pUG23 P _{ATG18} -Atg18-yeGFP-T _{CYC1}	L. Munzel (AG Thumm)
Atg18-yeGFP	pRS415 P _{ATG18} -Atg18-yeGFP-T _{CYC1}	This study
Atg2-GFP	pUG23 P _{MET25} -Atg2-GFP-T _{CYC1}	L. Munzel (AG Thumm)
GFP-Atg18	pUG36 P _{MET25} -GFP-Atg18-T _{CYC1}	(Dove et al., 2004)
GFP-Atg18 ^{P72AR73A}	pUG36 P _{MET25} -GFP-Atg18 ^{P72AR73A} -T _{CYC1}	This study
GFP-Atg18 ^{Δ7AB}	pUG36 P _{MET25} -GFP-Atg18 ^{Δ433-460} -T _{CYC1}	This study
GFP-Atg18 ^{FTTG}	pUG36 P _{MET25} -GFP-Atg18 ^{FTTG} -T _{CYC1}	(Dove et al., 2004)
GFP-Atg21	pUG36 P _{MET25} -GFP-Atg21-T _{CYC1}	R. Krick (AG Thumm)
GFP-Atg8	pRS316 P _{ATG8} -GFP-Atg8-T _{ATG8}	AG Thumm
GFP-Atg9	pRN295 P _{MET25} -GFP-Atg9-T _{ATG9}	T. Lang (AG Thumm)
GFP-Hsv2	pUG36 P _{MET25} -GFP-Hsv2-T _{CYC1}	AG Thumm
mCherry-Atg8	pRS315 P _{ATG8} -mCherry-Atg8-T _{ATG8}	F. Otto (AG Thumm)
mRFP-2xFYVE	pRS315 P _{TEF} -2xFYVE(HRS)-T _{CYC1}	AG Thumm
Myc-BirA*	pUG36 P _{MET25} -Myc-BirA*-T _{CYC1}	L. Munzel (AG Thumm)
Myc-BirA*-Atg18	pUG36 P _{MET25} -Myc-BirA*-Atg18-T _{CYC1}	L. Munzel (AG Thumm)

3. Materials and Methods

NLSNab2-mCherry	pRS413 P _{TEF1} -NLS _{Nab2} -mCherry	Michael Rout (The Rockefeller University, NY, USA)
pFa6a-HisMX6	Amp ^R ori P _{TEF1} -R-T _{CYC1}	(Gueldener, 2002)
pFa6a-hphNT1	Amp ^R ori P _{TEF1} -Hyg ^R -T _{CYC1}	(Janke et al., 2004)
pFa6a-kanMX6	Amp ^R ori P _{TEF1} -R-T _{CYC1}	(Guldener, 1996)
pFa6a-natNT2	Amp ^R ori P _{TEF1} -Nrs ^R -TADH ₁	(Janke et al., 2004)
pRS313	<i>CEN/ARS</i> Amp ^R ori <i>lacZ'</i> <i>HIS3</i>	(Sikorski & Hieter, 1989)
pRS315	<i>CEN/ARS</i> Amp ^R ori <i>lacZ'</i> <i>LEU2</i>	(Sikorski & Hieter, 1989)
pRS316	<i>CEN/ARS</i> Amp ^R ori <i>lacZ'</i> <i>URA3</i>	(Sikorski & Hieter, 1989)
pRS415	<i>CEN/ARS</i> Amp ^R ori <i>lacZ'</i> <i>LEU2</i>	(Simons et al., 1987)
pUG23		(Niedenthal et al., 1996)
pUG36	<i>CEN/ARS</i> Amp ^R ori <i>URA3</i> P _{MET25} -yeGFP- <i>lacZ'</i> /MCS- T _{CYC1}	(Niedenthal et al., 1996)
pYM25-mCherry	Amp ^R ori mCherry P _{TEF1} -Hyg ^R -T _{CYC1}	S. Karnebeck (AG Thumm)

3.1.11. Oligonucleotides

name	sequence
Vps35_S1	CGATAAAAGGAGGAGGACGAGAAAGAAGAAGCTGAAAAACACAATGcgtacgctgc aggtcgac
Vps35_S2	GTGTAGTTTTTTTTATCTTGGGCATGTACGAAGAGCAAGTACGTTATTTAACTAatc gatgaattcgagctcg
Vps35_S3	CATTGAAAGTCAAAGAGAAGTTGACGATCGTTTCAAAGTCATATATGTAcgtacgctg caggtcgac
Vac14_S2	CAGGTCCATTTCTTAACCAAAGATGCTTTCAATCAGGTAATGGGTAGTTAatcgatga attcgagctcg
Vac14_S3	GATAGTGGCAGTCTGCCATTCAACCGCAATGTATCCGATAAATTAATAAAAAcgtacg ctgcaggtcgac
Yck3-S1	GTGGTATCTCATTCTGAAGAAAAAGTGAAAAGGACGATAAGGAAAGATGCGTAC GCTGCAGGTCGAC
Yck3_S3	CATTTTGTCTAAAATATACAAATATTGTTGTTGCTGTTTTTGTGCTGTcgtacgctgc aggtcgac
Sap155_S2	CATATAAATTAATATATATATATACAAATTAAGAAAAGTACAAAACAATGTATCAa tcgatgaattcgagctcg
Sap155_S3	CTCGTAATTATAATGAAGATGCTGATAATGATAATGATTATGATCATGAACgtacgct gcaggtcgac

3. Materials and Methods

Pib2_S2	CATCAATAGTGACATCCTCTCTCGCTTGTCTCGCAAAAATGTTTCATCAatc gatga attcgagctcg
Pib2_S3	GGGCAGTGTTATCGGCTCTGTGCCTGCAAACCTGGAATTGGAGTAGTTTCcgtacgctg caggtcgac
Vtc3_S2	GTAAGTGGTACTTGTGTAATATATGTGTATATAAAAAATATACATGTTCTTAatc gatg aattcgagctcg
Vtc3_S3	CCCCGTACACTAAAACCAATTCAAGATTTTATCTTCAATTTGGTTGGGGAAcgtacgct gcaggtcgac
Cdc48_S2	GAAATGACTTGAATTTACGATTTAAAATAAAAAATATACCTGGCATATAACTAatc gat gaattcgagctcg
Cdc48_S3	GGTGCTGCATTTGGTTCTAATGCGGAGGAAGATGATGATTTGTATAGTcgtacgctgc aggtcgac
Snx3_S2	CATTCTTTTATATAATCTATATTATTTATTCACGTAAAAGAGTTCTTTTCAatc gatgaat tcgagctcg
Snx3_S3	CTGGTCTAAAGTTCTCGTGAGGTTTCATTGAAGCTGAAAAGTTTGTCGGCcggtacgct gcaggtcgac
Snf7_S2	GTAAGAACACCTTTTTTTTTCTTTTCATCTAAACCGCATAGAACACGTTCAatc gatga attcgagctcg
Snf7_S3	GAAGAAGATGAAGATGAAAAAGCATTAAAGAGAACTACAAGCAGAAATGGGGCTT cgtacgctgcaggtcgac
BK_6xHA_for	caaGATAAACGTCGACggttctgctgctagaATGtaccatacg
BK_6xHA_rev	catgtttatcaattgcacttttgagctagaagcgtaatc
BK_PSec4_for	ctcaCTATAGGGCGAATTGGAGCTCATAACTGGAAAGAGGAACAGCC
BK_PSec4_rev	cagaaccgtcgacGTTTATCTTGTTATGTTTATATTCTTTCTGGTG
BK_Sec4_for	gctcaaaagtCAATTGATAAACATGTCAGGCTTGAGAAC
BK_Sec4_rev	gaacaaaagctgggtaccGGGCCCTTTCTTGATTTTTTACCAATCGCC
BK_6xHA- Ykt6_for	GGCAGTCGACcggttctgctgctagaATGtaccatacg
BK_6xHA- Ykt6_rev	GATTCTCATCAATTGcacttttgagctagaagcgtaatc
BK_PYkt6_for	CTCACTATAGGGCGAATTGGAGCTCCTTTTGCTGTTGTTGTCATCTTC
BK_PYkt6_rev	gcagcagaaccgGTCGACTGCCAAAATAACTTCTCTAGTGATAC
BK_Ykt6_for	gctcaaaagtgaattgATGAGAATCTACTACATCGGTG
BK_Ykt6_rev	GAACAAAAGCTGGGTACCGGGCCCCATGGCCAAGTTGGTTAAGG
Vps26_S2	GAAAGAACAGAGAACCACATCTTCACCTTATTTAAGGTCGAGCTTTTCTAatc gatga attcgagctcg
Vps26_S3	GATGGCAGAAGATATTTTAAACAATCAGAAATAACATTGTACAGGACCCGGcgtacg ctgcaggtcgac
Vps29_S2	CTAATGTTTAGACATCATAGAAATGCATAAAAATGAAAATGGCTACCCTAatc gatga attcgagctcg
Vps29_S3	CGTTAATGGAGAAGTGAAGGTCGATAAAGTGGTTTATGAAAAGGAAcgtacgctgca ggtcgac

3. Materials and Methods

Sft2_S2	CATTATTTTCTTCTCAACTAATCAATTCAATATGCACTATGAATGATAATTCAatcg atgaattcgagctcg
Sft2_S3	GAGGATGTTAAGCTCTGCTGGTGTCAATTCGGCAAGAGGTGTTCTGCGCATCcgtag gctgcaggtcgac
Ear1_S2	CTGACCGGGGCTAGTGTTCAGCCTTACTATCTCATGCATTTTCGTATTAatcgaatgaa ttcgagctcg
Ear1_S3	GATCCCGAACAATTTTCAGAATTTGATGATTACGAAAGCAGGATGCATGGCATAcgt acgctgcaggtcgac
Ymr253c_S2	GAAAAGAAGGAAAAAATCATAGTAGAAACTGAGGAATTTATACTCGTCTTAatc gatgaattcgagctcg
Ymr253c_S3	GACGACGAAGAGAAGCTATTCCCCTGACAGAGTTTGACCTATCCGATTCTAAAcgt acgctgcaggtcgac
Kex2_S2	CTATAAGAAAAAATGCTATTTTGTAATTTGAAGCTTTCTGTACATATCGAATCAatc gatgaattcgagctcg
Kex2_S3	CCAATAAATTACAAGAATTACAGCCTGATGTTCCCTCCATCTTCCGGACGATCGcgtag gctgcaggtcgac
BK_Atg17- 7AB_for	CATCTTCATAACGCCTATACTTGATATGGTCATTACATGGG
BK_Atg18- 7AB_rev	CAAGTATAGGCGTTATGAAGATGGTCCCCATCAGG
Atg9_S2	GGAAACAGTTATATATATAGTTATATTGGATGATGTACACGACACAGTCTGCCatcg atgaattcgagctcg
Atg9_S3	GGTGTCTTAGGACTTGTTAAAGAGTATTACAAGAAGTCTGACGTCGGAAGAcgtacg ctgcaggtcgac
Atg18_P72AR73A _for	CAACCTGCGCTTTCAgCAgcGAGATTGCGTATAATC
Atg18_P72AR73A _rev	GATTATACGCAATCTCgcTGcTGAAAGCGCAGGTTG
Vps38_KO_loxP_f or	GATGGTTTTACCTATTAGGGATAGTAATCATAATTTAAAAATATGcagctgaagcttcgt acgc
Vps38_KO_loxP2 _rev	AAAGATTAATGGCAGTCCAAAAGAGATTTTTGATTTTCAGTCTA ^g catagggccactag tgatctg
Atg14_KO_loxP_f or	AAAAAGGGAAGTAAAAGTTAAAACTAGAATCCTAGTATGACATGcagctgaagcttc gtacgc
Atg14_KO_loxP_r ev	ACATGCAACTTTATACACACGGCAGGAAAAAAGTGCCTACTA ^g catagggccacta gtgatctg

3. Materials and Methods

3.2. Methods

3.2.1. Cultivation Conditions

3.2.1.1. Cultivation of *S. cerevisiae*

Yeast strains were either grown under nutrient rich conditions in yeast peptone dextrose (YPD) medium or in complete minimal (CM) medium (Table 3-7). The CM medium supplemented with all necessary amino acids was used to select for auxotrophy markers. For overexpression experiments using the *MET25* promoter methionine was added to CM without (w/o) L-methionine to a f.c. of 0.3 mM, if not stated otherwise.

Yeast cultures were grown at 30°C, while shaking at 220 rpm. Pre-cultures were inoculated and grown o/n to stationary phase and used to inoculate the main culture in the appropriate dilution. Cell density was measured photometrically at 600 nm (OD₆₀₀).

Strains were stored on plates at 4°C for up to six weeks. For long term storage cell cultures were grown o/n at 30°C and 220 rpm, mixed with glycerol to a final concentration of 15% (w/v) and stored at -80°C.

3.2.1.2. Cultivation of *E. coli*

E. coli strain XL1-blue and XL10-gold were used for cloning. Cells were cultivated in lysogeny broth (LB) supplemented with the selection marker ampicillin (Table 3-7). Selection of plasmid carrying clones was performed by plating the cells after transformation evenly on a LB amp plate and incubating overnight (o/n) at 37°C. Cells grown on plates were stored up to five weeks at 4°C, before patching them on fresh LB amp plates.

For long-term storage cells were grown o/n at 37°C and 220 rpm, mixed with glycerol to a final concentration (f.c.) of 30% (w/v) and stored at -80°C.

3.2.1.3. Nitrogen starvation

To induce nitrogen starvation cells were grown in selective medium to the appropriate OD, harvested (5 min, 2000 rpm) and washed once in SD-N. After a second centrifugation step (5 min, 2000 rpm) cells were resuspended in SD-N to an OD₆₀₀ of 10.

3. Materials and Methods

3.2.2. Molecular biological methods

3.2.2.1. DNA Isolation

3.2.2.1.1. Isolation of chromosomal DNA from Yeast

The NucleoSpin® Microbial DNA kit was used to isolate chromosomal yeast DNA. Cells were grown o/n in YPD medium, harvested and lysed according to manufacturer's instruction. DNA was isolated and solubilized in 70µL dH₂O.

3.2.2.1.2. Isolation of plasmid DNA from *E.coli*

Plasmids were purified from transformed *E.coli* strains using the Wizard® Plus SV Miniprep System from Promega. 5 mL culture were grown o/n in LB-Amp (37°C, 220 rpm), harvested (5000 rpm, 5 min) and further processed according to manufacturer's instructions. DNA was eluted in 150µl sterile dH₂O. DNA concentration was measured according to chapter 3.2.2.3.

3.2.2.1.3. Purification of DNA fragments

DNA fragments contaminated with enzymes or buffer after a reaction step or after gel electrophoresis were purified using the QIAquick Gel Extraction Kit (Qiagen) according to manufacturer's instructions. DNA was eluted in 30 µl sterile dH₂O and concentration was determined according to 3.2.2.3.

3.2.2.2. Agarose gel electrophoresis

Gel electrophoresis was used to analyze DNA samples after PCR or digestion as well as separating specific DNA fragments from each other. For this, 0.8 % (w/v) agarose were dissolved in TAE buffer (Table 3-8). 1 µg/ml ethidium bromide was added to make the DNA visible under UV light. DNA samples were mixed with 6x Purple Gel Loading Dye (NEB) and loaded in gel pockets with 5-10 µl TriDye™ 1 kb DNA Ladder (NEB) or 100 bp DNA Ladder (NEB) as a size reference. Electrophoresis was run at 120 V for 18-25 min. DNA bands were visualized and documented with a UV transilluminator (Biometra).

Fragments at the correct size were cut out of the gel and purified with the QIAquick Gel Extraction Kit (see 3.2.2.1.3) if necessary.

3. Materials and Methods

3.2.2.3. Determination of DNA concentration

Two methods were used to measure DNA concentration in a sample: concentration of plasmid DNA or yeast chromosomal DNA was determined using the NanoDrop^c UV/Vis spectrophotometer (Thermo Scientific)

DNA concentration of fragments after PCR or restriction was analyzed using gel electrophoresis (3.2.2.2). A volume of 2 µl DNA was mixed with 1 µl 6x Purple Gel Loading Dye (NEB) and loaded on a Gel with 10 µl TriDye™ 1 kb DNA Ladder (NEB). After visualization with UV light the intensity of the signal was compared to the reference (ladder with known DNA concentrations) and an approximated amount of DNA was determined.

3.2.2.4. Molecular Cloning

All plasmids made during this thesis are listed in Table 3-13. Most of them were constructed by using restriction digestion and ligation. Fragments containing the respective restriction sites were generated with PCR (chapter 3.2.2.4.1) and digested with the appropriate restriction enzyme (chapter 3.2.2.4.2). The target plasmid or backbone is digested with the same or matching restriction enzymes and the insert is then ligated into the backbone (chapter 3.2.2.4.3). Point mutations or smaller deletions were introduced with site-directed mutagenesis (chapter 3.2.2.4.4). More complex cloning strategies were performed with the NEBuilder Kit (chapter 3.2.2.4.5).

3.2.2.4.1. Polymerase Chain Reaction (PCR)

The KOD Hot Start DNA Polymerase (Merck) was used to amplify DNA fragments for molecular cloning or genomic integration, since its proofreading function prevents mutations in the finished construct. DNA sequences longer than 3,000 base pairs were multiplied with the KOD XL DNA polymerase, which was optimized for longer fragments. Oligonucleotides to use as primer were designed using SnapGene: between 18 to 25 base pairs aligned to sequence flanking the region of interest, with restriction sites inserted if necessary. PCRs were performed according to manufacturer's protocol, melting temperature and elongation time adjusted to the length of the amplicon and annealing temperature of the oligonucleotides.

3. Materials and Methods

3.2.2.4.2. Restriction

Fragments generated with PCR or plasmids were digested with restriction enzymes and buffers from NEB according to manufacturer's instructions. Restriction buffer and 1,5 µl of each enzyme were added to 5-10 µg DNA in a total volume of 50 µl and incubated for 3 h at the recommended temperature. Vector DNA (or the plasmid backbone) was further incubated with 1 µl CIP (calf intestinal alkaline phosphatase, NEB) to dephosphorylate 5' and 3' ends of DNA. This decreases the chance of self-ligation of the vector.

DNA fragments were purified with gel electrophoresis after restriction as described in chapters 3.2.2.1.3 and 3.2.2.2 and DNA concentration was determined as described in chapter 3.2.2.3.

3.2.2.4.3. Ligation

DNA fragments with compatible ends were ligated with the T4 DNA Ligase (NEB) according to manufacturer's instructions. DNA fragments were mixed with 1 µl T4 DNA Ligase and 2 µl T4 DNA Ligase Buffer in a total volume of 20 µl. The reaction was incubated for 30 – 60 min at room temperature or o/n at 16°C before transformation in *E.coli* (see chapter 3.2.2.6.1).

To optimize ligation a 3x excess of insert to vector was used with a total amount of 150-300 ng DNA. The amount of insert used was calculated with the following formula:

Equation 1: Formula used to determine optimal amount of insert

$$mass_{insert} (ng) = \frac{length_{insert} (bp) \times mass_{plasmid} (ng) \times 3}{length_{plasmid} (bp)}$$

3.2.2.4.4. Site-Directed Mutagenesis

Either the Quick-Change II Site-Directed Mutagenesis Kit or the QuickChange Lightning Site-Directed Mutagenesis Kit (Agilent) were used according to manufacturer's instructions to introduce point mutations or small deletions. Oligos with a length of 45-55 bp aligning to the adjacent regions but designed to contain the mutation or deletion were used to generate a linearized plasmid with the mutation. The constructs were then transformed in *E.coli* XL-Gold ultracompetent cells (see chapter 3.2.2.6.1). Plasmids were sequenced as described in chapter 3.2.2.8 to confirm mutation or deletion.

3. Materials and Methods

3.2.2.4.5. BuilderKit

The NEBuilder HiFi DNA Assembly Master Mix (NEB) was used to assemble multiple DNA fragments in a single cloning step. DNA fragments with appropriate overlaps were multiplied with specifically designed oligonucleotides, purified and incubated with linearized vector according to the manufacturer's protocol. For deletions of more than 30 bp oligonucleotides complementing the sequence adjacent to both sides of the deletion were used to amplify the whole plasmid. Gaps and nicks were filled and sealed by the NEBuilder Master Mix. The resulting double-stranded fully sealed plasmid was transformed in *E.coli* XL1-Blue (see 3.2.2.6.1).

3.2.2.5. Genome engineering based on homologous recombination

Chromosomal modification of the yeast genome were performed as described by (Gueldener, 2002; Guldener, 1996; Janke et al., 2004; Longtine et al., 1998). Cassettes containing tag or deletion as well as the marker were amplified with PCR, purified and transformed into highly competent yeast cells.

3.2.2.6. Transformation

3.2.2.6.1. Transformation of *E. coli*

E.coli XL1-Blue were either directly bought from Agilent or regrown and made chemically competent by the author of this study or a former member of the group (Dr. P. Rube) according to the protocol published by (Hanahan, 1983). Ultracompetent XL10-Gold were obtained from Agilent and used for site-directed mutagenesis (see chapter 3.2.2.4.4).

The frozen cells were gently thawed on ice for 15 min, 50-90 µl of the cell suspension were gently mixed with 10 µl plasmid DNA or ligation mix and incubated for another 30 min. The cells were then incubated at 42°C for 90 s to facilitate formation of pores and uptake of DNA. The Eppendorf tube was immediately placed on ice and 900 µl SOC medium was added. Cells were incubated at 37°C gently shaking for 1 h and then pelleted (3000 rpm, 5 min) and plated on LB agar plates containing the respective antibiotics (ampicillin if not otherwise stated) for plasmid selection. Plates were incubated o/n at 37°C and clones were used to inoculate 5 mL LB-Amp. Plasmid DNA

3. Materials and Methods

was isolated from the cultures (see chapter 3.2.2.1.2) and tested for the correct plasmid (see chapters 3.2.2.7 and 3.2.2.8).

3.2.2.6.1. Transformation of *S. cerevisiae*

Two different methods to introduce DNA into yeast cells were used. The first was used for plasmid DNA (“quick & dirty”). Here, 300µl of PEG in LiTE buffer (see Table 3-8) were mixed with 5 µl herring sperm DNA (10 mg/ml) and 5 µl of the respective plasmid/s. Yeast cells were added with a sterile tooth pick directly from agar plates. The reaction was then incubated for 30 min at 30°C to increase competency and then transferred to 42°C for 15 min. The cells were pelleted (3000 rpm, 5 min), resuspended in 50 µl sterile dH₂O and plated on the respective CM selection plate. Colonies formed after 2-3 days incubation at 30°C.

The second method was used for introducing chromosomal changes, e.g. tags or deletions, because a high transformation efficiency was necessary. Cells were grown in 50 mL YPD to log-phase (between 0.3 and 0.8) and harvested (2000 rpm, 5 min). The pellet was washed twice in 50 mL sterile dH₂O and then once in 2.5 mL LiOAc-Sorb buffer (see Table 3-8), before it was resuspended in 100-300 µl LiOAc-Sorb buffer. Aliquots of 50 µl were incubated for 15 min at 30°C. 300 µl PEG in LiTE buffer was added, as well as 5 µl herring sperm DNA (10 mg/mL) and 10 µL of the respective DNA fragment. After gently mixing the reaction was incubated for another 30 min at 30°C and then transferred to 42°C for an additional 15 min. Cells were then pelleted (2000 rpm, 5 min) and resuspended in 3 ml YPD medium. After 2-3 h regeneration at 30°C and 220 rpm, cells were again harvested and plated on the respective selection plate. After 3 d of incubation at 30°C colonies were patched on a fresh selection plate and incubated o/n at 30°C. Clones were then picked and used to inoculate 5 mL YPD medium, chromosomal DNA was isolated (see chapter 3.2.2.1.1). The modified chromosomal DNA was then verified by PCR (see chapter 3.2.2.7).

3.2.2.7. PCR to verify size of gene / plasmid

PCR was used to verify correct insertion of a tag or deletion of a gene. Chromosomal DNA was isolated from a cell culture (see chapter 3.2.2.1.2). Oligos complementing regions adjacent to insertion or deletion were chosen to amplify the area of interest.

3. Materials and Methods

The size of the resulting band after gel electrophoresis indicates if the chromosomal modification was successful.

Plasmids were analyzed using DreamTaq Green PCR Master Mix (2x) (ThermoScientific). This master mix contains a polymerase as well as dyes and a density reagent, that allows for direct loading on a gel after PCR. 0.5 µl primer binding on either side of the area of interest were added to a total volume of 25 µl MasterMix (1x). A sterile pipette tip was used to transfer a small amount of cell material into the mix and the PCR was run according to manufacturer's instructions.

3.2.2.8. Sequencing of DNA

All plasmids constructed in this group were further verified by sequencing performed by Microsynth Seqlab (Göttingen). For this, 12 µl plasmid DNA at a concentration of 80 ng/µl were mixed with 3 µl of the respective primer (10 times dilution → ??) and send to the lab. The results were analyzed using SnapGene.

3.2.3. Biochemical methods

3.2.3.1. Alkaline lysis of yeast cells

For alkaline lysis 2 OD₆₀₀ of yeast cells were pelleted (5000 rpm, 5 min) and resuspended in 1 ml alkaline lysis buffer (0.28 M NaOH, 1.125 % (v/v) β-mercaptoethanol). After 10 min incubation on ice (with occasionally vortexing) 150 µl 50% (v/v) trichloroacetic acid (TCA) was added. Samples were incubated on ice for another 10 min and all precipitated proteins were then pelleted (12700 rpm, 10 min, 4°C). The pellet was washed twice in 600 µl of -20°C acetone, dried for 10 min at 37°C to remove all of the remaining acetone and then resuspended in 100 µl 2xLämmli buffer (see Table 3-8).

3.2.3.2. Co-IP

The µMACS (magnetic activated cell sorting) System from Miltenyi Biotec was used for Co-IPs: superparamagnetic microbeads are conjugated to monoclonal antibodies against specific epitope tags (e.g. GFP, HA, Myc), which can bind to proteins of interest and isolate them using magnetic fields. The protocol recommended by the manufacturers was modified in this thesis.

3. Materials and Methods

Proteins were tagged with GFP (bait) or 3x/6xHA (prey) and grown in 90 ml of the respective selection medium to an OD₆₀₀ of 2-3. 200 OD₆₀₀ were harvested (2000 rpm, 5 min, 4°C), washed once in 15 ml 50 mM Tris HCl pH 7.5 and centrifugated again (2000 rpm, 5 min, 4°C). Pelleted cells were resuspended in 750 µl Co-IP lysis buffer (see Table 3-8) if not stated differently, 400 µl glass beads were added and the cells were harshly shaken for 30 min at 4°C to completely lyse cell walls. The suspension was then centrifugated (10000 x g, 10 min, 4°C) to remove cell debris and the supernatant was transferred into a fresh eppendorf vessel. 25 µl of the supernatant were taken as a loading control, mixed with 25 µl 2x Lämmli buffer and boiled for 5 min at 95°C. 50µl anti-GFP micro beads were added to the supernatant and incubated on ice for 30 min. Columns provided by Miltenyi Biotec were equilibrated with 150 µl Co-IP lysis buffer and the supernatant containing the micro beads is then loaded onto the columns. Typically, the columns are then washed 3x with 200 µl lysis buffer, 1x with 200 µl Co-IP wash buffer I and once with 200 µl 50 mM Tris-HCl pH 7.5 to remove remaining SDS. Proteins were eluted by adding 20 µl 2xLämmli buffer heated to 95°C to the columns and after 5 min incubation another 50 µl 2x Lämmli buffer at 95°C. Eluted proteins were boiled for 5 min at 95°C.

The concentration or addition of SDS to the Co-IP Wash buffer I was changed over time for some proteins, especially Atg21, since even small variations affected the binding affinity to Vps35.

3.2.3.3. SDS-PAGE

SDS-PAGE (Sodium-dodecyl sulfate polyacrylamide gel electrophoresis) was used to separate proteins by size, as described in (Lämmli, 1970). 2xLämmli-Buffer (see Table 3-8) was added to the protein, or the protein was directly dissolved in Lämmli-buffer, and boiled for 5 min at 95°C. 10-15 µl of the sample was loaded onto a SDS-Gel (separating gel: 0.375 M Tris pH 8.8, 10% (v/v) Rotiphorese® Gel 30 (37.5:1), 0.1% (w/v) SDS, 0.1% (w/v) APS, 0.5% (v/v) TEMED; separating gel: 0.14 M Tris pH 6.8, 5% (v/v) Rotiphorese® Gel 30 (37.5:1), 0.1% (w/v) SDS, 0.1% (w/v) APS, 0.5% (v/v) TEMED). Precision Plus Protein™ All Blue Prestained Protein Standard (Biowas used as a marker for molecular weight. The electrophoresis was run on a Mini-PROTEAN® electrophoresis cell at 150 V for approximately 1 h. The gel was then either used for

3. Materials and Methods

immunoblotting (see chapter 3.2.3.4) or Coomassie brilliant blue staining (see chapter 3.2.3.5).

3.2.3.4. Immunoblotting

Separated proteins were transferred to a PVDF (polyvinylidene difluoride) membrane according to (Towbin et al., 1979). The PVDF membrane was activated in 98% (v/v) ethanol and arranged with gel and blotting paper soaked in blotting buffer (see Table 3-8). A Mini Trans-Blot[®] Cell was used for the transfer at 75 mA per gel for 10 h at 4°C. Further cooling was achieved by adding a cooling element and constant stirring.

The membrane containing the proteins was then saturated in blocking solution (10 % (w/v) skim milk powder in 1x TBST) for 1 h at RT or o/n at 4°C. After washing the membrane 3x for 10 min in 25 mL 1x TBST it was then incubated with the primary antibody (for target and dilution see Table 3-5) for 3 h at RT or o/n at 4°C. Afterwards, the membrane was washed 3x for 10 min in 25 mL 1xTBST and incubated with the secondary antibody for 1 h at RT. While the primary antibody targeted epitopes of the protein of interest, the secondary antibody binds to the primary, but is typically coupled to HRP (horseradish peroxidase). This can be used to visualize the otherwise invisible protein. After removing excess secondary antibody by washing it again 3x for 10 min in 25 mL 1x TBST the membrane was treated for 5 min in the dark with Amersham[™] ECL[™] Western Blotting Detection Reagents (GE Healthcare) or the Pierce[™] ECL Plus Western-Blotting Substrate (Thermo Fisher Scientific) according to manufacturer's instructions. Development and documentation were performed with the LAS-3000 system and Amersham[™] ImageQuant[™] 800 (GE Healthcare). Quantification was done with Fiji (Schindelin et al., 2012).

Membranes were incubated in 10% (v/v) acetic acid for 10 min at RTT to remove the remaining antibodies and could then be decorated with different antibodies.

3.2.3.5. Coomassie brilliant blue staining

Coomassie brilliant blue (CBB) stains proteins and can therefore be used to visualize unspecific proteins after separation. The protocol used is based on (X. Wang et al., 2007) and modified according to (Pink et al., 2010). One major advantage of this method is its compatibility with mass spectrometry and was therefore used to stain proteins for the BioID assay.

3. Materials and Methods

After electrophoresis SDS gels were incubated for 1 h in CBB fixation buffer I (for all buffers and solutions see Table 3-8) and then for 2 h in CBB fixation buffer II to secure all proteins to the gel. The gel was then incubated in CBB staining solution o/n at 4°C. To remove unspecific staining (reduce background) the gel was first incubated in CBB destaining solution for 1 h and then ddH₂O. Documentation was done with the Perfection V850 Scanner (Epson).

3.2.4. DeltaVision

Optimal cell density for microscopy is between 2-10 OD₆₀₀. Cultures at lower ODs were centrifugated (2000 rpm, 5 min) and resuspended in 1/10 of its original medium. 4 µl yeast cell suspension were dropped on a microscope slide and fixed with a cover slip. DeltaVision immersion oil (N=1.520, GE Healthcare) was applied to the cover slip to minimize reflection. Fluorescence microscopy was performed with a DeltaVision[®] microscope (Olympus IX71, Applied Precision) equipped with the UPlanSApo x100,1.4 numerical aperture (NA), oil immersion objective, a CoolSNAP_{HQ2}[™] couple-charged device (CCD) camera and different filter sets (see Table 3-14). Imaging occurred with a 100x objective and 2x2 binning. At least 20 focal planes along the z-axis with a distance of 0.2 µm were captured and the resulting images were deconvolved using softWoRx[™] (Applied Precision) and further processed with Fiji (Schindelin et al., 2012).

Table 3-14: Filter sets for live-cell fluorescence microscopy used in this thesis

Filter Set		Central wavelength / bandpass		Fluorophore
		Excitation (nm)	Emission (nm)	
Blue	DAPI	390 / 18	435 / 48	BFP
Green	GFP	475 / 28	525 / 50	GFP
Red	mCherry	575 / 25	632 / 69	mCherry, RFP, FM4-64
DIC	POL	-50 / 28	-50 / 0	

3.2.5. BioID assay

A protocol for the proximity dependent biotin identification (BioID) assay in combination with the use of stable isotope labeling by amino acids (SILAC) was published by (Opitz et al., 2017) provided to this group by Dr. Oliver Valerius and the former member Dr. Nadine Opitz (Department of Molecular Microbiology and Genetics,

3. Materials and Methods

Georg-August-University, Göttingen. It was modified for this specific approach by the former member of this group, Dr. Lena Munzel. An overview of the workflow is depicted in Figure 3-1.

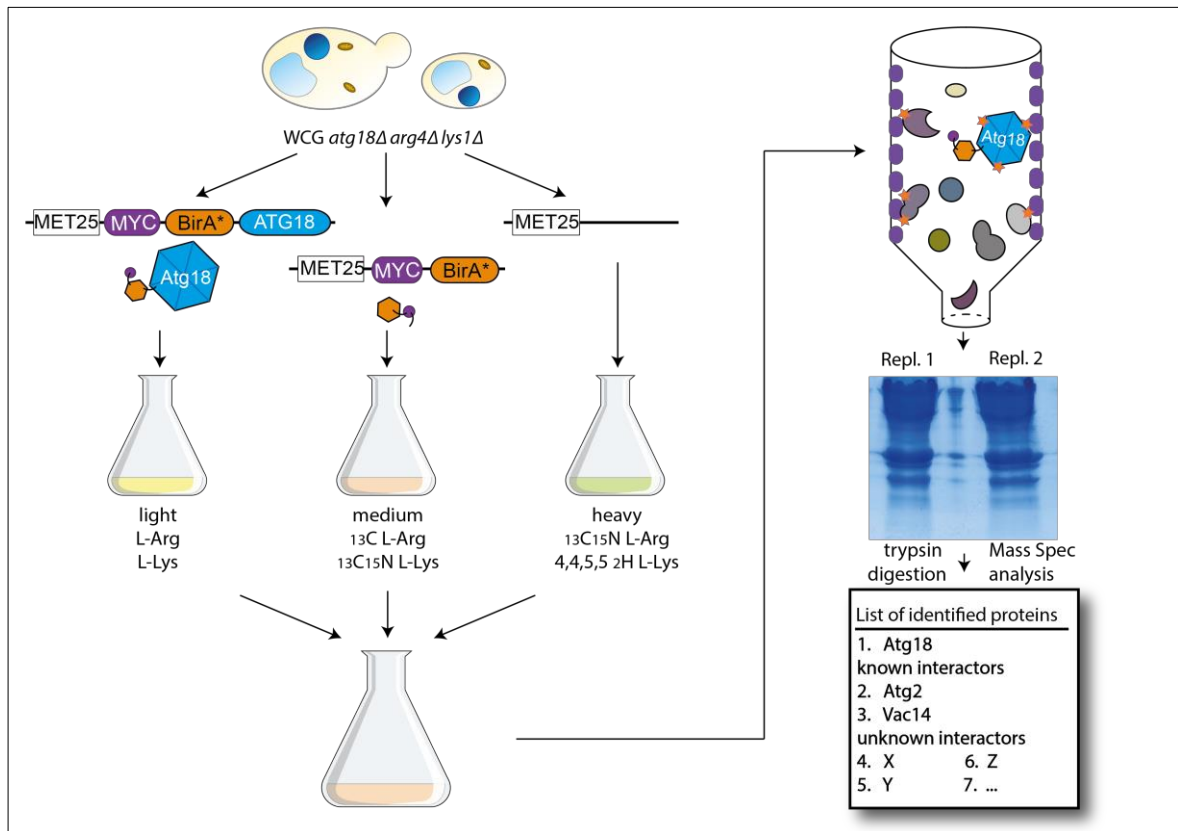


Figure 3-1: Workflow for the BioID assay

WCG *atg18Δ arg4Δ lys1Δ* strains expressing either the fusion protein (Atg18 N-terminally tagged with Myc-BirA*), Myc-BirA* or an empty plasmid under the control of a *MET25* promoter from a low-copy plasmid were grown in selection medium supplemented with 0.3 mM methionine, 10 μM biotin and isotope labeled arginine and lysine. Cells were harvested at an OD_{600} of 4, pooled and lysed with glass beads. Biotinylated proteins were purified using Strep-tactin columns, precipitated with TCA and resuspended in Lämmli buffer. After separation of the proteins on a SDS-gel proteins were digested with trypsin and analyzed using mass spectrometry.

3.2.5.1. Small scale

A preliminary experiment without the SILAC approach was performed to test the ability of the fusion proteins to biotinylate already known interaction partners. For this, 300 ml selection medium without methionine and supplemented with all necessary amino acids (not isotope labeled amino acids) and biotin to a f.c. of 10 μM was inoculated 1:500 from a pre-culture. Cells were grown to an OD_{600} of 4 and the equivalent of 800 ODs were harvested (2000 rpm, 5 min, 4°C). Harvested cells were washed twice in 15ml of ice cold 10 mM HEPES pH 7.9 and carefully resuspended in a total of 3 ml BioID Lysis buffer (see Table 3-8) for each strain. 750 μl of cells in lysis buffer were mixed with 400 μl glass beads and vortexed for 30 min at 4°C. Then SDS

3. Materials and Methods

was added to a f.c. of 4% (w/v) at RT and the proteins were denatured for 10 min at 65°C. After centrifugation of the samples (3000 x g, 5 min, RT) the supernatants were pooled and a loading sample of 30 µl taken, mixed with 30 µl of 4x Lämmli buffer and boiled for 10 min at 95°C. Biotinylated proteins were then isolated with Step-Tactin columns and precipitated with TCA as described in chapter 3.2.5.3 and resuspended in 2xLämmli buffer. The samples were then analyzed using SDS-PAGE and either stained with CBB or transferred to a PVDF membrane and visualized with antibodies (see chapters above).

3.2.5.2. BioID with SILAC approach

Three different strains expressing either the fusion protein Myc-BirA*-Atg18, the first control Myc-BirA* or the second control, an empty plasmid were grown separately in media supplemented with different combinations of stable isotopes of L-arginine and L-lysine as depicted in Figure 3-1.

An o/n preculture in normal selection medium was used to inoculate a second pre-culture with 10 mL of selection medium w/o methionine (dilution 1:100). The selection medium was supplemented with 50 mg/L of L-lysine and L-arginine in either its “light” version or “medium” and “heavy”, respectively (as indicated in Figure 3-1). The second pre-culture was incubated for 7 h and then used to inoculate the main culture to a final OD of 0.014. The main culture consisted of 75 ml of the same medium used for the second pre-culture but supplemented with 10 µM biotin. It was grown o/n for approximately 15-17 h to an OD₆₀₀ of 3-4.

200 ODs were harvested for each strain by centrifugation (2000 rpm, 10 min, 4°C) and washed once in 15 ml of ice cold 10 µM HEPES pH 7.9. After another centrifugation step (2000 rpm, 5 min, 4°C) cells were resuspended in 15 ml ice cold 10 µM HEPES pH 7.9 and the OD₆₀₀ of the cell suspensions was determined. Equal amounts of cells of each strain according to the measured OD were pooled together and harvested by centrifugation as before. The pellet was then resuspended in a total of 1.8 ml BioID Lysis buffer (see Table 3-8) and distributed to three 1.5 ml Protein LoBind Tube (Eppendorf) containing glass beads. Cells were vortexed for 30 min at 4°C and SDS was added to a f.c. of 4% (w/v). The proteins were denatured for 10 min at 65°C and cell debris as well as glass beads were removed by centrifuging the samples (3000 x g, 5 min, RT). The supernatant was pooled and a loading sample of 100 µl taken and stored

3. Materials and Methods

at -20°C. Biotinylated proteins were then isolated with Step-Tactin columns and precipitated with TCA as described in chapter 3.2.5.3.

3.2.5.3. Isolation of biotinylated proteins

Gravity flow Strep-Tactin® Sepharose® Columns (iba) were used to isolate biotinylated proteins from the supernatant. For this 1 ml columns were used to isolate biotinylated proteins for the BioID/SILAC experiment (0.2 ml columns were used for the small scale approach). After removal of the storage solution the columns were equilibrated with 4 ml washing buffer (1x buffer W (iba), 0.4% (w/v) SDS; 400 µl were used for the small scale approach). The cell lysate was applied to the column. After the lysate had completely entered the column it was washed with a total of 50 ml washing buffer (10 ml for small scale). Biotinylated proteins bound to the column were eluted with three times of 1 ml elution buffer (1x buffer W (iba), 10 mM biotin; 6x 100 µl for small scale) into 1.5 ml protein LoBind Tube (Eppendorf).

Proteins were precipitated by adding TCA to a f.c. of 10% (w/v) and incubated for 30 min on ice. Precipitated proteins were pelleted by centrifuging the samples (12700 rpm, 10 min, 4°C) and washed twice with 500 µl ice-cold acetone. Afterwards, the pellet was air dried and resuspended in a total of 30 µl 2xLämmli buffer (60 µl for small scale approach). 30 µl of the sample were loaded on a SDS-polyacrylamide gel and separated by SDS-PAGE. Proteins were visualized with a CBB staining and prepared for mass spectrometry. For the small scale approach, gels were either blotted after the SDS-PAGE or stained with CBB.

3.2.6. Mass spectrometry

3.2.6.1. Sample preparation

Samples were separated on a 10% SDS-polyacrylamide gel by SDS-PAGE and stained with Coomassie brilliant blue as described in chapter 3.2.3.5. Preparations of the samples for MS analysis were performed by Olaf Bernhard (Department of Cellular Biochemistry, University Medical Center Göttingen) according to (Opitz et al., 2017). For this, the sample lane was divided into 10 sections and each section was further cut into 2 x 2mm sized gel pieces. After digestion and purification the sample was vacuum dried to preserve the peptides.

3. Materials and Methods

3.2.6.2. LC-MS analysis

Liquid chromatography-mass spectrometry (LC-MS) analysis was performed by Dr. Oliver Valerius and Dr. Kerstin Schmitt (Department of Molecular Microbiology and Genetics, Georg-August-University Göttingen) with a Q exactive™ HF Hybrid Quadrupol-Orbitrap™ mass spectrometer (Thermo Fisher Scientific). Samples were resuspended in 20µl fresh LC-MS sample buffer (2% (v/v) acetonitrile, 0.1 % (v/v) formic acid) immediately before LC-MS analysis and incubated in an ultrasonic bath for 3 min to remove air bubbles.

Protein and biotin-site identification as well as SILAC-based quantification was performed with the MaxQuant 1.5.1.0 software (Max Planck Institute of Biochemistry). The Andromeda algorithm was used for searching a *UniProt*-derived *S. cerevisiae* specific database (<http://www.uniprot.org>, Proteome ID UP000002311, download 2019). Parameters were set according to (Opitz et al., 2017). Generated data were then further processed and filtered with the Perseus software. Additionally, the Proteome Discoverer™ 2.2 software (Thermo Fisher Scientific) was also used to identify candidates. The SequestHT and Mascot algorithms were used for database searches against a database specific for *S. cerevisiae* (SGD, 6110 entries, including common contaminants, S288C_ORF_database release version 2011, Stanford University).

3.2.7. Statistical analyses

Blots were quantified using the free software Fiji (Schindelin et al., 2012). Statistical analyses for Western blots as well as fluorescence microscopy were performed using GraphPad Prism® (GraphPad Software, USA). Graphs were plotted using the mean value together with the standard error of the mean (SEM). Statistical relevance was determined using the unpaired two-tailed t-test and is indicated in the graphs as follows: not significant (n.s. or no asterisk) for $p > 0.05$, * for $p < 0.05$, ** for $p < 0.01$, *** for $p < 0.001$ and **** for $p < 0.0001$.

4. Results

Most biochemical approaches to detect protein-protein interactions like affinity purification followed by mass spectrometry have distinct disadvantages. Before the protein complex or cellular organelle can be analyzed cells need to be lysed, proteins have to be isolated. This often happens under harsh conditions and many of the more fragile connections are lost. In addition to that, not all proteins are soluble outside of their normal environment, e.g. membrane proteins. These proteins precipitate before purification and cannot be identified.

In a proximity dependent labeling assay such as a BioID assay, proteins nearby are labeled *in vivo*. These already marked proteins can then be isolated and identified by mass spectrometry.

4.1. BioID

The BioID assay (shown in Figure 4-1) utilizes biotin protein ligases, enzymes responsible for the covalent attachment of biotin to carboxylases (Chapman-Smith & Cronan Jr, 1999). Since this modification is relatively rare in most organisms it allows for selective isolation of labeled proteins.

The *E.coli* ligase BirA (bifunctional ligase/repressor) regulates both biotinylation of acetyl-CoA carboxylase (Barker & Campbell, 1981b; Roux et al., 2012) and, by binding directly to the *bio* operon, its own expression levels (Barker & Campbell, 1981a). It catalyzes the formation of activated biotinyl-5'-AMP from biotin and ATP, which remains stably associated with BirA. This is facilitated through interaction with R118 and further stabilized by a salt-bridge between R118 and D176 (Weaver et al., 2001). Biotinyl-5'-AMP is then transferred to a lysine residue of the substrate.

The mutation of arginine 119 to glycine (R118G, from now on denoted as BirA*) results in a higher dissociation rate of biotinyl-5'-AMP (Kwon & Beckett, 2000), while it also blocks the protein from binding DNA. Furthermore, this variant showed a high level of promiscuous protein biotinylation in a proximity dependent manner (Choi-Rhee et al., 2008). A study in mammalian cells determined the practical labeling radius of BioID to be around 10 nm (D. I. Kim et al., 2014), dependent on exposure time. Fusion of BirA* to a protein of interest ('bait') therefore results in covalent biotinylation of all proteins in the immediate vicinity. These proteins can then be isolated using either antibodies

4. Results

against either biotin or streptavidin laced columns and are identified by mass spectrometry.

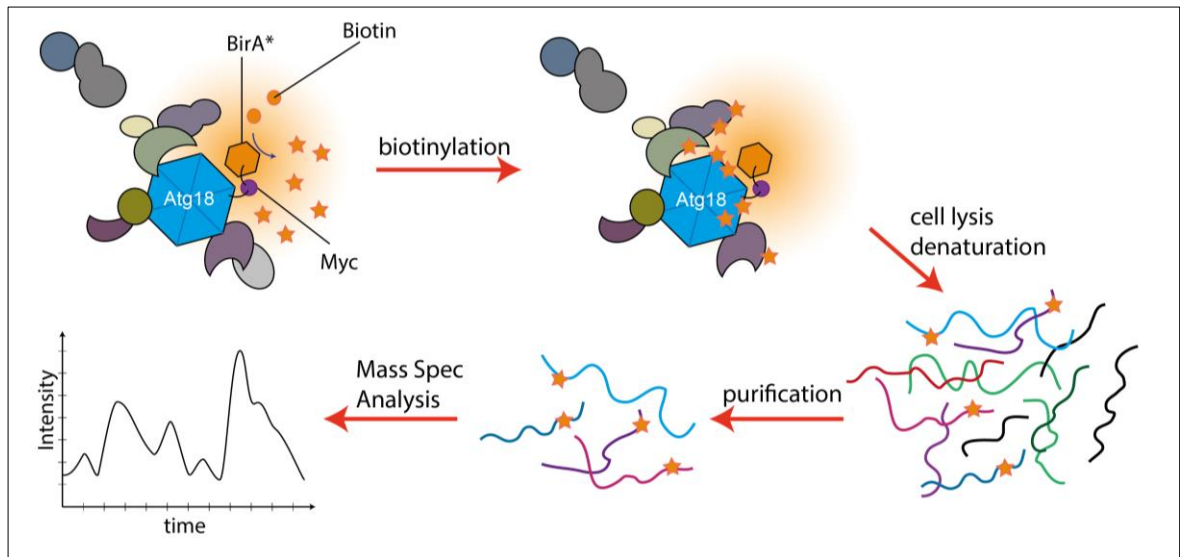


Figure 4-1: Schema for a proximity-based labeling assay.

Modified *E.coli* biotin ligase BirA* fused to the protein of interest (bait) activates biotin, which is released and can bind to accessible lysine residues of neighboring proteins. These proteins are denatured during cell lysis and purified using StrepTag columns with a high affinity towards biotin (affinity chromatography). Purified biotinylated proteins are then digested with trypsin and the peptides are identified with LC-MS.

4.1.1. Preliminary experiments

Atg18 was chosen as 'bait' for this experiment. It was tagged with BirA* and a Myc epitope tag was added N-terminally of BirA* to determine expression levels.

The preliminary experiments for the BioID assay were performed to identify the fusion protein with the highest stability and functionality and optimize the conditions used for the large-scale experiment. Stability and performance of the fusion protein could be impaired by a tag, therefore C- and N-terminally tagged Atg18 was analyzed for its functionality and expression level. Autophagic activity was tested with an Ape1 maturation assay: the vacuolar aminopeptidase 1 accumulates in the cytosol and is then transported via an autophagic process to the vacuole, named cvt (cytosol to vacuole targeting) pathway (Klionsky et al., 1992; Scott et al., 1997). Here, the protein is processed from its inactive precursor form (pApe1) to its active mature form (mApe1). This results in a size shift, which can be detected after immunoblotting. Atg18 is essential for all forms of autophagy, which includes the Cvt pathway (Barth et al., 2001). pApe1 and its maturation rate can therefore be used to determine the functionality of Atg18 fusion constructs in autophagy.

4. Results

Figure 4-2A shows almost no difference in the functionality of the two different fusion proteins: after 4h of starvation, nearly 100% of Ape1 is detected in its mature form in both Myc-BirA*-Atg18 and Atg18-Myc-BirA* expressing cells (see Figure 4-2B). Therefore, the location of the BirA* tag at either the C- or the N-terminus of Atg18 does not influence the function of the propeller in autophagy.

The functionality of some proteins is compromised by overexpression. For this reason, the Ape1 assay was performed with different concentrations of methionine in the medium to rule out a defect in Atg18 function if overexpressed under the control of a *MET25* promotor. A completely induced *MET25* promotor (no methionine in the medium) seems to slightly improve Ape1 maturation in non-starved cells, while no difference could be observed under starvation. This indicates a better performance of the fusion protein if overexpressed.

Figure 4-2C shows the expression levels of both constructs as well as BirA* alone at different methionine concentrations. All three bands were detected at the correct size, which indicates functioning expression and folding. Cells grown in CM medium without methionine expressed increased levels of fusion protein compared to medium supplemented with 0.3 mM methionine. This was as expected since the BirA* constructs were expressed with a *MET25* promotor, which is inhibited in the presence of methionine. Higher amounts of BirA* should result in a higher biotinylation rate of proteins in the vicinity of Atg18. This allows for the identification of highly dynamic interaction partners. Therefore, medium without methionine was chosen for the BioID assay in combination with the SILAC approach.

Both N- and C-terminally tagged Atg18 are active in the autophagic process, as the maturation rate of Ape1 was nearly at 100% for both proteins (Figure 4-2A,B). To select the optimal bait and test the premise a small scale BioID was performed. Atg2 is an already well-known interaction partner of Atg18 and forms a stable complex with the PROPPIN. It should therefore be biotinylated in the presence of BirA* tagged Atg18. Atg2 was tagged with a 3xHA epitope tag and expressed with both fusion proteins as well as Myc-BirA* as a control. All three constructs biotinylated proteins which were then isolated with a streptavidin column (Figure 4-2D). Only the full fusion proteins however precipitated together with the HA tagged Atg2 (Figure 4-2E), which proves the biotinylation of Atg2 dependent on the BirA* tagged Atg18. Decoration of the blot

4. Results

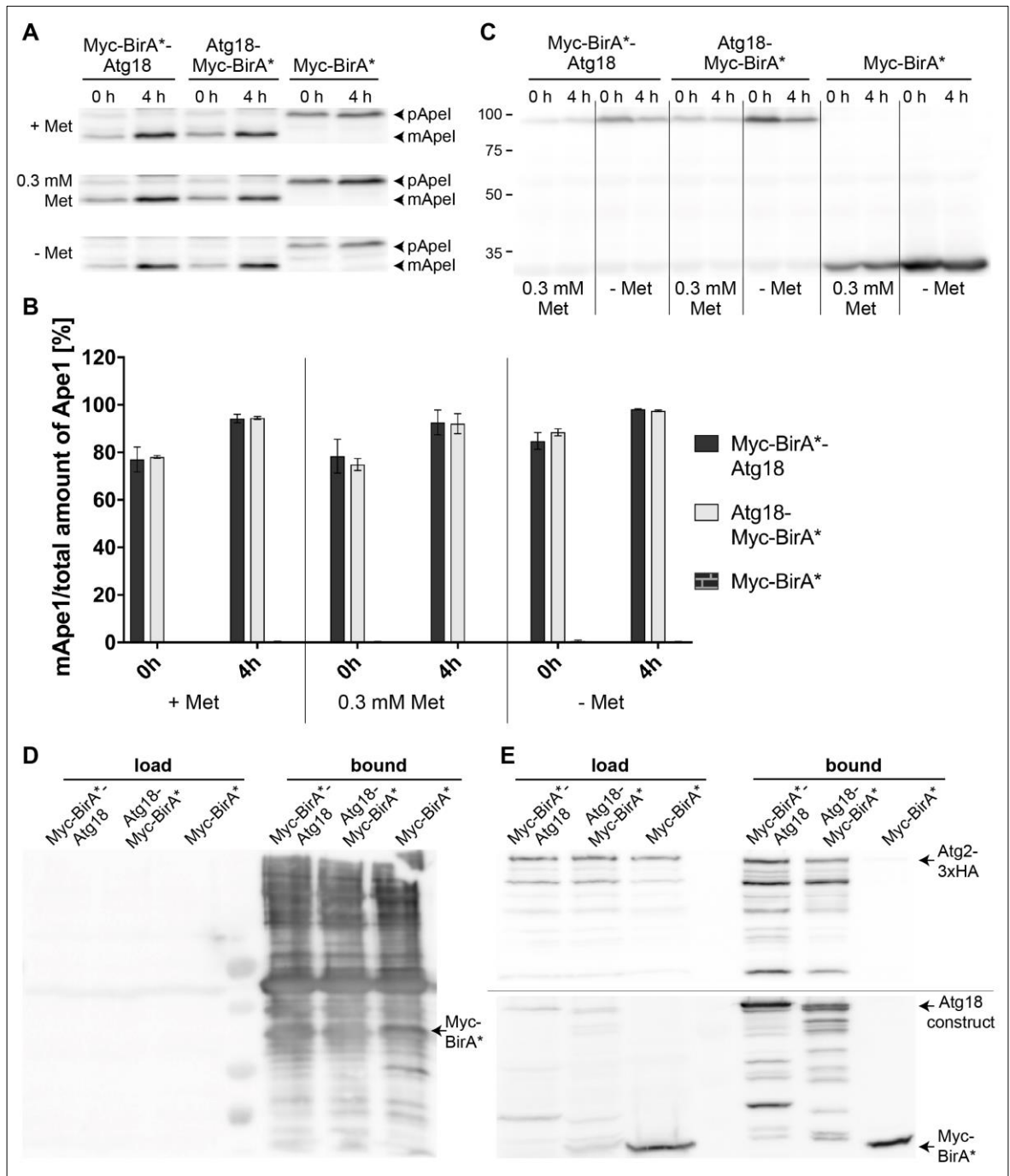


Figure 4-2: Preliminary experiments for BioID.

(A) Ape1 assay to determine the function of BirA* fusion proteins - *atg18Δ* strains expressing the constructs were grown at different methionine concentrations, harvested and alkaline lysed. Western Blots were decorated with antibodies against Ape1. **(B)** Quantification of Ape1 maturation rate (mApe1 to the total amount of Ape1) was measured in three independent experiments. Statistical relevance was determined with one sample t-test. **(C)** To determine expression levels of the fusion protein at different methionine concentrations cells were grown and treated as in (A), Western Blots were decorated with antibodies against Myc epitope. **(D + E)** A small scale BioID was performed to test the functionality of the fusion constructs with a known interactor of Atg18. Cells expressing the BirA* constructs together with Atg2-3xHA were grown in selection medium supplemented with biotin, harvested at OD₆₀₀ 4 and lysed. Cell lysate was loaded on a StrepTactin column to isolate biotinylated proteins. Blots were decorated with antibodies against biotin (StrepTag-HRP conjugate) **(D)** and HA and Myc, respectively **(E)**.

with antibodies against myc showed successful isolation of all three BirA* constructs, which is caused by self-biotinylation (depicted in Figure 4-2E, lower panel). It was

4. Results

concluded that proteins interacting with BirA* tagged Atg18 are biotinylated and can be isolated and identified with a BioID assay.

The degradation pattern of both Myc-BrA*-Atg18 and Atg18-Myc-BirA* suggest more stability for the N-terminally tagged protein, as less bands indicating degraded protein were detected after decorating the blot with antibodies against myc. It was therefore chosen for the following experiments.

4.1.2. BioID Results

Yeast cells have a relatively high background of naturally biotinylated proteins. To differentiate between those and proteins biotinylated by BirA* a SILAC (stable isotope labeling by amino acids in cell culture) approach was necessary (Ong et al., 2002). Here, stable isotope labeled amino acids added to the growth medium are transported into the cells and incorporated into proteins. Cells expressing the full construct, Myc-BirA*-Atg18, were grown in medium supplemented with 'light' amino acids (^{12}C L-Arg and ^{12}C ^{14}N L-Lys). Both control cultures, cells expressing Myc-BirA* or were transformed with an empty vector, were cultivated in medium supplemented with 'medium' amino acids (^{13}C L-Arg and ^{13}C ^{15}N L-Lys) or 'heavy' amino acids (^{13}C ^{15}N L-Arg and 4,4,5,5 ^2H L-Lys), respectively. The amino acids can be identified and differentiated using mass spectrometry, allowing for direct comparison between three different cultures and therefore three different strains. A strain with wildtype *ATG18* was chosen to reveal unspecific enrichments and naturally biotinylated proteins and a strain expressing only Myc-BirA* was used to eliminate unspecific BirA* dependent biotinylation.

The raw data obtained with the LC-MAS were subjected to database searches using the MaxQuant software and identified proteins were filtered according to relative enrichment from the strain expressing the full construct to the controls using the Perseus software (described in (Opitz et al., 2017)). Proteins enriched in the strain expressing the full construct, but not in either of the control strains, are in close proximity to Atg18 and could very well be previously unidentified interaction partners. To count as a hit or candidate, an enrichment of more than 20% compared to the controls had to be detected in at least two of three samples, show in in Figure 4-3A. Ticked lines are added at $\log_2 = 0.26$ (120%), everything to the right of the vertical line and on top of the horizontal line is enriched compared to the controls.

4. Results

Atg18 is a very prominent hit, it is highly enriched compared to both controls. This was expected since BirA* also biotinylates the protein it is fused to and Atg18 should therefore contain multiple biotinylation sites. All three known interactors, Atg2, Fab1 and Vac14, were also detected in at least two of three samples (shown in Figure 4-3A). This suggests a high success rate for this specific experiment.

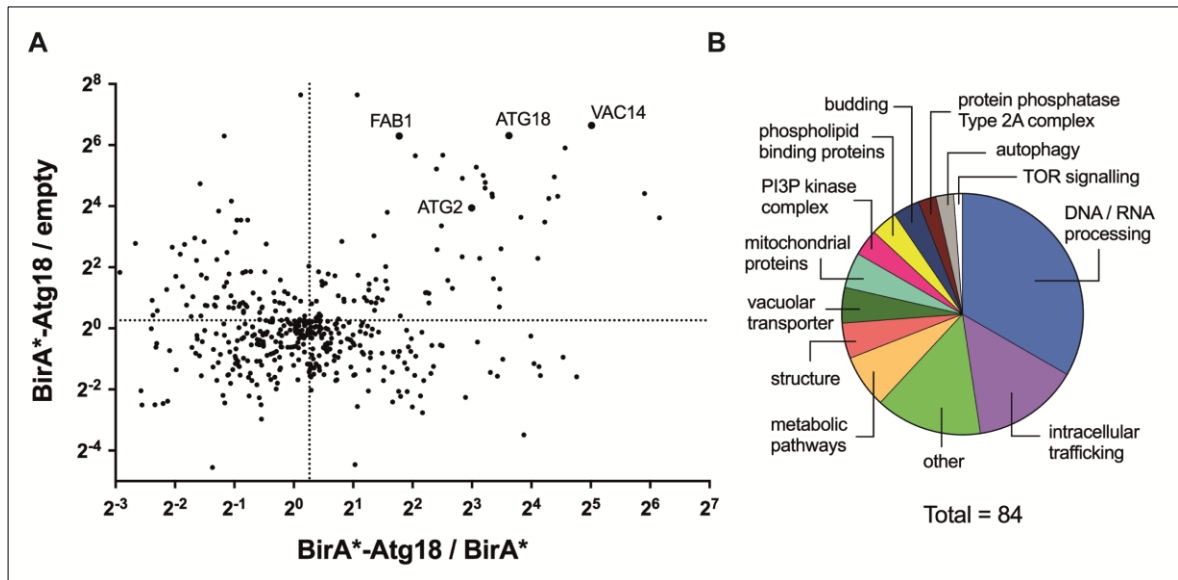


Figure 4-3: Results of the BioID performed to identify additional interaction partners of Atg18

(A) Scatter plot of all proteins identified in the BioID assay, with the signal ratio of BirA*-Atg18 to wt-Atg18 plotted against the signal ratio of BirA*-Atg to BirA* alone. Lines indicate the threshold of significance at 20% enrichment compared to the control (120% corresponds to a log₂ SILAC ratio of 0.26). **(B)** All 84 identified candidates were sorted according to their function.

Around 20% of all detected candidates are involved in DNA or RNA processing (see Figure 4-3B), several subunits of ribosomes were identified. Biotinylation probably occurred during the process of translation and can be seen as background. Comparing the results of the complete fusion protein to BirA* alone should have eliminated these hits. However, it probably took longer to synthesize the full Myc-BirA*-Atg18 compared to just Myc-BirA*. This could explain the relatively high amount of biotinylated proteins that are part of DNA or RNA processing detected among the enriched candidates. It could also indicate an involvement of Atg18 in ribophagy. Several of the identified proteins were located at the vacuolar membrane such as the vacuolar transporter Vtc3 or Avt4, or phospholipid binding proteins like Pib2. A list of the most promising candidates can be seen in Table 4-1. Here, a ranking was attempted based on detection of biotinylation site(s), the enrichment compared to the controls and the number of unique peptides identified.

4. Results

Apart from Atg18, biotinylation sites for two other proteins were identified, namely Snx3 and Ykt6. Snx3 is a sorting nexin (SNX) and forms a complex with the retromer components Vps26, Vps29 and Vps35 (Lucas et al., 2016). The last protein was also detected in the BioID assay as an interactor of Atg18. The retromer complex together with Snx3 is involved in the retrieval of late Golgi resident membrane proteins from endosomes or vacuole (Ma & Burd, 2020; Voos & Stevens, 1998) and is discussed in more detail in chapter 4.2.

Ykt6 is an essential SNARE functioning in the yeast secretory pathway (McNew et al., 1997). It participates in retrograde transport to the cis-Golgi as well as membrane traffic to the vacuole and vacuolar fusion (Kweon et al., 2003). Recently, it has also been implied in autophagosome fusion with the vacuole (Bas, Papinski, Licheva, et al., 2018). The BioID assay clearly hints toward an interaction between the SNARE and Atg18, which could occur at the vacuolar membrane or the pre-autophagosomal membrane or both.

Table 4-1: List of the most interesting BioID hits

gene	biotin sites	BirA*- Atg18/Bira*	BirA*- Atg18/empty	unique peptides	Coverage [%]
ATG18	4	12.3	79.4	26	67,8
SNX3*	1	4.2	26.8	4	30,9
YKT6*	1	2.1	3.4	13	79
VAC14		32.3	99.9	9	16,2
YCK3*		71.3	12.3	8	21,2
SAP155*		23.7	59.8	7	7,8
VPS35*		9.3	24.1	8	11,3
PIB2*		5.7	50	9	23,8
VTC3*		6.7	14.1	15	20,6
FAB1		2.6	52	4	1,8
SEC4*		14.2	12.5	2	10,4
SNF7*		6.9	2.1	4	19,6
CDC48*		2.6	8.2	11	18,4
AVT4*		9.1	32.2	2	3,9
ATG2		8	15.4	4	3,3

Yck3 is a membrane associated casein kinase I isoform in yeast (Wang et al., 1996). It is involved in vacuolar fusion, where it negatively regulates the HOPS tethering complex. The HOPS complex associates with the GTPase Ypt7 in its GTP bound form to

4. Results

establish fusion at the vacuole (Cabrera et al., 2009; LaGrassa & Ungermann, 2005; Seals et al., 2000; Sun et al., 2004).

Sap155 (Sit4p associated protein 155) is a regulatory subunit of the type 2A-related phosphatase Sit4 (suppressor of initiation of transcription) (Arndt et al., 1989; Luke et al., 1996). The phosphatase is required for different steps of the eukaryotic cell cycle, for example, execution of Start and bud formation (Sutton et al., 1991) and acts downstream of the TOR signaling complex (Di Como & Arndt, 1996).

Snf7 is a subunit of the ESCRT-III complex and involved in protein sorting into the MVB pathway ((Babst et al., 2002), reviewed in (Piper & Katzmann, 2010)). Snf7 was recently suggested to function in autophagy: deletion of SNF7 resulted in a complete autophagic defect (Zhou et al., 2019).

4.1.3. Autophagic and endosomal interactions

Two distinct functions of Atg18 are known: it is essential for autophagy and in maintaining vacuolar morphology. The original aim of this thesis was to differentiate the two processes and identify proteins selective for one process. A second BioID was performed to achieve this. Atg18 binds to PtdIns3P, which is primarily detected at the preautophagosomal membrane, and PtdIns(3,5)P₂, which is synthesized at the endosome and the vacuolar membrane. PtdIns 3-kinase activity at the IM is dependent on Atg14 (see chapter 2.3.5.2), while Vps38 does not affect autophagy. However, transport and sorting of vacuolar proteins such as CPY are defective in *vps38Δ* but not in *atg14Δ* (Kihara et al., 2001). Deletion of *ATG14* should therefore redirect most if not all of Atg18 to the vacuolar and endosomal membrane, while most Atg18 should localize to the preautophagosomal membrane in a *vps38Δ* strain (see Figure 4-4).

A BioID assay combined with the SILAC approach can then be utilized to identify proteins enriched in an *atg14Δ* strain (Atg18 mostly at the endosomes) compared to a *vps38Δ* strain (Atg18 mostly at the autophagosome). Strains expressing Myc-BirA*-Atg18 and with either a deletion of *ATG14* or *VPS38* were compared to a wildtype strain expressing Myc-BirA*. Since the SILAC approach allows for three different conditions only one control could be done. Therefore, filtering out background hits was not as rigorous as before and the results are not as reliable.

Proteins enriched in *vps38Δ* but not in *atg14Δ* are expected to interact with Atg18 at the PAS or autophagosome (Figure 4-5, upper left quadrant). Candidates which are

4. Results

more involved with endosomal functions should be enriched in an *atg14Δ* strain (Figure 4-5, lower right quadrant).

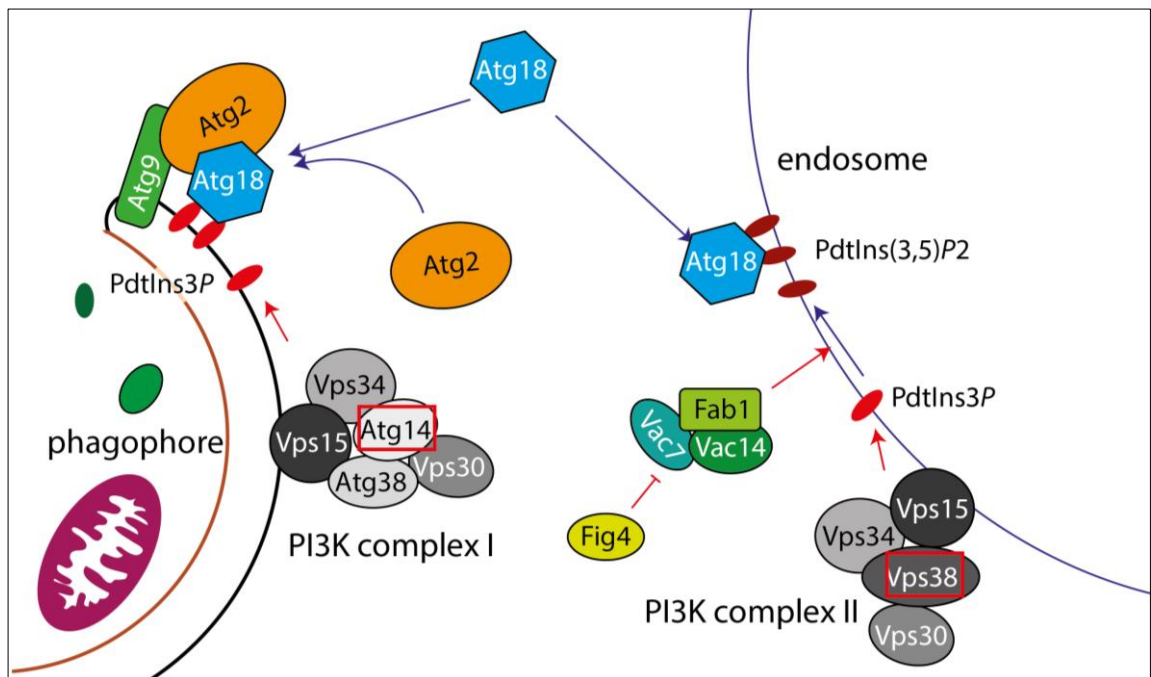


Figure 4-4: Membrane recruitment of Atg18 depends on two PtdIns 3-kinase complexes.

PI3 kinase complex I contains Vps34, Vps15, Vps30, Atg38 and Atg14. It functions at the growing IM / phagophore, where it phosphorylates PtdIns. PI3-kinase complex II catalyzes the same reaction at endosomes. PtdIns3P is then transported to the vacuolar membrane after the endosome fuses with the vacuole. Unlike the first complex PI3KCII does not contain Atg14 but Vps38.

Interestingly, Atg2 is enriched in both strains, as depicted in Figure 4-5. One explanation for this result could be the formation of a cytosolic Atg2-Atg18 complex, which is not dependent on membrane association of Atg18. Furthermore, it was shown that Atg2 is able to recruit Atg18 to the membrane. This enables Atg18 to localize to the autophagosomal membrane, even with decreased levels of PtdIns3P. This further relativizes the results for other proteins identified as enriched in both strains, as predominantly autophagic related candidates are also enriched in *atg14Δ* strains. Both the kinase Yck3 and the ESCRT-III subunit Snf7 were also enriched in both strains, which could suggest a role in autophagy as well as endosomal trafficking (Figure 4-5). The vacuolar SNARE Ykt6 was not enriched in the *vps38Δ* strain, implicating its interaction with Atg18 occurred mainly at the vacuolar or endosomal membrane. This is similar to Vps35 and Snx3, as both were enriched in an *atg14Δ* strain, but not in the *vps38Δ* strain. This suggests a role in the endosomal pathway but not in autophagy.

4. Results

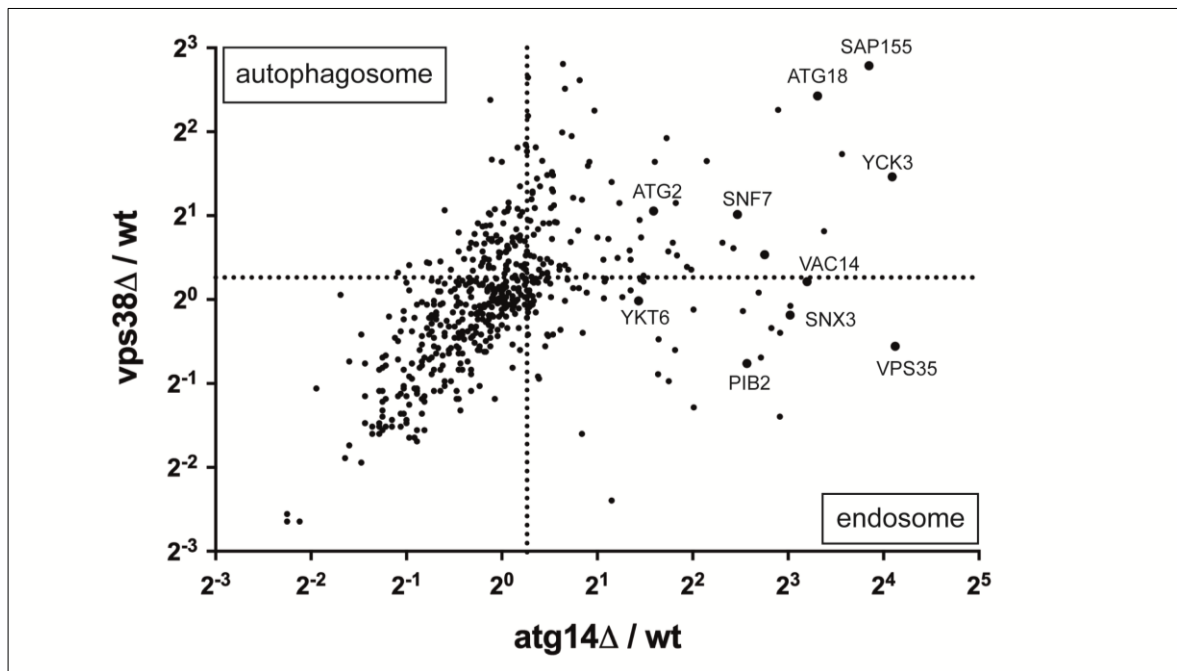


Figure 4-5: BioID to distinguish between endosomal and autophagic interaction partners.

Scatter plot of all proteins identified in the BioID assay, with the ratio of signal in *vps38Δ* to wildtype plotted against the ratio of signal in *atg14Δ* to wildtype. Proteins depicted in the upper left quadrant are enriched in a strain able to perform autophagy, while proteins in the lower right quadrant are involved in endosomal/vacuolar processes.

The accuracy of this method is a big issue and any conclusions have to be carefully considered. PtdIns concentrations are very fluid and dependent on several kinases and phosphatases. PtdIns3P is transported to the vacuole during autophagy, independent of Vps38 function. They can also be generated by dephosphorylation of other PtdInsPs at the endosomal or vacuolar membrane. It is therefore not possible to completely exclude the possibility of remaining PtdIns3P or PtdIns(3,5)P₂ at the pre-autophagosomal or endosomal membrane, respectively. Atg18 is also able to interact with the peripheral membrane protein Atg2, which further complicates the matter. Conclusions from this experiment are more speculation than fact, with one exception: It further confirms the previously identified candidates Sap155, Yck3, Vps35, Snx3, Pib2, Ykt6 and Snf7 as interaction partners of Atg18.

4.1.4. Validation of BioID candidates

Although the BioID assay was shown to reliably detect known interactors of Atg18, previously unknown binding partners of Atg18 should be validated by independent means. In order to confirm the interaction of At18 with candidates detected in the BioID assay (see chapter 4.1.2), Co-IPs were carried out. This was performed with all candidates listed in Table 4-1, with the exception of the already known interactors of

4. Results

Atg18, namely Fab1. Atg2 was chosen to serve as a control in the CoIP experiments. Although interaction with Vac14 was previously confirmed with a Two-hybrid assay Co-IPs with both proteins were never successful (Jin et al., 2008).

All Co-IPs were performed with GFP tagged Atg18 as bait and HA-tagged candidates as prey. For their detection in western blot, all non-essential genes were chromosomally tagged with a C-terminal 6xHA epitope tag. Essential genes, *SEC4* and *YKT6*, were cloned together with their endogenous promotor on a low-copy plasmid and the tag was inserted between promotor and gene. To test the expression levels of the HA tagged genes cultures inoculated with the new strains were grown to stationary phase, harvested and alkaline lysed. The blots were decorated with antibodies against HA and are shown in Figure 4-6.

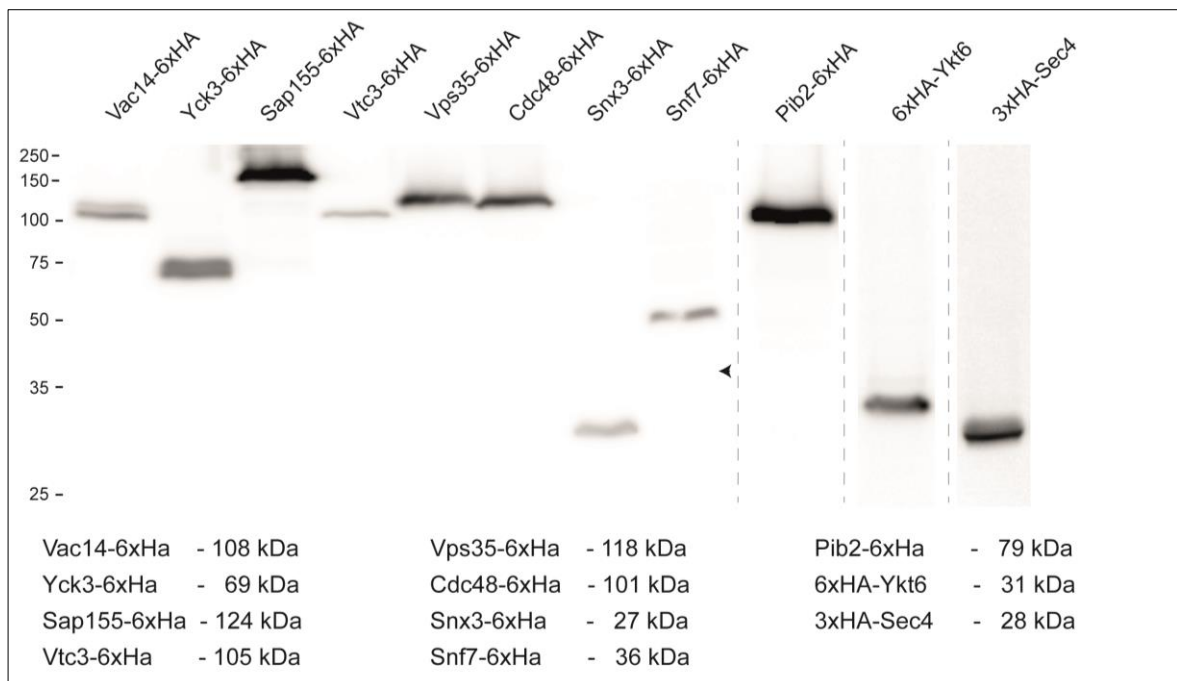


Figure 4-6: Expression level and protein size of HA tagged BioID candidates-

Candidates were tagged with a C-terminal 6xHA epitope and expressed from the chromosome, with the exception of Ykt6 and Sec4. The essential genes were tagged at the N-terminal and expressed from a plasmid. Cells were grown in selection medium to a stationary phase (OD_{600} 4-5), harvested and alkaline lysed. Western blots were decorated with antibodies against HA. An arrow indicates the expected size for Snf7-6xHA.

All expressed 6xHA fusion proteins were detected in the expected molecular weight range, except for Snf7-6xHA, and showed reasonable expression levels, with the exception of Avt4-6xHA. The band for Snf7p was detected at 50 kDa in all of the tested clones, while the molecular size was calculated as 36 kDa (shown in Figure 4-6, arrow indicate expected position). A control PCR of the gene however generated a PCR

4. Results

product of the correct size. Therefore, Snf7-6xHA was included in the following experiments.

The faint signal observed for the vacuolar transporter Avt4 could either be caused by a very low expression level or difficulties with isolation from the membrane during cell lysis. Due to the problem of detecting Avt4-6xHA experiments with the protein were discontinued.

4.1.4.1. GFP-Traps with endogenous promotor

Co-IPs were performed with the μ MACS system from Miltenyi Biotec. The 6xHA tagged candidates chosen from the candidates detected with the BioID assay (see previous chapter) were expressed together with either Atg18-GFP or GFP alone as a control from a low copy plasmid under the control of an *ATG18* promotor. Cells were grown to OD₆₀₀ 2-3, harvested and processed according to the protocol for Co-IPs (see chapter 3.2.3.2). The first Co-IPs with endogenously expressed Atg18 were performed with lysis buffer and wash buffer provided by the manufacturer.

To verify the functionality of the μ MACS system for this specific approach and establish a working protocol the well-known interactor Atg2 was chosen as a control. The HA-tagged protein co-precipitates with Atg18-GFP but not with GFP alone, as can be seen in Figure 4-7. This establishes a well performing protocol for coimmunoprecipitating the known interactor Atg2 with Atg18 and was now used to test all other candidates from the BioID assay (see Table 4-1, candidates marked with an asterisk). From these, only Sap155 and Vps35 could be detected in the bound fraction of Atg18-GFP but not in the control (see Figure 4-7).

Pib2, Sec4 and Yck3 co-precipitated with Atg18-GFP, but also with GFP alone (data not shown), indicating unspecific binding of the proteins to the beads. Repeating the experiment with slightly harsher washing conditions (SDS added to a final concentration of 0.05% (w/v)) to break the unspecific binding resulted in a complete loss of bound protein. The other tested proteins did not show any binding to Atg18-GFP or GFP alone (data not shown).

The logical next step was to further improve the experimental set up in order to stabilize the complexes and therefore enable co-immunoprecipitation with the bait.

4. Results

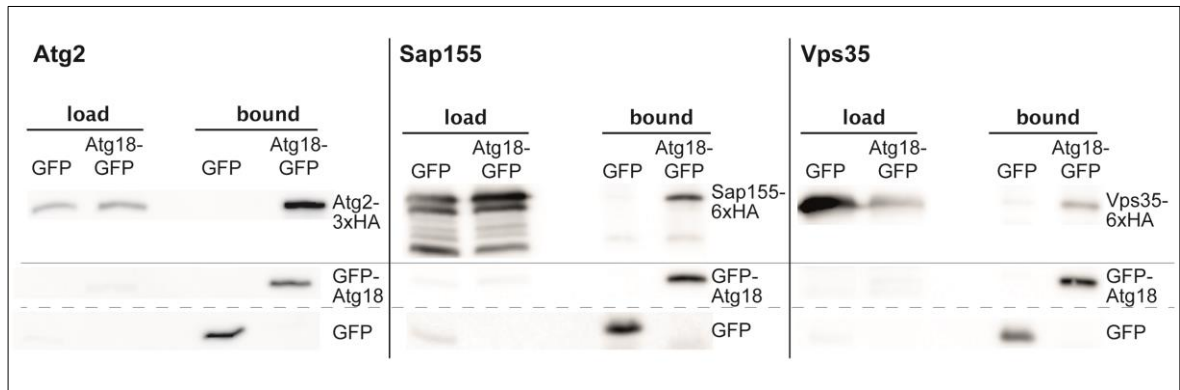


Figure 4-7: Both Vps35 and Sap155 co-precipitate with Atg18 at endogenous levels.

Co-IPs were performed with *atg18Δ* strains expressing HA tagged prey from the chromosome (Atg2-3xHA, Sap155-6xHA or Vps35-6xHA) together with GFP tagged bait (GFP of Atg18-GFP) expressed from plasmids at similar levels from an *Atg8* and *Atg18* promoter, respectively. Cells were grown in selection medium to an OD_{600} of 2-3, harvested and processed according to the manufacturer's protocol and with lysis buffer and wash buffers provided with the kit. Load and bound samples were analyzed with a Western blot decorated with antibodies against HA and GFP.

4.1.4.2. GFP-Traps with overexpressed Atg18

Cell lysis is mostly a harsh process and more fragile complexes are destroyed before they can be isolated and analyzed. One way to circumvent this is the *in vivo* introduction of chemical links between proteins in a complex that survive cell lysis and prevents the complex from breaking apart. One such chemical reagent is DSP (Dithiobis (succinimidylpropionate)), which forms covalent amide bonds between primary amines. It is lipophilic and membrane-permeable and can be used to stabilize intracellular complexes. Since the chemical is unable to pass the yeast cell wall it has to be removed prior to incubation with DSP. This can be achieved by spheroplastation, a process in which the cell wall is enzymatically degraded. However, this approach did not improve the amount of Vps35 detected in the bound fraction of Atg18-GFP (data not shown) and was therefore discarded.

A second potential improvement was the overexpression of N-terminally tagged Atg18 with a *MET25* promoter in combination with the adaptation of lysis and washing conditions. Although the GFP-tag does not seem to affect the autophagic activity of Atg18, it does perhaps interfere with binding to different interactors. Therefore, N-terminally tagged GFP-Atg18 was chosen as bait in the following experiments instead of the C-terminally tagged Atg18-GFP previously used.

To validate the conditions chosen for the new experimental set-up the already confirmed interactor Vps35, chromosomally tagged with a 6xHA epitope tag, was included in the performed experiments. The signal of Vps35-6xHA detected in the

4. Results

bound fraction was improved compared to the previous experiments, as can be seen in Figure 4-8. Furthermore, the known interactor Vac14 could also be shown to co-precipitate with GFP-Atg18 (Figure 4-8). Remarkably, an interaction between the two proteins was so far only demonstrated by yeast two-hybrid studies, but could not be reproduced in co-immunoprecipitation experiments (Jin et al., 2008).

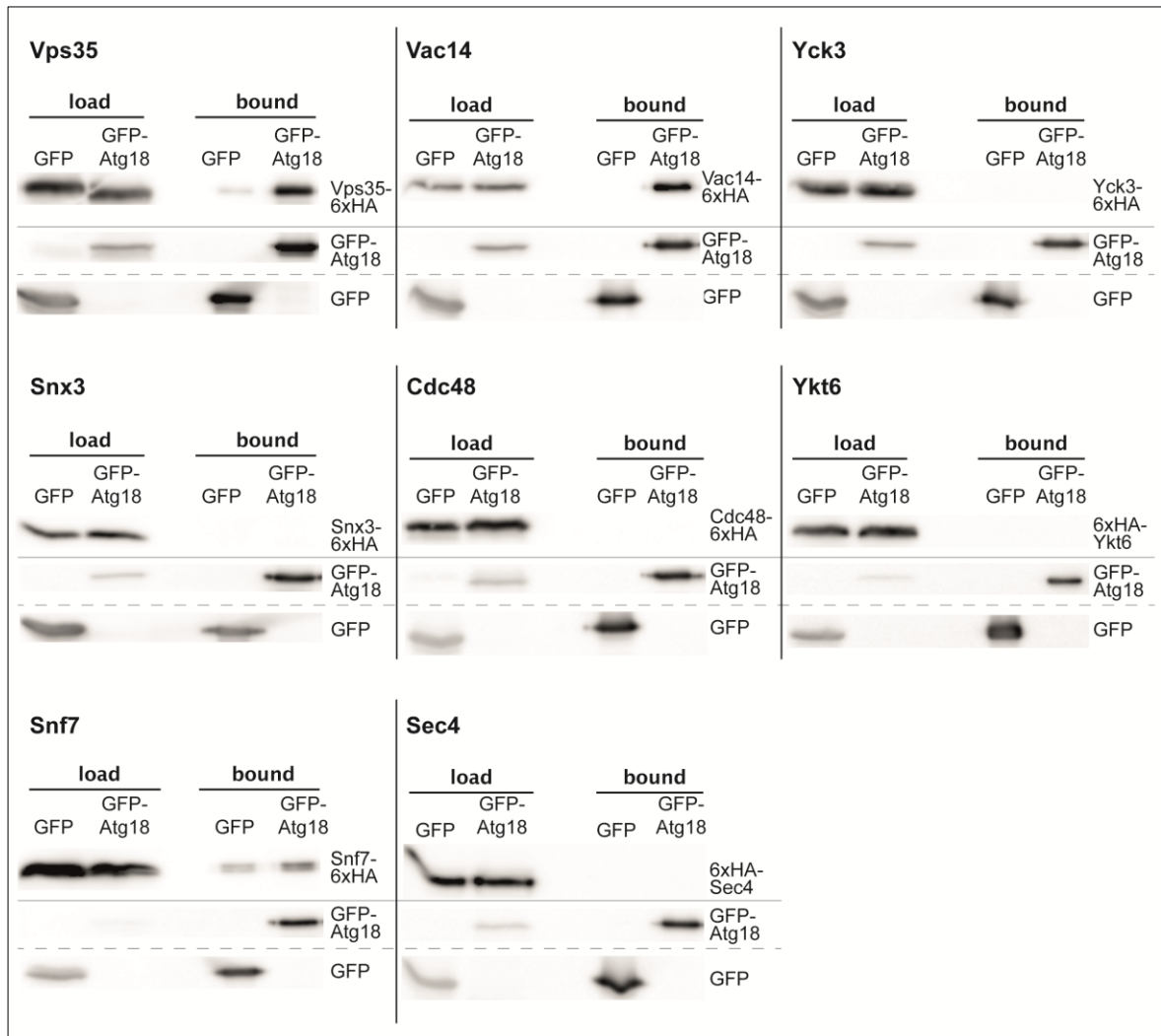


Figure 4-8: Overexpression of Atg18 with a *MET25* promotor improves co-immunoprecipitation.

Co-IPs were performed with *atg18Δ* strains expressing C-terminally 6xHA tagged prey from the chromosome (Vps35, Vac14, Yck3, Snx3, Cdc48, Snf7) or N-terminally 6xHA tagged prey from a plasmid (Ykt6, Sec4) together with GFP tagged bait (GFP of Atg18-GFP) expressed from plasmids with a *MET25* promotor. Cells were grown in selection medium supplemented with 0.3 mM methionine to an OD_{600} of 2-3, harvested and processed according to protocol. Load and bound samples were analyzed with a Western blot decorated with antibodies against HA and GFP.

The improved experimental set-up was used to test all previous candidates, with the exception of the vacuolar transporter Vtc3 and Sap155, the latter of which was previously confirmed. The signal for Vtc3 was very faint, similar to the other vacuolar transporter Avt4 and the protein was therefore not included in the following experiments.

4. Results

Snf7-6xHA was found in the bound fraction of GFP-Atg18 but could also be detected in the control although slightly weaker. Harsher conditions to stop unspecific binding (higher concentrations of detergent in the wash buffer) resulted in a complete loss of the signal in the bound fractions (data not shown). Either the observed binding of Snf7 in the first experiment was completely unspecific or the interaction was too fragile to survive the washing conditions used in the second experiment. The difference between observed and calculated molecular weight of the protein could also be an explanation: it could be caused by a mutation in the stop codon, resulting in an additional non-functional tag or domain hindering interaction with other proteins.

Although the interaction of neither Snx3-6xHA nor 6xHA-Ykt6 with GFP-Atg18 could be confirmed with this approach a connection is still highly likely. Sec4, Yck3, Pib2 and Cdc48 could not be further confirmed with this experiment.

4.1.4.3. Effect of nitrogen starvation on binding

Starvation in nitrogen free medium (SD-N) activates macroautophagy. Autophagy activation might increase the interaction with GFP-Atg18 with candidates that are potentially involved in the process of autophagy. This could lead to an enhancement of the signal in the bound fraction of GFP-Atg18. Reversely, autophagy activation could also decrease the interaction of GFP-Atg18 with proteins not involved in autophagy due to its enhanced recruitment to the PAS. However, this effect is probably not as strong in this approach, since Atg18 is overexpressed and should be present in abundance.

Cultures of strains expressing HA tagged candidates and GFP tagged Atg18 were grown in selective medium to an OD₆₀₀ of 2-3, either directly harvested and either directly processed or transferred to SD-N and starved for 2h before processing. The Co-IPs were performed according to the protocol, with lysis and washing conditions as described in chapter 3.2.3.2.

Starvation had no effect on the interaction between GFP-Atg18 and Sap155-6xHA, as can be seen in Figure 4-9. The signal of bound Sap155-6xHA was neither increased nor decreased after 2h of starvation in SD-N.

4. Results

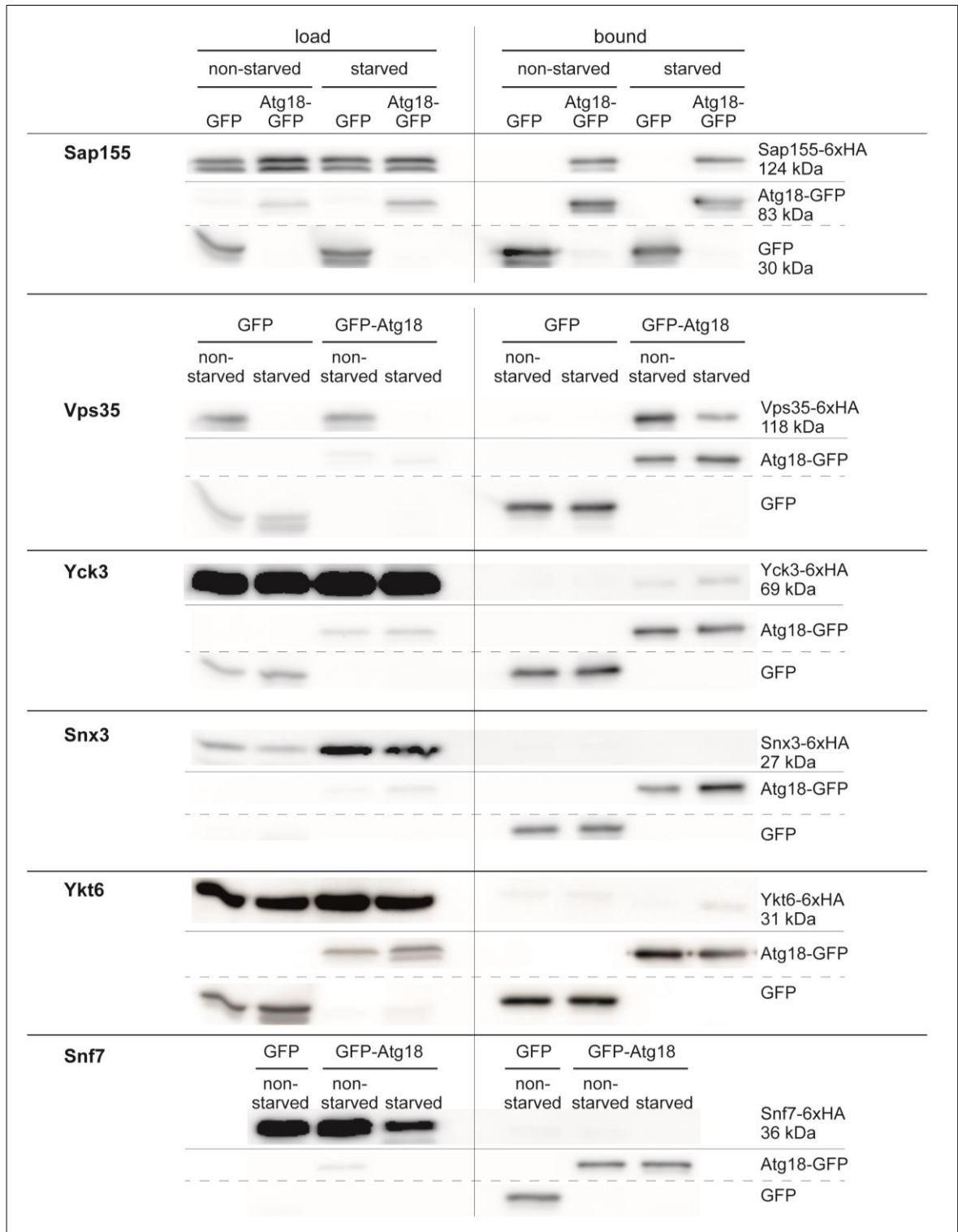


Figure 4-9: Effect of nitrogen starvation on binding to Atg18.

Co-IPs were performed with *atg18Δ* strains expressing C-terminally 6xHA tagged prey from the chromosome (Sap155, Vps35, Yck3, Snx3, Snf7) or N-terminally 6xHA tagged prey from a plasmid (Ykt6) together with GFP tagged bait (GFP or Atg18-GFP) expressed from plasmids with a *MET25* promoter. Cells were grown in selection medium supplemented with 0.3 mM methionine to an OD₆₀₀ of 2-3 and transferred to SD-N. Cells were harvested after 2h f starvation and processed according to protocol. Load and bound samples were analyzed with a Western blot decorated with antibodies against HA and GFP.

4. Results

Vps35 was degraded during autophagy since the signal in the load sample was consistently weaker after starvation. The amount of Vps35-6xHA found in the bound fraction of GFP-Atg18 remained the same or slightly reduced (Figure 4-9). However, compared with the strongly reduced concentration of Vps35-6xHA in the load sample affinity of Vps35-6xHA seems to be enhanced after two hours of starvation. This implies a function of the interaction between Vps35 and Atg18 more related to autophagy and less to endosomal trafficking.

An interaction could be detected for the casein kinase Yck3, which was not seen in previous experiments. The signal was enhanced after starvation, implying a function related to autophagy.

6xHA-Ykt6 showed weak binding after 2 h starvation, but the signal was only marginally stronger than in the control. Repetitions of the experiment could not reproduce the result and an interaction between Ykt6 and Atg18 could therefore not be confirmed.

Similar to previous experiments neither Snx3-6xHA nor Snf7-6xHA were detected in the bound fraction of GFP-Atg18. This does not imply a false positive for the BioID results. Many interactions and complexes are lost during cell lysis or protein purification, which was the main reason to perform a BioID approach. Not all of the results can therefore be validated with Co-IPs.

4.1.1. Autophagic activity

An involvement in autophagy cannot be excluded for any of the candidates, therefore the autophagic activity was analyzed in the absence of the candidates. For this, non-essential proteins identified in the BioID with the exception of vacuolar transporter Avt4 and Vtc3 were chosen (see Table 4-1).

An Ape1 maturation assay as described previously was done to determine if any of the discovered candidates function in autophagy. Strains from the Euroscarf collection containing deletions of the main BioID hits were grown to an OD₆₀₀ of 4, starved in SD-N for up to 4 h and analyzed for Ape1 maturation (see Figure 4-10A).

Most strains showed no effect in regards to autophagy: Ape1 was processed at the same rate in wildtype as in *sap155Δ*, *yck3Δ*, *snx3Δ* and *pib2Δ*. This does not exclude a function related to autophagy, as they could also be redundant and therefore non-essential.

4. Results

However, *vac14Δ* shows a strong phenotype in unstarved cells, which can be seen in Figure 4-10A: autophagic activity is significantly decreased compared to the wildtype. This effect is gone after 4h of starvation, the ratio of mature to premature Ape1 is similar to wildtype. This is surprising since Vac14 was not implicated in autophagy before. It functions as a regulator of Fab1, a PtdIns3P-kinase (see chapter 2.4.3) and is involved in vacuolar morphology (Dove et al., 2002).

Both Vps35 and Snf7 showed a significant reduction in autophagic activity compared to the wildtype in unstarved cells but also after 4h starvation in nitrogen free medium. Both proteins are involved in protein sorting: Vps35 is a subunit of the retromer complex and functions in retrograde transport of late-Golgi proteins (Seaman et al., 1997), while Snf7 is involved in protein sorting into the MVB pathway ((Babst et al., 2002), reviewed in (Piper & Katzmann, 2010)).

Cvt vesicle contain a large amount of Ape1 and one successful fusion with the vacuole causes a high ratio of mature to premature Ape1. An Ape1 assay is for this reason not a good quantitative measure of autophagic activity. Therefore, a free GFP assay was performed to further analyze strains with a mild autophagic phenotype. GFP-Atg8 is recruited to the PAS and stays at the autophagosome until it fuses with the vacuole. Here, vacuolar hydrolases break down the autophagic body and Atg8, but GFP cannot be degraded in the vacuole. The amount of GFP accumulated in the vacuole is therefore a quantitative measure of autophagic activity. GFP-Atg8 was expressed in BY strains deleted for either *VPS35*, *VAC14* or *SNF7* (Figure 4-10B). Cells were grown to log-phase, harvested and starved in SD-N according to the protocol used by (Zhou et al., 2019).

Although *vac14Δ* strains still demonstrated a mild decrease in autophagic activity, the difference to the wildtype was no longer significant. The reduced ratio of free GFP is probably a result of a disturbance in PtdInsPs metabolism as a consequence of improper Fab1 kinase function.

Cvt vesicle contain a large amount of Ape1 and one successful fusion with the vacuole causes a high ratio of mature to premature Ape1. An Ape1 assay is for this reason not a good quantitative measure of autophagic activity. Therefore, a free GFP assay was performed to further analyze strains with a mild autophagic phenotype. GFP-Atg8 is recruited to the PAS and stays at the autophagosome until it fuses with the vacuole.

4. Results

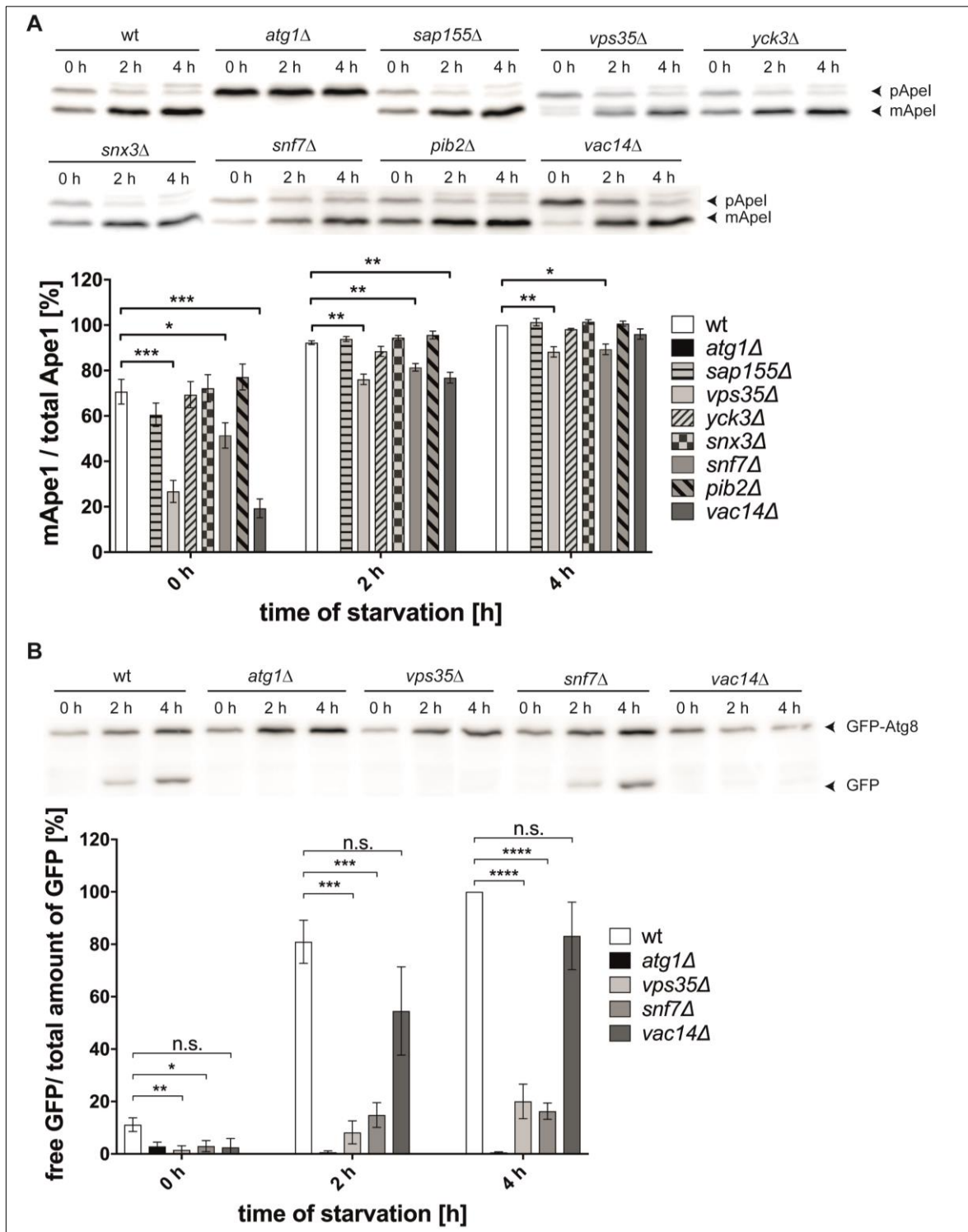


Figure 4-10: Autophagic activity in BioID candidate knockout strains.

(A) Ape1 maturation assay: Strains with a deletion in one candidate each were grown in CM to stationary phase (OD_{600} of 4) and transferred to SD-N. After starvation cells were harvested and alkaline lysed. **(B)** GFP assay: Strains with a deletion in one candidate each and expressing GFP-Atg8 from a plasmid were grown to mid-log phase (OD_{600} of 0.5-1) and transferred to SD-N. After starvation cells were harvested and alkaline lysed. Western blots were decorated with antibodies against GFP. Quantification of GFP-Atg8 degradation rate (free GFP to the total amount of GFP and GFP-Atg8) was measured in three independent experiments. Statistical relevance was determined with one sample t-test. 4 h sample of wildtype was set to 100%.

Here, vacuolar hydrolases break down the autophagic body and Atg8, but GFP is not degraded in the vacuole. The amount of GFP accumulated in the vacuole is therefore a

4. Results

quantitative measure of autophagic activity. GFP-Atg8 was expressed in BY strains deleted for either *VPS35*, *VAC14* or *SNF7* (Figure 4-10B). Cells were grown to log-phase, harvested and starved in SD-N according to the protocol used by (Zhou et al., 2019). Although *vac14Δ* strains still demonstrated a mild decrease in autophagic activity, the difference to the wildtype was no longer significant. The reduced ratio of free GFP is probably a result of a disturbance in PtdInsP metabolism as a consequence of improper Fab1 kinase function.

A significant decrease in autophagic activity was observed for cells with a deletion in *SNF7*, which is still detectable after 4h starvation. However, autophagy is not completely abolished as published by (Zhou et al., 2019). The effect is only detected in cells starved during the mid-log phase. Transferring stationary cells to SD-N causes a much weaker phenotype.

Deletion of *VPS35* impaired autophagy significantly, as can be seen in Figure 4-10B. This effect was stronger for the GFP assay compared with the Ape1 assay. This could partially be caused by the stage in which the cells were transferred to medium without nitrogen. *Vps35* was previously shown to negatively affect autophagic activity if deleted (Dengjel et al., 2012). Deletion of other retromer subunits such as *Vps29* lead to similar results, as did a knockout of the sorting nexins *Vps5* and *Vps17*. Both *Vps5* and *Vps17* are essential for several retromer mediated cargo transport. So far it is unknown if the reduced autophagic activity is a result of protein mislocalization at the endosomes or if the retromer complex is directly involved in autophagy. A study done in mammalian cells with a mutated version of *Vps35* (*VPS35* D620N, found in patients with Parkinson's disease) described a defect in ATG9A cycling, caused by weakened binding of the mutated *Vps35* to the WASH complex (Zavodszky et al., 2014).

4. Results

4.1.2. Vps35 colocalizes with Atg18

The strongest interaction with Atg18 could be detected for Sap155, Vps35 and Vac14. However, since the complex containing Atg18 and Vac14 was already published (Botelho et al., 2008; Jin et al., 2008), it was not chosen for further experiments.

Cell lysis is a necessary step for Co-IPs, which naturally destroys separating compartments in the cell. Furthermore, the conditions necessary for cell lysis differ from the normal intracellular environment and abnormal protein interaction could be a result. Therefore, location of both Sap155 and Vps35 in relation to Atg18 in the living cell were determined to further confirm the interaction.

Both Sap155 and Vps35 were chromosomally tagged with mCherry and expressed together with Atg18-GFP under the control of an *ATG18* promoter from a low copy plasmid. The cells were grown to different ODs (between 3-4 and 5-6) and analyzed with fluorescent microscopy (Figure 4-11A). The signal for Sap155 was very weak and mostly distributed in the cytosol. A version tagged with the brighter GFP was also examined but showed the same results: a diffuse signal in the cytosol. It was not possible to quantify colocalization or the lack thereof with Atg18.

Vps35-mCherry was localized to puncta in the periphery of the cell, very likely endosomes, as expected. Around 40% of all Atg18 dots colocalized with Vps35-mCherry in cells with an OD₆₀₀ between 3 and 4, as shown in Figure 4-11B. Less colocalization was observed in cells with higher ODs. Cells at OD₆₀₀ between 5 and 6 are already in the later stages of growth, with scarce nutrients. Activation of autophagy recruits more Atg18 to the PAS and reduces the endosomal pool.

Vps35 was identified as an interactor of Atg18 in the BioID assay and further validated by Co-IP and fluorescent microscopy. It is known to form a complex with Snx3, which was also detected in the BioID and contained one identified biotinylation site. Deletion of *VPS35* severely impacts autophagic activity. For all these reasons it was chosen for further analyses.

4. Results

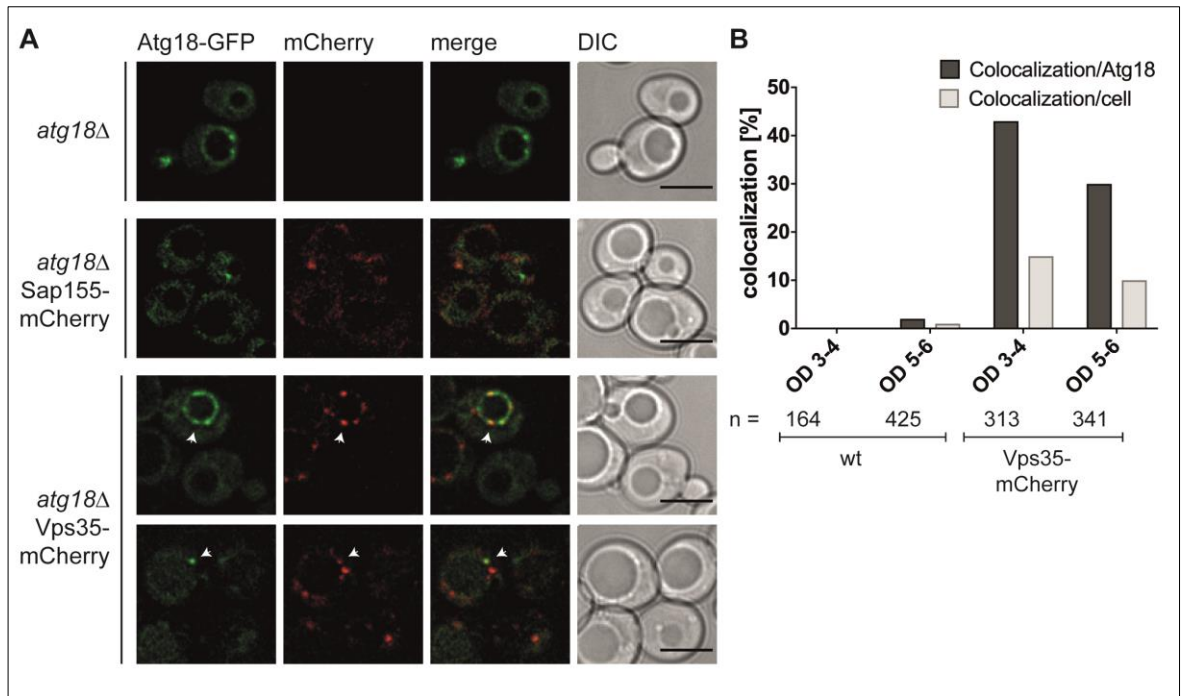


Figure 4-11: Co-localization of Atg18 with Vps35 and Sap155.

Analysis of the localization of Sap155-mCherry and Vps35-mCherry using fluorescence microscopy. *atg18Δ* strains expressing either chromosomally tagged Sap155-mCherry, Vps35-mCherry together with Atg18-GFP with an endogenous promoter from a plasmid were grown in selection medium to a stationary phase (OD₆₀₀ 3-4) or late stationary phase (OD₆₀₀ 5-6) and analyzed with fluorescent microscopy. White arrows indicate a colocalization. The number of Atg18 punctae and the number of colocalizations of GFP and mCherry signal were counted. Scale bar is set to 5 μm.

4. Results

4.2. Vps35

Vps35 was first described in 1989 as a protein involved in vacuolar protein targeting (vpt) (Robinson et al., 1988) or sorting (vps) (Rothman et al., 1989). Its deletion leads to the mislocalization of several native vacuolar proteins such as the vacuolar

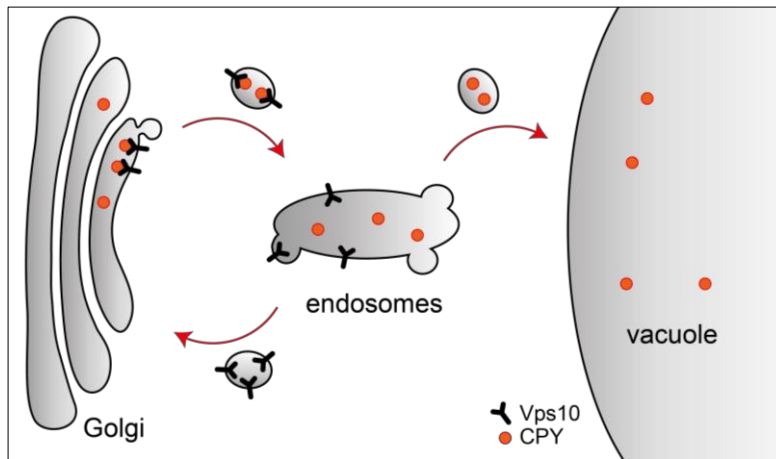


Figure 4-12: Model of Vps10 trafficking in yeast.

The Vps10 receptor binds CPY in its premature form in the late Golgi and transports it to the endosomes, where it dissociates. CPY is then delivered to the vacuole, while Vps10 is recycled to the Golgi by the retromer complex.

carboxypeptidase Y (CPY). The transport pathways involved in CPY sorting are shown in Figure 4-12. CPY is sorted into vesicles by the transmembrane receptor Vps10 and then trafficked to the late endosome and the vacuole. Vps10 is not delivered to the vacuole

but recycled from late endosomes to the Golgi. This process requires Vps35 and the retromer complex (Nothwehr et al., 1996). Several late Golgi membrane proteins have been identified to be retromer cargo (Ma & Burd, 2020). The complex is conserved across all eukaryotes, as most of the involved proteins have mammalian homologues, and mutations or deletions have been linked to severe neurodegenerative disorders such as Alzheimer's disease or Parkinson's disease (reviewed in (Abubakar et al., 2017)).

4.2.1. Vps35 binds to all PROPPINs

Atg18 shares many similarities with the two other PROPPINs, Atg21 and Hsv2. Although BioID assays with both Atg21 and Hsv2 did not identify Vps35 as a potential interactor a connection could not be excluded. Therefore, Co-IPs with HA tagged Vps35 and either GFP-tagged *ATG21* or *HSV2* expressed with a *MET25* promoter were performed. Initial experiments showed no binding (Atg21) or weak binding (Hsv2) compared to Atg18 (data not shown). After reducing the concentration of detergent in the wash buffer Vps35 co-precipitated with both Atg21 and Hsv2, although in lower amounts compared to Atg18 (see Figure 4-13A). The signal for GFP-Atg21 was also

4. Results

weaker than GFP-Atg18, indicating a similar binding affinity of both PROPPINs towards Vps35. The milder wash buffer was not able to remove all unspecific binding since the signal for Vps35 could also be detected in the controls.

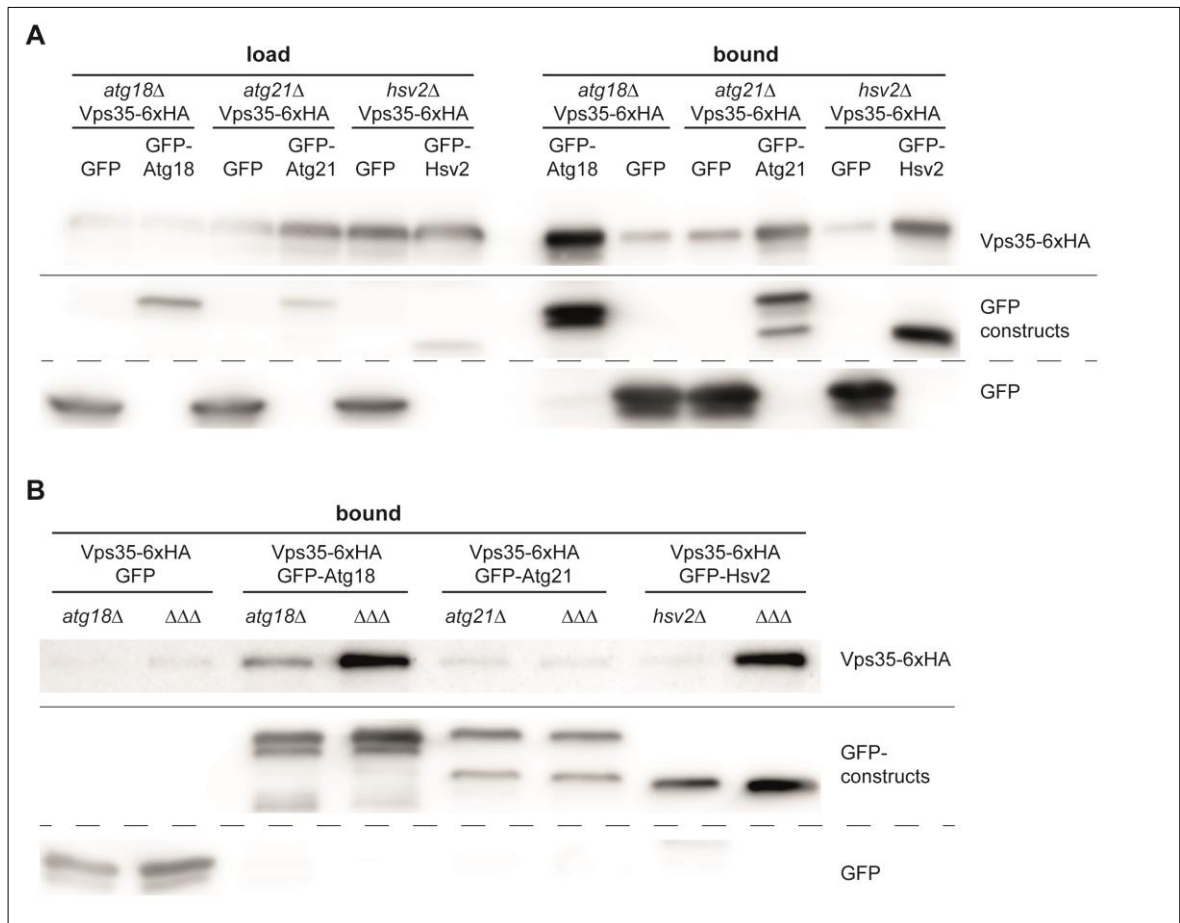


Figure 4-13: Vps35 interacts with all three PROPPINs.

(A) Co-IPs were performed to analyze the interaction between Vps35 and different PROPPINs. Strains with a deletion in either *ATG18*, *ATG21* or *HSV2* and expressing chromosomally tagged *VPS35-6xHA* (prey) together with GFP tagged bait (GFP, GFP-ATG18, GFP-ATG21 or GFP-HSV2) with a *MET25* promoter from a plasmid were grown in selection medium to an OD_{600} of 2-3, harvested and processed according to protocol (wash buffer w/o SDS). Load and bound samples were analyzed with a Western blot decorated with antibodies against HA and GFP. **(B)** Co-IPs were performed in *atg18Δ atg21Δ hsv2Δ* ($\Delta\Delta\Delta$) triple knockout strains to rule out indirect binding mediated by other PROPPINs. Strains with a deletion in either *ATG18*, *ATG21*, *HSV2* or all three ($\Delta\Delta\Delta$) and expressing chromosomally tagged *VPS35-6xHA* (prey) together with GFP tagged bait (GFP, GFP-ATG18, GFP-ATG21 or GFP-HSV2) with a *MET25* promoter from a plasmid were grown in selection medium to an OD_{600} of 2-3, harvested and processed according to protocol (wash buffer with 0.025% (w/v) SDS). Load and bound samples were analyzed with a Western blot decorated with antibodies against HA and GFP.

Interestingly, the PROPPINs compete with each other for binding to Vps35, as deletion of the other two increased the amount of bound Vps35-6xHA. Unfortunately, the signal for the Co-IP with Atg21 was too weak to analyze under the used conditions.

4. Results

4.2.2. Atg18 competes with Vps17/Vps5

The retromer core complex or cargo selection complex (CSC) consists of Vps35, Vps26 and Vps29 (Seaman, 2021; Seaman et al., 1997, 1998). Vps35 forms a right-handed α -solenoid with Vps26 and Vps29 bound to the N- and C- terminal regions, respectively (Hierro et al., 2007; Norwood et al., 2011). The complex seems to be shaped like a flexible stick of around 21 nm in length. Most cargo is recognized and recruited by Vps35 (Nothwehr et al., 1999, 2000), but Vps26 also plays a role in cargo selection (Suzuki et al., 2019). Both Vps26 and Vps29 seem to stabilize Vps35 and its interaction with the endosomal membrane (Reddy & Seaman, 2001). Although Vps29 has structural similarities to metal binding phosphoesterases and the metal binding residues are conserved no substantial phosphoesterase activity could be detected (Collins et al., 2005). None of the CSC components interact with the membrane directly and are therefore not able to shape or even bind to the membrane on their own.

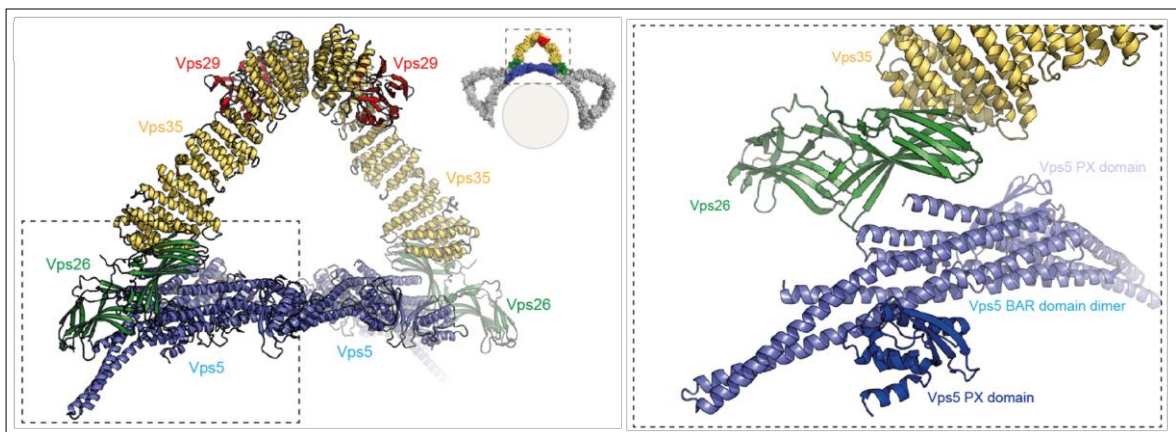


Figure 4-14: Crystal structure of *C. thermophilum* retromer in complex with Vps5.

Vps35 (yellow) forms dimers, binds to Vps29 (red) at its C-terminal end and with Vps26 (green) at its N-terminal end. Contact with the SNX-BAR protein Vps5 (blue) is mediated by Vps26. Adapted from (Chen et al., 2019).

Two additional proteins have been identified to be involved in Vps10 recycling, the SNX-BAR family members Vps5 and Vps17 (Chen et al., 2019; Horazdovsky et al., 1997; Kohrer & Emr, 1993; Ma & Burd, 2020; Steven F. Nothwehr & Hindes, 1997). Both proteins are sorting nexins (SNX) peripherally associated with the membrane and form complexes with each other and the CSC (Seaman et al., 1998). A crystal structure of the retromer in complex with Vps5 showed contact between Vps26 and Vps5, connecting the CSC to endosomal membranes (Kovtun et al., 2018). Sorting nexins are defined by a PtdIns3P-binding phox homology (PX) domain targeting them to membranes and sometimes also contain a BAR (bin/amphiphysin/Rvs161) domain to induce

4. Results

membrane curvature (reviewed in (Worby & Dixon, 2002)). According to a crystal structure with Vps5, Vps26, Vps29 and Vps35 (Kovtun et al., 2018), Vps5 associates with the endosomal membrane, where it forms curved homodimers (heterodimers with Vps17 under cellular conditions) through contact mediated by the BAR domain and the PX domain. Interaction with Vps26 recruits the CSC and further interconnects Vps5 (each Vps26 contains several Vps5 binding sites). Vps35 arches away from the membrane surface and dimerizes through a conserved region at the apex of each arch (Chen et al., 2019; Kovtun et al., 2018), as can be seen in Figure 4-14. Oligomerization of the retromer in complex with Vps5 is thought to result in the formation of tubules coated by the complex. In this model both Vps29 and Vps35 as well as Vps26 to a smaller degree are exposed to the cytosol and are accessible to recruit cargo proteins.

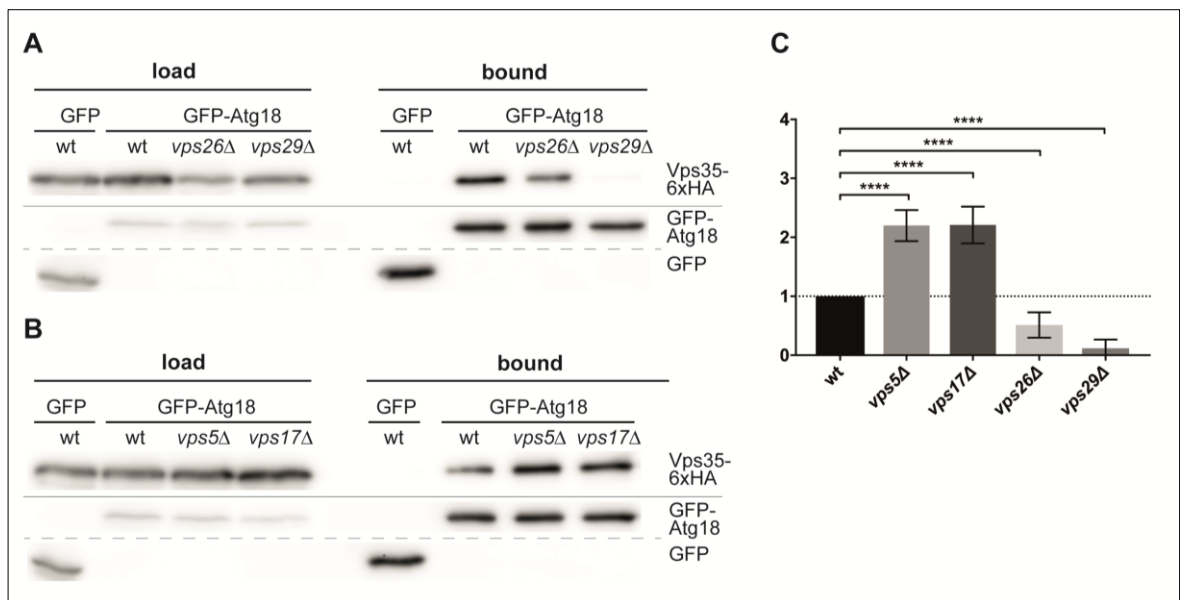


Figure 4-15: Atg18 competes with the SNX-Bar-part of the retromer complex.

(A) Co-IPs were performed to analyze the function of the other retromer components in stabilizing the interaction. Strains with a deletion in either *VPS26* or *VPS29* and expressing chromosomally tagged *VPS35-6xHA* (prey) together with GFP tagged bait (GFP, GFP-ATG18) with a *MET25* promoter from a plasmid were grown in selection medium supplemented with 0.3 mM methionine to an OD_{600} of 2-3, harvested and processed according to protocol. Load and bound samples were analyzed with Western blots decorated with antibodies against HA and GFP. **(B)** Co-IPs were performed to analyze the function of sorting nexins associated with retromer. Strains with a deletion in either *VPS5* or *VPS17* and expressing chromosomally tagged *VPS35-6xHA* (prey) together with GFP tagged bait (GFP, GFP-ATG18) with a *MET25* promoter from a plasmid were grown in selection medium supplemented with 0.3 mM methionine to an OD_{600} of 2-3, harvested and processed according to protocol. Load and bound samples were analyzed with Western blots decorated with antibodies against HA and GFP. **(C)** Quantification of the amount of bound prey for at least three independent experiments. The ratio of HA signal to GFP signal in the bound fraction was used to determine the amount of *Vps35-6xHA* bound to *GFP-Atg18*. The ratios were normalized to wildtype ratio developed on the same blot and at the same time. Statistical relevance was determined using the unpaired two-tailed t-test. Error bars indicate SEM, asterisks indicate p-values.

To analyze the function of the interaction of Atg18 with Vps35 and the retromer complex Co-IPs were performed in strains with HA epitope tagged Vps35 depleted for different retromer subunits (see Figure 4-15). The binding of Vps35 to Atg18 was

4. Results

dependent on the retromer subunit Vps29, as no Vps35 could be detected in the bound fraction of the Co-IP (see Figure 4-15A). A direct interaction between Atg18 and Vps29 is unlikely, since Vps29 did not co-precipitate with Atg18 (Figure 4-16B) and was not detected in the BioID assay. However, deletion of Vps29 has a destabilizing effect on Vps35 (Collins et al., 2005), which probably weakens the interaction between Vps35 and Atg18. A similar but weaker effect was seen in *vps26Δ* cells: although Vps35 could still co-precipitate with Atg18 the amount of bound protein was significantly reduced (see Figure 4-15A,C). Atg18 forms a complex with Vps26 dependent on Vps35, as Vps26-6xHA co-purifies with GFP-Atg18 in the presence of Vps35, but not in a *vps35Δ* strain (see Figure 4-16A). These results indicate the formation of Atg18 in complex with the retromer core components, with direct interaction between Atg18 and Vps35.

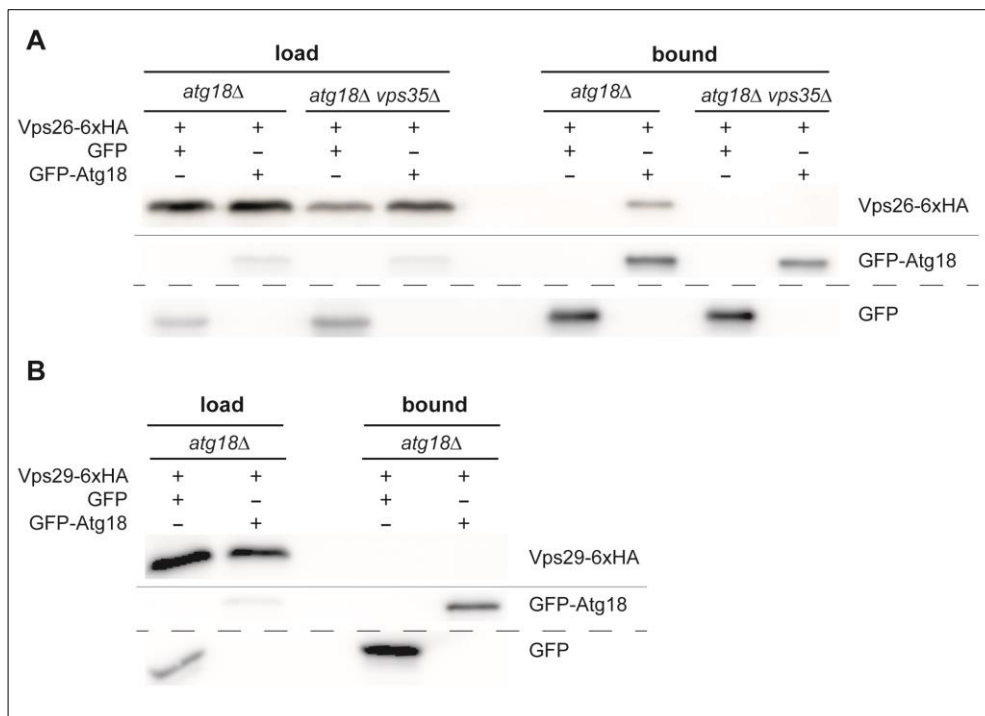


Figure 4-16: Interaction of Atg18 and Vps26 is mediated by Vps35.

GFP-Traps with either Vps26- or Vps29-6xHA were performed for a more detailed analysis of the interaction between retromer and Atg18. **(A)** *atg18Δ* or *atg18Δ vps35Δ* strains expressing chromosomally tagged VPS26-6xHA (prey) together with GFP tagged bait (GFP, GFP-ATG18) with a *MET25* promoter from a plasmid were grown in selection medium supplemented with 0.3 mM methionine to an OD_{600} of 2-3, harvested and processed according to protocol. Load and bound samples were analyzed with Western blots decorated with antibodies against HA and GFP. **(B)** Strains with a deletion of *ATG18* expressing chromosomally tagged VPS26-6xHA (prey) together with GFP tagged bait (GFP, GFP-ATG18) with a *MET25* promoter from a plasmid were grown in selection medium supplemented with 0.3 mM methionine to an OD_{600} of 2-3, harvested and processed according to protocol. Load and bound samples were analyzed with Western blots decorated with antibodies against HA and GFP.

Deletion of either *VPS5* or *VPS17* increased the amount of Vps35 bound to Atg18 more than twofold, as can be seen in Figure 4-15B,C. There are two possible reasons for that: In the first scenario, Atg18 would be a normal cargo of the retromer complex and its

4. Results

recycling would be dependent on all subunits. Atg18 would still be recruited by Vps35 to the cargo selection complex in the absence of Vps5 or Vps17, although the recycling machinery is stalled. Consequently, Atg18 would remain bound to Vps35 and slowly accumulate. However, although Atg18 can bind to PtdIns3P and PtdIns(3,5)P₂ and associates with the membrane, it is not a membrane protein and therefore not a typical retromer cargo.

In the second scenario Atg18 would compete with Vps5/Vps17 for binding to Vps35. The main function of the SNX-BAR proteins is membrane recruitment and deformation. Atg18 contains a hydrophobic loop, which is inserted into the membrane. This induces a slight membrane curvature, which causes tubulation during oligomerization (Gopaldass et al., 2017; Scacioc et al., 2017). Atg18 could therefore take on the role of membrane shaping and induction of scission in the absence of SNX-BAR proteins Vps5 and Vps17. A depletion of *VPS5* and *VPS17* would result in the increased formation of a so far unknown complex containing Atg18 and the retromer components.

Interestingly, a similar function has already been described for the sorting nexin Snx3, which could be involved in this complex. Snx3 was also detected in the BioID assay as an interactor of Atg18, with one identified biotinylation site (see chapter 4.1.2). The protein was identified as another component of the retrieval machinery important for the localization of some cargo such as Kex2 but not Vps10 (Voos & Stevens, 1998). Retrograde transport mediated by retromer affects a lot of different cargo proteins but needs to be highly selective. Sorting nexins in different combinations acting as cargo-specific adaptors widen the spectrum of recognized proteins (Harrison et al., 2014; Strohlic et al., 2007). A crystal structure of the retromer in complex with Snx3 shows the sorting nexin connecting to both Vps35 and Vps26 while binding to PtdIns3P at the membrane (Lucas et al., 2016). So far the only recognizable motif of Snx3 is the PX domain (Worby & Dixon, 2002), which allows for membrane association via PtdIns but not membrane deformation. A potential explanation for Atg18 interacting with both Vps35 and Snx3 could be the formation of a unknown cargo recycling complex. The retromer subunits would recognize and recruit cargo, while Snx3 and Atg18 would organize membrane association and tubulation.

4. Results

4.2.3. **Atg18 is not necessary for typical retromer activity**

Snx3 together with the retromer core complex is essential for the sorting of several membrane proteins such as Kex2 (Voos & Stevens, 1998). Kex2 is a membrane bound serine protease involved in the endoproteolytic processing of precursor proteins (Fuller et al., 1989) and localized to the late Golgi (Bryant & Boyd, 1993; Franzusoff et al., 1991). Recently, an effort has been made to discover new cargo proteins trafficked by retromer and sorting nexins (Bean et al., 2017). One of the identified putative cargo proteins of both retromer and Snx3 was Ear1. The endosomal protein interacts with the ubiquitin ligase Rsp5 and is required for MVB sorting of membrane proteins targeted to the vacuole (Léon et al., 2008).

Atg18 function in recycling retromer cargo dependent on Snx3 was analyzed with an assay described by Bean et al., (2017): cargo proteins Kex2 and Ear1 were tagged with GFP and expressed in strains deleted for either *ATG18* and *ATG21* or all three PROPPINs. The localization of the tagged proteins was analyzed in relation to the vacuolar membrane, which was stained with the lipophilic dye FM4-64.

In wildtype cells, both proteins localized to multiple puncta in the cytosol, likely to be late Golgi or endosomes as described by the literature. No or almost no GFP reached the vacuole (see Figure 4-17). In contrast, a missorting to the vacuole was observed for both proteins in *vps35Δ* cells: Ear1-GFP was transported to the vacuolar lumen in 45% of the cells (Figure 4-17B), while Kex2-GFP was detected at the vacuolar membrane in 65% of the cells (Figure 4-17D). Deletion of either *ATG18* and *ATG21* or all three PROPPINs did not cause the same effect: although a small amount of GFP was transported to the vacuole (around 8% for Ear1), most of the signal for Ear1-GFP and Kex2-GFP remained localized to cytosolic puncta, which can be observed in Figure 4-17A and C. This indicates functional retrograde trafficking from the endosomes to the Golgi.

Snx3 contains a PX domain which is sufficient for association with the membrane, but unable to induce membrane curvature. A complex of the retromer components Vps26, Vps29 and Vps35 together with Snx3 was therefore thought to be unable to induce tubulation without further proteins. *In vitro* experiments with GUVs (giant unilamellar yesicles) demonstrated membrane remodeling activity of Snx3, which is enhanced in

4. Results

the presence of cargo (Purushothaman & Ungermann, 2018). The retromer core complex in combination with Snx3 and a transmembrane cargo protein is therefore sufficient to induce tubulation and does not need additional proteins. Membrane curvature induced by Atg18 might not be necessary for retromer function in a complex with Snx3 *in vitro*, although it cannot be excluded *in vivo*. The small difference to the wildtype as shown in Figure 4-17 can be explained by the function of Atg18 at the vacuolar membrane: the vacuole is abnormally swollen in *atg18Δ* cells, which is probably caused by a defect in membrane fission. This could indirectly or directly affect the function of the retromer at the vacuolar membrane, but does not necessarily implicate Atg18 as part of the retromer.

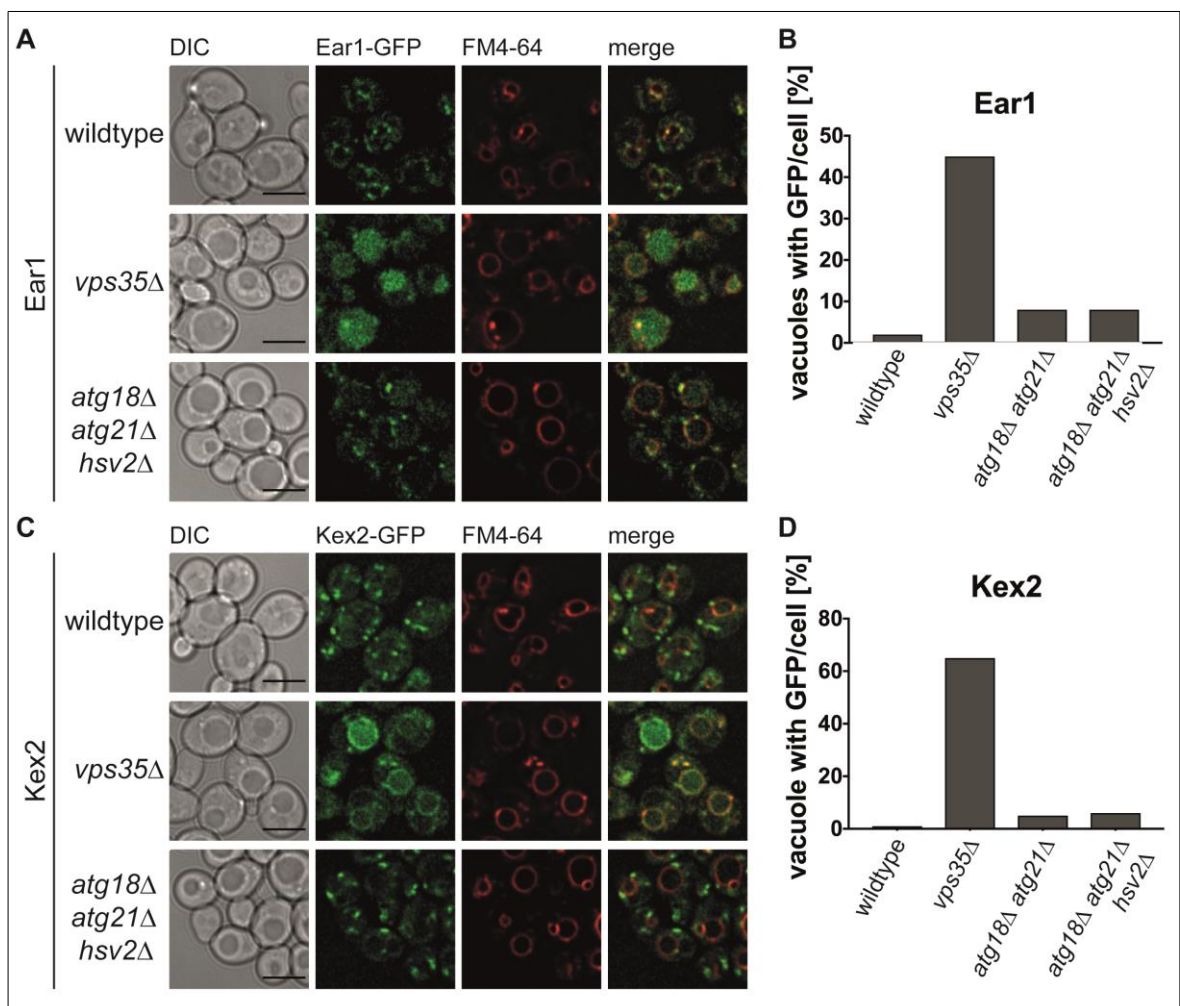


Figure 4-17: Atg18 does not function in Ear1 and Kex2 recycling mediated by retromer.

A sorting assay was performed to determine a function of Atg18 in retromer mediated retrograde transport. Known retromer cargo Ear1 (A+B) and Kex2 (C+D) were C-terminally tagged with GFP and expressed from the chromosome in either wildtype, *vps35Δ*, *atg18Δ atg21Δ* or *atg18Δ atg21Δ hsv2Δ* strains. Cells were grown in selection medium to mid-log phase and incubated in fresh medium supplemented with FM4-64 for 30 min. After incubating the cells in fresh medium w/o FM4-64 cells were analyzed using fluorescence microscopy. Scale bar is set to 5 μ m. (B+D) Statistical analysis was performed with an average of 280 cells per condition, with a minimum of 150 cells. Cells with increased GFP signal inside the vacuole (compared to the signal in the cytosol) were counted and the ratio of cells with stained vacuole to total amount of cells was calculated.

4. Results

4.2.4. Interaction depends partially on membrane association of Atg18

The association of Atg18 with the membrane is mediated by the conserved FRRG motif (see chapter 2.4.1). Replacement of Arg285 and Arg286 with Thr reduces affinity to PtdIns3P and PtdIns(3,5)P₂ significantly and Atg18^{FTTG} is mostly cytosolic. This impairs its function in retrograde trafficking as well as selective and non-selective autophagy, (Dove et al., 2004; Obara, Sekito, et al., 2008), although some autophagic activity could be observed after starvation (Krick et al., 2006). The retromer complex is responsible for retrograde transport of membrane proteins. Assuming that Atg18 could as well be a cargo of retromer complex it was analyzed whether cytosolic Atg18^{FTTG} was still able to interact with Vps35.

Strains expressing Vps35-6xHA were transformed with plasmids containing either wildtype GFP-ATG18 or the mutated GFP-ATG18^{FTTG} and a Co-IP was performed. Interestingly, Vps35 was still able to form a complex with Atg18^{FTTG} (see Figure 4-18A), although the amount of bound Vps35 is reduced compared to wildtype Atg18 (see Figure 4-18B). Additional deletion of both *ATG21* and *HSV2* enhanced the signal of bound Vps35-6xHA, as previously described (chapter 4.2.1).

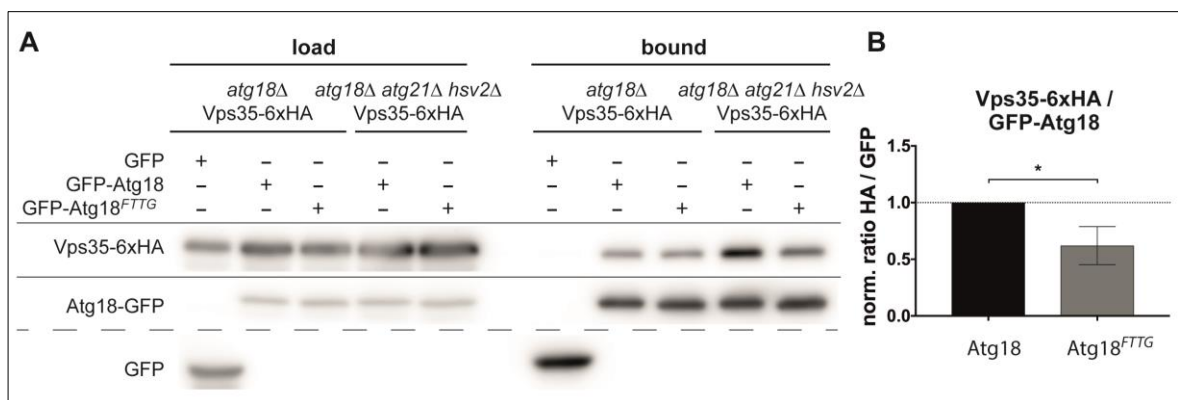


Figure 4-18: Interaction between Vps35 and cytosolic Atg18^{FTTG} is reduced.

(A) Co-IPs to analyze the role of Atg18 membrane association during retromer mediated transport. *atg18Δ* or *atg18Δ atg21Δ hsv2Δ* strains expressing chromosomally tagged VPS35-6xHA (prey) together with GFP tagged bait (GFP, GFP-ATG18, GFP-Atg18^{FTTG}) with a *MET25* promoter from a plasmid were grown in a selection medium supplemented with 0.3 mM methionine to an OD₆₀₀ of 2-3, harvested and processed according to protocol. Load and bound samples were analyzed with Western blots decorated with antibodies against HA and GFP. **(B)** Quantification of the amount of bound prey for at least three independent experiments. The ratio of HA signal to GFP signal in the bound fraction was used to determine the amount of Vps35-6xHA to GFP-Atg18/GFP-Atg18^{FTTG} in the *atg18Δ* strain (functional wildtype). The ratios were normalized to the ratio for GFP-Atg18 developed on the same blot and at the same time. Statistical relevance was determined using the unpaired two-tailed t-test. Error bars indicate SEM, asterisks indicate p-values.

4. Results

The results indicate a reduced interaction between Vps35 and cytosolic Atg18. Macroautophagy and pexophagy progress to some extent in the presence of Atg18^{FTTG} (Krick et al., 2006), although it is unable to rescue the defect in vacuolar morphology (Dove et al., 2004). Therefore, it can be assumed that the residual binding of Atg18^{FTTG} to PtdIns3P is sufficient for partial localization to the PAS and the formation of a complex with Atg2, which is essential for the autophagic process. Atg2 was observed at the PAS in the absence of Atg18 (Rieter et al., 2013) and could recruit Atg18^{FTTG}. Interaction of Vps35 and Atg18^{FTTG} could indicate a role of the retromer complex during or downstream of autophagy.

4.2.5. Atg18 is mislocalized in *vps35Δ*

In a wildtype strain, Atg18 localizes to the vacuolar membrane (Guan et al., 2001) and endosomes (Krick, Henke, et al., 2008), while a small amount can also be found at the PAS (Reggiori et al., 2004). As illustrated in Figure 4-19, in 12% of wildtype cells Atg18-GFP was observed at the vacuolar membrane. In contrast to this, Atg18-GFP accumulated at the vacuolar membrane in 20% of the *VPS35* depleted cells. Interestingly, some of the Atg18 signal seemed to localize to the membrane of small ring-like structures associated or at least in close proximity to the vacuole and not to the vacuolar membrane itself. The localization of Atg18-GFP to punctuate structures in the cytosol, likely to be endosomes or the PAS, was reduced compared to the wildtype. The number of puncta per cell was decreased from 54% per cell in wildtype to 28% per cell in a *vps35Δ* strain (Figure 4-19B).

Atg18 is recruited to the PAS during starvation. Almost no signal could be observed at the vacuolar membrane of wildtype cells after 2h of nitrogen starvation (Figure 4-19A). This was different in *vps35Δ* strains: although the number of cells with Atg18 at the vacuolar membrane was reduced compared to unstarved cells, 8% and 7% showed the characteristic ring after 2h and 4h, respectively. However, in starved cells Atg18-GFP increasingly accumulated at the small ring-like structures described above. The number of cells with this particular phenotype increased from 6% in non-starved cells to 24% and 25% after 2h and 4h of starvation, respectively (Figure 4-19B, at ring-like structures).

4. Results

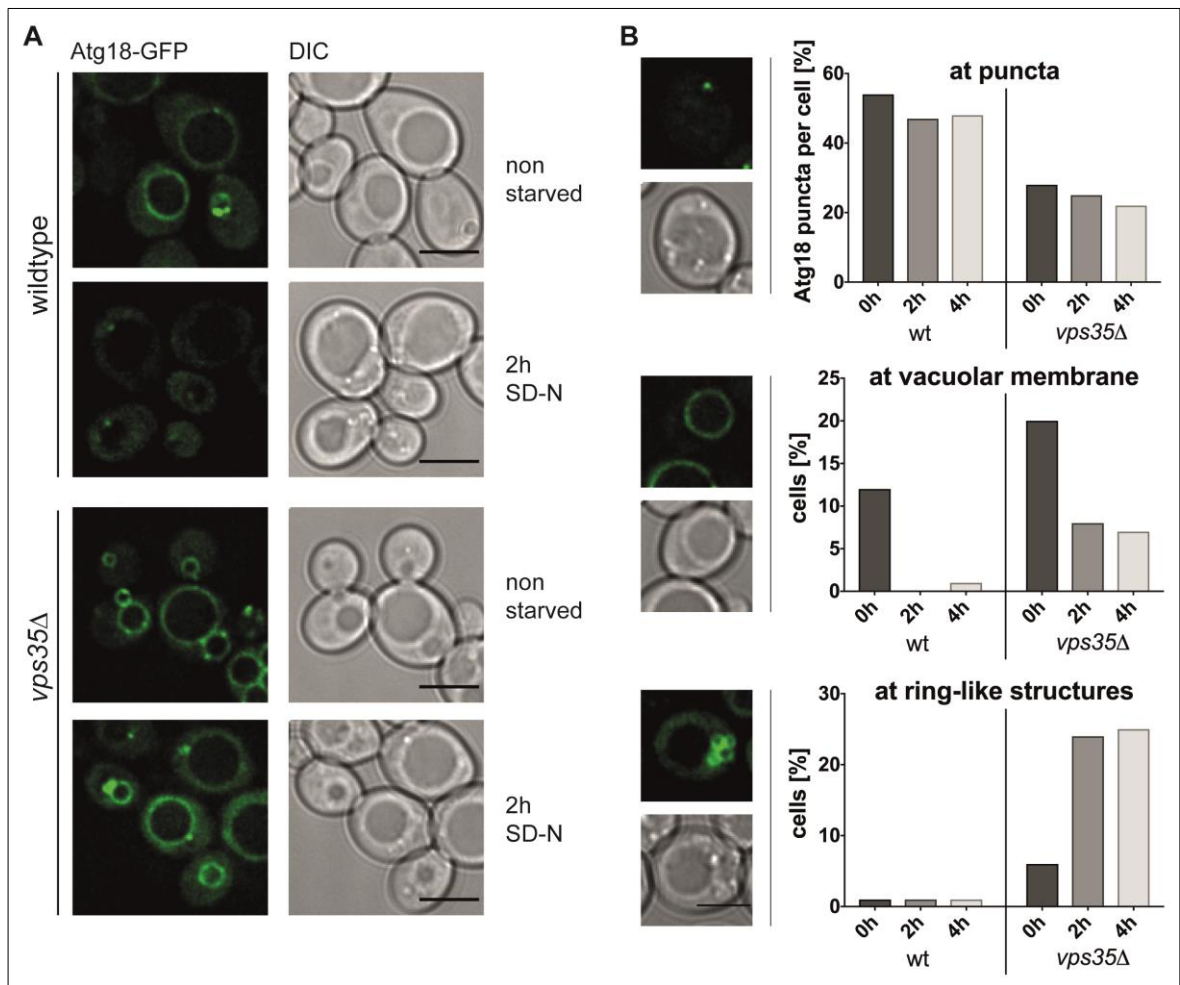


Figure 4-19: Localization of Atg18 is dependent on Vps35.

Fluorescence microscopy was performed to analyze the localization of Atg18 in *vps35Δ* cells. **(A)** Either *atg18Δ* (functional wildtype) or *atg18Δ vps35Δ* strains (functional *vps35Δ*) expressing Atg18-GFP with an endogenous promoter from a plasmid were grown in selection medium to an OD_{600} of 2-3 and transferred to SD-N medium. Cells were analyzed after 0h, 2h or 4h starvation. Scale bar is set to 5 μ m. **(B)** Three different morphological features were defined – Atg18 enriched at puncta (upper panel), at the vacuolar membrane (middle) or at ring-like structures adjacent to the vacuole (lower panel). Atg18 positive puncta were counted and divided by the total amount of cells (puncta per cell) for the upper panel. For the middle and lower panel, cells containing either Atg18 enriched at the vacuolar membrane or at small ring-like structures were counted and divided by the total amount of cells (% cells containing the indicated structure).

The nature of the small ring like structures is not yet known. Since starvation enhances the accumulation a connection to autophagy is very likely. Closure and subsequent fusion of the mature autophagosome with the vacuolar membrane has to be tightly regulated, but the factors involved in the organization are still not completely known. Recycling of Atg18 or other Atgs mediated by the retromer complex could be a signal for autophagosome maturation and induce fusion.

Another reason for the occurrence of the ring-like structures could be a defect in the endosome-vacuole fusion machinery, caused by the deletion of *VPS35*. Retromer plays an important role in membrane protein sorting at the Golgi and endosomes. A defect

4. Results

in this transport pathway has a severe impact on many processes in the cell. For example, Neo1 is a P4-type ATPase flippase, it translocates phospholipids like PE from the luminal to the cytosolic leaflet of the membrane to establish asymmetry (Muthusamy et al., 2009; Takar et al., 2016). It was shown to be a cargo of retromer and Snx3 and is mislocated to the vacuolar membrane in *vps35Δ* or *snx3Δ* (Dalton et al., 2017). PE is suggested to be an important regulator of Ypt7 and SNARE mediated vacuolar fusion (Wu et al., 2016) It is conjugated with Atg8 in immature autophagosomes, which could further block fusion with the vacuolar membrane. Because of its conical shape, it could also affect membrane formation and lipid packing. A defect in retromer could also impact directly or indirectly localization of vacuolar SNAREs, resulting in the accumulation of enlarged late endosomes at the vacuolar membrane.

4.2.6. Atg18 colocalizes with FM4-64

To identify the origin of the ring-like structures the endosomal and vacuolar membranes were stained with different methods. FM4-64 is a lipophilic styryl dye that stains membranes (Vida & Emr, 1995). Endocytic processes transport it to late endosomes and then the vacuole. Either wildtype or *vps35Δ* cells expressing Atg18-GFP were incubated with FM4-64 for at least 30 min (unstarved) or 2h (starved) and examined with fluorescence microscopy.

Atg18-GFP co-localized with the vacuolar membrane stained by FM4-64 in non-starved cell of both wildtype and *vps35Δ* strain, which can be observed in Figure 4-20A. Starvation caused the accumulation of Atg18-GFP at cytosolic puncta in wildtype cells, which were not stained with FM4-64 and are likely to be autophagic structures. Almost no co-localization with FM4-64 was observed.

In *vps35Δ* cells Atg18-GFP stayed localized to the vacuolar membrane comparable to the cells before starvation and also localized to the ring-like structures described above, both stained with the dye. This indicates that the structures observed in a *VPS35* deletion strain are either part of the endosomal system or originate from the vacuole. Since FM4-64 stains endosomes as well as the vacuolar membrane it is not possible to differentiate between the two compartments using this dye. A marker specific for either the endosome or the vacuole is necessary.

4. Results

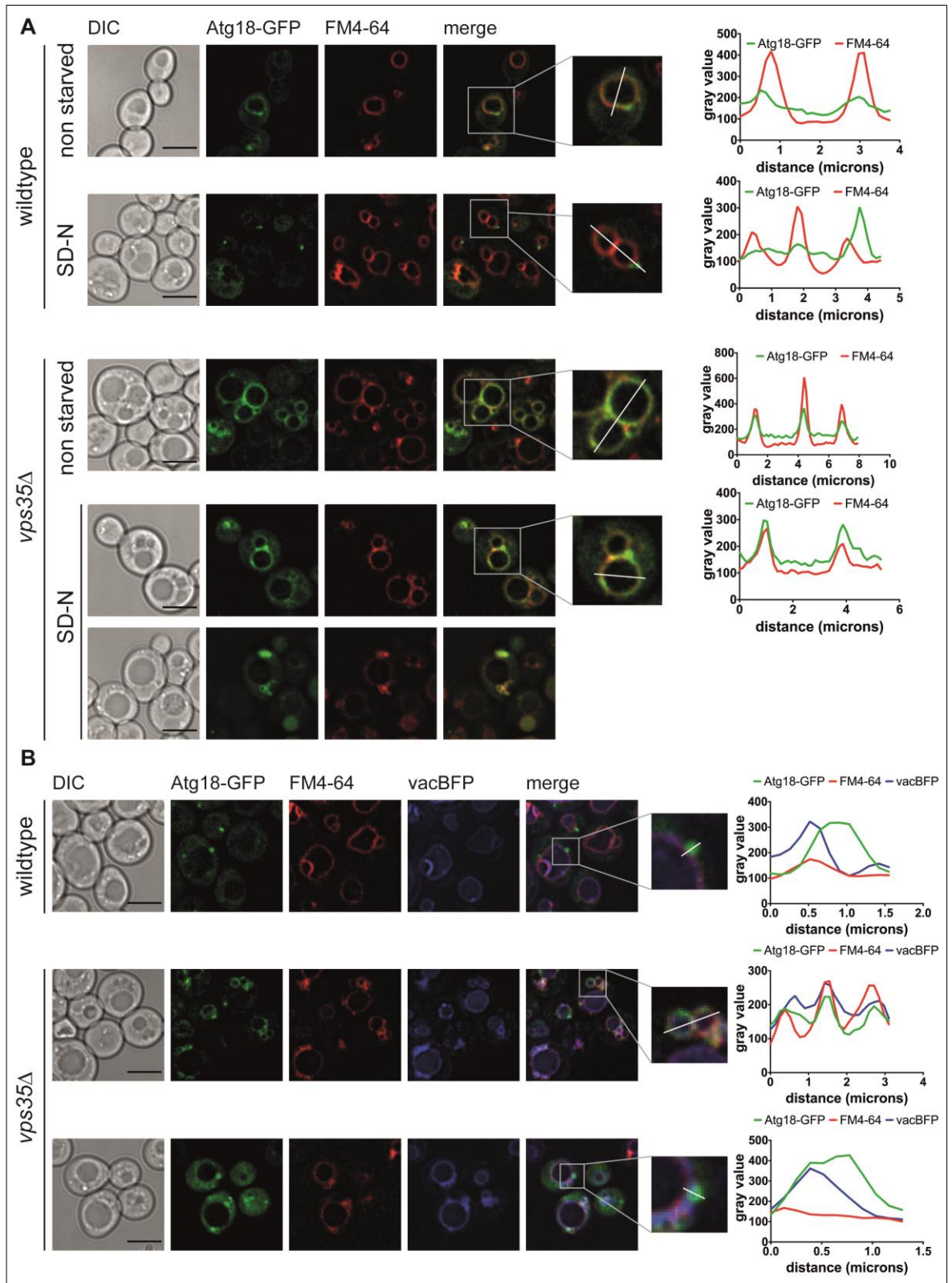


Figure 4-20: Atg18 localizes partially with the endosomal and vacuolar membrane.

Cells were stained with either FM4-64 or vacBFP to determine the location of the missorted Atg18. *atg18Δ* or *atg18Δ vps35Δ* strains expressing Atg18-GFP with an endogenous promoter from plasmid were grown to an OD_{600} of 2-3 and transferred to SD-N medium. Cells were analyzed after 0h, 2h or 4h starvation. Fluorescence profiles were measured using FIJI and plotted against distance using GraphPad Prism. Scale bar is set to 5 μ m. **(A)** Vacuolar and endosomal membrane were stained with FM4-64: cells were incubated with either fresh medium or SD-N containing FM4-64 (non-starved and starved, respectively) before analysis with the fluorescence microscopy.

4. Results

(B) Cells expressed Atg18-GFP together with vacBFP (3xtagBFP-Pho8) from the chromosome. The vacuolar membrane was stained with vacBFP in addition to FM4-64, to differentiate between vacuolar and endosomal membrane.

The product of the PHO8 gene is the repressible vacuolar alkaline phosphatase (ALP) (Kaneko et al., 1982), an integral membrane protein (Klionsky & Emr, 1989). ALP is transported from the late Golgi directly to the vacuolar membrane mediated by the AP-3 (adaptor protein) complex (Cowles et al., 1997; Stepp et al., 1997). Fused to BFP it can be used to mark the vacuolar membrane as vacBFP (3xtagBFP-Pho8).

VacBFP colocalized with FM4-64 but not with Atg18-GFP in wildtype cells after starvation, depicted in Figure 4-20B. Deletion of *VPS35* led to the accumulation of Atg18-GFP at vacuolar structures marked with vacBFP and endosomal structures stained with FM4-64. Some of the ring like structures decorated with Atg18-GFP found in *vps35Δ* cells were positive for both FM4-64 and vacBFP. Vps35 belongs to the class A vps mutants (Raymond et al., 1992), indicating no or only small changes in vacuolar morphology upon deletion. Staining with FM4-64 and vacBFP indicates a change in the vacuolar morphology caused by deletion of *VPS35* (data not shown) which is enhanced after starvation. It has to be pointed out that although the AP-3 transport pathway is independent of most vps proteins, deletion of *VPS35* results in the missorting of “intermediate” levels of ALP (Klionsky & Emr, 1989). Mislocalization of vacBFP to the endosomes can therefore not be excluded.

Atg18 binds to PtdIns3P and PtdIns(3,5)P₂, which is localized at the PAS and the endosomal and vacuolar membranes. A deletion in *VPS35* could affect the distribution of phospholipids in the cell and therefore also the distribution of Atg18. RFP-2xFYVE binds exclusively to PtdIns3P (Gillooly, 2000) and can be used to detect its distribution in the cell. RFP-2xFYVE accumulates at the vacuolar membrane in both wildtype and *vps35Δ* cells before and after starvation and it is also present at the ring like structures exclusively seen in cells without Vps35 (see Supp. Figure 7-2). However, in starved wildtype cells the only colocalization with Atg18 could be observed at cytosolic puncta likely to be either PAS or endosomes, while in *vps35Δ* cells Atg18-GFP partially colocalized with RFP-2xFYVE positive membrane structures. The signal for Atg18-GFP was weaker compared to other experiments since both Atg18 and FYVE compete for binding to PtdIns3P and RFP-2xFYVE was overexpressed with a TEF promotor (Gillooly, 2000). All these results indicate that in the absence of Vps35 Atg18 is

4. Results

mislocalized to the vacuolar and endosomal membrane during starvation and this is not caused by an abnormal PtdIns3P distribution.

A part of the small ring-like structures were not positive for either FM4-64 or vacBFP, indicating the presence of structures formed independent of the vacuole such as autophagosomes.

4.2.7. Atg18 accumulates at the autophagosome/PAS in *vps35Δ* cells

The ring-like structures accumulated at the vacuolar membrane in starved *vps35Δ* cells could be autophagosomes. If this assumption is correct they should also be positive for proteins found at the PAS or the mature autophagosome. To test this, cells with a deletion of *VPS35* were transformed with plasmids containing Atg18-GFP and mCherry-Atg8. Atg8 is recruited to the PAS in the early stages of phagophore formation and remains at the autophagosome until degradation in the vacuole. It is therefore a good marker for autophagosomes. The results are shown in Figure 4-21.

Overall, the amount of Atg8 dots per cell observed in both wildtype and *vps35Δ* remained the same before and during starvation (see Figure 4-21A,B). Deletion of *VPS35* increased the number of puncta in the cytosol slightly in non-starved cells (from 13% in wildtype cells to 19% in *vps35Δ* cells). Interestingly, after 2h of starvation 33% of all cells contained Atg8 positive puncta, which is a more than twofold increase compared to the wildtype. The number of Atg8 positive puncta in the cells was reduced to levels comparable to the wildtype after 4h of starvation. This might indicate a bottleneck somewhere in the process. Another striking detail is the fact that 35% of mCherry-Atg8 puncta were also positive for Atg18-GFP in the absence of *VPS35* compared to only 16% in the wildtype (see Figure 4-21C). This was increased to up to 49% during starvation, while only 18% of mCherry-Atg8 puncta were positive for Atg18-GFP after 2h starvation in the wildtype. Colocalization with the small ring-like structures, which were only observed in *vps35Δ* cells, was comparable: almost 50% of them either colocalized with mCherry-Atg8 or contained mCherry signal. This number was still at 38% after 4h starvation. The results strongly indicate that the depletion of *VPS35* causes an accumulation of Atg18 at the autophagosomal membrane and that either AP closure or fusion with the vacuole was the limiting step.

4. Results

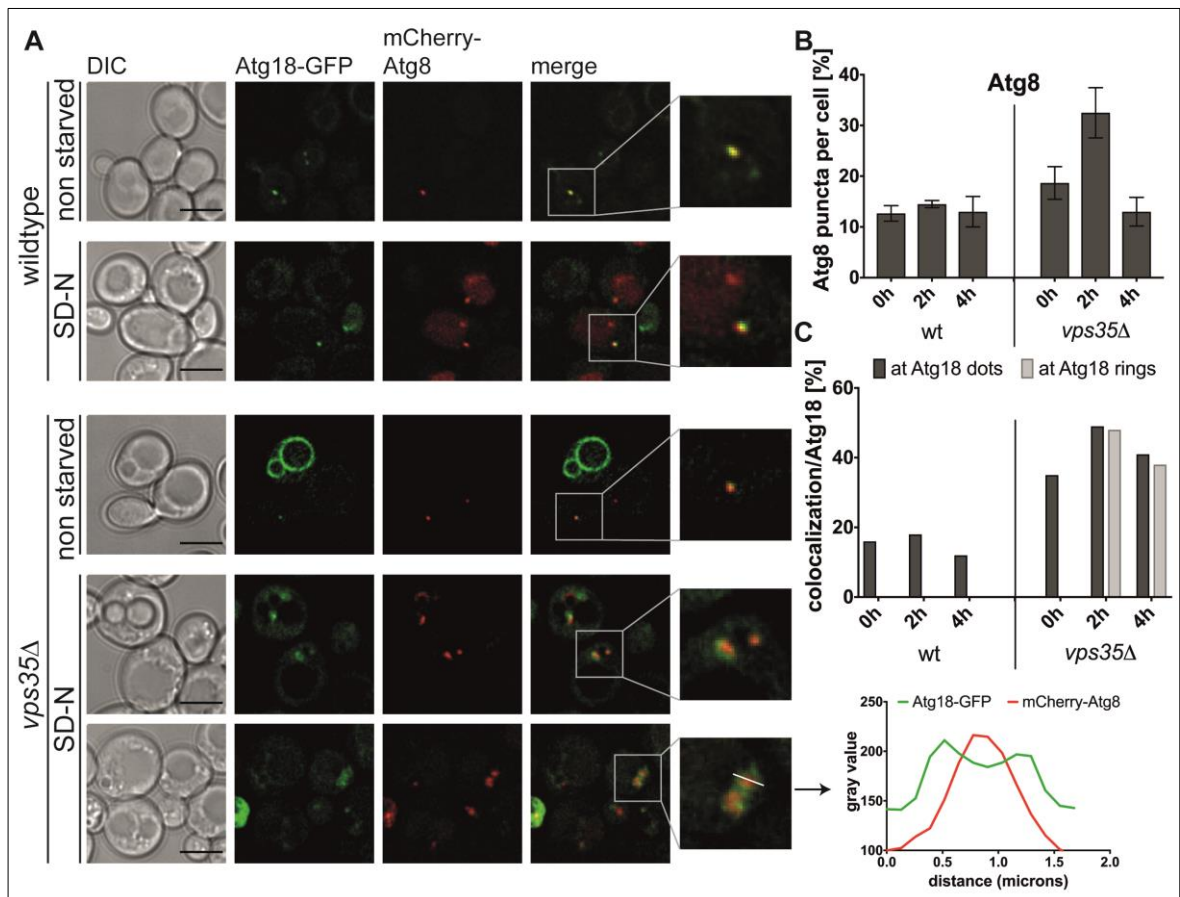


Figure 4-21: Atg18 is enriched at autophagosomes in *vps35Δ* cells.

Atg18 was tagged with GFP and expressed with the PAS marker mCherry-Atg8 to analyze the identity of the small vesicular structures found in *vps35Δ* cells. **(A)** *atg18Δ* or *atg18Δ vps35Δ* strains expressing Atg18-GFP and mCherry-Atg8 with endogenous promoters from plasmids were grown to an OD_{600} of 2-3 and transferred to SD-N medium. Cells were analyzed using fluorescent microscopy after 0h, 2h or 4h of starvation. Scale bar is set to 5 μm. Fluorescence profile for the lower panel was measured using FIJI and plotted against distance using GraphPad Prism. **(B)** The ratio of cells containing Atg8 puncta was determined by dividing the amount of Atg8 positive puncta by the total amount of cells in two independent experiments, with a minimum of 200 cells per condition. **(C)** The amount of colocalizations between Atg8 and Atg18 positive puncta or ring-like structures was counted and divided by the total number of Atg18 positive structures. Statistical analyses were performed with a minimum of 200 cells per condition.

Another PAS marker was used for further confirmation. Ape1 is a cargo of the Cvt pathway and due to its nature a marker for the earliest stage of the autophagic process. It accumulates in the cytosol and is recognized by a specific receptor, which in turn recruits the autophagic machinery. Ape1 tagged with RFP was expressed together with Atg18-GFP in wildtype and *vps35Δ* cells and starved for two and four hours. The results are depicted in Figure 4-22.

The amount of Ape1 dots per cell remained between 34% and 39% during starvation in wildtype cells (Figure 4-22B). 10% of these dots are positive for Atg18-GFP before and after starvation, as depicted in Figure 4-22A. Deletion of *VPS35* increases the number of Ape1 complexes in the cytosol after 4h of starvation to 63% per cell, in

4. Results

comparison to only 37% per cell in wildtype. A third of the Ape1 puncta were positive for Atg18-GFP after 2h of starvation, which then slightly decreases. Another 15% were surrounded by a ring of Atg18-GFP, marking this as an autophagosome containing Ape1.

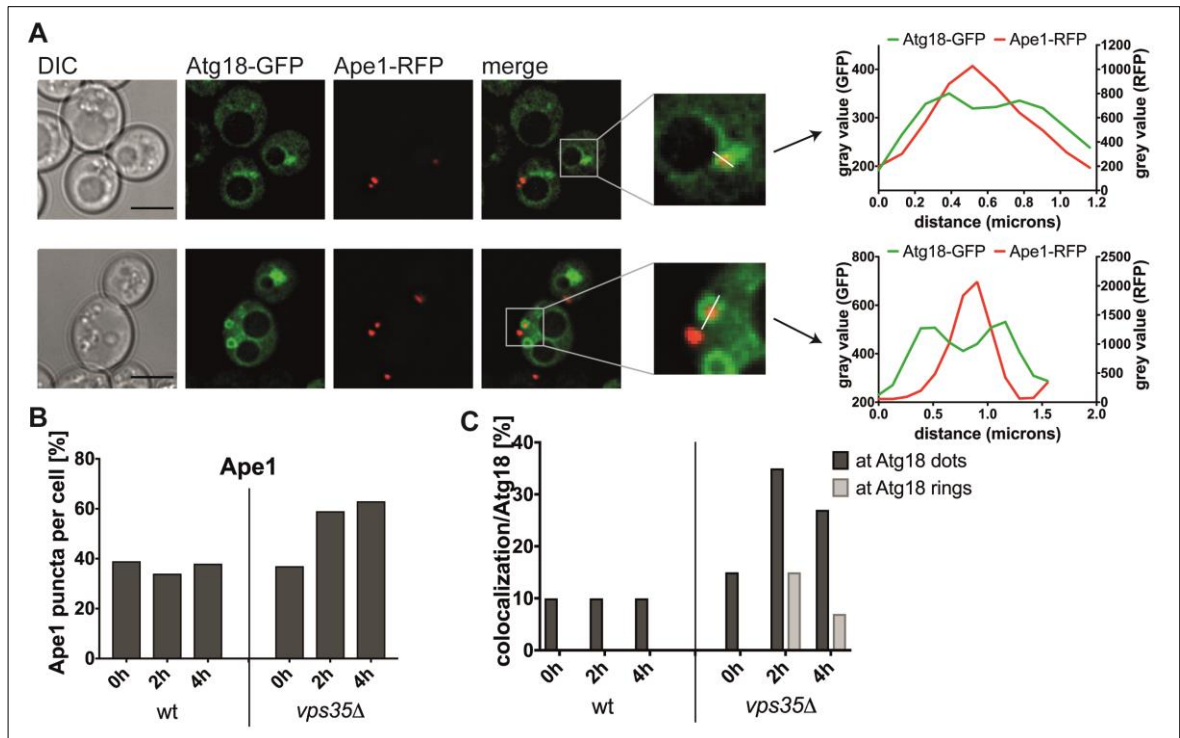


Figure 4-22: Atg18 positive structures colocalize with Ape1.

Atg18-GFP was expressed with the autophagosomal cargo Ape1-RFP to confirm the enrichment of Atg18 at autophagosomal structures. **(A)** *atg18Δ* or *atg18Δ vps35Δ* strains expressing Atg18-GFP and Ape1-RFP with endogenous promoters from plasmids were grown to an OD₆₀₀ of 2-3 and transferred to SD-N medium. Cells were analyzed after 0h, 2h or 4h starvation. Scale bar is set to 5 μm. Fluorescence profiles were measured using FIJI and plotted against distance using GraphPad Prism. **(B)** The ratio of Ape1 positive punctae to the total amount of cells was determined with a minimum of 200 cells per condition. **(C)** The amount of colocalizations between Ape1 and Atg18 positive punctae or ring-like structures was counted and divided by the total number of Atg18 positive structures. Statistical analyses was performed with a minimum of 200 cells per condition.

To further confirm these results the experiment was repeated with a *vps35Δ ypt7Δ* strain. Ypt7 is a GTPase necessary for autophagosome fusion with the vacuole, deletion leads to the accumulation of sealed autophagosomes in the cytosol (J. Kim et al., 1999; Kirisako et al., 1999). Deletion of both *VPS35* and *YPT7* should therefore result in the accumulation of sealed autophagosomes covered with Atg18 (Zhou et al., 2017). However, GFP-Atg8 was distributed in the cytosol, as only a diffuse signal could be detected and no puncta were visible. GFP-Atg8 was therefore not recruited to the PAS, which could be caused by either a complete block in autophagy induction or a defect specifically in Atg8 recruitment to the IM. Deletion of both *YPT7* and *VPS35* results in

4. Results

severe protein sorting and fusion defects of the endosomal system and an effect on autophagic proteins is highly likely.

Part of the ring-like structures detected in *VPS35* deletion strains are positive for PAS marker mCherry-Atg8 or Ape1-RFP. The mCherry tagged Atg8 was expressed from a plasmid in addition to chromosomally expressed Atg8. Therefore, autophagosomes can also be formed without the mCherry tagged protein. This together with the fact that only a small part of autophagosomes contain Ape1 during starvation could be an explanation for ring-like structures not positive for either PAS marker.

However, the results indicate an involvement of the retromer complex in the recycling of Atg18 from the autophagosome either before fusion with the vacuole occurs or from the vacuolar membrane after fusion. The accumulation of autophagosomes could also indicate a defect with the fusion process itself, which could be caused by a shortage of vacuolar SNAREs. Defective endosomal recycling as a result of impaired retromer function could lead to the mislocalization of proteins involved in fusion events at the vacuole. This could also explain the presence of ring-like structures stained with FM4-64, as the lipophilic dye is normally not observed at autophagosomes. This could be large endosomes or pinched off vacuole decorated with Atg18.

4.2.8. Vps35 is recruited to the PAS

For the retromer complex to be directly involved in autophagy its components have to be recruited to the PAS or autophagosome. To test this *VPS35* was tagged chromosomally with mCherry and expressed together with the PAS marker GFP-Atg8. The functionality of the tagged Vps35 in autophagic activity was assessed with an Ape1 maturation and a free GFP-assay (see Suppl. Figure 7-1A-C). Activity of Vps35-mCherry in autophagy was reduced compared to wildtype Vps35, but still functional. Additionally, a CPY maturation assay was performed to analyze the function of Vps35 in recycling the CPY receptor Vps10 (see Suppl. Figure 7-1D). The ratio of mature CPY to the total amount of CPY in strains expressing only *VPS35*-mCherry was comparable to wildtype strains after starvation.

The results of the co-localization assay of Vps35-mCherry and GFP-Atg8 are depicted in Figure 4-23. 7% of all Atg8 dots colocalized with Vps35-mCherry in non-starved cells, as depicted in Figure 4-23. Starvation did only marginally affect colocalization, after 4h in nitrogen free medium only 6% of GFP-Atg8 puncta were positive for Vps35-

4. Results

mCherry. This further indicates a role of Vps35 during autophagy. The low number of puncta positive for both signals imply a highly dynamic situation, where Vps35 would only colocalize very briefly with the PAS or autophagosome.

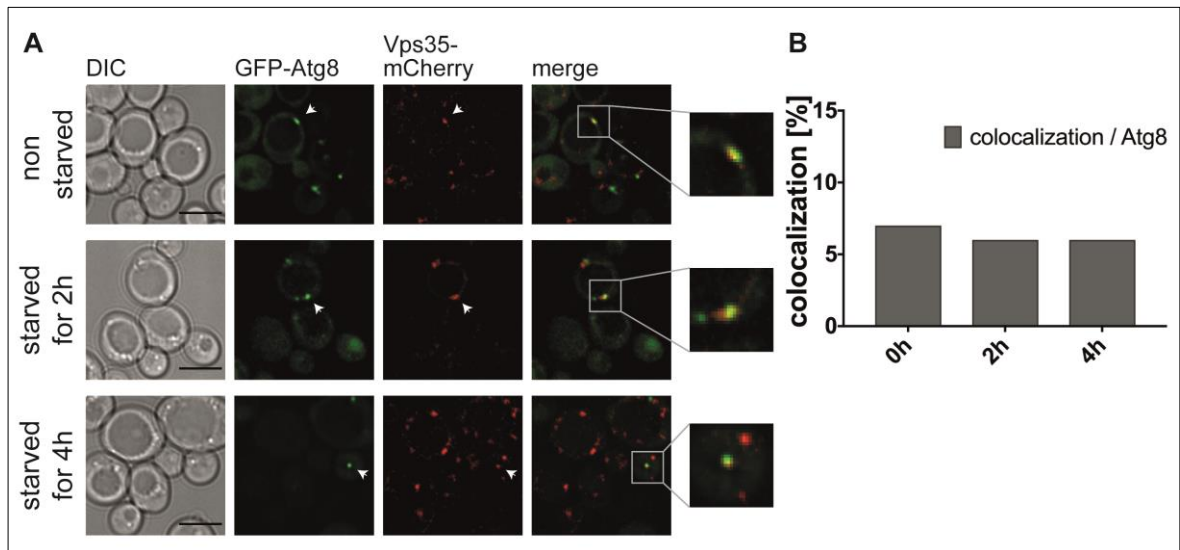


Figure 4-23: Vps35 co-localizes with the PAS marker Atg8.

Vps35-mCherry was expressed together with the PAS marker GFP-Atg8 to determine a possible recruitment of Vps35 to the PAS. **(A)** *atg8Δ* strains expressing chromosomally tagged VPS35-mCherry and GFP-Atg8 with an endogenous promoter from plasmid were grown to an OD₆₀₀ of 2-3 and transferred to SD-N medium. Cells were analyzed after 0h, 2h or 4h starvation. Scale bar is set to 5 μm. Fluorescence profile was measured using FIJI and plotted against distance using GraphPad Prism. **(B)** The amount of colocalizations between Atg8 and Vps35 positive punctae was counted and divided by the total number of Atg8 dots. Statistical analysis was performed with a minimum of 200 cells per condition.

4.2.9. Binding site of Vps35 at Atg18

It is necessary to determine the interface between Vps35 and Atg18. Knowing the exact binding site of Vps35 on Atg18 could lead to Atg18 mutants selectively unable to bind Vps35. The function of the interaction could then be analyzed without the need for knockout mutants. Deletions in both *VPS35* and *ATG18* have a widespread impact on cellular pathways. Protein sorting is defective in *vps35Δ* strains, which also affects autophagy. The impact of an interaction between Vps35 and Atg18 would easily be overlooked under these conditions.

It was hypothesized that the binding of Vps35 to Atg18 could exclude the interaction with Atg2, which could in turn be a trigger for the release of Atg9. The complex containing Atg9, Atg2 and Atg18 is located to the outer rim of the growing phagophore and the release of Atg2 and Atg9 as well as recycling of Atg18 could trigger autophagosome closure or fusion with the vacuolar membrane. In that case Vps35 and Atg2 would compete for the same binding site on Atg18. To test this assumption, two

4. Results

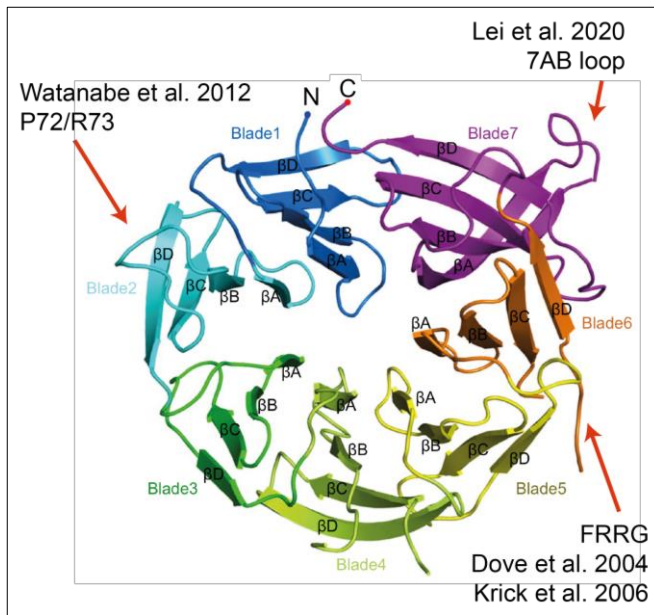


Figure 4-24: Crystal structure of ScAtg18 with indicated Atg2 binding sites.

Blades are displayed in different colors, red arrows indicate regions involved in binding to either Atg2 at blade 2 and blade 7 or PtdInsPs at blade 5 and 6. Adapted from (Lei *et al.*, 2020)

published binding regions for Atg2 were mutated and binding of Vps35 to Atg18 was analyzed with a Co-IP. Blade 2 of Atg18 has been identified as essential for PAS targeting and interaction with Atg2, indicated in Figure 4-24 (Rieter *et al.*, 2013; Watanabe *et al.*, 2012). Mutation of both Pro72 and Arg73 to Ala resulted in reduced autophagic activity and blocked binding to Atg2.

CoIPs with chromosomally expressed *ATG2-3xHA* and *GFP-ATG18^{P72AR73A}* expressed under the control of a *MET25* promoter from a plasmid showed a strongly reduced binding between Atg2 and *Atg18^{P72AR73A}*. *Atg2-3xHA* was still able to bind normal Atg18 (Figure 4-25A). The mutation did not affect binding between Atg18 and Vps35, although the interaction seemed to be slightly but not significantly reduced (Figure 4-25B).

Another potential binding site for Atg2 was discovered with the crystal structure of *S. cerevisiae*: ScAtg18 has an extended loop between βA and βB of Blade 7 in comparison to other members of the PROPPIN family. *Atg18^{Δ7AB}*, in which the 7AB loop (amino acids 433-460) was deleted, showed defects in autophagy and markedly decreased binding to Atg2 (Lei *et al.*, 2020).

Deletion of the 7AB loop however did not weaken the interaction between Atg18 and Atg2, as the amount of Atg2-3xHA bound to GFP-*Atg18^{Δ7AB}* was not reduced compared to GFP-Atg18 (Figure 4-25C). The result contradicts the data published by (Lei *et al.*, 2020), where the amount of Atg2 bound to *Atg18^{Δ7AB}* was significantly reduced. Curiously, the interaction between Vps35-6xHA and *Atg18^{Δ7AB}* seemed to be enhanced, as more Vps35-6xHA can be found in the bound fraction compared to GFP-Atg18. Quantification determines this to be not significant since there were variations in the observed signal strength. Therefore, both binding sites analyzed in this experiment have no impact on binding between Vps35 and Atg18.

4. Results

This does not exclude the possibility of an overlap between the binding sites of Atg2 and Vps35 on Atg18, as amino acids other than P27R73 could be involved in the interaction between Atg18 and the retromer subunit. Another possibility is the formation of a complex containing both Atg2 and Vps35 bound to Atg18.

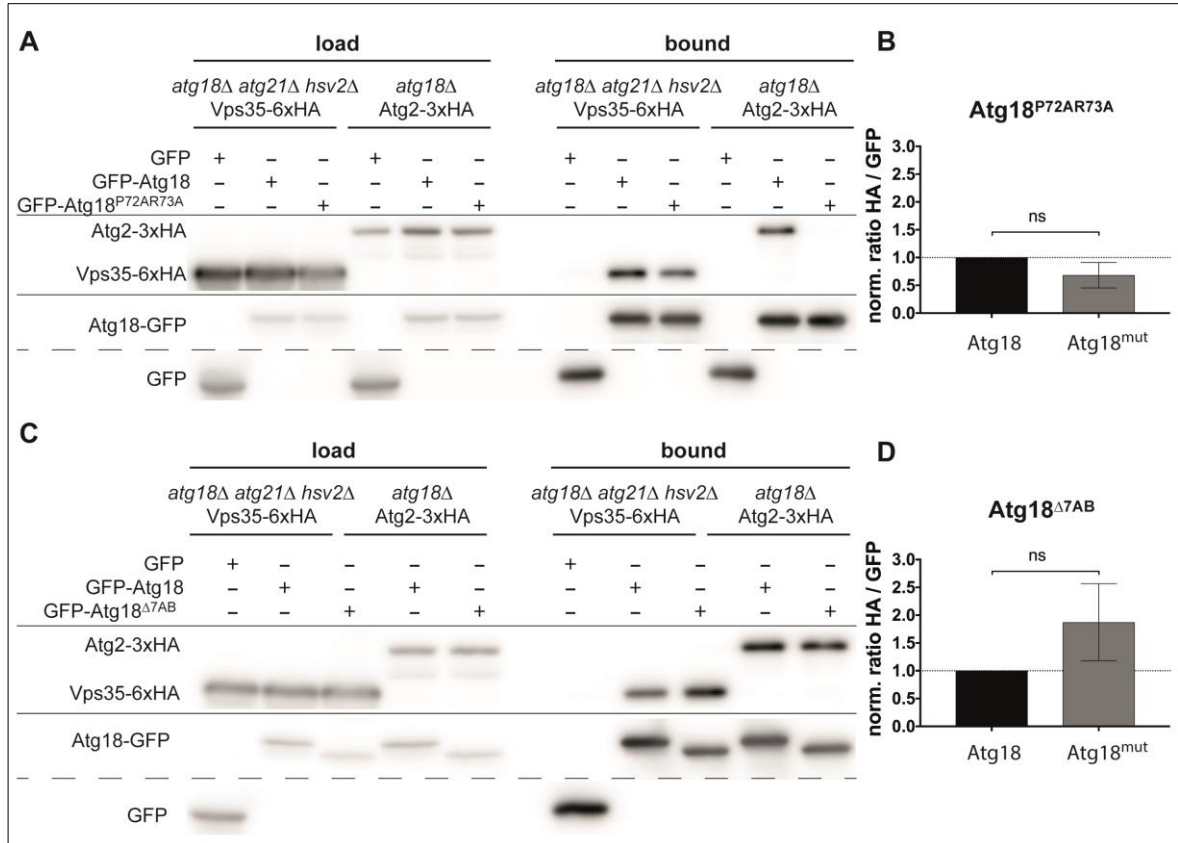


Figure 4-25: Vps35 does not bind Atg18 via known Atg2 binding sites.

Mutated Atg18 with reduced affinity towards Atg2 was used in a Co-IP with Vps35 to determine if the binding sites of Atg2 and Vps35 to Atg18 overlap. **(A)** Either *atg18Δ atg21Δ hsv2Δ* strains expressing chromosomally tagged Vps35-6xHA or *atg18Δ* strains expressing chromosomally tagged Atg2-3xHA together with GFP tagged bait (GFP, GFP-ATG18 or GFP-Atg18^{P72AR73A}) with a *MET25* promoter from a plasmid were grown in selection medium supplemented with 0.3 mM methionine to an OD₆₀₀ of 2-3, harvested and processed according to protocol. Load and bound samples were analyzed with Western blots decorated with antibodies against HA and GFP. **(C)** The experiment was performed as described in (A), but with GFP-Atg18^{Δ7AB} instead of GFP-Atg18^{P72AR73A}. **(B+D)** Quantification of the amount of bound prey for at least three independent experiments. The ratio of HA signal to GFP signal in the bound fraction was used to determine the amount of Vps35-6xHA to the GFP-Atg18 variants. The ratios were normalized (norm.) to the ratio determined for GFP-Atg18 developed on the same blot and at the same time. Statistical relevance was determined using the unpaired two-tailed t-test. Error bars indicate SEM, asterisks indicate p-values.

4.2.10. Interaction of Vps35 with Atg2 and Atg9

Atg18 forms a complex with Atg2 to recruit Atg9 to the PAS. Results of the Co-IP experiments with mutated Atg18 revealed that Vps35 might not compete with Atg2 for its binding to Atg18. Therefore, a simultaneous interaction of Vps35 and Atg2 would be possible. In this case, interaction of Vps35 with other components of the Atg18 complex at the PAS, namely Atg2 and Atg9, is very likely. To examine this hypothesis

4. Results

Co-IPs with *GFP-ATG2*, *GFP-ATG18* or *GFP-ATG9* expressed under the control of a *MET25* promoter from plasmids in different knockout strains together with chromosomally expressed VPS35-6xHA were performed. Neither Atg2 nor Atg9 are required for binding of Vps35 to Atg18, as Vps35-6xHA co-precipitated with GFP-Atg18 in the absence of Atg2 (see Figure 4-26B) and Atg9 (see Figure 4-26C). Interestingly, Vps35-6xHA also precipitated with GFP-Atg2 as can be seen in Figure 4-26A. A binding of Vps35 to Atg2 can also be detected in the absence of Atg18, the interaction is therefore not dependent on the PROPPIN. The amount of Vps35 co-purified with Atg2 was low compared to Atg18, indicating a lower affinity or an indirect connection.

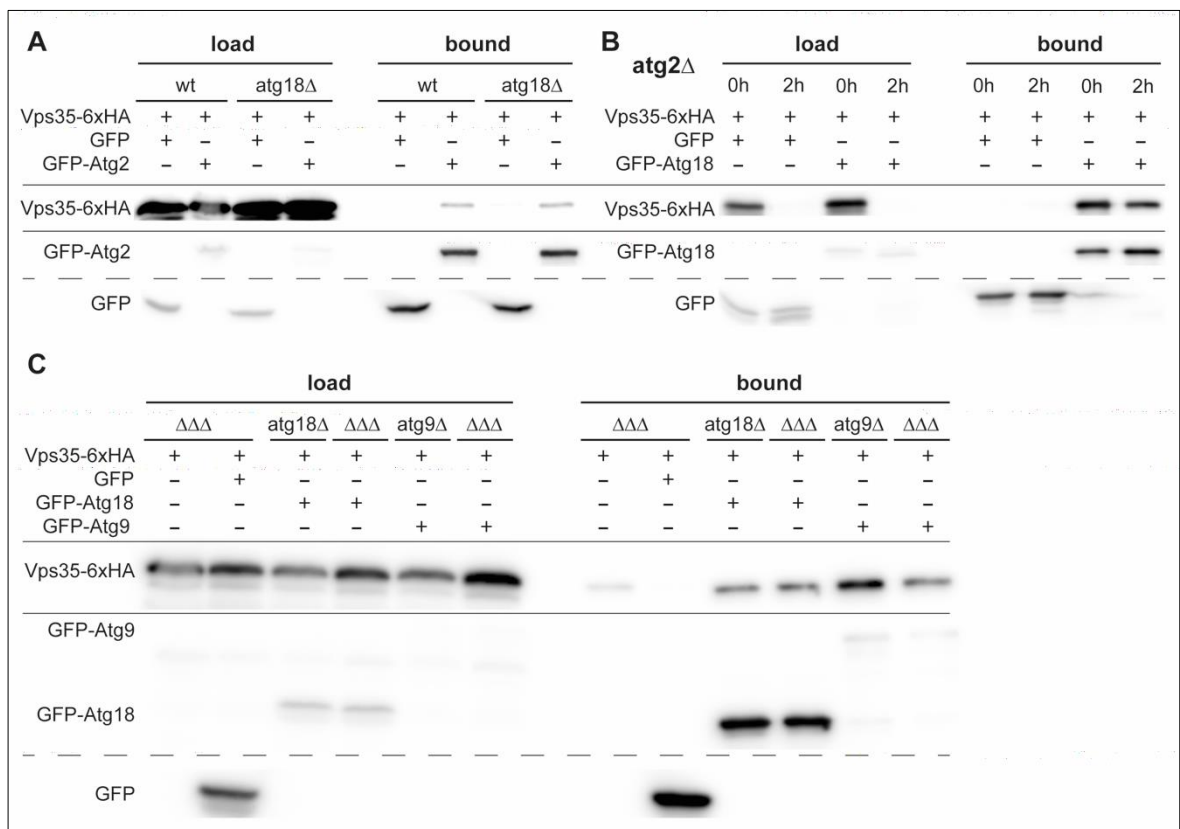


Figure 4-26: Vps35 copurifies with Atg9 and Atg2 independent of Atg18.

GFP-Traps were performed to analyze interaction between Vps35 and the Atg2-Atg18 complex and Atg9, respectively. Strains with different GFP- and HA-tagged proteins are grown in selection medium supplemented with 0.3 mM methionine to an OD₆₀₀ of 2-3, harvested and processed according to protocol. Load and bound samples were analyzed with Western blots decorated with antibodies against HA and GFP. **(A)** Chromosomally tagged VPS35-6xHA (prey) was expressed together with GFP tagged bait (GFP, GFP-ATG2) with a *MET25* promoter from plasmid in either a wildtype or *atg18Δ* strain. **(B)** Chromosomally tagged VPS35-6xHA (prey) was expressed together with GFP tagged bait (GFP, GFP-ATG18) with a *MET25* promoter from plasmid in an *atg2Δ* strain. Cells were starved in SD-N for 2h, before the Co-IP was performed. **(C)** Chromosomally tagged VPS35-6xHA (prey) was expressed together with GFP tagged bait (GFP, GFP-ATG18, GFP-ATG9) with a *MET25* promoter from plasmid in either a functional wildtype (*atg18Δ* or *atg9Δ*, respectively) or a triple knockout strain (*atg18Δ atg2Δ atg9Δ - ΔΔΔ*).

Atg9 is the only transmembrane protein involved at this stage of autophagy and is thought to be removed before fusion with the vacuole occurs. For this reason, it would

4. Results

be an excellent cargo of the retromer complex. Vps35-6xHA co-precipitates with GFP-Atg9, as can be observed in Figure 4-26C. The amount of bound Vps35 is slightly lower in an *atg18Δ atg2Δ* strain, but Atg9 and Vps35 are still able to interact. The signal detected for GFP-Atg9 after decorating the same blot with antibodies against GFP was weaker compared to the signal for Atg18 (Figure 4-26C). Atg9 is a transmembrane protein, which is more difficult to isolate than cytosolic proteins. More Atg9 is lost during cell lysis and purification compared to Atg18. The ratio of bound Vps35-6xHA to prey is therefore much higher for Atg9 than for Atg18. This indicates a stronger and more stable interaction between Atg9 and Vps35. Since the low amount of purified Atg9 is not enough to saturate the magnetic beads unspecific binding of Vps35-6xHA to the beads is possible. To exclude this possibility cells expressing only Vps35-6xHA and no GFP were used as a control. Although some HA-tagged protein was detected in the control, the signal was weaker compared to the amount of Vps35-6xHA bound to GFP-Atg9.

All of these results led to the conclusion, that Vps35 can form a complex with both Atg18 and Atg9 independent of each other. Atg2 could be linked to Vps35 via Atg9, although a direct connection between Atg2 and Vps35 cannot be ruled out at this point. This however could indicate a role of the retromer complex in retrieving Atg9 from the autophagosome.

4.2.1. Localization of Atg2 and Atg9 in *vps35Δ* cells

If recycling of Atg2 or Atg9 from the autophagosome is mediated by the retromer complex and this step is necessary for vacuole fusion, both proteins should accumulate with the PAS marker Atg8 in a *vps35Δ* strain and this should be enhanced during starvation. Both Atg2 and Atg9 were chromosomally tagged with GFP at the C-terminus and expressed in wildtype and *vps35Δ* strains together with mCherry-Atg8 with endogenous promoter from a plasmid as a PAS marker.

The amount of colocalization of Atg9-GFP and mCherry-Atg8 was reduced in the absence of Vps35: 45% of all Atg8 dots colocalized with Atg9 in wildtype cells, while the rate was reduced to 26% in a *vps35Δ* strain (Figure 4-27A,B). This did not change during starvation.

4. Results

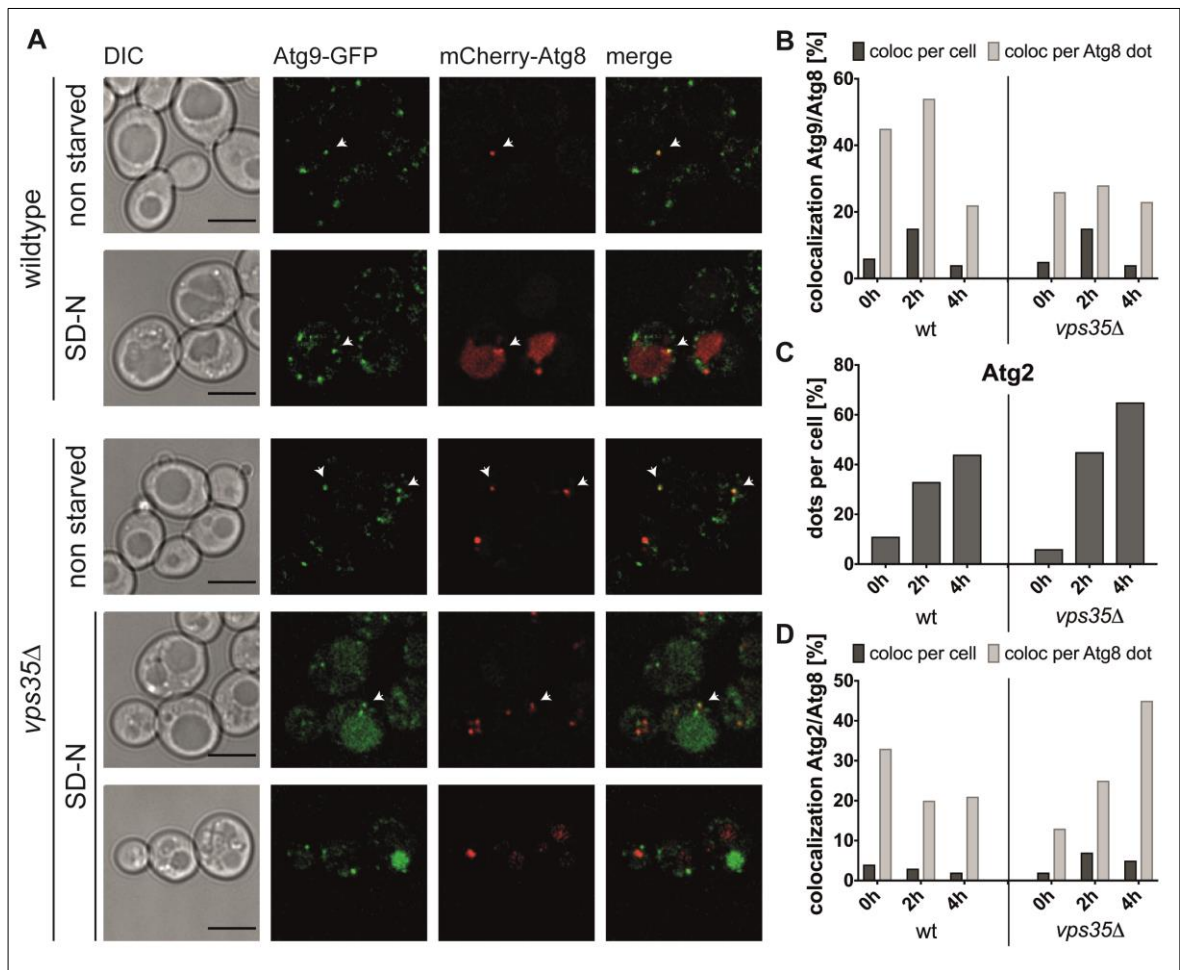


Figure 4-27: Recycling of Atg9 from the mature autophagosome is not dependent on Vps35.

Localization of Atg9 in the absence of Vps35 was analyzed using fluorescence microscopy to test if the transmembrane protein is recycled by retromer. **(A)** Wildtype or *vps35Δ* strains expressing chromosomally tagged Atg9-GFP together with the PAS marker mCherry-Atg8 with an endogenous promoter from plasmid were grown to an OD_{600} of 2-3 and transferred to SD-N medium. Cells were analyzed after 0h, 2h or 4h starvation. White arrows indicate puncta positive for Atg8 and Atg9. Scale bar is set to 5 μm. **(B)** The number of Atg8 and Atg9 positive puncta as well as colocalizations were counted to calculate the rate of colocalization per cell and per Atg8 dots. **(C+D)** The localization of Atg2 dependent on Vps35 was analyzed with fluorescent microscopy. Wildtype or *vps35Δ* strains expressing chromosomally tagged Atg2-GFP together with the PAS marker mCherry-Atg8 with an endogenous promoter from plasmid were grown and treated as described in (A). **(C)** The number of Atg2-GFP positive dots was counted and divided by the total amount of cells. **(D)** The number of Atg8 and Atg2 positive puncta as well as colocalizations were counted to calculate the rate of colocalization per cell and per Atg8 dots.

Atg9 could also be recycled from the vacuolar membrane after the fusion of the autophagosome with the vacuole. Deletion of *VPS35* should then result in the accumulation of Atg9 at the vacuolar membrane, similar to Atg18. But experiments with GFP tagged Atg9 demonstrated no increased GFP signal at the vacuolar membrane after nitrogen starvation. Remarkably, free GFP accumulated in the vacuolar lumen, which was not observed in wildtype cells (Figure 4-27A). Atg9 is a transmembrane protein with both N- and C- terminal at the cytosolic side of the membrane leaflet (Matoba et al., 2020). The fusion of the autophagosome with the vacuole would not result in GFP on the luminal side of the vacuole. Atg9 would have to be mislocalized to

4. Results

the inner leaflet of the growing phagophore, which would locate the protein in the autophagosome and the autophagic body. For this reason, the increased amount of free GFP in *vps35Δ* cells after starvation is unlikely to be caused by a defect in Atg9 retrieval from the autophagosome. Together the data indicates that deletion of *VPS35* might result in a defect in Atg9 sorting to either a peripheral Atg9 pool or the PAS. Instead, Atg9 might be partially missorted into MVB vesicles at the late endosomes and transported to the vacuolar lumen. A similar missorting was already observed in mammalian cells, where Atg9A trafficking is affected by mutations in *VPS35* (Zavodszky et al., 2014). Although a direct interaction between both proteins was not observed, some ATG9A colocalized with mammalian VPS35. In cells expressing the mutant *VPS35^{D620N}* ATG9A was mislocalized to an abnormal perinuclear compartment. No GFP signal was detected in the vacuoles of *vps35Δ* cells expressing Atg2-GFP and mCherry-Atg8. The distribution of Atg2-GFP during starvation seemed to be affected by a deletion of *VPS35*: the amount of Atg2 positive puncta in the cytosol was increased compared to the wildtype, 65% per cell after 4h starvation compared to 44% in the wildtype (see Figure 4-27C). Additionally, colocalization of mCherry-Atg8 and Atg2-GFP is increased: 28% of all Atg8 puncta were positive for Atg2 in the wildtype, while deletion of *VPS35* increased this to 45%. However, due to the low number of Atg8 dots after 4h of nitrogen starvation the significance is questionable. 13 out of 29 Atg8 dots colocalized in 261 counted *vps35Δ* cells, while 6 out of 28 dots colocalized in 292 counted wildtype cells. Unlike Atg18, Atg2 is not accumulated at the vacuolar membrane. This indicates that Atg18 is the only membrane associated protein recycled from the autophagosomal or vacuolar membrane mediated by the retromer complex in combination with Snx3.

5. Discussion

Autophagy is essential in maintaining the balance between anabolism, synthesis of new amino acids and precursors, and catabolism, the breakdown of cellular components. It was the topic of intense research over the last decades, culminating in a Nobel prize. A major breakthrough was the discovery of the molecular components of the autophagic machinery by genetic screens in yeasts. Since then many of the complex processes have been described in more detail. However, vital functions such as the *de novo* formation of the double membrane or the homotypic fusion of the autophagosomal membrane edges are still unknown or speculation.

This thesis is an attempt to shed some light on the functions of Atg18 in autophagy and other cellular processes by identifying and characterizing previously unknown interaction partners.

5.1. BioID

5.1.1. Proximity-based labeling assays

Proximity-dependent labeling assays have been developed in response to an old problem: for most biochemical approaches a complex needs to be isolated before it can be analyzed. The steps necessary for isolation, e.g. cellular disruption, purification, often destroy more fragile interactions. Labeling complexes *in vivo* coupled to mass spectrometry is a useful tool to map whole protein interactomes (Chen & Perrimon, 2017). The protein of interest (bait) is fused to an enzyme that covalently tags neighboring proteins. Three major approaches have been developed for proximity-dependent labeling: proximity-dependent biotin identification (BioID), horseradish peroxidase (HRP) and engineered ascorbate peroxidase (APEX).

The BioID assay has been described in chapter 4.1: a mutated more promiscuous version of the *E. coli* biotin ligase BirA catalyzes the conversion of biotin to the highly reactive biotinoyl-5'-AMP, which is released from the enzyme and covalently tags neighboring proteins at lysine residues (Choi-Rhee et al., 2008; Roux et al., 2012). Both HRP and APEX assay use similar methods: they are activated by H₂O₂ and catalyze the conversion of the substrate, biotin-phenol, into a highly reactive radical, which then

5. Discussion

binds to electron-rich amino acids such as tyrosine residues of nearby proteins (Jiang et al., 2012; Martell et al., 2012).

Both HRP and APEX assay have the advantage of creating radicals that can be detected with an electron microscope, verifying the location of a complex in the cell. This is not possible with the BioID assay. However, unlike the biotin used for the BioID assay which is actively imported into the cell, HRP and APEX prefer biotin-phenol as substrate. This molecule does not effectively penetrate yeast cell walls, high osmolarity and disruption of cell wall integrity by treatment with zymolyase are necessary. Another difference is the duration of treatment: APEX and HRP proximity labeling generate short-lived but highly reactive radicals, the half-life of radicals determined for APEX is just 1 ms (Rhee et al., 2013), with a labeling radius of less than 20 nm (Chen et al., 2015). Biotin-5'-AMP has a half-life of minutes and should therefore have a wider labeling range (DeMoss et al., 1956). However, with 10-15 nm the effective biotinylation radius seems to be shorter (Kim et al., 2014). It has to be pointed out that the range of the two different systems was evaluated under completely different conditions and in different organisms, which probably affect the labeling radius. Since APEX has such rapid kinetics it is optimal for observing short interactions, such as during acute responses. With optimal labeling time between 15 to 24 hours, the BioID assay is better to detect whole protein complexes and the changes over a longer period of time.

5.1.2. Optimization of the BioID assay

Several attempts to improve the function of the BirA* ligase have been made (Xu et al., 2021). One of the first innovations was the design of BioID2, a substantially smaller ligase lacking the N-terminal DNA-binding domain (D. I. Kim et al., 2016). The location as well as the function of the fusion protein is improved due to the smaller size of the tag. It also shows a higher affinity to biotin and is therefore functional at lower biotin concentrations (Samavarchi-Tehrani et al., 2020). The ligase BaSu was engineered from *Bacillus subtilis* to study RNA-protein interactions and was proposed to show an improved signal-to-noise ration compared to BirA* as well as faster kinetics (Ramanathan et al., 2018). Later studies were unable to confirm this, which led to the development of TurboID and the much smaller miniTurbo (Branon et al., 2018). Directed evolution was used to generate mutants of the *E.coli* ligase BirA* with

5. Discussion

improved functions. The resulting enzyme was able to catalyze as many biotinylations in 10 min as BioID in 18 hours and had an overall 3-6 fold increase in activity compared to BirA*. This enables shorter incubation times, minimizing the chance of false positives. The stronger signal also allows the use of TurboID for low-abundant proteins, which so far could not be used in a BioID.

5.1.3. Atg18 interactome

The BioID assay was used to analyze the interactome of Atg18. For this, the ligase BirA* was fused to the bait protein Atg18. Since BirA* releases activated biotinoyl-5'-AMP into its vicinity, the covalently bound fusion protein should always be biotinylated and therefore be identified as a prominent hit by mass spectrometry.

Four biotinylation sites were identified for Atg18 and the protein was enriched compared to both controls. Furthermore, three of the known interactors of Atg18, Atg2, Fab1 and Vac14, were also identified as candidates. While Vac14 is known to interact with Atg18 as a result of two-hybrid experiments, Co-IPs with Atg18 and Vac14 were unsuccessful until now (Jin et al., 2008). The binding of both proteins to each other was clearly demonstrated in Figure 4-8. All these results confirm the BioID assay as functional and identified candidates can be considered as potential interactors of Atg18.

84 proteins in total were found to be enriched in a sample containing Myc-BirA*-Atg18 compared to the control (see Figure 4-3). 28 of them are involved in DNA and RNA processing, as described in chapter 4.1.2. Since BirA* is fused to the N-terminus of Atg18 in these experiments, it is translated before Atg18 and briefly stuck to the ribosomes, while the rest of the fusion protein is synthesized. The BirA* domain might already be functional and could activate and release biotin while still bound to the ribosome. This would increase the chance of ribosomal proteins being biotinylated, especially compared to BirA* alone, which is released directly after its synthesis. This could explain why DNA and RNA processing proteins are enriched as a result and cannot be identified and filtered out as background.

Interestingly, several of the proteins identified contained either a phospholipid binding site (Pib2) or are associated with the membrane such as the vacuolar transporter Avt4 and Vtc3. Candidates detected in a BioID do not have to interact with the bait protein, as biotinylation is not specific. They only have to be in the vicinity of the biotin ligase,

5. Discussion

while longer exposure further increases the radius and therefore the chances of biotinylation. An example for this could be membrane proteins that locate to lipid rafts and are therefore in close proximity to each other, although they do not necessarily interact with one another. For this reason, the candidates from the BioID assay with Atg18 should be carefully validated by an independent method.

Furthermore, proteins in a highly fluctuating complex have a reduced chance of biotinylation, even if they are in a complex with the bait protein. Another important aspect is the accessibility of lysine residues, as they might be inside the protein or covered by other interaction partners. Activated biotin is unable to react with these residues and the protein is therefore not isolated.

Proteins can be part of several complexes and it is impossible to separate components of one complex from the other. One approach to solve this problem is a split-BioID (Schopp et al., 2017): the catalytic enzyme is split into two inactive fragments and can only regain function if both units are brought into contact. This can be achieved by fusion of the fragments to two proteins interacting in a specific complex. The assay used in this thesis was a BioID with a promiscuous BirA* ligase. However, for the purpose of distinguishing two separate processes as the function of Atg18 in autophagy (in a complex with Atg2 and Atg9) or the function in maintaining vacuolar morphology (interacting with the Fab1 kinase complex), an approach based on a split-BioID could be useful. Here, a similar effect was attempted by depleting localized PtdIns3P pools at either the PAS or the endosomal membrane. The result however was not as promising as expected, with several of the previously discovered candidates missing from the screen, for example, the regulator subunit of Fab1 kinase, Vac14. Since the identified proteins could only be compared to one control and not two as in the previous experiment, it is very likely that more false positives were detected.

12 of the Proteins identified as interaction partners of Atg18 are part of intracellular trafficking pathways: the ESCRT subunit Snf7 for example is involved in endosomal protein sorting, while the kinase Yck3 regulates fusion events at the vacuole. Both will be discussed in later chapters (chapter 5.1.6 and chapter 5.1.5, respectively).

One interesting candidate is Ykt6, which had one identified biotinylation site and is therefore a very promising potential interactor of Atg18. Unfortunately, Co-IPs were not conclusive, but an interaction is nevertheless highly likely (chapter 5.1.7).

5. Discussion

Several of the candidates found with the BioID assay have been identified in previous manually curated or high-throughput assays (indicated by a black line in Figure 5-1).

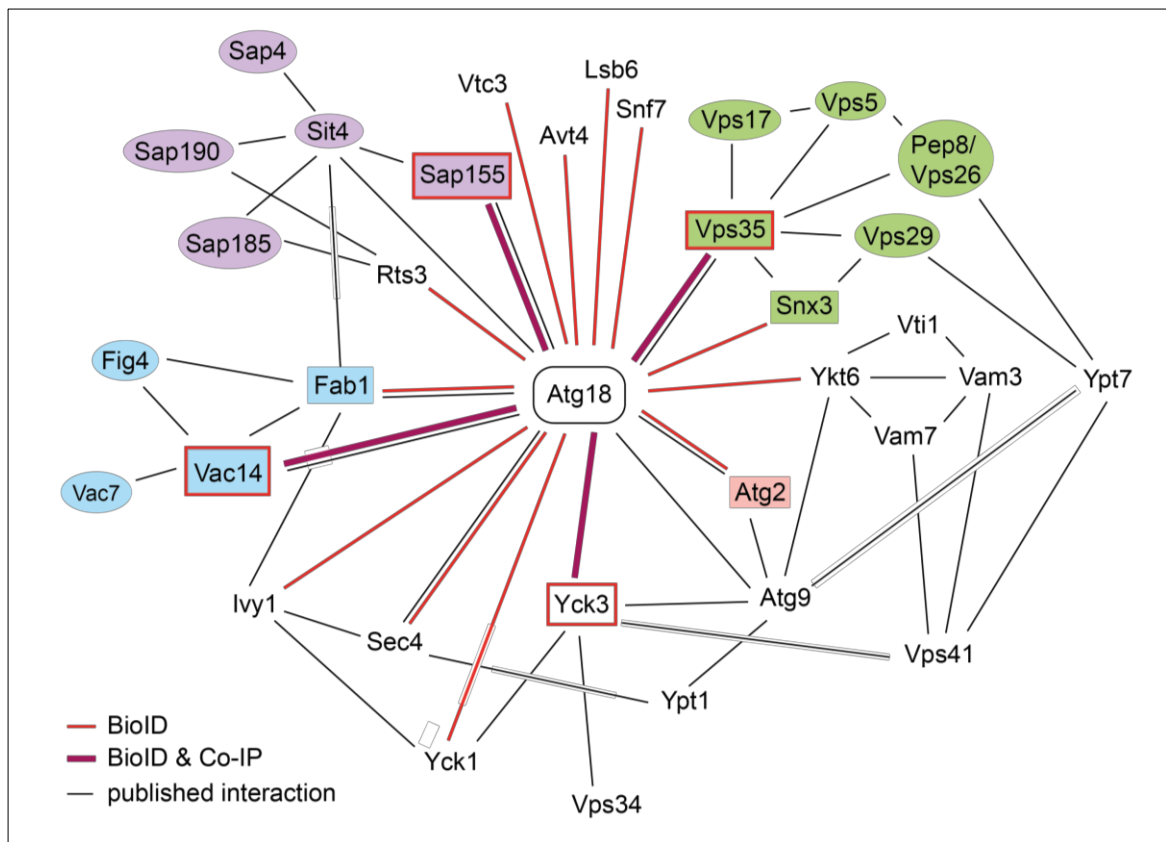


Figure 5-1: Map of interactions between Atg18 and other proteins.

Data accumulated from the Saccharomyces Genome Database (www.yeastgenome.org).

For example, Sap155 was detected in this experiment, but also in two independent previously published high-throughput assays (Ho et al., 2002; Krogan et al., 2006). Sap155 regulates the phosphatase Sit4, which was also identified as an Atg18 interactor in a high-throughput affinity capture assay coupled with MS (Ho et al., 2002). A connection of Sap155 with Atg18 seems to be independent of membrane association, as the Sit4 regulator is enriched in *atg14Δ* as well as *vps38Δ* strains. A possible function of the interaction between Atg18 and the Sit4 complex will be discussed later (chapter 5.1.4).

Interaction of Atg18 with Vps35 and Vps29 was previously described by (Graef et al., 2013), Vps35 was a prominent candidate in the BioID assay and could also be confirmed with Co-IPs. It was also shown to interact with another BioID candidate, Snx3, which was so far unknown as interactor of Atg18. Both interactions seem to occur at the endosome, as Vps35 and Snx3 were enriched in an *atg14Δ* strain compared to the deletion of *VPS38*. This will be further analyzed and discussed in chapter 5.2.

5. Discussion

5.1.4. Sap155 and the phosphatase Sit4

The BioID candidate Sap155 was previously briefly described in chapter 4.1.2. It was the first candidate validated with a Co-IP and a strong signal in the bound fraction of Atg18 was observed. An interaction of Atg18 with this protein was not detected in previous high-throughput assays searching for Atg18 interactors.

Cellular functions are often regulated by protein phosphorylation. Two encoding genes for the catalytic subunit of the protein phosphatase 2A (PP2A) have been identified in *S. cerevisiae* as well as three PP2A related phosphatases, one of which is *SIT4* (Zabrocki et al., 2002). They act downstream of the nutrient sensor TORC1 (described in chapter 2.3.5.7), which regulates protein biosynthesis, ribosomal biogenesis, growth and cell cycle events. Sit4 is regulated by four Sit4-associated proteins of different size, Sap155, Sap185, Sap190 and Sap5 (Luke et al., 1996; Sutton et al., 1991). Tap42 is also associated with Sit4 independent of the SAPs (Di Como & Arndt, 1996). In its phosphorylated form, the protein shows a high affinity towards Sit4 as well as the other phosphatases and forms a complex. Treatment with the Tor1 inhibitor rapamycin or loss of TORC1 function disassembles the complex and releases both Tap42 and Sit4, which is thought to activate the phosphatase (Di Como & Arndt, 1996; Jiang & Broach, 1999).

TORC1 was observed to play an important role in autophagy regulation by phosphorylating Atg13. This inhibits the formation and activation of the Atg1 kinase complex, which blocks autophagy. However, the exact mechanism of how the inactivation of TORC1 mediates Atg13 dephosphorylation is still unknown. The major regulatory component directly downstream of TORC1 is Tap42 and this protein is not involved in inducing autophagy (Kamada et al., 2000). An interaction between Atg18 and the Sit4 regulator Sap155 is probably also not involved in the mechanism, as Atg18 recruitment to the PAS is downstream of the Atg1 kinase complex (Suzuki et al., 2013). However, the phosphatase Sit4 could be involved in the dephosphorylation of Atg1 during autophagy induction and the deactivation of the Atg1 kinase complex. This is thought to regulate the disassembly of the autophagic machinery after autophagosome formation. This could be regulated by Sap155 and the PtdIns effector Atg18. A change in autophagic activity upon deletion of *SAP155* could not be observed (see chapter 4.1.1), which could indicate no function of Sap155 in autophagy. However, yeast

5. Discussion

expresses three known homologues to Sap155, which could indicate a redundancy of the Sit4 regulators.

Atg18 contains several phosphorylation sites at its hydrophobic loop, which are thought to regulate membrane association. Phosphorylation of the loop decreases membrane affinity of Atg18 in *P. pastoris*. This affected vacuolar morphology as well as micropexophagy and seemed to occur strictly at the vacuolar membrane (Tamura et al., 2013). The kinases and phosphatases involved are not yet known. The phosphatase Sit4 in complex with its regulator Sap155 could function in the dephosphorylation of Atg18, promoting membrane association and vacuolar fission events or could act as signal for Atg9 recycling.

5.1.5. Yck3 regulates vacuolar fusion events

Another enzyme involved in phosphoregulation at the vacuole/endosome is an isoform of the yeast casein kinase I named Yck3 (Wang et al., 1996). The membrane-associated protein is transported to the vacuole mediated by the AP-3-dependent transport pathway (Sun et al., 2004). Deletion of *YCK3* affects vacuolar morphology during hypertonic stress: exposure to high concentrations of salt caused vacuolar fragmentation to maintain the osmotic balance similar to wildtype. But while the vacuoles in wildtype stayed small and fragmented, vacuoles in the absence of Yck3 became large again in a SNARE dependent manner (LaGrassa & Ungermann, 2005). Yck3 phosphorylates the HOPS complex subunits Vps41 and Vam3 and negatively regulates membrane tethering during fusion events at the vacuole (Cabrera et al., 2009). Interestingly, phosphorylation of the HOPS complex subunit Vps41 mediated by Yck3 does not completely block fusion. Tethering with Ypt7 in its active GTP bound form is still possible (Zick & Wickner, 2012). Yck3 is also speculated to play a role during budding events at the vacuolar membrane, as homotypic vacuolar fusion of tubules just pinched off from the vacuolar membrane must be inhibited (LaGrassa & Ungermann, 2005).

Yck3 was a candidate identified in both BioID assays performed, it seemed to interact with Atg18 independent of membrane localization. It also coimmunoprecipitated with Atg18, further validating an interaction. Interestingly, the amount of Yck3 bound to Atg18 was slightly increased after 2h of nitrogen starvation. This was not expected, as Yck3 is exclusively located to the vacuolar membrane. However, if Atg18 is not recycled

5. Discussion

from the autophagosome but from the vacuolar membrane, bulk autophagy could transiently increase the Atg18 concentration at the vacuole.

Atg18 is required for maintaining vacuolar morphology during hyperosmotic stress, as deletion causes a swollen vacuole during high salt concentrations (Dove et al., 2004). The phosphorylation status of its hydrophobic loop is thought to regulate its activity and membrane association (see chapter above). Yck3 depletion causes a partial defect in PpAtg18 phosphorylation (Tamura et al., 2013). The HOPS complex responsible for membrane tethering and Atg18 involved in membrane fission events seem to be counterparts in regulating vacuolar morphology and Yck3 could play a role in balancing both processes at the vacuolar membrane.

5.1.6. Snf7 could be involved in autophagosome closure

The ESCRT (endosomal sorting complexes required for transport) machinery has long been in discussion as a mechanism of autophagosome closure (Hurley, 2015). It is part of the MVB pathway, described in chapter 2.2.1. Four different multimeric complexes have been identified and are thought to act sequentially to recruit ubiquitinated cargo into invaginations of the endosomal membrane, which bud inwards and are ultimately severed to form ILVs (Lefebvre et al., 2018; Schöneberg et al., 2017).

Early studies found a connection between the ESCRT machinery and autophagosome maturation (Rusten et al., 2007). However, this was very controversial as other studies found a requirement of functional MVBs for efficient autophagic degradation, which would provide an explanation for previously observed phenotypes (Filimonenko et al., 2007). Regardless of that the homotypic fusion of the autophagosomal edges shares some similarities with the membrane scission catalyzed by the ESCRT-III complex (Hurley & Hanson, 2010).

Recent publications propose a role of ESCRT components, notably Snf7, in autophagosome closure (Zhou et al., 2019). Deletion of Snf7 caused a complete block in autophagic activity and led to the accumulation of unsealed autophagosomes decorated with Atgs. An interaction between Snf7 and Atg17 was suggested to recruit parts of the ESCRT machinery to the unsealed autophagosome. Snf7 was found in the BioID assay and is therefore a potential interactor for Atg18. Atg18 could be involved

5. Discussion

in recruiting Snf7 to the phagophore, which could then induce the disassembly of the Atg9/Atg2/Atg18 complex.

However, the complete block of Ape1 maturation in *snf7Δ* strains as described in (Zhou et al., 2019) could not be reproduced, although autophagic activity was significantly reduced under specific conditions. Interaction of Snf7 with Atg18 seems not to be limited to the autophagosome, since Snf7 was also enriched in the *atg14Δ* strain (see chapter 4.1.3 and Figure 4-5). A function at the endosomal membrane is therefore also a possibility.

5.1.7. Fusion with vacuole requires Ykt6

Ykt6 was discovered in the BioID as a potential binding partner of Atg18. One biotinylation site was identified, which is a very strong indicator of a direct interaction. The R-SNARE Ykt6 forms a complex with the Q-SNAREs Vam3 (Q_a), Vti1 (Q_b) and Vam7 (Q_c), which is required for autophagosome-vacuole fusion (Bas, Papinski, Licheva, et al., 2018; Darsow et al., 1997; Dilcher et al., 2001; Gao, Reggiori, et al., 2018; von Mollard & Stevens, 1999). Vam3, Vti1 and Vam7 are located at the vacuolar membrane, while Ykt6 was detected at the autophagosome (Bas, Papinski, Licheva, et al., 2018; Gao, Reggiori, et al., 2018).

Ykt6 localizes to the PAS during the early stages of autophagy, before autophagosome completion. A recent study observed a defect in Ykt6 recruitment after deletion of the ER-resident Dsl1 complex. This complex is involved in the fusion of COPI-coated vesicles and was previously shown to interact with Ykt6 (Andag et al., 2001; Meiringer et al., 2011). COPII coated vesicles were observed as a potential membrane source for the nascent autophagosome. It was therefore hypothesized, that Ykt6 is sorted into COPII-coated vesicles dependent on the ER-resident Dsl1 complex and delivered to the PAS (Gao et al., 2020). Random fusion of the immature autophagosome is blocked by direct phosphorylation of Ykt6 mediated by the Atg1 kinase complex (Barz et al., 2020; Gao et al., 2020).

Both Atg18 and Ykt6 are located at the autophagosomal membrane and the BioID results suggest an interaction. Ykt6 was shown to colocalize with Atg9 and Ape1 in the absence of Atg2, recruitment to the PAS is therefore not dependent on the Atg2-Atg18 complex (Gao et al., 2020). The dephosphorylation stage of Ykt6 could also act as a

5. Discussion

signal for autophagosome maturation and induce disassembly of the autophagic machinery.

So far not enough is known about the interaction between Ykt6 and Atg18 to propose a hypothesis.

5. Discussion

5.2. Vps35 and Snx3

5.2.1. Atg18 forms complex with Retromer

Atg18 interacts with Vps35, as demonstrated with a BioID assay as well as Co-IPs. Furthermore, both proteins can be found at the endosomal membrane and experiments with a fluorescence microscope confirmed colocalization of 40% of all Atg18-GFP puncta with Vps35-mCherry (Figure 4-11).

Vps35 is part of a peripheral membrane complex that regulates and mediates retrograde trafficking from the endosome to the Golgi, the so-called retromer complex. It is also named cargo recognition or selection complex (CRC or CSC) and retromer core complex. It consists of three subunits, Vps35 itself, Vps26 and Vps29. In addition to Vps35 Atg18 was able to interact with Vps26 in the presence of Vps35 but not in a *vps35Δ* strain. Deletion of *VPS26* did not completely block the interaction between Atg18 and Vps35, as Vps26 is not required for complex formation (Seaman et al., 1998). Interaction between Vps35 and Vps29 is essential to stabilize Vps35, which explains the loss of binding between Atg18 and Vps35 in a *vps29Δ* strain. Furthermore, mutating the FRRG motif responsible for PtdIns3P binding to the functionally defect FTTG also affects the affinity between Atg18 and the retromer subunit.

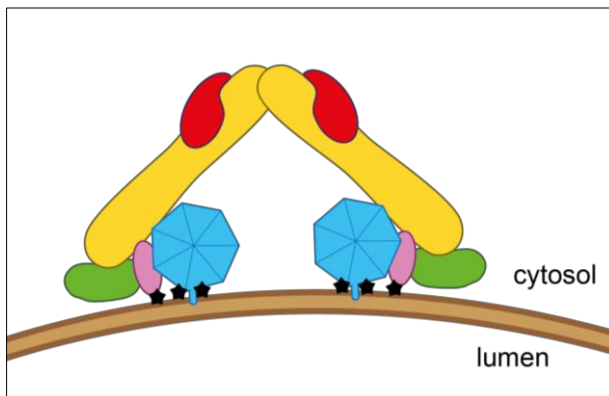


Figure 5-2: Model of retromer in complex with Atg18.

Atg18 (blue) interacts with Vps35 (yellow) and Snx3 (pink), while binding to the membrane mediated by a hydrophobic loop and PtdIns3P (black). Vps35 is in a complex with Vps29 (red) and Vps26 (green).

Altogether the results suggest the formation of a complex with Atg18 and retromer subunits Vps35, Vps26 and Vps29. A direct connection between Atg18 and Vps26 cannot be ruled out, as it could be stabilized by Vps35 and therefore not detectable in a *vps35Δ* strain. Association of Atg18 with PtdIns3P recruits the complex to the membrane.

Early studies attributed two additional proteins to the retromer complex, the membrane associated Vps5 and Vps17. Retrograde trafficking of the first and best described retromer cargo, Vps10, was blocked in their absence (Nothwehr et al., 1996; Seaman et al., 1998). None of the components of the retromer core complex (Vps26, Vps29, Vps35) are able to bind to

5. Discussion

the membrane or induce curvature, therefore an interaction with integral membrane proteins or sorting nexins is essential. Sorting nexins are characterized by a phosphoinositidephosphate-binding PX domain (phagocyte oxidase (phox) homology domain) targeting these proteins to cellular membranes containing PtdIns3P (reviewed in (Worby & Dixon, 2002)). Both Vps5 and Vps17 are SNX proteins and furthermore contain a BAR (bin/amphiphysin/Rvs161) domain with a curved form. Dimerization results in the characteristic “banana-shape” (reviewed in (Mim & Unger, 2012; Ren et al., 2006; van Weering et al., 2010). Binding to membranes induces membrane curvature or tubulation of formerly round spheres (Takei et al., 1999). The retromer complex was therefore thought to contain the SNX-BAR proteins Vps5 and Vps17 in addition to Vps26, Vps29 and Vps35.

More recent publications propose a more flexible model for the complex mediating retrograde traffic: here, the heterotrimeric retromer complex recognizes and recruits cargo, while SNX proteins bind to the membrane and induce curvature to form tubules. Interactions between components of both subcomplexes facilitate the concentration of cargo at the tubular structures and eventual fission of retrograde vesicles (Ma & Burd, 2019).

The function of the retromer complex is highly diverse, it has been linked to many different cellular processes such as the establishment of cellular polarity, regulation of morphology and apoptotic cell clearance (Burd & Cullen, 2014). Mutations in retromer components or deficiency are thought to be involved in an increasing number of human diseases. So has the loss of retromer been linked to the risk for Alzheimer’s disease (Siegenthaler & Rajendran, 2012) and mutations in *VPS35* and *VPS26* have been associated with late-onset familial Parkinson’s disease and type 2 diabetes, respectively (Kooner et al., 2011; Zimprich et al., 2011). The retromer core complex is thought to predate the last common eukaryotic ancestor and is highly conserved among all eukaryotes (Koumandou et al., 2011). A variety of sorting nexins specific for selected cargo and transport pathways expands the repertoire of proteins trafficked from the endosome (Ma et al., 2017). The SNX-BAR domain protein Mvp1 was recently shown to promote fission of Vps5-Vps17-coated tubules at the endosome (Chi et al., 2014), together with the dynamin-like protein Vps1 (Ma et al., 2017). Interestingly, deletion of either *VPS5* or *VPS17* increased the amount of Vps35 bound to Atg18 more

5. Discussion

than two-fold (chapter 4.2.2), which hints at an alternative pathway in competition to Vps5/Vps17.

Another SNX involved in endosomal protein sorting mediated by retromer is Snx3 (Harterink et al., 2011; Strohlic et al., 2007; Voos & Stevens, 1998). Snx3 was also detected in the BioID assay as a potential interactor of Atg18. One biotinylation site was identified, which further confirms a connection to the PROPPIN. Unfortunately, Snx3 could not be co-precipitated with Atg18; but is nonetheless a likely interaction partner due to its connection with retromer. Unlike Vps5 and Vps17 it belongs to the 'PX-only' sub-family of sorting nexins and can therefore bind to PtdIns3P but not induce membrane tubulation (Worby & Dixon, 2002). Snx3 was shown to interact with Vps35 at its N-terminal end close to the membrane and with Vps26, both with multiple interfaces (Chen et al., 2019; Lucas et al., 2016), as shown in Figure 5-3. This is required for membrane recruitment of retromer as well as binding and sequestering cargo proteins into recycling transport intermediates. A recent study in *S. cerevisiae* proposed a different model for interaction between the CRC and sorting nexins: they were able to coimmunoprecipitate Vps35 and Vps29 with Vps5 in the absence of Vps26. This implies a direct connection between Vps35 and/or Vps29 with the sorting nexins (Suzuki et al., 2019). The different findings could be explained by an interaction between sorting nexins and CSC mediated by the cargo, as the Co-IP experiments were conducted *in vivo*.

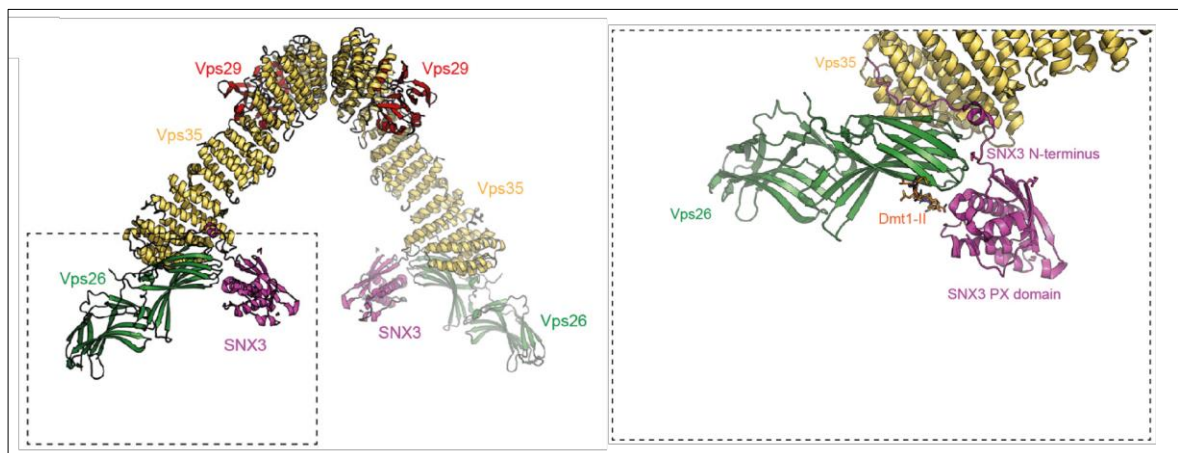


Figure 5-3: Model of SNX3 in complex with retromer based on an alignment of the crystal structure of human SNX3 bound to Vps35 and Vps26 from *C. thermophilum*.

SNX3 (magenta) interacts with Vps35 (yellow) and Vps26 (green), Vps29 (red) interacts with and stabilizes Vps35. Adapted from (Chen et al., 2019)

The exact mechanism of inducing membrane curvature remains unknown. Atg18 contains an unstructured hydrophobic loop at blade 6 between the two lipid binding

5. Discussion

sites (Baskaran et al., 2012; Krick et al., 2012; Watanabe et al., 2012), which undergoes a transformation into an amphipathic α -helix upon contact with lipids (Gopaldass et al., 2017). This loop is necessary and sufficient to induce tubulation of GUVs if recruited to the membrane via PtdIns3P or PtdIns(3,5)P₂. A complex containing retromer, Snx3 and Atg18 could therefore recruit cargo (via retromer and Snx3) associate with the membrane (via Snx3 and Atg18) and induce membrane tubulation (via Atg18). Both Snx3 and Atg18 would thereby take over the function of SNX-BAR proteins Vps5 and Vps17. A model of this is shown in Figure 5-2.

Interestingly, both Atg21 and Hsv2 are also able to interact with Vps35 (chapter 4.2.1) and Vps35 was detected in a BioID assay with Atg21 as bait (unpublished data from Dr. Lena Munzel). Vps35 could also be co-purified with Atg21 (unpublished data from Dr. Lena Munzel). For this, the binding site for Vps35 at Atg18 needs to be highly conserved among all PROPPINs. It also opens up the possibility that Atg18 is redundant in its function with Vps35 and can easily be replaced with either Atg21 or Hsv2. Vps35 self-dimerizes to form multiprotein complexes and this megacomplex could also contain different PROPPINs.

5.2.2. Function of Atg18 in retromer activity

An early hypothesis regarding the function of Atg18 in complex with retromer was membrane shaping during cargo sequestration. As previously mentioned Snx3 only contains a PX domain and is unable to induce membrane curvature. Atg18 could be recruited by Vps35 to retromer coated endosomal membranes or the PAS. Insertion of the hydrophobic loop together with the high concentration of Atg18 could cause the formation of endosomal tubular carriers (ETCs) and scission of retromer vesicles from the endosome. This idea was tested with several known cargos of the retromer mediated retrograde transport. Both Ear1 and Kex2 have been introduced in chapter 4.2.3 as cargo of retromer and Snx3. Defects in the retromer complex result in missorting of both proteins to the vacuolar membrane. Neither deletion of *ATG18* and *ATG21* nor of all three PROPPINs causes the same phenotype, disproving the hypothesis. However, although most of the GFP tagged cargo localized to puncta in the cytosol a small but noticeable amount of GFP ended up in the vacuole or at the vacuolar membrane. Atg18 was suggested to be required for PtdIns(3,5)P₂-dependent retrograde transport from the vacuole to the Golgi via endosome (Dove et al., 2004).

5. Discussion

Parallel to Kex2 and Ear1 two additional cargos of the endosomal retrograde transport pathway were analyzed for their location in an *atg18Δ atg21Δ hsv2Δ* strain. Ymr253c is a putative protein with unknown function and was recently described as a retromer cargo dependent on Vps5 and Vps17 (Bean et al., 2017). The same study also identified the membrane protein Sft2 as cargo of the retromer independent recycling pathway mediated by Snx4. Both proteins showed behavior similar to Ear1 and Kex2 in a triple knockout strain of the PROPPINs. While most of the GFP tagged cargo localized to the endosome and Golgi (puncta in the cytosol), some of the vacuoles contained GFP signal (data not shown). This indicates a general role of Atg18 in retrograde trafficking not restricted to Vps35 and retromer. A function in membrane scission during vesicle fission could be an explanation for this (Gopaldass et al., 2017).

5.2.3. Connection between Vps35 and autophagy

Defects in the vacuolar protein sorting are known to impair autophagy and deletion of retromer subunits *VPS35* and *VPS29* causes a decrease in autophagic activity (Dengjel et al., 2012). Similar results were observed during this thesis; as Ape1 maturation as well as the accumulation of free GFP after degradation of GFP-Atg8 in the vacuole were reduced (see chapter 4.1.1). *VPS35* deletion blocks retrograde sorting of proteins, which leads to mislocalization of several different proteins. This could indirectly affect autophagic efficiency if proteins necessary for the process are distributed to the wrong location.

Results of the BioID assay with mutants defective in either PI3-kinase complex I or II might indicate a function of Vps35 at the vacuolar membrane and not the PAS. The protein was enriched in an *atg14Δ* strain, but not after deletion of *VPS38* (Figure 4-5). However, experiments with fluorescence microscopy of Vps35-mCherry and GFP-Atg8 as a PAS or autophagosome marker showed colocalization between Vps35 and the IM or autophagosome (see chapter 4.2.8). This indicates a previously unknown direct connection between the retromer and autophagy. Retromer is known to recycle integral or peripheral membrane proteins. Several Atg proteins are associated with the autophagosomal membrane during or after phagophore closure, which have to be removed before fusion with the vacuolar membrane occurs. One of them is the transmembrane protein Atg9, which can be found in a complex with Atg2-Atg18.

5. Discussion

5.2.4. Atg9 localization is mediated by retromer

Atg9 is localized to small single membrane vesicles at the periphery of the cell. Early reports suggested a localization at the mitochondria since Atg9 could often be found nearby (Mari et al., 2010; Reggiori et al., 2004). More recent studies indicate an Atg9 pool at peripheral structures derived from the late Golgi and endosomal system, comparable to mammalian cells (Ohashi & Munro, 2010). The membrane proteins Atg23 and Atg27 are involved in maintaining the Atg9 pool and deletion of either *ATG23* or *ATG27* caused a major decrease in the brightness of the Atg9 puncta at the periphery of the cell (Backues et al., 2015). Atg27 is sorted to the vacuolar membrane, its recycling to the Golgi is dependent on the sorting nexin Snx4 and the retromer complex. The Snx4-related family of SNX-BAR proteins contains three members: Snx4, Snx41 and Atg20. Genetic epistasis tests suggested a role in recycling proteins from the early endosome (or 'post-Golgi' endosome), as opposed to the late endosome ('pre-vacuolar' endosome) for SNX-BAR proteins Vps5 and Vps17 (Hetzema et al., 2003). Atg27 is transported from the vacuolar membrane to the endosomes mediated by the Snx4 complex and then delivered to the Golgi dependent on the retromer complex (Ma et al., 2017; Suzuki & Emr, 2018). A deletion of *VPS35* results in missorting of Atg27, which also affects Atg9 localization. *vps35Δ* strains show a defect in autophagy, which is more severe in cells at log-phase (see Figure 4-10). This could be caused by mislocalization of Atg9 or impaired recruitment to the PAS. Indeed, localization of Atg9-GFP with the PAS marker mCherry-Atg8 was reduced in *vps35Δ* cells even after 4h of starvation (Figure 4-27). This effect is less severe in cells transferred to nitrogen free medium at a higher OD, since the maturation rate of Ape1 is closer to wildtype cells (see Figure 4-10). Autophagy is induced by a lack of nutrients and cells harvested at higher ODs could already experience the first signs of starvation, with increased expression levels of *ATG9* and other Atgs. This could give the cells a head start in the induction of autophagy that cells harvested in log-phase are unable to catch up to. Interestingly, Atg9 interacts with Vps35 in the absence of Atg2 and Atg18 (chapter 4.2.10). This indicates a direct role of the retromer complex in maintaining Atg9 localization at the late Golgi/ early endosomes. Atg9-GFP was partially transported to the vacuolar lumen in the absence of Vps35, as some of the vacuoles contained GFP. Atg9 is located to the edges of the growing phagophore and recycled either before

5. Discussion

fusion with the vacuole occurs or from the vacuolar membrane after the fusion event. If recycling occurs afterwards, Atg9 has to be limited to the outer membrane of the autophagosome, otherwise it would be transported to the vacuolar lumen and degraded. Due to the location of both the C- and the N-terminus on the cytosolic side of the membrane GFP could only reach the vacuolar lumen in *vps35Δ* cells if Atg9 is located on the inside of the autophagosome. This could suggest a defect in recycling of Atg9 from the phagophore before closure, which might result in an accumulation of the transmembrane protein in the autophagosome. Another way for GFP fused to Atg9 to be transported into the vacuole is the MVB pathway, where the protein is sorted into intraluminal vesicles (ILVs) at the late endosome. If Atg9 accumulates at the late endosome as a result in defective retrograde transport from the endosome to the Golgi, it could be incorporated into ILVs and transported into the vacuolar lumen. This mechanism might play a minor role in Atg9 localization, since not all cells contained GFP in their vacuoles.

Another possible reason for the interaction between Atg9 and Vps35 seen in Figure 4-26 is a role of the retromer complex in recycling Atg9 from either the autophagosome or the vacuolar membrane. Atg9 is the only transmembrane protein of the core autophagic machinery and localizes to the growing phagophore early in the process. It is not degraded in the vacuole but recycled to the endosomal Atg9 pool. Retromer is responsible for the retrograde transport of transmembrane proteins from the endosomes to the Golgi and it was also shown to function at the vacuolar membrane. Deletion of *VPS35* did not result in an accumulation of Atg9 at closed autophagosomes or the vacuolar membrane. However, it is possible that Atg9 is transported in a pathway comparable to Atg27: transport from the vacuolar membrane to the endosome could be mediated by Snx4 or an unknown complex, while the retromer complex would only be responsible for the last step from endosome to Golgi. If this is true, Atg9 should accumulate at the endosomes if *VPS35* is deleted, missorted into MVB vesicles and transported to the vacuolar lumen. This would explain the elevated amount of GFP in the vacuolar lumen after starvation. A recent study on potential cargoes of either Retromer or Snx4 did not detect Atg9 among the analyzed proteins (Bean et al., 2017).

5. Discussion

5.2.5. Vps35 affects Atg18 localization

Unlike Atg9 the membrane associated protein Atg18 is mislocalized in a *VPS35* deletion strain, as demonstrated in chapter 4.2.5. In the absence of a functional retromer, Atg18-GFP localizes to the vacuolar membrane and to small vesicle like structures adjacent to the vacuole. This phenotype is enhanced after starvation.

Vps35 belongs to the class A *vps* mutants as deletion causes only mild disturbances in vacuolar morphology (Banta et al., 1988; Raymond et al., 1992). The WCG background strain mostly used for this thesis has only one large vacuole under normal conditions, unlike the SEY background analyzed in the publications. This could have an effect on the morphological changes seen in *VPS35* deletion strains. A similar vacuolar morphology was observed in WCG wildtype and *VPS35* deletion strains, with one or less often two large vacuoles per cell. After nitrogen starvation, more than 50% of the cells contain either more than one vacuole of the same size or accumulate small ring-like structures near the vacuole (data not shown).

Vacuolar fragmentation requires the PtdIns3P 5-kinase Fab1 (Cooke et al., 1998; Dove et al., 1997) and is accelerated in the presence of Atg18 (Zieger & Mayer, 2012). Accumulation of Atg18 at the vacuolar membrane caused by the absence of *Vps35* could increase fission and vacuolar fragmentation. However, deletion of both *ATG18* and *VPS35* results in enlarged vacuoles with several small ring-like structures accumulated at the vacuolar membrane (data not shown). Therefore, high levels of Atg18 should not cause the phenotype observed in *vps35Δ* cells.

Overexpression of the Rab like GTPase Ypt7 results in vacuole invaginations, caused by massive membrane expansion (Balderhaar et al., 2010). Ypt7 recruits the HOPS complex and promotes the fusion of endosomes and vacuoles. Overexpression of Ypt7 is thought to induce this event before the retromer can recycle sufficient amounts of proteins and membrane lipids. Defects in the retromer could also cause membrane expansion of the vacuole, as recycling of membrane lipids from the endosome to the Golgi is reduced. Furthermore, the retromer complex was shown to function at the vacuolar membrane together with Ypt7 and the dynamin homolog Vps1 (Arlt, Reggiori, et al., 2015). Recycling of endosomal SNAREs from the vacuolar membrane is necessary for efficient fusion and this could be mediated by retromer. Defective retrograde transport could therefore impair endosomal fusion with the vacuole and cause

5. Discussion

accumulation of late endosomes. The amphipathic loop of Atg18 could cause a preferred integration of the protein in highly curved membranes, which would explain the accumulation of Atg18-GFP at the structures.

Nitrogen starvation enhances the accumulation of small ring-like structures and colocalization experiments with Atg18-GFP and mCherry-Atg8 have identified part of these structures as autophagosomes. This indicates a defect in the fusion of the autophagosome with the vacuolar membrane.

5.2.6. Atg18 is cargo of retromer

The autophagosomes accumulated in a *VPS35* deletion strain are completely decorated with Atg18-GFP, as shown in Figure 4-19. Atg18 is not a membrane protein, but membrane association is mediated by two PtdIns3P or PtdIns(3,5)P₂ binding sites together with a hydrophobic loop at blade 6. The protein forms a complex with Atg2 and is located to the membrane during autophagy. Since the localization of membrane associated Atg18 is dependent on the presence of Vps35 it could be a cargo of retromer in complex with the sorting nexin Snx3.

Snx3 contains a PX domain for membrane association but is unable to shape membranes (Worby & Dixon, 2002). However, the sorting nexin was shown to induce tubulation in the presence of specific membrane bound cargo proteins (Purushothaman & Ungermann, 2018). Atg18 with its hydrophobic loop could therefore be sufficient to induce the formation of tubules coated with Snx3 and the multimeric retromer complex. The mechanism of membrane scission is still not known, although this could be triggered by the presence of Atg18. The PROPPIN was shown to initiate tubulation and membrane scission in GUVs (Gopaldass et al., 2017).

In the proposed model Atg18 would be recruited to the PAS during autophagy induction, stayed bound as part of the machinery and would be recycled at some point during or after autophagosome closure mediated by retromer in complex with Snx3. A model of this is depicted in Figure 5-4.

Recycling of Atg18 in a retromer dependent manner could happen at two locations: it could either be sorted into retromer coated vesicles at the autophagosome before fusion with the vacuole occurs or from the vacuolar membrane after fusion.

5. Discussion

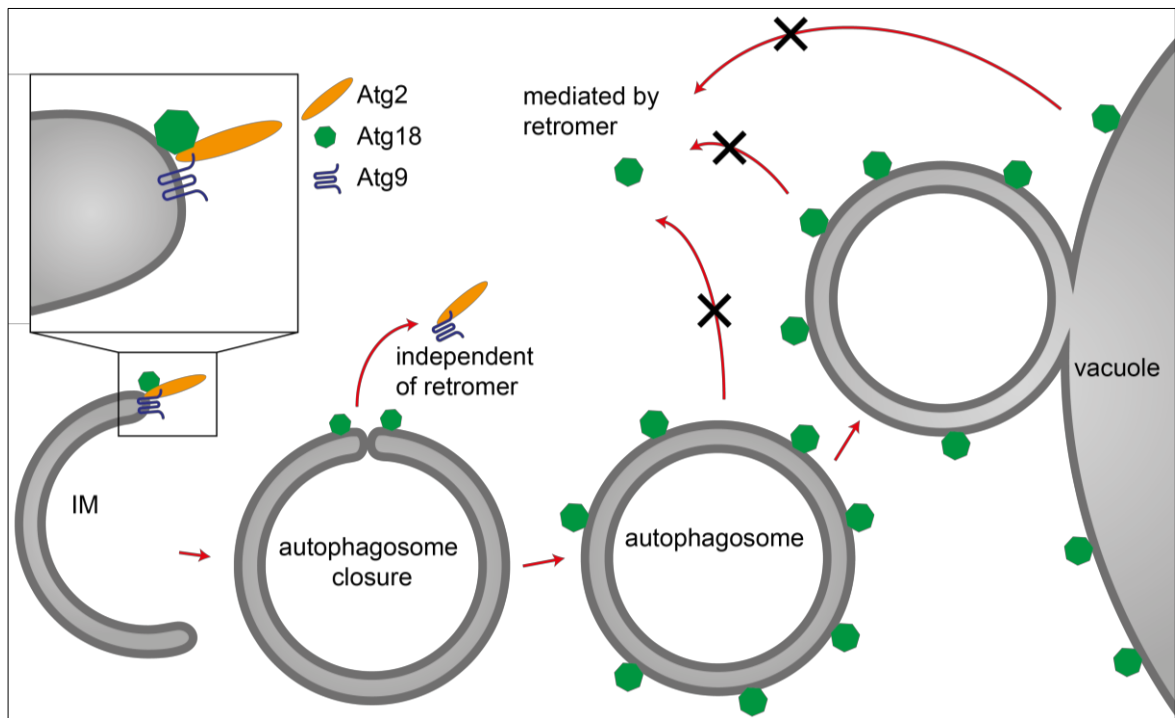


Figure 5-4: Hypothetical model for Atg18 localization in the absence of Vps35.

Atg18 localizes to the edges of the expanding IM, mediated by association with Atg2 and Atg9. Before, during or after sealing the AP Atg2 and Atg9 might be recycled from the AP in a Vps35-independent manner. Atg18 would remain at the autophagosomal membrane and would be transported to the vacuolar membrane during fusion of the AP with the vacuole. Reduced efficiency of the fusion event might cause accumulation of Atg18 covered APs adjacent to the vacuole.

Atg18 is a PtdInsP effector and levels of PtdIns at the autophagosomal membrane have been discussed as a sign for autophagosome maturation. The presence or absence of Atg18 could signal the next step in autophagy: disassembly of the autophagic machinery and/or fusion with the vacuole. Autophagic activity is significantly reduced in a *VPS35* deletion strain and the mCherry signal seen in the vacuole of cells expressing mCherry-Atg8 after starvation is weak compared to wildtype cells. This could be caused by Atg9 mislocalization as discussed in chapter 5.2.4. But here the defect is in the early stages of autophagy: recruitment of Atg9 is reduced in a *VPS35* deletion strain, as the amount of colocalization between Atg9 and Atg8 is decreased. This would not result in the accumulation of autophagosomes as seen in a *vps35Δ* strain, which implies a partial block in either autophagosome closure or fusion of the autophagosome with the vacuole. The incomplete disassembly of the autophagic machinery, with Atg18 as an example, would impair efficient fusion with the vacuole and cause the accumulation of sealed autophagosomes. Interestingly, a mammalian homologue to Atg18, WDR45/45B, was shown to be dispensable for autophagosome closure but essential for fusion of the AP with the lysosome in neural cells (Ji et al., 2021).

5. Discussion

However, a defect in retrograde trafficking could also affect components of the fusion machinery such as Ykt6 and cause partial mislocalization. Indeed, deletion of retromer causes a redistribution of the vacuolar SNARE Vam3, which is also implicated in fusion of the autophagosome with the vacuole (Arlt, Reggiori, et al., 2015). Fusion with the vacuole would not be completely abolished but slowed down as loss of recycling would result in a higher demand for newly synthesized proteins. This would explain the low but still present autophagic activity in *VPS35* deletion strains. In this scenario, Atg18 would still be enriched at the AP and vacuolar membrane, but would not act as a signal for autophagosome maturation. Retromer has been shown to recycle proteins from the vacuole (Arlt, Auffarth, et al., 2015) and defective retrograde transport mediated by retromer would explain the accumulation of Atg18 at the vacuole.

Atg18 is also cytosolic and could be recruited to the vacuolar membrane independent of autophagic activity, as a low amount of Atg18-GFP can be detected at the vacuolar membrane in wildtype cells. Furthermore, deletion of *VPS35* causes a decrease in autophagic activity, with less autophagosomes fusing with the vacuole. Therefore, a block in Atg18 recycling after autophagy cannot completely explain the accumulation of Atg18 at the vacuolar membrane. The PtdIns3P distribution is not significantly altered in a *vps35Δ* strain compared to the wildtype, as observed with RFP-2xFYVE. The FYVE domain, however, is unable to bind to PtdIns3,5P₂, which could differ from the wildtype and might explain some of the changes in Atg18 localization.

However, the interaction observed for Atg18 and Vps35 indicates a more direct role of Vps35 in Atg18 localization.

5.2.7. Replacing Atg2 with Vps35

Interestingly, Atg18 is evenly distributed over the membrane of the vesicle like structures found in *VPS35* deletion strains. Atg18 localizes to the edges of the IM during expansion, which is mediated by the interaction between Atg2 and Atg9 (Gómez-Sánchez et al., 2018). Loss of this localization implies the absence of Atg9 and/or Atg2, neither of which could be detected in increased levels at the small vesicle like structures identified as autophagosomes.

Both the PtdIns3P binding sites formed by the FRRG motif located at the outer rim of the PROPPIN and the hydrophobic loop between blade 6CD mediate binding to the membrane. Depending on the orientation of Atg18 (indicated in Figure 5-2), the

5. Discussion

binding site for Atg2 at blade 2 could be blocked by Vps35 (Watanabe et al., 2012). Replacement of Atg2 with Vps35 during phagophore closure would release Atg2 from the Atg2-Atg18 complex and disassemble the Atg9 complex. Vps35 was able to co-immunoprecipitate with Atg9 in the absence of both Atg18 and Atg2, as discussed in chapter 5.2.4. However, its absence did not cause the accumulation of Atg9 at autophagosomes or the vacuolar membrane.

Mutating the known binding site of Atg2 on Atg18, P72A73 (Watanabe et al., 2012) to alanine did not reduce the affinity of Vps35 to Atg18, which indicates interaction with different amino acid residues for Vps35. Another region implied to function in the interaction between Atg18 and Atg2 is an extended loop at Blade 7, as deletion decreases the affinity of Atg2 towards Atg18 (Lei et al., 2020). However, this observation could not be reproduced in this study. Furthermore, the deletion of this loop had no effect on the interaction between Atg18 and Vps35. Therefore, a simultaneous binding of both Atg2 and Vps35 to Atg18 cannot be excluded. Vps35-6xHA coimmunoprecipitated with GFP-Atg2, albeit the amount of bound Vps35 was very low compared to the amount of Vps35 bound to Atg18. This indicates a lower affinity of Vps35 towards Atg2 or, more probable, an indirect interaction either mediated by Atg18 or Atg9. A direct interaction of Vps35 and Atg2 as well as its dependency on the presence of Atg18 could be analyzed in recombinant pulldown experiments.

The binding interface of Atg18 and Vps35 is still unknown. One of the difficulties of uncovering the function of a complex between Atg18 and Vps35 is the variety of cellular processes which is affected by both proteins. Deletion of *VPS35* causes defects in endosomal protein sorting, which also affects autophagic proteins. Deletion of *ATG18* not only blocks autophagy but also alters vacuolar morphology and affects endosomal and vacuolar sorting pathways. Specifically blocking the interaction between Atg18 and Vps35 could help to determine which of the different functions depend on a complex of both proteins. This could be achieved by determining the binding site(s) and introducing mutations. A sorting signal for retromer cargo has been defined as $\emptyset X [L/M/V]$ where \emptyset is F/Y/W (Cullen & Steinberg, 2018; Seaman, 2007; Suzuki et al., 2019). This conserved sequence can also be found on proteins not involved in retrograde transport and is therefore not sufficient for cargo sorting. Recognition of cargo is mostly thought to be mediated by Vps26 (Cui et al., 2017; Lucas

5. Discussion

et al., 2016) and Vps35 (Nothwehr et al., 2000) with more than one interface to adapt to several different cargos (Suzuki et al., 2019). Identification of the amino acid residues involved in Atg18 and Vps35 interaction is therefore of utmost importance.

5.2.8. Atg18 and retromer involved in fusion of autophagosome with the vacuole?

Recruitment of human retromer CRC to the endosome is mediated by the GTPase Rab7 and dependent on Rab5 (Rojas et al., 2008; Seaman et al., 2009). The yeast homologue to Rab7 is the Rab7 like GTPase Ypt7, which is localized to the late endosome and the vacuole (Balderhaar et al., 2010). Overexpression of the GTPase increases fusion with the vacuole and causes massive membrane expansion and invaginations as well as accumulation of retromer cargo such as Vps10 at the vacuolar surface (Balderhaar et al., 2010). This is thought to be a result of premature fusion of the endosomal vesicles with the vacuole, as fusion occurs before all relevant proteins are recycled by the retromer. Several studies have observed an interaction between Ypt7 and the retromer and a conserved region on repeat 5-7 of Vps35 has been identified as a binding site for Ypt7 (Liu et al., 2012; Priya et al., 2015). Although Ypt7 is not essential for retromer association to cargo proteins it greatly enhances the recruitment of Vps35, Vps26 and Vps29 to the membrane (Purushothaman et al., 2017). It is then replaced by sorting nexins to induce membrane curvature.

Ypt7 is recruited and activated by its GEF, the Mon1-Ccz1 complex (Nordmann et al., 2010; C.-W. Wang et al., 2003). The yeast homologue to mammalian Rab5 GTPase Vps21 in concert with the CORVET complex is thought to recruit the Mon1-Ccz1 complex to the late endosome (Nordmann et al., 2010). Here it acts as GEF to Ypt7 and activates it, which allows Ypt7 to recruit the HOPS complex and induce fusion with the vacuole. Furthermore, the Mon1-Ccz1 complex is recruited to the autophagosomal membrane and is important for the fusion of the autophagosome with the vacuole (Hegedűs et al., 2016; C.-W. Wang et al., 2002). Ccz1 is able to bind to Atg8 via a LIR motif at its C-terminus (Gao, Langemeyer, et al., 2018) and interaction of the complex with Atg21 was observed in this lab (unpublished data). Recent studies also found the Rab5 like GTPase Vps21 localized to the autophagosome (Chen et al., 2014; Zhou et al., 2017). This could further support the association of Ypt7 with the autophagosome together with PtdIns3P present at the membrane and the Mon1-Ccz1 complex.

5. Discussion

Ypt7 associated with the autophagosomal membrane could facilitate recruitment of the retromer complex mediated by its interaction with Vps35 (depicted in Figure 5-5). The retromer cargo Atg18 can also bind Vps35 and enhance the process. Ypt7 is then replaced by either the sorting nexin Snx3 or Atg18 itself, as SNX-BAR proteins were shown to compete with Ypt7 for retromer binding (Arlt, Reggiori, et al., 2015). Ypt7 would then be free to recruit the HOPS complex and assemble SNAREs to mediate fusion and Atg18 would be recycled by the retromer complex from the autophagosomal membrane or the vacuolar membrane after the fusion event.

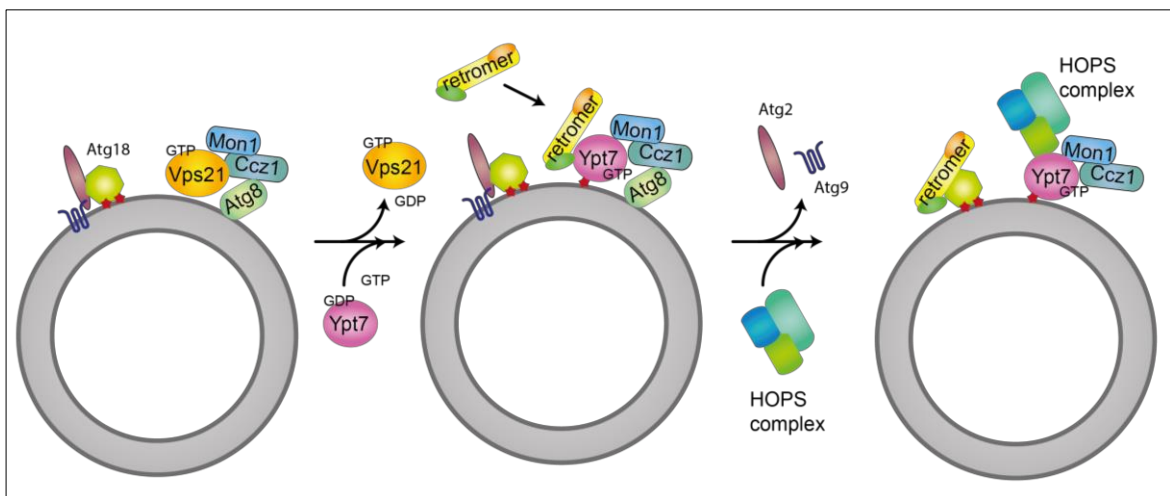


Figure 5-5: Proposed model for retromer recruitment to the autophagosome.

Atg8 recruits the GEF Mon1-Ccz 1 complex to the autophagosome, which is potentially supported by interaction with the Rab5 like Vps21 and the PROPPIN Atg21. The GEF then recruits activated Ypt7-GTP, which also depends on PtdIns3P at the membrane. Ypt7 enhances recruitment of retromer to its cargo, here Atg18, and is ultimately replaced as binding partner of Vps35 and is free to recruit the HOPS complex.

Conclusion and Outlook

The aim of this thesis was the discovery of previously unknown interaction partners of Atg18. Several interesting and promising candidates were identified with a proximity-dependent labeling assay in combination with a SILAC approach. So far three of these candidates, Vps35, Sap155 and Yck3, could be further validated using independent methods, which confirms the overall approach. Other candidates such as Ykt6 and Snx3 remain very interesting, although they could not be confirmed via independent means so far.

Two of the candidates were selected for further analysis. Vps35 is a subunit of the retromer and together with the sorting nexin Snx3 involved in retrograde transport of membrane associated proteins. Atg18 forms a complex with Vps35, the other retromer components Vps26 and Vps29 and probably also Snx3. This interaction was shown to be involved in Atg18 localization, as deletion of *VPS35* caused accumulation of Atg18 at the vacuolar membrane as well as at autophagosomes. It was concluded, that retromer is involved in the recycling of Atg18 from the membrane either before or after autophagosome-vacuole fusion.

The absence of Vps35 leads to massive defects in endosomal protein sorting, which affects Atg9 localization and also autophagy. This makes it difficult to differentiate between a phenotype directly related to an interaction between Atg18 and Vps35 or a general defect in the endosomal trafficking pathway. A solution to this problem is the identification of the binding interface of the proteins. A putative cargo recognition motif for Vps35 has been identified, however cargo recruitment is likely to necessitate more than one binding site. A crystal structure of Atg18 in complex with Vps35, Vps26, Vps29 and Snx3 could be an approach to learn more about the interaction and the function of the newly identified complex.

Additionally, an interaction between the integral membrane protein Atg9 and Vps35 was observed. Since all experiments were conducted *in vivo*, Co-IPs with recombinant proteins should be repeated *in vitro*.

6. Bibliography

- Abreu, S., Kriegenburg, F., Gómez-Sánchez, R., Mari, M., Sánchez-Wandelmer, J., Skytte Rasmussen, M., Soares Guimarães, R., Zens, B., Schuschnig, M., Hardenberg, R., Peter, M., Johansen, T., Kraft, C., Martens, S., & Reggiori, F. (2017). Conserved Atg8 recognition sites mediate Atg4 association with autophagosomal membranes and Atg8 deconjugation. *EMBO Reports*, *18*(5), 765–780.
- Abubakar, Y., Zheng, W., Olsson, S., & Zhou, J. (2017). Updated Insight into the Physiological and Pathological Roles of the Retromer Complex. *International Journal of Molecular Sciences*, *18*(8), 1601.
- Agarraberes, F. A., & Dice, J. F. (2001). A molecular chaperone complex at the lysosomal membrane is required for protein translocation. *Journal of Cell Science*, *114*(Pt 13), 2491–2499.
- Andag, U., Neumann, T., & Schmitt, H. D. (2001). The Coatamer-interacting Protein Dsl1p Is Required for Golgi-to-Endoplasmic Reticulum Retrieval in Yeast. *Journal of Biological Chemistry*, *276*(42), 39150–39160.
- Araki, Y., Ku, W.-C., Akioka, M., May, A. I., Hayashi, Y., Arisaka, F., Ishihama, Y., & Ohsumi, Y. (2013). Atg38 is required for autophagy-specific phosphatidylinositol 3-kinase complex integrity. *Journal of Cell Biology*, *203*(2), 299–313.
- Arlt, H., Auffarth, K., Kurre, R., Lisse, D., Piehler, J., & Ungermann, C. (2015). Spatiotemporal dynamics of membrane remodeling and fusion proteins during endocytic transport. *Molecular Biology of the Cell*, *26*(7), 1357–1370.
- Arlt, H., Reggiori, F., & Ungermann, C. (2015). Retromer and the dynamin Vps1 cooperate in the retrieval of transmembrane proteins from vacuoles. *Journal of Cell Science*, *128*(4), 645–655.
- Arndt, K. T., Styles, C. A., & Fink, G. R. (1989). A suppressor of a HIS4 transcriptional defect encodes a protein with homology to the catalytic subunit of protein phosphatases. *Cell*, *56*(4), 527–537.
- Ashford, T. P., & Porter, K. R. (1962). CYTOPLASMIC COMPONENTS IN HEPATIC CELL LYOSOMES. *Journal of Cell Biology*, *12*(1), 198–202.
- Axe, E. L., Walker, S. A., Manifava, M., Chandra, P., Roderick, H. L., Habermann, A., Griffiths, G., & Ktistakis, N. T. (2008). Autophagosome formation from membrane compartments enriched in phosphatidylinositol 3-phosphate and dynamically connected to the endoplasmic reticulum. *Journal of Cell Biology*, *182*(4), 685–701.
- Baba, M., Takeshige, K., Baba, N., & Ohsumi, Y. (1994). Ultrastructural analysis of the autophagic process in yeast: detection of autophagosomes and their characterization. *Journal of Cell Biology*, *124*(6), 903–913.
- Babst, M., Katzmann, D. J., Estepa-Sabal, E. J., Meerloo, T., & Emr, S. D. (2002). ESCRT-III: An endosome-associated heterooligomeric protein complex required for MVB sorting. *Developmental Cell*, *3*(2), 271–282.
- Backues, S. K., Orban, D. P., Bernard, A., Singh, K., Cao, Y., & Klionsky, D. J. (2015). Atg23 and Atg27 Act at the Early Stages of Atg9 Trafficking in *S. cerevisiae*. *Traffic*, *16*(2), 172–190.
- Balderhaar, H. J. K., Arlt, H., Ostrowicz, C., Bröcker, C., Sündermann, F., Brandt, R., Babst, M., & Ungermann, C. (2010). The Rab GTPase Ypt7 is linked to retromer-mediated receptor recycling and fusion at the yeast late endosome. *Journal of Cell Science*,

6. Bibliography

- 123(23), 4085–4094.
- Banta, L. M., Robinson, J. S., Klionsky, D. J., & Emr, S. D. (1988). Organelle assembly in yeast: characterization of yeast mutants defective in vacuolar biogenesis and protein sorting. *Journal of Cell Biology*, 107(4), 1369–1383.
- Barker, D. F., & Campbell, A. M. (1981a). Genetic and biochemical characterization of the birA gene and its product: Evidence for a direct role of biotin holoenzyme synthetase in repression of the biotin operon in *Escherichia coli*. *Journal of Molecular Biology*, 146(4), 469–492.
- Barker, D. F., & Campbell, A. M. (1981b). The birA gene of *Escherichia coli* encodes a biotin holoenzyme synthetase. *Journal of Molecular Biology*, 146(4), 451–467.
- Barlowe, C. (1994). COPII: A membrane coat formed by Sec proteins that drive vesicle budding from the endoplasmic reticulum. *Cell*, 77(6), 895–907.
- Barr, F. A. (2013). Rab GTPases and membrane identity: Causal or inconsequential? *Journal of Cell Biology*, 202(2), 191–199.
- Barth, H., Meiling-Wesse, K., Epple, U. D., & Thumm, M. (2001). Autophagy and the cytoplasm to vacuole targeting pathway both require Aut10p. *FEBS Letters*, 508(1), 23–28.
- Barth, H., Meiling-Wesse, K., Epple, U. D., & Thumm, M. (2002). Mai1p is essential for maturation of proaminopeptidase I but not for autophagy. *FEBS Letters*, 512(1–3), 173–179.
- Barz, S., Kriegenburg, F., Henning, A., Bhattacharya, A., Mancilla, H., Sánchez-Martín, P., & Kraft, C. (2020). Atg1 kinase regulates autophagosome-vacuole fusion by controlling SNARE bundling. *EMBO Reports*, 21(12).
- Bas, L., Papinski, D., & Kraft, C. (2018). Ykt6 mediates autophagosome-vacuole fusion. *Molecular & Cellular Oncology*, 5(6), e1526006.
- Bas, L., Papinski, D., Licheva, M., Torggler, R., Rohringer, S., Schuschnig, M., & Kraft, C. (2018). Reconstitution reveals Ykt6 as the autophagosomal SNARE in autophagosome–vacuole fusion. *Journal of Cell Biology*, 217(10), 3656–3669.
- Baskaran, S., Ragusa, M. J., Boura, E., & Hurley, J. H. (2012). Two-Site Recognition of Phosphatidylinositol 3-Phosphate by PROPPINs in Autophagy. *Molecular Cell*, 47(3), 339–348.
- Bean, B. D. M., Davey, M., & Conibear, E. (2017). Cargo selectivity of yeast sorting nexins. *Traffic*, 18(2), 110–122.
- Bonangelino, C. J., Nau, J. J., Duex, J. E., Brinkman, M., Wurmser, A. E., Gary, J. D., Emr, S. D., & Weisman, L. S. (2002). Osmotic stress-induced increase of phosphatidylinositol 3,5-bisphosphate requires Vac14p, an activator of the lipid kinase Fab1p. *Journal of Cell Biology*, 156(6), 1015–1028.
- Botelho, R. J., Efe, J. A., Teis, D., & Emr, S. D. (2008). Assembly of a Fab1 Phosphoinositide Kinase Signaling Complex Requires the Fig4 Phosphoinositide Phosphatase. *Molecular Biology of the Cell*, 19(10), 4273–4286.
- Bowers, K., & Stevens, T. H. (2005). Protein transport from the late Golgi to the vacuole in the yeast *Saccharomyces cerevisiae*. *Biochimica et Biophysica Acta - Molecular Cell Research*, 1744(3 SPEC. ISS.), 438–454.
- Branon, T. C., Bosch, J. A., Sanchez, A. D., Udeshi, N. D., Svinkina, T., Carr, S. A., Feldman, J. L., Perrimon, N., & Ting, A. Y. (2018). Efficient proximity labeling in living cells and organisms with TurboID. *Nature Biotechnology*, 36(9), 880–898.

6. Bibliography

- Bryant, N. J., & Boyd, A. (1993). Immunoisolation of Kex2p-containing organelles from yeast demonstrates colocalisation of three processing proteinases to a single Golgi compartment. *Journal of Cell Science*, *106* (Pt 3(3), 815–822.
- Budovskaya, Y. V., Stephan, J. S., Deminoff, S. J., & Herman, P. K. (2005). An evolutionary proteomics approach identifies substrates of the cAMP-dependent protein kinase. *Proceedings of the National Academy of Sciences of the United States of America*, *102*(39), 13933–13938.
- Budovskaya, Y. V., Stephan, J. S., Reggiori, F., Klionsky, D. J., & Herman, P. K. (2004). The Ras/cAMP-dependent Protein Kinase Signaling Pathway Regulates an Early Step of the Autophagy Process in *Saccharomyces cerevisiae*. *Journal of Biological Chemistry*, *279*(20), 20663–20671.
- Burd, C., & Cullen, P. J. (2014). Retromer: A Master Conductor of Endosome Sorting. *Cold Spring Harbor Perspectives in Biology*, *6*(2), a016774–a016774.
- Busse, R. A., Scacioc, A., Krick, R., Pérez-Lara, Á., Thumm, M., & Kühnel, K. (2015). Characterization of PROPPIN-Phosphoinositide Binding and Role of Loop 6CD in PROPPIN-Membrane Binding. *Biophysical Journal*, *108*(9), 2223–2234.
- Cabrera, M., Ostrowicz, C. W., Mari, M., LaGrassa, T. J., Reggiori, F., & Ungermann, C. (2009). Vps41 Phosphorylation and the Rab Ypt7 Control the Targeting of the HOPS Complex to Endosome–Vacuole Fusion Sites. *Molecular Biology of the Cell*, *20*(7), 1937–1948.
- Cadwell, K., & Debnath, J. (2018). Beyond self-eating: The control of nonautophagic functions and signaling pathways by autophagy-related proteins. *Journal of Cell Biology*, *217*(3), 813–822.
- Carlsson, S. R., & Simonsen, A. (2015). Membrane dynamics in autophagosome biogenesis. *Journal of Cell Science*, *128*(2), 193–205.
- Cebollero, E., & Reggiori, F. (2009). Regulation of autophagy in yeast *Saccharomyces cerevisiae*. *Biochimica et Biophysica Acta (BBA) - Molecular Cell Research*, *1793*(9), 1413–1421.
- Cebollero, E., van der Vaart, A., Zhao, M., Rieter, E., Klionsky, D. J., Helms, J. B., & Reggiori, F. (2012). Phosphatidylinositol-3-Phosphate Clearance Plays a Key Role in Autophagosome Completion. *Current Biology*, *22*(17), 1545–1553.
- Chapman-Smith, A., & Cronan Jr, J. E. (1999). Molecular Biology of Biotin Attachment to Proteins. *The Journal of Nutrition*, *129*(2), 477S–484S.
- Chen, C. L., Hu, Y., Udeshi, N. D., Lau, T. Y., Wirtz-Peitz, F., He, L., Ting, A. Y., Carr, S. A., & Perrimon, N. (2015). Proteomic mapping in live *Drosophila* tissues using an engineered ascorbate peroxidase. *Proceedings of the National Academy of Sciences of the United States of America*, *112*(39), 12093–12098.
- Chen, C. L., & Perrimon, N. (2017). Proximity-dependent labeling methods for proteomic profiling in living cells. *Wiley Interdisciplinary Reviews: Developmental Biology*, *6*(4), e272.
- Chen, K. E., Healy, M. D., & Collins, B. M. (2019). Towards a molecular understanding of endosomal trafficking by Retromer and Retriever. *Traffic*, *20*(7), 465–478.
- Chen, Y., Zhou, F., Zou, S., Yu, S., Li, S., Li, D., Song, J., Li, H., He, Z., Hu, B., Björn, L. O., Lipatova, Z., Liang, Y., Xie, Z., & Segev, N. (2014). A Vps21 endocytic module regulates autophagy. *Molecular Biology of the Cell*, *25*(20), 3166–3177.
- Cheong, H., Nair, U., Geng, J., & Klionsky, D. J. (2008). The Atg1 Kinase Complex Is Involved in the Regulation of Protein Recruitment to Initiate Sequestering Vesicle

6. Bibliography

- Formation for Nonspecific Autophagy in *Saccharomyces cerevisiae*. *Molecular Biology of the Cell*, 19(2), 668–681.
- Chi, R. J., Liu, J., West, M., Wang, J., Odorizzi, G., & Burd, C. G. (2014). Fission of SNX-BAR-coated endosomal retrograde transport carriers is promoted by the dynamin-related protein Vps1. *Journal of Cell Biology*, 204(5), 793–806.
- Chiang, H. L., & Dice, J. F. (1988). Peptide sequences that target proteins for enhanced degradation during serum withdrawal. *Journal of Biological Chemistry*, 263(14), 6797–6805.
- Chiang, H. L., Terlecky, S., Plant, C., & Dice, J. (1989). A role for a 70-kilodalton heat shock protein in lysosomal degradation of intracellular proteins. *Science*, 246(4928), 382–385.
- Choi-Rhee, E., Schulman, H., & Cronan, J. E. (2008). Promiscuous protein biotinylation by *Escherichia coli* biotin protein ligase. *Protein Science*, 13(11), 3043–3050.
- Chowdhury, S., Otomo, C., Leitner, A., Ohashi, K., Aebersold, R., Lander, G. C., & Otomo, T. (2018). Insights into autophagosome biogenesis from structural and biochemical analyses of the ATG2A-WIPI4 complex. *Proceedings of the National Academy of Sciences*, 115(42), E9792–E9801.
- Collins, B. M., Skinner, C. F., Watson, P. J., Seaman, M. N. J., & Owen, D. J. (2005). Vps29 has a phosphoesterase fold that acts as a protein interaction scaffold for retromer assembly. *Nature Structural & Molecular Biology*, 12(7), 594–602.
- Cooke, F. T., Dove, S. K., McEwen, R. K., Painter, G., Holmes, A. B., Hall, M. N., Michell, R. H., & Parker, P. J. (1998). The stress-activated phosphatidylinositol 3-phosphate 5-kinase Fab1p is essential for vacuole function in *S. cerevisiae*. *Current Biology*, 8(22), 1219–1222.
- Cowles, C. R. (1997). Novel Golgi to vacuole delivery pathway in yeast: identification of a sorting determinant and required transport component. *The EMBO Journal*, 16(10), 2769–2782.
- Cowles, C. R., Odorizzi, G., Payne, G. S., & Emr, S. D. (1997). The AP-3 Adaptor Complex Is Essential for Cargo-Selective Transport to the Yeast Vacuole. *Cell*, 91(1), 109–118.
- Cuervo, A. M. (2010). Chaperone-mediated autophagy: selectivity pays off. *Trends in Endocrinology & Metabolism*, 21(3), 142–150.
- Cuervo, A. M., & Dice, J. F. (1996). A Receptor for the Selective Uptake and Degradation of Proteins by Lysosomes. *Science*, 273(5274), 501–503.
- Cui, T.-Z., Peterson, T. A., & Burd, C. G. (2017). A CDC25 family protein phosphatase gates cargo recognition by the Vps26 retromer subunit. *ELife*, 6, 1–18.
- Cullen, P. J., & Steinberg, F. (2018). To degrade or not to degrade: mechanisms and significance of endocytic recycling. *Nature Reviews Molecular Cell Biology*, 19(11), 679–696.
- Dalton, L. E., Bean, B. D. M., Davey, M., & Conibear, E. (2017). Quantitative high-content imaging identifies novel regulators of Neol1 trafficking at endosomes. *Molecular Biology of the Cell*, 28(11), 1539–1550.
- Darsow, T., Rieder, S. E., & Emr, S. D. (1997). A multispecificity syntaxin homologue, Vam3p, essential for autophagic and biosynthetic protein transport to the vacuole. *Journal of Cell Biology*, 138(3), 517–529.
- Davis, S., & Ferro-Novick, S. (2015). Ypt1 and COPII vesicles act in autophagosome biogenesis and the early secretory pathway. *Biochemical Society Transactions*, 136

6. Bibliography

- 43(1), 92–96.
- Davis, S., Wang, J., Zhu, M., Stahmer, K., Lakshminarayan, R., Ghassemian, M., Jiang, Y., Miller, E. A., & Ferro-Novick, S. (2016). Sec24 phosphorylation regulates autophagosome abundance during nutrient deprivation. *ELife*, 5(NOVEMBER2016), 1–22.
- De Craene, J.-O., Bertazzi, D., Bär, S., & Friant, S. (2017). Phosphoinositides, Major Actors in Membrane Trafficking and Lipid Signaling Pathways. *International Journal of Molecular Sciences*, 18(3), 634.
- de Duve, C. (1963). The Lysosome. *Scientific American*, 208(5), 64–73.
- DeMoss, J. A., Genuth, S. M., & Novelli, G. D. (1956). THE ENZYMATIC ACTIVATION OF AMINO ACIDS VIA THEIR ACYL-ADENYLATE DERIVATIVES. *Proceedings of the National Academy of Sciences*, 42(6), 325–332.
- Dengjel, J., Høyer-Hansen, M., Nielsen, M. O., Eisenberg, T., Harder, L. M., Schandorff, S., Farkas, T., Kirkegaard, T., Becker, A. C., Schroeder, S., Vanselow, K., Lundberg, E., Nielsen, M. M., Kristensen, A. R., Akimov, V., Bunkenborg, J., Madeo, F., Jäättelä, M., & Andersen, J. S. (2012). Identification of Autophagosome-associated Proteins and Regulators by Quantitative Proteomic Analysis and Genetic Screens. *Molecular & Cellular Proteomics*, 11(3), M111.014035.
- Deretic, V., Saitoh, T., & Akira, S. (2013). Autophagy in infection, inflammation and immunity. *Nature Reviews Immunology*, 13(10), 722–737.
- Di Como, C. J., & Arndt, K. T. (1996). Nutrients, via the Tor proteins, stimulate the association of Tap42 with type 2A phosphatases. *Genes & Development*, 10(15), 1904–1916.
- Dilcher, M., Köhler, B., & Von Mollard, G. F. (2001). Genetic Interactions with the Yeast Q-SNARE VTI1 Reveal Novel Functions for the R-SNARE YKT6. *Journal of Biological Chemistry*, 276(37), 34537–34544.
- Dooley, H. C., Razi, M., Polson, H. E. J., Girardin, S. E., Wilson, M. I., & Tooze, S. A. (2014). WIPI2 Links LC3 Conjugation with PI3P, Autophagosome Formation, and Pathogen Clearance by Recruiting Atg12–5–16L1. *Molecular Cell*, 55(2), 238–252.
- Dove, S. K., Cooke, F. T., Douglas, M. R., Sayers, L. G., Parker, P. J., & Michell, R. H. (1997). Osmotic stress activates phosphatidylinositol-3,5-bisphosphate synthesis. *Nature*, 390(6656), 187–192.
- Dove, S. K., McEwen, R. K., Mayes, A., Hughes, D. C., Beggs, J. D., & Michell, R. H. (2002). Vac14 controls PtdIns(3,5)P₂ synthesis and Fab1-dependent protein trafficking to the multivesicular body. *Current Biology*, 12(11), 885–893.
- Dove, S. K., Piper, R. C., McEwen, R. K., Yu, J. W., King, N. C., Hughes, D. C., Thuring, J., Holmes, A. B., Cooke, F. T., Michell, R. H., Parker, P. J., & Lemmon, M. A. (2004). Svp1p defines a family of phosphatidylinositol 3,5-bisphosphate effectors. *EMBO Journal*, 23(9), 1922–1933.
- Duex, J. E., Tang, F., & Weisman, L. S. (2006). The Vac14p-Fig4p complex acts independently of Vac7p and couples PI3,5P₂ synthesis and turnover. *Journal of Cell Biology*, 172(5), 693–704.
- Duina, A. A., Miller, M. E., & Keeney, J. B. (2014). Budding Yeast for Budding Geneticists: A Primer on the *Saccharomyces cerevisiae* Model System. *Genetics*, 197(1), 33–48.
- Dupont, N., Chauhan, S., Arko-Mensah, J., Castillo, E. F., Masedunskas, A., Weigert, R., Robenek, H., Proikas-Cezanne, T., & Deretic, V. (2014). Neutral lipid stores and lipase PNPLA5 contribute to autophagosome biogenesis. *Current Biology*, 24(6),

6. Bibliography

- 609–620.
- Efe, J. A., Botelho, R. J., & Emr, S. D. (2005). The Fab1 phosphatidylinositol kinase pathway in the regulation of vacuole morphology. *Current Opinion in Cell Biology*, *17*(4), 402–408.
- Efe, J. A., Botelho, R. J., & Emr, S. D. (2007). Atg18 Regulates Organelle Morphology and Fab1 Kinase Activity Independent of Its Membrane Recruitment by Phosphatidylinositol 3,5-Bisphosphate. *Molecular Biology of the Cell*, *18*(11), 4232–4244.
- Epple, U. D., Eskelinen, E.-L., & Thumm, M. (2003). Intravacuolar Membrane Lysis in *Saccharomyces cerevisiae*. *Journal of Biological Chemistry*, *278*(10), 7810–7821.
- Epple, U. D., Suriapranata, I., Eskelinen, E.-L., & Thumm, M. (2001). Aut5/Cvt17p, a Putative Lipase Essential for Disintegration of Autophagic Bodies inside the Vacuole. *Journal of Bacteriology*, *183*(20), 5942–5955.
- Fader, C. M., Sánchez, D. G., Mestre, M. B., & Colombo, M. I. (2009). TI-VAMP/VAMP7 and VAMP3/cellubrevin: two v-SNARE proteins involved in specific steps of the autophagy/multivesicular body pathways. *Biochimica et Biophysica Acta - Molecular Cell Research*, *1793*(12), 1901–1916.
- Farré, J.-C., & Subramani, S. (2016). Mechanistic insights into selective autophagy pathways: lessons from yeast. *Nature Reviews Molecular Cell Biology*, *17*(9), 537–552.
- Feyder, S., De Craene, J.-O., Bär, S., Bertazzi, D., & Friant, S. (2015). Membrane Trafficking in the Yeast *Saccharomyces cerevisiae* Model. *International Journal of Molecular Sciences*, *16*(1), 1509–1525.
- Filimonenko, M., Stuffers, S., Raiborg, C., Yamamoto, A., Malerød, L., Fisher, E. M. C., Isaacs, A., Brech, A., Stenmark, H., & Simonsen, A. (2007). Functional multivesicular bodies are required for autophagic clearance of protein aggregates associated with neurodegenerative disease. *Journal of Cell Biology*, *179*(3), 485–500.
- Franzusoff, A., Redding, K., Crosby, J., Fuller, R. S., & Schekman, R. (1991). Localization of components involved in protein transport and processing through the yeast Golgi apparatus. *Journal of Cell Biology*, *112*(1), 27–37.
- Fujioka, Y., Suzuki, S. W., Yamamoto, H., Kondo-Kakuta, C., Kimura, Y., Hirano, H., Akada, R., Inagaki, F., Ohsumi, Y., & Noda, N. N. (2014). Structural basis of starvation-induced assembly of the autophagy initiation complex. *Nature Structural and Molecular Biology*, *21*(6), 513–521.
- Fujita, N., Itoh, T., Omori, H., Fukuda, M., Noda, T., & Yoshimori, T. (2008). The Atg16L Complex Specifies the Site of LC3 Lipidation for Membrane Biogenesis in Autophagy. *Molecular Biology of the Cell*, *19*(5), 2092–2100.
- Fuller, R. S., Brake, A., & Thorner, J. (1989). Yeast prohormone processing enzyme (KEX2 gene product) is a Ca²⁺-dependent serine protease. *Proceedings of the National Academy of Sciences*, *86*(5), 1434–1438.
- Gao, J., Kurre, R., Rose, J., Walter, S., Fröhlich, F., Piehler, J., Reggiori, F., & Ungermann, C. (2020). Function of the SNARE Ykt6 on autophagosomes requires the Dsl1 complex and the Atg1 kinase complex. *EMBO Reports*, *21*(12), 1–18.
- Gao, J., Langemeyer, L., Kümmel, D., Reggiori, F., & Ungermann, C. (2018). Molecular mechanism to target the endosomal Mon1-Ccz1 GEF complex to the pre-autophagosomal structure. *ELife*, *7*, 1–18.

6. Bibliography

- Gao, J., Reggiori, F., & Ungermann, C. (2018). A novel in vitro assay reveals SNARE topology and the role of Ykt6 in autophagosome fusion with vacuoles. *Journal of Cell Biology*, *217*(10), 3670–3682.
- Gary, J. D., Sato, T. K., Stefan, C. J., Bonangelino, C. J., Weisman, L. S., & Emr, S. D. (2002). Regulation of Fab1 phosphatidylinositol 3-phosphate 5-kinase pathway by Vac7 protein and Fig4, a polyphosphoinositide phosphatase family member. *Molecular Biology of the Cell*, *13*(4), 1238–1251.
- Gary, J. D., Wurmser, A. E., Bonangelino, C. J., Weisman, L. S., & Emr, S. D. (1998). Fab1p Is Essential for PtdIns(3)P 5-Kinase Activity and the Maintenance of Vacuolar Size and Membrane Homeostasis. *Journal of Cell Biology*, *143*(1), 65–79.
- Gavin, A.-C., Bösch, M., Krause, R., Grandi, P., Marzioch, M., Bauer, A., Schultz, J., Rick, J. M., Michon, A.-M., Cruciat, C.-M., Remor, M., Höfert, C., Schelder, M., Brajenovic, M., Ruffner, H., Merino, A., Klein, K., Hudak, M., Dickson, D., ... Superti-Furga, G. (2002). Functional organization of the yeast proteome by systematic analysis of protein complexes. *Nature*, *415*(6868), 141–147.
- Ge, L., Zhang, M., & Schekman, R. (2014). Phosphatidylinositol 3-kinase and COPII generate LC3 lipidation vesicles from the ER-Golgi intermediate compartment. *ELife*, *3*(November), 1–13.
- Geng, J., Baba, M., Nair, U., & Klionsky, D. J. (2008). Quantitative analysis of autophagy-related protein stoichiometry by fluorescence microscopy. *Journal of Cell Biology*, *182*(1), 129–140.
- Geng, J., Nair, U., Yasumura-Yorimitsu, K., & Klionsky, D. J. (2010). Post-Golgi Sec Proteins Are Required for Autophagy in *Saccharomyces cerevisiae*. *Molecular Biology of the Cell*, *21*(13), 2257–2269.
- Gillooly, D. J. (2000). Localization of phosphatidylinositol 3-phosphate in yeast and mammalian cells. *The EMBO Journal*, *19*(17), 4577–4588.
- Goffeau, A., Barrell, B. G., Bussey, H., Davis, R. W., Dujon, B., Feldmann, H., Galibert, F., Hoheisel, J. D., Jacq, C., Johnston, M., Louis, E. J., Mewes, H. W., Murakami, Y., Philippsen, P., Tettelin, H., & Oliver, S. G. (1996). Life with 6000 Genes. *Science*, *274*(5287), 546–567.
- Goldberg, A. L. (2003). Protein degradation and protection against misfolded or damaged proteins. *Nature*, *426*(6968), 895–899.
- Gomes de Mesquita, D. S., van den Hazel, H. B., Bouwman, J., & Woldringh, C. L. (1996). Characterization of new vacuolar segregation mutants, isolated by screening for loss of proteinase B self-activation. *European Journal of Cell Biology*, *71*(3), 237–247.
- Gómez-Sánchez, R., Rose, J., Guimarães, R., Mari, M., Papinski, D., Rieter, E., Geerts, W. J., Hardenberg, R., Kraft, C., Ungermann, C., & Reggiori, F. (2018). Atg9 establishes Atg2-dependent contact sites between the endoplasmic reticulum and phagophores. *Journal of Cell Biology*, *217*(8), 2743–2763.
- Gopaldass, N., Fauvet, B., Lashuel, H., Roux, A., & Mayer, A. (2017). Membrane scission driven by the PROPPIN Atg18. *The EMBO Journal*, *36*(22), 3274–3291.
- Graef, M., Friedman, J. R., Graham, C., Babu, M., & Nunnari, J. (2013). ER exit sites are physical and functional core autophagosome biogenesis components. *Molecular Biology of the Cell*, *24*(18), 2918–2931.
- Guan, J., Stromhaug, P. E., George, M. D., Habibzadegah-Tari, P., Bevan, A., Dunn, W. A., & Klionsky, D. J. (2001). Cvt18/Gsa12 Is Required for Cytoplasm-to-Vacuole

6. Bibliography

- Transport, Pexophagy, and Autophagy in *Saccharomyces cerevisiae* and *Pichia pastoris*. *Molecular Biology of the Cell*, 12(12), 3821–3838.
- Gueldener, U. (2002). A second set of loxP marker cassettes for Cre-mediated multiple gene knockouts in budding yeast. *Nucleic Acids Research*, 30(6), 23e – 23.
- Guldener, U. (1996). A new efficient gene disruption cassette for repeated use in budding yeast. *Nucleic Acids Research*, 24(13), 2519–2524.
- Hailey, D. W., Rambold, A. S., Satpute-Krishnan, P., Mitra, K., Sougrat, R., Kim, P. K., & Lippincott-Schwartz, J. (2010). Mitochondria Supply Membranes for Autophagosome Biogenesis during Starvation. *Cell*, 141(4), 656–667.
- Hanada, T., Noda, N. N., Satomi, Y., Ichimura, Y., Fujioka, Y., Takao, T., Inagaki, F., & Ohsumi, Y. (2007). The Atg12-Atg5 conjugate has a novel E3-like activity for protein lipidation in autophagy. *Journal of Biological Chemistry*, 282(52), 37298–37302.
- Hanahan, D. (1983). Studies on transformation of *Escherichia coli* with plasmids. *Journal of Molecular Biology*, 166(4), 557–580.
- Hardwick, J. S., Kuruvilla, F. G., Tong, J. K., Shamji, A. F., & Schreiber, S. L. (1999). Rapamycin-modulated transcription defines the subset of nutrient-sensitive signaling pathways directly controlled by the Tor proteins. *Proceedings of the National Academy of Sciences*, 96(26), 14866–14870.
- Harrison, M. S., Hung, C.-S., Liu, T. T., Christiano, R., Walther, T. C., & Burd, C. G. (2014). A mechanism for retromer endosomal coat complex assembly with cargo. *Proceedings of the National Academy of Sciences*, 111(1), 267–272.
- Harterink, M., Port, F., Lorenowicz, M. J., McGough, I. J., Silhankova, M., Betist, M. C., van Weering, J. R. T., van Heesbeen, R. G. H. P., Middelkoop, T. C., Basler, K., Cullen, P. J., & Korswagen, H. C. (2011). A SNX3-dependent retromer pathway mediates retrograde transport of the Wnt sorting receptor Wntless and is required for Wnt secretion. *Nature Cell Biology*, 13(8), 914–923.
- He, C., Baba, M., Cao, Y., & Klionsky, D. J. (2008). Self-Interaction Is Critical for Atg9 Transport and Function at the Phagophore Assembly Site during Autophagy. *Molecular Biology of the Cell*, 19(12), 5506–5516.
- Hegedűs, K., Takáts, S., Boda, A., Jipa, A., Nagy, P., Varga, K., Kovács, A. L., & Juhász, G. (2016). The Ccz1-Mon1-Rab7 module and Rab5 control distinct steps of autophagy. *Molecular Biology of the Cell*, 27(20), 3132–3142.
- Herman, P. K., & Emr, S. D. (1990). Characterization of VPS34, a gene required for vacuolar protein sorting and vacuole segregation in *Saccharomyces cerevisiae*. *Molecular and Cellular Biology*, 10(12), 6742–6754.
- Herman, P. K., Stack, J. H., DeModena, J. A., & Emr, S. D. (1991). A novel protein kinase homolog essential for protein sorting to the yeast lysosome-like vacuole. *Cell*, 64(2), 425–437.
- Herman, P. K., Stack, J. H., & Emr, S. D. (1991). A genetic and structural analysis of the yeast Vps15 protein kinase: Evidence for a direct role of Vps15p in vacuolar protein delivery. *EMBO Journal*, 10(13), 4049–4060.
- Hettema, E. H., Lewis, M. J., Black, M. W., & Pelham, H. R. B. (2003). Retromer and the sorting nexins Snx4/41/42 mediate distinct retrieval pathways from yeast endosomes. *EMBO Journal*, 22(3), 548–557.
- Hickey, C. M., & Wickner, W. (2010). HOPS initiates vacuole docking by tethering membranes before trans-SNARE complex assembly. *Molecular Biology of the Cell*,

6. Bibliography

- 21(13), 2297–2305.
- Hierro, A., Rojas, A. L., Rojas, R., Murthy, N., Effantin, G., Kajava, A. V., Steven, A. C., Bonifacino, J. S., & Hurley, J. H. (2007). Functional architecture of the retromer cargo-recognition complex. *Nature*, *449*(7165), 1063–1067.
- Hirata, E., Shirai, K., Kawaoka, T., Sato, K., Kodama, F., & Suzuki, K. (2021). Atg15 in *Saccharomyces cerevisiae* consists of two functionally distinct domains. *Molecular Biology of the Cell*, mbc.E20-07-0500.
- Ho, R., & Stroupe, C. (2015). The HOPS/class C Vps complex tethers membranes by binding to one Rab GTPase in each apposed membrane. *Molecular Biology of the Cell*, *26*(14), 2655–2663.
- Ho, Y., Ho, Y., Gruhler, A., Gruhler, A., Heilbut, A., Heilbut, A., Bader, G. D., Moore, L., Moore, L., Adams, S. L., Adams, S. L., Millar, A., Millar, A., Taylor, P., Taylor, P., Bennett, K., Bennett, K., Boutilier, K., Boutilier, K., ... Tyers, M. (2002). Systematic identification of protein complexes in *Saccharomyces cerevisiae* by mass spectrometry. *Nature*, *415*(6868), 180–183.
- Horazdovsky, B. F., Davies, B. A., Seaman, M. N. J., McLaughlin, S. A., Yoon, S. H., & Emr, S. D. (1997). A sorting nexin-1 homologue, Vps5p, forms a complex with Vps17p and is required for recycling the vacuolar protein-sorting receptor. *Molecular Biology of the Cell*, *8*(8), 1529–1541.
- Hurley, J. H. (2015). ESCRTs are everywhere. *Embo J*, *34*(19), 2398–2407.
- Hurley, J. H., & Hanson, P. I. (2010). Membrane budding and scission by the ESCRT machinery: it's all in the neck. *Nature Reviews Molecular Cell Biology*, *11*(8), 556–566.
- Hutchins, M. U., & Klionsky, D. J. (2001). Vacuolar Localization of Oligomeric α -Mannosidase Requires the Cytoplasm to Vacuole Targeting and Autophagy Pathway Components in *Saccharomyces cerevisiae*. *Journal of Biological Chemistry*, *276*(23), 20491–20498.
- Ichimiya, T., Yamakawa, T., Hirano, T., Yokoyama, Y., Hayashi, Y., Hirayama, D., Wagatsuma, K., Itoi, T., & Nakase, H. (2020). Autophagy and Autophagy-Related Diseases: A Review. *International Journal of Molecular Sciences*, *21*(23), 8974.
- Ichimura, Y., Kirisako, T., Takao, T., Satomi, Y., Shimonishi, Y., Ishihara, N., Mizushima, N., Tanida, I., Kominami, E., Ohsumi, M., Noda, T., & Ohsumi, Y. (2000). A ubiquitin-like system mediates protein lipidation. *Nature*, *408*(6811), 488–492.
- Ishihara, N., Hamasaki, M., Yokota, S., Suzuki, K., Kamada, Y., Kihara, A., Yoshimori, T., Noda, T., & Ohsumi, Y. (2001). Autophagosome requires specific early sec proteins for its formation and NSF/SNARE for vacuolar fusion. *Molecular Biology of the Cell*, *12*(11), 3690–3702.
- Jain, B. P., & Pandey, S. (2018). WD40 Repeat Proteins: Signalling Scaffold with Diverse Functions. *Protein Journal*, *37*(5), 391–406.
- Janke, C., Magiera, M. M., Rathfelder, N., Taxis, C., Reber, S., Maekawa, H., Moreno-Borchart, A., Doenges, G., Schwob, E., Schiebel, E., & Knop, M. (2004). A versatile toolbox for PCR-based tagging of yeast genes: New fluorescent proteins, more markers and promoter substitution cassettes. *Yeast*, *21*(11), 947–962.
- Jao, C. C., Ragusa, M. J., Stanley, R. E., & Hurley, J. H. (2013). A HORMA domain in Atg13 mediates PI 3-kinase recruitment in autophagy. *Proceedings of the National Academy of Sciences*, *110*(14), 5486–5491.
- Jeffries, T. R., Dove, S. K., Michell, R. H., & Parker, P. J. (2004). PtdIns-specific MPR

6. Bibliography

- Pathway Association of a Novel WD40 Repeat Protein, WIPI49. *Molecular Biology of the Cell*, 15(6), 2652–2663.
- Jensen, D., & Schekman, R. (2011). COPII-mediated vesicle formation at a glance. *Journal of Cell Science*, 124(1), 1–4.
- Ji, C., Zhao, H., Chen, D., Zhang, H., & Zhao, Y. G. (2021). β -propeller proteins WDR45 and WDR45B regulate autophagosome maturation into autolysosomes in neural cells. *Current Biology*, 1–12.
- Jiang, S., Kotani, N., Ohnishi, T., Miyagawa-Yamaguchi, A., Tsuda, M., Yamashita, R., Ishiura, Y., & Honke, K. (2012). A proteomics approach to the cell-surface interactome using the enzyme-mediated activation of radical sources reaction. *Proteomics*, 12(1), 54–62.
- Jiang, Y., & Broach, J. R. (1999). Tor proteins and protein phosphatase 2A reciprocally regulate Tap42 in controlling cell growth in yeast. *EMBO Journal*, 18(10), 2782–2792.
- Jin, N., Chow, C. Y., Liu, L., Zolov, S. N., Bronson, R., Davisson, M., Petersen, J. L., Zhang, Y., Park, S., Duex, J. E., Goldowitz, D., Meisler, M. H., & Weisman, L. S. (2008). VAC14 nucleates a protein complex essential for the acute interconversion of PI3P and PI(3,5)P2 in yeast and mouse. *The EMBO Journal*, 27(24), 3221–3234.
- Juris, L., Montino, M., Rube, P., Schlotterhose, P., Thumm, M., & Krick, R. (2015). PI3P binding by Atg 21 organises Atg 8 lipidation. *The EMBO Journal*, 34(4), 1–20.
- Kabeya, Y., Kamada, Y., Baba, M., Takikawa, H., Sasaki, M., & Ohsumi, Y. (2005). Atg17 Functions in Cooperation with Atg1 and Atg13 in Yeast Autophagy. *Molecular Biology of the Cell*, 16(5), 2544–2553.
- Kabeya, Y., Mizushima, N., Ueno, T., Yamamoto, A., Kirisako, T., Ohsumi, Y., & Yoshimori, T. (2000). LC3, a mammalian homologue of yeast Apg8p, is localized in autophagosome membranes after processing. *The EMBO Journal*, 19(21), 5720–5728.
- Kamada, Y., Funakoshi, T., Shintani, T., Nagano, K., Ohsumi, M., & Ohsumi, Y. (2000). Tor-Mediated Induction of Autophagy via an Apg1 Protein Kinase Complex. *Journal of Cell Biology*, 150(6), 1507–1513.
- Kamada, Y., Yoshino, K., Kondo, C., Kawamata, T., Oshiro, N., Yonezawa, K., & Ohsumi, Y. (2010). Tor Directly Controls the Atg1 Kinase Complex To Regulate Autophagy. *Molecular and Cellular Biology*, 30(4), 1049–1058.
- Kametaka, S., Okano, T., Ohsumi, M., & Ohsumi, Y. (1998). Apg14p and Apg6/Vps30p form a protein complex essential for autophagy in the yeast, *Saccharomyces cerevisiae*. *Journal of Biological Chemistry*, 273(35), 22284–22291.
- Kane, P. M. (2007). The long physiological reach of the yeast vacuolar H⁺-ATPase. *Journal of Bioenergetics and Biomembranes*, 39(5–6), 415–421.
- Kaneko, Y., Toh-e, A., & Oshima, Y. (1982). Identification of the genetic locus for the structural gene and a new regulatory gene for the synthesis of repressible alkaline phosphatase in *Saccharomyces cerevisiae*. *Molecular and Cellular Biology*, 2(2), 127–137.
- Kanki, T., Wang, K., Cao, Y., Baba, M., & Klionsky, D. J. (2009). Atg32 Is a Mitochondrial Protein that Confers Selectivity during Mitophagy. *Developmental Cell*, 17(1), 98–109.
- Katzmann, D. J., Odorizzi, G., & Emr, S. D. (2002). Receptor downregulation and multivesicular-body sorting. *Nature Reviews Molecular Cell Biology*, 3(12), 893–

6. Bibliography

905.

- Kaufmann, A., Beier, V., Franquelim, H. G., & Wollert, T. (2014). Molecular mechanism of autophagic membrane-scaffold assembly and disassembly. *Cell*, *156*(3), 469–481.
- Kiel, J. A. K. W., Rechinger, K. B., van der Klei, I. J., Salomons, F. A., Titorenko, V. I., & Veenhuis, M. (1999). The *Hansenula polymorpha* PDD1 gene product, essential for the selective degradation of peroxisomes, is a homologue of *Saccharomyces cerevisiae* Vps34p. *Yeast*, *15*(9), 741–754.
- Kihara, A., Noda, T., Ishihara, N., & Ohsumi, Y. (2001). Two Distinct Vps34 Phosphatidylinositol 3-Kinase Complexes Function in Autophagy and Carboxypeptidase Y Sorting in *Saccharomyces cerevisiae*. *Journal of Cell Biology*, *152*(3), 519–530.
- Kim, D. I., Jensen, S. C., Noble, K. A., KC, B., Roux, K. H., Motamedchaboki, K., & Roux, K. J. (2016). An improved smaller biotin ligase for BioID proximity labeling. *Molecular Biology of the Cell*, *27*(8), 1188–1196.
- Kim, D. I., KC, B., Zhu, W., Motamedchaboki, K., Doye, V., & Roux, K. J. (2014). Probing nuclear pore complex architecture with proximity-dependent biotinylation. *Proceedings of the National Academy of Sciences*, *111*(24), E2453–E2461.
- Kim, J., Dalton, V. M., Eggerton, K. P., Scott, S. V., & Klionsky, D. J. (1999). Apg7p/Cvt2p Is Required for the Cytoplasm-to-Vacuole Targeting, Macroautophagy, and Peroxisome Degradation Pathways. *Molecular Biology of the Cell*, *10*(5), 1337–1351.
- Kim, J., Scott, S. V., Oda, M. N., & Klionsky, D. J. (1997). Transport of a Large Oligomeric Protein by the Cytoplasm to Vacuole Protein Targeting Pathway. *Journal of Cell Biology*, *137*(3), 609–618.
- Kirisako, T., Baba, M., Ishihara, N., Miyazawa, K., Ohsumi, M., Yoshimori, T., Noda, T., & Ohsumi, Y. (1999). Formation Process of Autophagosome Is Traced with Apg8/Aut7p in Yeast. *Journal of Cell Biology*, *147*(2), 435–446.
- Kirisako, T., Ichimura, Y., Okada, H., Kabeya, Y., Mizushima, N., Yoshimori, T., Ohsumi, M., Takao, T., Noda, T., & Ohsumi, Y. (2000). The Reversible Modification Regulates the Membrane-Binding State of Apg8/Aut7 Essential for Autophagy and the Cytoplasm to Vacuole Targeting Pathway. *Journal of Cell Biology*, *151*(2), 263–276.
- Kiššová, I. B., Salin, B., Schaeffer, J., Bhatia, S., Manon, S., & Camougrand, N. (2007). Selective and Non-Selective Autophagic Degradation of Mitochondria in Yeast. *Autophagy*, *3*(4), 329–336.
- Klionsky, D. J., Cueva, R., & Yaver, D. S. (1992). Aminopeptidase I of *Saccharomyces cerevisiae* is localized to the vacuole independent of the secretory pathway. *Journal of Cell Biology*, *119*(2), 287–299.
- Klionsky, D. J., & Emr, S. D. (1989). Membrane protein sorting: biosynthesis, transport and processing of yeast vacuolar alkaline phosphatase. *The EMBO Journal*, *8*(8), 2241–2250.
- Kohrer, K., & Emr, S. D. (1993). The yeast VPS17 gene encodes a membrane-associated protein required for the sorting of soluble vacuolar hydrolases. *Journal of Biological Chemistry*, *268*(1), 559–569.
- Komatsu, M., Tanida, I., Ueno, T., Ohsumi, M., Ohsumi, Y., & Kominami, E. (2001). The C-terminal Region of an Apg7p/Cvt2p is Required for Homodimerization and is Essential for its E1 Activity and E1-E2 Complex Formation. *Journal of Biological*

6. Bibliography

- Chemistry*, 276(13), 9846–9854.
- Kooner, J. S., Saleheen, D., Sim, X., Sehmi, J., Zhang, W., Frossard, P., Been, L. F., Chia, K.-S., Dimas, A. S., Hassanali, N., Jafar, T., Jowett, J. B. M., Li, X., Radha, V., Rees, S. D., Takeuchi, F., Young, R., Aung, T., Basit, A., ... Chambers, J. C. (2011). Genome-wide association study in individuals of South Asian ancestry identifies six new type 2 diabetes susceptibility loci. *Nature Genetics*, 43(10), 984–989.
- Kotani, T., Kirisako, H., Koizumi, M., Ohsumi, Y., & Nakatogawa, H. (2018). The Atg2-Atg18 complex tethers pre-autophagosomal membranes to the endoplasmic reticulum for autophagosome formation. *Proceedings of the National Academy of Sciences*, 115(41), 10363–10368.
- Koumandou, V. L., Klute, M. J., Herman, E. K., Nunez-Miguel, R., Dacks, J. B., & Field, M. C. (2011). Evolutionary reconstruction of the retromer complex and its function in *Trypanosoma brucei*. *Journal of Cell Science*, 124(9), 1496–1509.
- Kovtun, O., Leneva, N., Bykov, Y. S., Ariotti, N., Teasdale, R. D., Schaffer, M., Engel, B. D., Owen, D. J., Briggs, J. A. G., & Collins, B. M. (2018). Structure of the membrane-assembled retromer coat determined by cryo-electron tomography. In *Nature* (Vol. 561, Issue 7724, pp. 561–564).
- Kraft, C., Deplazes, A., Sohrmann, M., & Peter, M. (2008). Mature ribosomes are selectively degraded upon starvation by an autophagy pathway requiring the Ubp3p/Bre5p ubiquitin protease. *Nature Cell Biology*, 10(5), 602–610.
- Krämer, L., & Ungermann, C. (2011). HOPS drives vacuole fusion by binding the vacuolar SNARE complex and the Vam7 PX domain via two distinct sites. *Molecular Biology of the Cell*, 22(14), 2601–2611.
- Krick, R., Busse, R. A., Scacioc, A., Stephan, M., Janshoff, A., Thumm, M., & Kühnel, K. (2012). Structural and functional characterization of the two phosphoinositide binding sites of PROPPINs, a β -propeller protein family. *Proceedings of the National Academy of Sciences*, 109(30), E2042–E2049.
- Krick, R., Henke, S., Tolstrup, J., & Thumm, M. (2008). Dissecting the localization and function of Atg18, Atg21 and Ygr223c. *Autophagy*, 4(7), 896–910.
- Krick, R., Muehe, Y., Prick, T., Bremer, S., Schlotterhose, P., Eskelinen, E.-L., Millen, J., Goldfarb, D. S., & Thumm, M. (2008). Piecemeal Microautophagy of the Nucleus Requires the Core Macroautophagy Genes. *Molecular Biology of the Cell*, 19(10), 4492–4505.
- Krick, R., Tolstrup, J., Appelles, A., Henke, S., & Thumm, M. (2006). The relevance of the phosphatidylinositolphosphat-binding motif FRRGT of Atg18 and Atg21 for the Cvt pathway and autophagy. *FEBS Letters*, 580(19), 4632–4638.
- Kriegenburg, F., Bas, L., Gao, J., Ungermann, C., & Kraft, C. (2019). The multi-functional SNARE protein Ykt6 in autophagosomal fusion processes. *Cell Cycle*, 18(6–7), 639–651.
- Krogan, N. J., Cagney, G., Yu, H., Zhong, G., Guo, X., Ignatchenko, A., Li, J., Pu, S., Datta, N., Tikuisis, A. P., Punna, T., Peregrín-Alvarez, J. M., Shales, M., Zhang, X., Davey, M., Robinson, M. D., Paccanaro, A., Bray, J. E., Sheung, A., ... Greenblatt, J. F. (2006). Global landscape of protein complexes in the yeast *Saccharomyces cerevisiae*. *Nature*, 440(7084), 637–643.
- Kuma, A., Mizushima, N., Ishihara, N., & Ohsumi, Y. (2002). Formation of the ~350-kDa Apg12-Apg5-Apg16 multimeric complex, mediated by Apg16 oligomerization, is essential for autophagy in yeast. *Journal of Biological Chemistry*, 277(21), 18619–

6. Bibliography

- 18625.
- Kunz, J. B., Schwarz, H., & Mayer, A. (2004). Determination of Four Sequential Stages during Microautophagy in Vitro. *Journal of Biological Chemistry*, 279(11), 9987–9996.
- Kvam, E., & Goldfarb, D. S. (2007). Nucleus-vacuole junctions and piecemeal microautophagy of the nucleus in *S. cerevisiae*. *Autophagy*, 3(2), 85–92.
- Kweon, Y., Rothe, A., Conibear, E., & Stevens, T. H. (2003). Ykt6p Is a Multifunctional Yeast R-SNARE That Is Required for Multiple Membrane Transport Pathways to the Vacuole. *Molecular Biology of the Cell*, 14(5), 1868–1881.
- Kwon, K., & Beckett, D. (2000). Function of a conserved sequence motif in biotin holoenzyme synthetases. *Protein Science*, 9(8), 1530–1539.
- LaGrassa, T. J., & Ungermann, C. (2005). The vacuolar kinase Yck3 maintains organelle fragmentation by regulating the HOPS tethering complex. *Journal of Cell Biology*, 168(3), 401–414.
- Lämmler, U. (1970). Cleavage of Structural Proteins during the Assembly of the Head of Bacteriophage T4. *Nature*, 227(5259), 680–685.
- Lang, T., Reiche, S., Straub, M., Bredschneider, M., & Thumm, M. (2000). Autophagy and the cvt Pathway Both Depend onAUT9. *Journal of Bacteriology*, 182(8), 2125–2133.
- Leber, R., Silles, E., Sandoval, I. V., & Mazón, M. J. (2001). Yol082p, a Novel CVT Protein Involved in the Selective Targeting of Aminopeptidase I to the Yeast Vacuole. *Journal of Biological Chemistry*, 276(31), 29210–29217.
- Lee, M. C. S., Miller, E. A., Goldberg, J., Orci, L., & Schekman, R. (2004). Bi-directional protein transport between the ER and Golgi. *Annual Review of Cell and Developmental Biology*, 20(1), 87–123.
- Lefebvre, C., Legouis, R., & Culetto, E. (2018). ESCRT and autophagies: Endosomal functions and beyond. *Seminars in Cell and Developmental Biology*, 74, 21–28.
- Lei, Y., Tang, D., Liao, G., Xu, L., Liu, S., Chen, Q., Li, C., Duan, J., Wang, K., Wang, J., Sun, B., Li, Z., Dai, L., Cheng, W., Qi, S., & Lu, K. (2020). The crystal structure of Atg18 reveals a new binding site for Atg2 in *Saccharomyces cerevisiae*. *Cellular and Molecular Life Sciences*.
- Léon, S., Erpapazoglou, Z., & Haguenaer-Tsapis, R. (2008). Ear1p and Ssh4p Are New Adaptors of the Ubiquitin Ligase Rsp5p for Cargo Ubiquitylation and Sorting at Multivesicular Bodies. *Molecular Biology of the Cell*, 19(6), 2379–2388.
- Levine, B., & Kroemer, G. (2019). Biological Functions of Autophagy Genes: A Disease Perspective. *Cell*, 176(1–2), 11–42.
- Li, W., Li, J., & Bao, J. (2012). Microautophagy: lesser-known self-eating. *Cellular and Molecular Life Sciences*, 69(7), 1125–1136.
- Liu, T. T., Gomez, T. S., Sackey, B. K., Billadeau, D. D., & Burd, C. G. (2012). Rab GTPase regulation of retromer-mediated cargo export during endosome maturation. *Molecular Biology of the Cell*, 23(13), 2505–2515.
- Liu, X., Mao, K., Yu, A. Y. H., Omairi-Nasser, A., Austin, J., Glick, B. S., Yip, C. K., & Klionsky, D. J. (2016). The Atg17-Atg31-Atg29 Complex Coordinates with Atg11 to Recruit the Vam7 SNARE and Mediate Autophagosome-Vacuole Fusion. *Current Biology*, 26(2), 150–160.
- Liu, Y., & Okamoto, K. (2021). Regulatory mechanisms of mitophagy in yeast.

6. Bibliography

- Biochimica et Biophysica Acta (BBA) - General Subjects*, 1865(5), 129858.
- Longtine, M. S., Mckenzie III, A., Demarini, D. J., Shah, N. G., Wach, A., Brachet, A., Philippsen, P., & Pringle, J. R. (1998). Additional modules for versatile and economical PCR-based gene deletion and modification in *Saccharomyces cerevisiae*. *Yeast*, 14(10), 953–961.
- Lucas, M., Gershlick, D. C., Vidaurrazaga, A., Rojas, A. L., Bonifacino, J. S., & Hierro, A. (2016). Structural Mechanism for Cargo Recognition by the Retromer Complex. *Cell*, 167(6), 1623-1635.e14.
- Luke, M. M., Della Seta, F., Di Como, C. J., Sugimoto, H., Kobayashi, R., & Arndt, K. T. (1996). The SAP, a new family of proteins, associate and function positively with the SIT4 phosphatase. *Molecular and Cellular Biology*, 16(6), 2744–2755.
- Ma, M., & Burd, C. G. (2019). Retrograde trafficking and quality control of yeast synaptobrevin, Snc1, are conferred by its transmembrane domain. *Molecular Biology of the Cell*, 30(14), 1729–1742.
- Ma, M., & Burd, C. G. (2020). Retrograde trafficking and plasma membrane recycling pathways of the budding yeast *Saccharomyces cerevisiae*. *Traffic*, 21(1), 45–59.
- Ma, M., Burd, C. G., & Chi, R. J. (2017). Distinct complexes of yeast Snx4 family SNX-BARs mediate retrograde trafficking of Snc1 and Atg27. *Traffic*, 18(2), 134–144.
- Maeda, S., Otomo, C., & Otomo, T. (2019). The autophagic membrane tether ATG2A transfers lipids between membranes. *ELife*, 8, 1–24.
- Mao, K., Chew, L. H., Inoue-Aono, Y., Cheong, H., Nair, U., Popelka, H., Yip, C. K., & Klionsky, D. J. (2013). Atg29 phosphorylation regulates coordination of the Atg17-Atg31-Atg29 complex with the Atg11 scaffold during autophagy initiation. *Proceedings of the National Academy of Sciences of the United States of America*, 110(31).
- Mari, M., Griffith, J., Rieter, E., Krishnappa, L., Klionsky, D. J., & Reggiori, F. (2010). An Atg9-containing compartment that functions in the early steps of autophagosome biogenesis. *Journal of Cell Biology*, 190(6), 1005–1022.
- Martell, J. D., Deerinck, T. J., Sancak, Y., Poulos, T. L., Mootha, V. K., Sosinsky, G. E., Ellisman, M. H., & Ting, A. Y. (2012). Engineered ascorbate peroxidase as a genetically encoded reporter for electron microscopy. *Nature Biotechnology*, 30(11), 1143–1148.
- Matoba, K., Kotani, T., Tsutsumi, A., Tsuji, T., Mori, T., Noshiro, D., Sugita, Y., Nomura, N., Iwata, S., Ohsumi, Y., Fujimoto, T., Nakatogawa, H., Kikkawa, M., & Noda, N. N. (2020). Atg9 is a lipid scramblase that mediates autophagosomal membrane expansion. *Nature Structural & Molecular Biology*.
- Matsuura, A., Tsukada, M., Wada, Y., & Ohsumi, Y. (1997). Apg1p, a novel protein kinase required for the autophagic process in *Saccharomyces cerevisiae*. *Gene*, 192(2), 245–250.
- McNew, J. A., Sogaard, M., Lampen, N. M., Rothman, J. E., Ye, R. R., Machida, S., Lacomis, L., Tempst, P., & Sollner, T. H. (1997). Ykt6p, a Prenylated SNARE Essential for Endoplasmic Reticulum-Golgi Transport. *Journal of Biological Chemistry*, 272(28), 17776–17783.
- Meiling-Wesse, K., Barth, H., Voss, C., Barmark, G., Murén, E., Ronne, H., & Thumm, M. (2002). Yeast Mon1p/Aut12p functions in vacuolar fusion of autophagosomes and cvt-vesicles. *FEBS Letters*, 530(1–3), 174–180.
- Meiringer, C. T. A., Rethmeier, R., Auffarth, K., Wilson, J., Perz, A., Barlowe, C., Schmitt,

6. Bibliography

- H. D., & Ungermann, C. (2011). The Dsl1 protein tethering complex is a resident endoplasmic reticulum complex, which interacts with five soluble NSF (N-ethylmaleimide-sensitive factor) attachment protein receptors (SNAREs): Implications for fusion and fusion regulation. *Journal of Biological Chemistry*, *286*(28), 25039–25046.
- Michell, R. H., & Dove, S. K. (2009). A protein complex that regulates PtdIns(3,5)P₂ levels. *The EMBO Journal*, *28*(2), 86–87.
- Michell, R. H., Heath, V. L., Lemmon, M. A., & Dove, S. K. (2006). Phosphatidylinositol 3,5-bisphosphate: metabolism and cellular functions. *Trends in Biochemical Sciences*, *31*(1), 52–63.
- Mim, C., & Unger, V. M. (2012). Membrane curvature and its generation by BAR proteins. *Trends in Biochemical Sciences*, *37*(12), 526–533.
- Mitchener, J. S., Shelburne, J. D., Bradford, W. D., & Hawkins, H. K. (1976). Cellular autophagocytosis induced by deprivation of serum and amino acids in HeLa cells. *American Journal of Pathology*, *83*(3), 485–498.
- Mizushima, N., & Komatsu, M. (2011). Autophagy: Renovation of Cells and Tissues. *Cell*, *147*(4), 728–741.
- Mizushima, N., Noda, T., & Ohsumi, Y. (1999). Apg16p is required for the function of the Apg12p-Apg5p conjugate in the yeast autophagy pathway. *EMBO Journal*, *18*(14), 3888–3896.
- Mizushima, N., Noda, T., Yoshimori, T., Tanaka, Y., Ishii, T., George, M. D., Klionsky, D. J., Ohsumi, M., & Ohsumi, Y. (1998). A protein conjugation system essential for autophagy. *Nature*, *395*(6700), 395–398.
- Mizushima, N., Yoshimori, T., & Ohsumi, Y. (2011). The Role of Atg Proteins in Autophagosome Formation. *Annual Review of Cell and Developmental Biology*, *27*(1), 107–132.
- Mochida, K., Oikawa, Y., Kimura, Y., Kirisako, H., Hirano, H., Ohsumi, Y., & Nakatogawa, H. (2015). Receptor-mediated selective autophagy degrades the endoplasmic reticulum and the nucleus. *Nature*, *522*(7556), 359–362.
- Mollereau, B., & Walter, L. (2019). Is WDR45 the missing link for ER stress-induced autophagy in beta-propeller associated neurodegeneration? *Autophagy*, *15*(12), 2163–2164.
- Mortimore, G. E., & Schworer, C. M. (1977). Induction of autophagy by amino-acid deprivation in perfused rat liver. *Nature*, *270*(5633), 174–176.
- Motley, A. M., Nuttall, J. M., & Hettema, E. H. (2012). Pex3-anchored Atg36 tags peroxisomes for degradation in *Saccharomyces cerevisiae*. *The EMBO Journal*, *31*(13), 2852–2868.
- Munzel, L., Neumann, P., Otto, F. B., Krick, R., Metje-Sprink, J., Kroppen, B., Karedla, N., Enderlein, J., Meinecke, M., Ficner, R., & Thumm, M. (2020). Atg21 organizes Atg8 lipidation at the contact of the vacuole with the phagophore. *Autophagy*, 1–21.
- Muthusamy, B. P., Natarajan, P., Zhou, X., & Graham, T. R. (2009). Linking phospholipid flippases to vesicle-mediated protein transport. *Biochimica et Biophysica Acta - Molecular and Cell Biology of Lipids*, *1791*(7), 612–619.
- Nair, U., Yen, W. L., Mari, M., Cao, Y., Xie, Z., Baba, M., Reggiori, F., & Klionsky, D. J. (2012). A role for Atg8-PE deconjugation in autophagosome biogenesis. *Autophagy*, *8*(5), 780–793.
- Nakatogawa, H., Ishii, J., Asai, E., & Ohsumi, Y. (2012). Atg4 recycles inappropriately

6. Bibliography

- lipidated Atg8 to promote autophagosome biogenesis. *Autophagy*, 8(2), 177–186.
- Neiman, A. M. (2005). Ascospore Formation in the Yeast *Saccharomyces cerevisiae*. *Microbiology and Molecular Biology Reviews*, 69(4), 565–584.
- Niedenthal, R. K., Riles, L., Johnston, M., & Hegemann, J. H. (1996). Green fluorescent protein as a marker for gene expression and subcellular localization in budding yeast. *Yeast (Chichester, England)*, 12(8), 773–786.
- Noda, N. N., Kumeta, H., Nakatogawa, H., Satoo, K., Adachi, W., Ishii, J., Fujioka, Y., Ohsumi, Y., & Inagaki, F. (2008). Structural basis of target recognition by Atg8/LC3 during selective autophagy. *Genes to Cells*, 13(12), 1211–1218.
- Noda, N. N., Ohsumi, Y., & Inagaki, F. (2010). Atg8-family interacting motif crucial for selective autophagy. *FEBS Letters*, 584(7), 1379–1385.
- Noda, N. N., Satoo, K., Fujioka, Y., Kumeta, H., Ogura, K., Nakatogawa, H., Ohsumi, Y., & Inagaki, F. (2011). Structural basis of Atg8 activation by a homodimeric E1, Atg7. *Molecular Cell*, 44(3), 462–475.
- Noda, T., Kim, J., Huang, W.-P., Baba, M., Tokunaga, C., Ohsumi, Y., & Klionsky, D. J. (2000). Apg9p/Cvt7p Is an Integral Membrane Protein Required for Transport Vesicle Formation in the Cvt and Autophagy Pathways. *Journal of Cell Biology*, 148(3), 465–480.
- Noda, T., & Ohsumi, Y. (1998). Tor, a Phosphatidylinositol Kinase Homologue, Controls Autophagy in Yeast. *Journal of Biological Chemistry*, 273(7), 3963–3966.
- Nordmann, M., Cabrera, M., Perz, A., Bröcker, C., Ostrowicz, C., Engelbrecht-Vandré, S., & Ungermann, C. (2010). The Mon1-Ccz1 complex is the GEF of the late endosomal Rab7 homolog Ypt7. *Current Biology*, 20(18), 1654–1659.
- Norwood, S. J., Shaw, D. J., Cowieson, N. P., Owen, D. J., Teasdale, R. D., & Collins, B. M. (2011). Assembly and Solution Structure of the Core Retromer Protein Complex. *Traffic*, 12(1), 56–71.
- Nothwehr, S. F., Bruinsma, P., & Strawn, L. A. (1999). Distinct Domains within Vps35p Mediate the Retrieval of Two Different Cargo Proteins from the Yeast Prevacuolar/Endosomal Compartment. *Molecular Biology of the Cell*, 10(4), 875–890.
- Nothwehr, S. F., Bryant, N. J., & Stevens, T. H. (1996). The newly identified yeast GRD genes are required for retention of late-Golgi membrane proteins. *Molecular and Cellular Biology*, 16(6), 2700–2707.
- Nothwehr, S. F., Ha, S. A., & Bruinsma, P. (2000). Sorting of yeast membrane proteins into an endosome-to-Golgi pathway involves direct interaction of their cytosolic domains with Vps35p. *Journal of Cell Biology*, 151(2), 297–309.
- Nothwehr, S. F., & Hines, A. E. (1997). The yeast VPS5/GRD2 gene encodes a sorting nexin-1-like protein required for localizing membrane proteins to the late Golgi. *Journal of Cell Science*, 110 (Pt 9(9), 1063–1072.
- Novick, P., Ferro, S., & Schekman, R. (1981). Order of events in the yeast secretory pathway. *Cell*, 25(2), 461–469.
- Novick, P., Field, C., & Schekman, R. (1980). Identification of 23 complementation groups required for post-translational events in the yeast secretory pathway. *Cell*, 21(1), 205–215.
- Novikoff, A. B., & Essner, E. (1962). CYTOLYSOMES AND MITOCHONDRIAL DEGENERATION. *Journal of Cell Biology*, 15(1), 140–146.

6. Bibliography

- Obara, K., Noda, T., Niimi, K., & Ohsumi, Y. (2008). Transport of phosphatidylinositol 3-phosphate into the vacuole via autophagic membranes in *Saccharomyces cerevisiae*. *Genes to Cells*, *13*(6), 537–547.
- Obara, K., & Ohsumi, Y. (2008). Dynamics and function of PtdIns(3) P in autophagy. *Autophagy*, *4*(7), 952–954.
- Obara, K., Sekito, T., Niimi, K., & Ohsumi, Y. (2008). The Atg18-Atg2 Complex Is Recruited to Autophagic Membranes via Phosphatidylinositol 3-Phosphate and Exerts an Essential Function. *Journal of Biological Chemistry*, *283*(35), 23972–23980.
- Ohashi, Y., & Munro, S. (2010). Membrane delivery to the yeast autophagosome from the golgi-endosomal system. *Molecular Biology of the Cell*, *21*(22), 3998–4008.
- Ohashi, Y., Soler, N., García Ortégón, M., Zhang, L., Kirsten, M. L., Perisic, O., Masson, G. R., Burke, J. E., Jakobi, A. J., Apostolakis, A. A., Johnson, C. M., Ohashi, M., Ktistakis, N. T., Sachse, C., & Williams, R. L. (2016). Characterization of Atg38 and NRBF2, a fifth subunit of the autophagic Vps34/PIK3C3 complex. *Autophagy*, *12*(11), 2129–2144.
- Oku, M., Maeda, Y., Kagohashi, Y., Kondo, T., Yamada, M., Fujimoto, T., & Sakai, Y. (2017). Evidence for ESCRT- and clathrin-dependent microautophagy. *Journal of Cell Biology*, *216*(10), 3263–3274.
- Ong, S.-E., Blagoev, B., Kratchmarova, I., Kristensen, D. B., Steen, H., Pandey, A., & Mann, M. (2002). Stable Isotope Labeling by Amino Acids in Cell Culture, SILAC, as a Simple and Accurate Approach to Expression Proteomics. *Molecular & Cellular Proteomics*, *1*(5), 376–386.
- Opitz, N., Schmitt, K., Hofer-Pretz, V., Neumann, B., Krebber, H., Braus, G. H., & Valerius, O. (2017). Capturing the Asc1p/Receptor for Activated C Kinase 1 (RACK1) Microenvironment at the Head Region of the 40S Ribosome with Quantitative BioID in Yeast. *Molecular & Cellular Proteomics*, *16*(12), 2199–2218.
- Orenstein, S. J., & Cuervo, A. M. (2010). Chaperone-mediated autophagy: Molecular mechanisms and physiological relevance. *Seminars in Cell & Developmental Biology*, *21*(7), 719–726.
- Osawa, T., Ishii, Y., & Noda, N. N. (2020). Human ATG2B possesses a lipid transfer activity which is accelerated by negatively charged lipids and WIPI4. *Genes to Cells*, *25*(1), 65–70.
- Osawa, T., Kotani, T., Kawaoka, T., Hirata, E., Suzuki, K., Nakatogawa, H., Ohsumi, Y., & Noda, N. N. (2019). Atg2 mediates direct lipid transfer between membranes for autophagosome formation. *Nature Structural and Molecular Biology*, *26*(4), 281–288.
- Osawa, T., & Noda, N. N. (2019). Atg2: A novel phospholipid transfer protein that mediates de novo autophagosome biogenesis. *Protein Science*, *28*(6), 1005–1012.
- Otomo, T., Chowdhury, S., & Lander, G. C. (2018). The Rod-Shaped ATG2A-WIPI4 Complex Tethers Membranes In Vitro. *Contact*, *1*(1), 251525641881993.
- Otto, F. B., & Thumm, M. (2020). Nucleophagy-implications for microautophagy and health. *International Journal of Molecular Sciences*, *21*(12), 1–14.
- Papinski, D., Schuschnig, M., Reiter, W., Wilhelm, L., Barnes, C. A., Maiolica, A., Hansmann, I., Pfaffenwimmer, T., Kijanska, M., Stoffel, I., Lee, S. S., Brezovich, A., Lou, J. H., Turk, B. E., Aebersold, R., Ammerer, G., Peter, M., & Kraft, C. (2014). Early Steps in Autophagy Depend on Direct Phosphorylation of Atg9 by the Atg1 Kinase.

6. Bibliography

- Molecular Cell*, 53(3), 471–483.
- Parrish, W. R., Stefan, C. J., & Emr, S. D. (2004). Essential Role for the Myotubularin-related Phosphatase Ymr1p and the Synaptojanin-like Phosphatases Sjl2p and Sjl3p in Regulation of Phosphatidylinositol 3-Phosphate in Yeast. *Molecular Biology of the Cell*, 15(8), 3567–3579.
- Parzych, K. R., Ariosa, A., Mari, M., & Klionsky, D. J. (2018). A newly characterized vacuolar serine carboxypeptidase, Atg42/Ybr139w, is required for normal vacuole function and the terminal steps of autophagy in the yeast *Saccharomyces cerevisiae*. *Molecular Biology of the Cell*, 29(9), 1089–1099.
- Parzych, K. R., & Klionsky, D. J. (2014). An Overview of Autophagy: Morphology, Mechanism, and Regulation. *Antioxidants & Redox Signaling*, 20(3), 460–473.
- Pasteur, L. (1879). Studies on Fermentation. *London MacMillan & Co.*
- Peters, C., Baars, T. L., Bühler, S., & Mayer, A. (2004). Mutual Control of Membrane Fission and Fusion Proteins. *Cell*, 119(5), 667–678.
- Pink, M., Verma, N., Rettenmeier, A. W., & Schmitz-Spanke, S. (2010). CBB staining protocol with higher sensitivity and mass spectrometric compatibility. *ELECTROPHORESIS*, 31(4), 593–598.
- Piper, R. C., & Katzmann, D. J. (2010). Biogenesis and function of MVBs. *Annual Review of Cell and Developmental Biology*, 23, 519–547.
- Priya, A., Kalaidzidis, I. V., Kalaidzidis, Y., Lambright, D., & Datta, S. (2015). Molecular Insights into Rab7-Mediated Endosomal Recruitment of Core Retromer: Deciphering the Role of Vps26 and Vps35. *Traffic*, 16(1), 68–84.
- Proikas-Cezanne, T., Takacs, Z., Donnes, P., & Kohlbacher, O. (2015). WIPI proteins: essential PtdIns3P effectors at the nascent autophagosome. *Journal of Cell Science*, 128(2), 207–217.
- Puri, C., Renna, M., Bento, C. F., Moreau, K., & Rubinsztein, D. C. (2013). Diverse autophagosome membrane sources coalesce in recycling endosomes. *Cell*, 154(6), 1285–1299.
- Purushothaman, L. K., Arlt, H., Kuhlee, A., Raunser, S., & Ungermann, C. (2017). Retromer-driven membrane tubulation separates endosomal recycling from Rab7/Ypt7-dependent fusion. *Molecular Biology of the Cell*, 28(6), 783–791.
- Purushothaman, L. K., & Ungermann, C. (2018). Cargo induces retromer-mediated membrane remodeling on membranes. *Molecular Biology of the Cell*, 29(22), 2709–2719.
- Ragusa, M. J., Stanley, R. E., & Hurley, J. H. (2012). Architecture of the Atg17 Complex as a Scaffold for Autophagosome Biogenesis. *Cell*, 151(7), 1501–1512.
- Ramanathan, M., Majzoub, K., Rao, D. S., Neela, P. H., Zarnegar, B. J., Mondal, S., Roth, J. G., Gai, H., Kovalski, J. R., Siprashvili, Z., Palmer, T. D., Carette, J. E., & Khavari, P. A. (2018). RNA–protein interaction detection in living cells. *Nature Methods*, 15(3), 207–212.
- Rao, Y., Perna, M. G., Hofmann, B., Beier, V., & Wollert, T. (2016). The Atg1-kinase complex tethers Atg9-vesicles to initiate autophagy. *Nature Communications*, 7.
- Ravikumar, B., Moreau, K., Jahreiss, L., Puri, C., & Rubinsztein, D. C. (2010). Plasma membrane contributes to the formation of pre-autophagosomal structures. *Nature Cell Biology*, 12(8), 747–757.
- Raymond, C. K., Howald-Stevenson, I., Vater, C. A., & Stevens, T. H. (1992).

6. Bibliography

- Morphological classification of the yeast vacuolar protein sorting mutants: evidence for a prevacuolar compartment in class E vps mutants. *Molecular Biology of the Cell*, 3(12), 1389–1402.
- Reddy, J. V., & Seaman, M. N. J. (2001). Vps26p, a Component of Retromer, Directs the Interactions of Vps35p in Endosome-to-Golgi Retrieval. *Molecular Biology of the Cell*, 12(10), 3242–3256.
- Reggiori, F., & Klionsky, D. J. (2002). Autophagy in the Eukaryotic Cell. *Eukaryotic Cell*, 1(1), 11–21.
- Reggiori, F., & Klionsky, D. J. (2013). Autophagic Processes in Yeast: Mechanism, Machinery and Regulation. *Genetics*, 194(2), 341–361.
- Reggiori, F., Tucker, K. A., Stromhaug, P. E., & Klionsky, D. J. (2004). The Atg1-Atg13 complex regulates Atg9 and Atg23 retrieval transport from the pre-autophagosomal structure. *Developmental Cell*, 6(1), 79–90.
- Reggiori, F., & Ungermann, C. (2017). Autophagosome Maturation and Fusion. *Journal of Molecular Biology*, 429(4), 486–496.
- Ren, G., Vajjhala, P., Lee, J. S., Winsor, B., & Munn, A. L. (2006). The BAR Domain Proteins: Molding Membranes in Fission, Fusion, and Phagy. *Microbiology and Molecular Biology Reviews*, 70(1), 37–120.
- Rhee, H. W., Zou, P., Udeshi, N. D., Martell, J. D., Mootha, V. K., Carr, S. A., & Ting, A. Y. (2013). Proteomic mapping of mitochondria in living cells via spatially restricted enzymatic tagging. *Science*, 339(6125), 1328–1331.
- Rieter, E., Vinke, F., Bakula, D., Cebollero, E., Ungermann, C., Proikas-Cezanne, T., & Reggiori, F. (2013). Atg18 function in autophagy is regulated by specific sites within its β -propeller. *Journal of Cell Science*, 126(2), 593–604.
- Robinson, J. S., Klionsky, D. J., Banta, L. M., & Emr, S. D. (1988). Protein sorting in *Saccharomyces cerevisiae*: isolation of mutants defective in the delivery and processing of multiple vacuolar hydrolases. *Molecular and Cellular Biology*, 8(11), 4936–4948.
- Rojas, R., van Vlijmen, T., Mardones, G. A., Prabhu, Y., Rojas, A. L., Mohammed, S., Heck, A. J. R., Raposo, G., van der Sluijs, P., & Bonifacino, J. S. (2008). Regulation of retromer recruitment to endosomes by sequential action of Rab5 and Rab7. *Journal of Cell Biology*, 183(3), 513–526.
- Romanov, J., Walczak, M., Ibiricu, I., Schüchner, S., Ogris, E., Kraft, C., & Martens, S. (2012). Mechanism and functions of membrane binding by the Atg5-Atg12/Atg16 complex during autophagosome formation. *EMBO Journal*, 31(22), 4304–4317.
- Rothman, J. H., Howald, I., & Stevens, T. H. (1989). Characterization of genes required for protein sorting and vacuolar function in the yeast *Saccharomyces cerevisiae*. *The EMBO Journal*, 8(7), 2057–2065.
- Roux, K. J., Kim, D. I., Raida, M., & Burke, B. (2012). A promiscuous biotin ligase fusion protein identifies proximal and interacting proteins in mammalian cells. *Journal of Cell Biology*, 196(6), 801–810.
- Rudge, S. A., Anderson, D. M., & Emr, S. D. (2004). Vacuole Size Control: Regulation of PtdIns(3,5)P₂ Levels by the Vacuole-associated Vac14-Fig4 Complex, a PtdIns(3,5)P₂-specific Phosphatase. *Molecular Biology of the Cell*, 15(1), 24–36.
- Rusten, T. E., Vaccari, T., Lindmo, K., Rodahl, L. M. W., Nezis, I. P., Sem-Jacobsen, C., Wendler, F., Vincent, J. P., Brech, A., Bilder, D., & Stenmark, H. (2007). ESCRTs and Fab1 Regulate Distinct Steps of Autophagy. *Current Biology*, 17(20), 1817–1825.

6. Bibliography

- Saitou, H., Nishimura, T., Muramatsu, K., Kodera, H., Kumada, S., Sugai, K., Kasai-Yoshida, E., Sawaura, N., Nishida, H., Hoshino, A., Ryujin, F., Yoshioka, S., Nishiyama, K., Kondo, Y., Tsurusaki, Y., Nakashima, M., Miyake, N., Arakawa, H., Kato, M., ... Matsumoto, N. (2013). De novo mutations in the autophagy gene WDR45 cause static encephalopathy of childhood with neurodegeneration in adulthood. *Nature Genetics*, *45*(4), 445–449.
- Sakai, Y., Oku, M., van der Klei, I. J., & Kiel, J. A. K. W. (2006). Pexophagy: Autophagic degradation of peroxisomes. *Biochimica et Biophysica Acta (BBA) - Molecular Cell Research*, *1763*(12), 1767–1775.
- Sakoh-Nakatogawa, M., Matoba, K., Asai, E., Kirisako, H., Ishii, J., Noda, N. N., Inagaki, F., Nakatogawa, H., & Ohsumi, Y. (2013). Atg12–Atg5 conjugate enhances E2 activity of Atg3 by rearranging its catalytic site. *Nature Structural & Molecular Biology*, *20*(4), 433–439.
- Salvador, N., Aguado, C., Horst, M., & Knecht, E. (2000). Import of a Cytosolic Protein into Lysosomes by Chaperone-mediated Autophagy Depends on Its Folding State. *Journal of Biological Chemistry*, *275*(35), 27447–27456.
- Samavarchi-Tehrani, P., Samson, R., & Gingras, A. C. (2020). Proximity dependent biotinylation: Key enzymes and adaptation to proteomics approaches. *Molecular and Cellular Proteomics*, *19*(5), 757–773.
- Sánchez-Wandelmer, J., Kriegenburg, F., Rohringer, S., Schuschnig, M., Gómez-Sánchez, R., Zens, B., Abreu, S., Hardenberg, R., Hollenstein, D., Gao, J., Ungermann, C., Martens, S., Kraft, C., & Reggiori, F. (2017). Atg4 proteolytic activity can be inhibited by Atg1 phosphorylation. *Nature Communications*, *8*(1), 295.
- Sawa-Makarska, J., Baumann, V., Coudevylle, N., von Bülow, S., Nogellova, V., Abert, C., Schuschnig, M., Graef, M., Hummer, G., & Martens, S. (2020). Reconstitution of autophagosome nucleation defines Atg9 vesicles as seeds for membrane formation. *Science (New York, N.Y.)*, *369*(6508).
- Scacioc, A., Schmidt, C., Hofmann, T., Urlaub, H., Kühnel, K., & Pérez-Lara, Á. (2017). Structure based biophysical characterization of the PROPPIN Atg18 shows Atg18 oligomerization upon membrane binding. *Scientific Reports*, *7*(1), 14008.
- Schindelin, J., Arganda-Carreras, I., Frise, E., Kaynig, V., Longair, M., Pietzsch, T., Preibisch, S., Rueden, C., Saalfeld, S., Schmid, B., Tinevez, J.-Y., White, D. J., Hartenstein, V., Eliceiri, K., Tomancak, P., & Cardona, A. (2012). Fiji: an open-source platform for biological-image analysis. *Nature Methods*, *9*(7), 676–682.
- Schöneberg, J., Lee, I.-H., Iwasa, J. H., & Hurley, J. H. (2017). Reverse-topology membrane scission by the ESCRT proteins. *Nature Reviews Molecular Cell Biology*, *18*(1), 5–17.
- Schopp, I. M., Amaya Ramirez, C. C., Debeljak, J., Kreibich, E., Skribbe, M., Wild, K., & Béthune, J. (2017). Split-BioID a conditional proteomics approach to monitor the composition of spatiotemporally defined protein complexes. *Nature Communications*, *8*(1), 15690.
- Schu, P., Takegawa, K., Fry, M., Stack, J. H., Waterfield, M., & Emr, S. D. (1993). Phosphatidylinositol 3-kinase encoded by yeast VPS34 gene essential for protein sorting. *Science*, *260*(5104), 88–91.
- Schuck, S. (2020). Microautophagy – distinct molecular mechanisms handle cargoes of many sizes. *Journal of Cell Science*, *133*(17), jcs246322.
- Schütter, M., Giavalisco, P., Brodesser, S., & Graef, M. (2020). Local Fatty Acid

6. Bibliography

- Channeling into Phospholipid Synthesis Drives Phagophore Expansion during Autophagy. *Cell*, 180(1), 135-149.e14.
- Scott, S. V., Baba, M., Ohsumi, Y., & Klionsky, D. J. (1997). Aminopeptidase I Is Targeted to the Vacuole by a Nonclassical Vesicular Mechanism. *Journal of Cell Biology*, 138(1), 37-44.
- Scott, S. V., Guan, J., Hutchins, M. U., Kim, J., & Klionsky, D. J. (2001). Cvt19 is a receptor for the cytoplasm-to-vacuole targeting pathway. *Molecular Cell*, 7(6), 1131-1141.
- Seals, D. F., Eitzen, G., Margolis, N., Wickner, W. T., & Price, A. (2000). A Ypt/Rab effector complex containing the Sec1 homolog Vps33p is required for homotypic vacuole fusion. *Proceedings of the National Academy of Sciences*, 97(17), 9402-9407.
- Seaman, M. N. J. (2007). Identification of a novel conserved sorting motif required for retromer-mediated endosome-to-TGN retrieval. *Journal of Cell Science*, 120(14), 2378-2389.
- Seaman, M. N. J. (2021). The Retromer Complex: From Genesis to Revelations. *Trends in Biochemical Sciences*.
- Seaman, M. N. J., Harbour, M. E., Tattersall, D., Read, E., & Bright, N. (2009). Membrane recruitment of the cargo-selective retromer subcomplex is catalysed by the small GTPase Rab7 and inhibited by the Rab-GAP TBC1D5. *Journal of Cell Science*, 122(14), 2371-2382.
- Seaman, M. N. J., Marcusson, E. G., Cereghino, J. L., & Emr, S. D. (1997). Endosome to Golgi Retrieval of the Vacuolar Protein Sorting Receptor, Vps10p, Requires the Function of the VPS29, VPS30, and VPS35 Gene Products. *Journal of Cell Biology*, 137(1), 79-92.
- Seaman, M. N. J., McCaffery, J. M., & Emr, S. D. (1998). A membrane coat complex essential for endosome-to-Golgi retrograde transport in yeast. *Journal of Cell Biology*, 142(3), 665-681.
- Sekito, T., Kawamata, T., Ichikawa, R., Suzuki, K., & Ohsumi, Y. (2009). Atg17 recruits Atg9 to organize the pre-autophagosomal structure. *Genes to Cells*, 14(5), 525-538.
- Sherman, F. (2002). Getting started with yeast. In *Methods in Enzymology* (Vol. 350, Issue 02, pp. 3-41).
- Shima, T., Kirisako, H., & Nakatogawa, H. (2019). COPII vesicles contribute to autophagosomal membranes. *Journal of Cell Biology*, 218(5), 1503-1510.
- Shintani, T., & Klionsky, D. J. (2004). Cargo Proteins Facilitate the Formation of Transport Vesicles in the Cytoplasm to Vacuole Targeting Pathway. *Journal of Biological Chemistry*, 279(29), 29889-29894.
- Shintani, T., Mizushima, N., Ogawa, Y., Matsuura, A., Noda, T., & Ohsumi, Y. (1999). Apg10p, a novel protein-conjugating enzyme essential for autophagy in yeast. *EMBO Journal*, 18(19), 5234-5241.
- Siegenthaler, B. M., & Rajendran, L. (2012). Retromers in Alzheimer's Disease. *Neurodegenerative Diseases*, 10(1-4), 116-121.
- Sikorski, R. S., & Hieter, P. (1989). A system of shuttle vectors and yeast host strains designed for efficient manipulation of DNA in *Saccharomyces cerevisiae*. *Genetics*, 122(1), 19-27.
- Simons, R. W., Houman, F., & Kleckner, N. (1987). Improved single and multicopy lac-based cloning vectors for protein and operon fusions. *Gene*, 53(1), 85-96.

6. Bibliography

- Slobodkin, M. R., & Elazar, Z. (2013). The Atg8 family: multifunctional ubiquitin-like key regulators of autophagy. *Essays in Biochemistry*, *55*, 51–64.
- Smith, T. F., Gaitatzes, C., Saxena, K., & Neer, E. J. (1999). The WD repeat: a common architecture for diverse functions. *Trends in Biochemical Sciences*, *24*(5), 181–185.
- Stack, J. H., DeWald, D. B., Takegawa, K., & Emr, S. D. (1995). Vesicle-mediated protein transport: regulatory interactions between the Vps15 protein kinase and the Vps34 PtdIns 3-kinase essential for protein sorting to the vacuole in yeast. *Journal of Cell Biology*, *129*(2), 321–334.
- Stack, J. H., Herman, P. K., Schu, P. V., & Emr, S. D. (1993). A membrane-associated complex containing the Vps15 protein kinase and the Vps34 PI 3-kinase is essential for protein sorting to the yeast lysosome-like vacuole. *The EMBO Journal*, *12*(5), 2195–2204.
- Steinfeld, N., Lahiri, V., Morrison, A., Metur, S. P., Klionsky, D. J., & Weisman, L. S. (2021). Elevating PI3P drives select downstream membrane trafficking pathways. *Molecular Biology of the Cell*, *32*(2), 143–156.
- Stenmark, H., Aasland, R., & Driscoll, P. C. (2002). The phosphatidylinositol 3-phosphate-binding FYVE finger. *FEBS Letters*, *513*(1), 77–84.
- Stephan, J. S., Yeh, Y. Y., Ramachandran, V., Deminoff, S. J., & Herman, P. K. (2009). The Tor and PKA signaling pathways independently target the Atg1/Atg13 protein kinase complex to control autophagy. *Proceedings of the National Academy of Sciences of the United States of America*, *106*(40), 17049–17054.
- Stepp, J. D., Huang, K., & Lemmon, S. K. (1997). The Yeast Adaptor Protein Complex, AP-3, Is Essential for the Efficient Delivery of Alkaline Phosphatase by the Alternate Pathway to the Vacuole. *Journal of Cell Biology*, *139*(7), 1761–1774.
- Stirnemann, C. U., Petsalaki, E., Russell, R. B., & Müller, C. W. (2010). WD40 proteins propel cellular networks. *Trends in Biochemical Sciences*, *35*(10), 565–574.
- Strochlic, T. I., Setty, T. G., Sitaram, A., & Burd, C. G. (2007). Grd19/Snx3p functions as a cargo-specific adapter for retromer-dependent endocytic recycling. *Journal of Cell Biology*, *177*(1), 115–125.
- Sun, B., Chen, L., Cao, W., Roth, A. F., & Davis, N. G. (2004). The Yeast Casein Kinase Yck3p Is Palmitoylated, then Sorted to the Vacuolar Membrane with AP-3-dependent Recognition of a YXX ϕ Adaptor Sorting Signal. *Molecular Biology of the Cell*, *15*(3), 1397–1406.
- Sutton, A., Lin, F., Sarabia, M. J. F., & Arndt, K. T. (1991). The SIT4 Protein Phosphatase Is Required in Late G1 for Progression into S Phase. *Cold Spring Harbor Symposia on Quantitative Biology*, *56*(4), 75–81.
- Suzuki, K., Akioka, M., Kondo-Kakuta, C., Yamamoto, H., & Ohsumi, Y. (2013). Fine mapping of autophagy-related proteins during autophagosome formation in *Saccharomyces cerevisiae*. *Journal of Cell Science*, *126*(11), 2534–2544.
- Suzuki, K., Kirisako, T., Kamada, Y., Mizushima, N., Noda, T., & Ohsumi, Y. (2001). The pre-autophagosomal structure organized by concerted functions of APG genes is essential for autophagosome formation. *EMBO Journal*, *20*(21), 5971–5981.
- Suzuki, K., Kubota, Y., Sekito, T., & Ohsumi, Y. (2007). Hierarchy of Atg proteins in pre-autophagosomal structure organization. *Genes to Cells*, *12*(2), 209–218.
- Suzuki, S. W., Chuang, Y.-S., Li, M., Seaman, M. N. J., & Emr, S. D. (2019). A bipartite sorting signal ensures specificity of retromer complex in membrane protein recycling. *Journal of Cell Biology*, *218*(9), 2876–2886.

6. Bibliography

- Suzuki, S. W., & Emr, S. D. (2018). Membrane protein recycling from the vacuole/lysosome membrane. *Journal of Cell Biology*, *217*(5), 1623–1632.
- Suzuki, S. W., Yamamoto, H., Oikawa, Y., Kondo-Kakuta, C., Kimura, Y., Hirano, H., & Ohsumi, Y. (2015). Atg13 HORMA domain recruits Atg9 vesicles during autophagosome formation. *Proceedings of the National Academy of Sciences*, *112*(11), 3350–3355.
- Takar, M., Wu, Y., & Graham, T. R. (2016). The Essential Neo1 Protein from Budding Yeast Plays a Role in Establishing Aminophospholipid Asymmetry of the Plasma Membrane. *Journal of Biological Chemistry*, *291*(30), 15727–15739.
- Takatori, S., Tatematsu, T., Cheng, J., Matsumoto, J., Akano, T., & Fujimoto, T. (2016). Phosphatidylinositol 3,5-Bisphosphate-Rich Membrane Domains in Endosomes and Lysosomes. *Traffic*, *17*(2), 154–167.
- Takei, K., Slepnev, V. I., Haucke, V., & De Camilli, P. (1999). Functional partnership between amphiphysin and dynamin in clathrin-mediated endocytosis. *Nature Cell Biology*, *1*(1), 33–39.
- Takehige, K., Baba, M., Tsuboi, S., Noda, T., & Ohsumi, Y. (1992). Autophagy in yeast demonstrated with proteinase-deficient mutants and conditions for its induction. *Journal of Cell Biology*, *119*(2), 301–312.
- Tamura, N., Oku, M., Ito, M., Noda, N. N., Inagaki, F., & Sakai, Y. (2013). Atg18 phosphoregulation controls organellar dynamics by modulating its phosphoinositidebinding activity. *Journal of Cell Biology*, *202*(4), 685–698.
- Tan, D., Cai, Y., Wang, J., Zhang, J., Menon, S., Chou, H.-T., Ferro-Novick, S., Reinisch, K. M., & Walz, T. (2013). The EM structure of the TRAPPIII complex leads to the identification of a requirement for COPII vesicles on the macroautophagy pathway. *Proceedings of the National Academy of Sciences*, *110*(48), 19432–19437.
- Tanida, I., Mizushima, N., Kiyooka, M., Ohsumi, M., Ueno, T., Ohsumi, Y., & Kominami, E. (1999). Apg7p/Cvt2p: A novel protein-activating enzyme essential for autophagy. *Molecular Biology of the Cell*, *10*(5), 1367–1379.
- Teter, S. A., Eggerton, K. P., Scott, S. V., Kim, J., Fischer, A. M., & Klionsky, D. J. (2001). Degradation of Lipid Vesicles in the Yeast Vacuole Requires Function of Cvt17, a Putative Lipase. *Journal of Biological Chemistry*, *276*(3), 2083–2087.
- Thumm, M. (2000). Structure and function of the yeast vacuole and its role in autophagy. *Microscopy Research and Technique*, *51*(6), 563–572.
- Thumm, M., Busse, R. A., Scacioc, A., Stephan, M., Janshoff, A., Kühnel, K., & Krick, R. (2013). It takes two to tango. *Autophagy*, *9*(1), 106–107.
- Thumm, M., Egner, R., Koch, B., Schlumpberger, M., Straub, M., Veenhuis, M., & Wolf, D. H. (1994). Isolation of autophagocytosis mutants of *Saccharomyces cerevisiae*. *FEBS Letters*, *349*(2), 275–280.
- Towbin, H., Staehelin, T., & Gordon, J. (1979). Electrophoretic transfer of proteins from polyacrylamide gels to nitrocellulose sheets: procedure and some applications. *Proceedings of the National Academy of Sciences*, *76*(9), 4350–4354.
- Tsukada, M., & Ohsumi, Y. (1993). Isolation and characterization of autophagy-defective mutants of *Saccharomyces cerevisiae*. *FEBS Letters*, *333*(1–2), 169–174.
- Tucker, K. A., Reggiori, F., Dunn, W. A., & Klionsky, D. J. (2003). Atg23 Is Essential for the Cytoplasm to Vacuole Targeting Pathway and Efficient Autophagy but Not Pexophagy. *Journal of Biological Chemistry*, *278*(48), 48445–48452.
- Valverde, D. P., Yu, S., Boggavarapu, V., Kumar, N., Lees, J. A., Walz, T., Reinisch, K. M., &

6. Bibliography

- Melia, T. J. (2019). ATG2 transports lipids to promote autophagosome biogenesis. *Journal of Cell Biology*, 218(6), 1787–1798.
- van der Vaart, A., Griffith, J., & Reggiori, F. (2010). Exit from the Golgi is required for the expansion of the autophagosomal phagophore in yeast *Saccharomyces cerevisiae*. *Molecular Biology of the Cell*, 21(13), 2270–2284.
- van Weering, J. R. T., Verkade, P., & Cullen, P. J. (2010). SNX–BAR proteins in phosphoinositide-mediated, tubular-based endosomal sorting. *Seminars in Cell & Developmental Biology*, 21(4), 371–380.
- Velikkakath, A. K. G., Nishimura, T., Oita, E., Ishihara, N., & Mizushima, N. (2012). Mammalian Atg2 proteins are essential for autophagosome formation and important for regulation of size and distribution of lipid droplets. *Molecular Biology of the Cell*, 23(5), 896–909.
- Vida, T. A., & Emr, S. D. (1995). A new vital stain for visualizing vacuolar membrane dynamics and endocytosis in yeast. *Journal of Cell Biology*, 128(5), 779–792.
- von Mollard, G. F., & Stevens, T. H. (1999). The *Saccharomyces cerevisiae* v-SNARE Vti1p Is Required for Multiple Membrane Transport Pathways to the Vacuole. *Molecular Biology of the Cell*, 10(6), 1719–1732.
- Voos, W., & Stevens, T. H. (1998). Retrieval of Resident Late-Golgi Membrane Proteins from the Prevacuolar Compartment of. 140(3), 577–590.
- Wang, C.-W., Stromhaug, P. E., Kauffman, E. J., Weisman, L. S., & Klionsky, D. J. (2003). Yeast homotypic vacuole fusion requires the Ccz1–Mon1 complex during the tethering/docking stage. *Journal of Cell Biology*, 163(5), 973–985.
- Wang, C.-W., Stromhaug, P. E., Shima, J., & Klionsky, D. J. (2002). The Ccz1-Mon1 Protein Complex Is Required for the Late Step of Multiple Vacuole Delivery Pathways. *Journal of Biological Chemistry*, 277(49), 47917–47927.
- Wang, J., Menon, S., Yamasaki, A., Chou, H.-T., Walz, T., Jiang, Y., & Ferro-Novick, S. (2013). Ypt1 recruits the Atg1 kinase to the preautophagosomal structure. *Proceedings of the National Academy of Sciences*, 110(24), 9800–9805.
- Wang, X., Hoekstra, M. F., DeMaggio, A. J., Dhillon, N., Vancura, A., Kuret, J., Johnston, G. C., & Singer, R. A. (1996). Prenylated isoforms of yeast casein kinase I, including the novel Yck3p, suppress the *gcs1* blockage of cell proliferation from stationary phase. *Molecular and Cellular Biology*, 16(10), 5375–5385.
- Wang, X., Li, X., & Li, Y. (2007). A modified Coomassie Brilliant Blue staining method at nanogram sensitivity compatible with proteomic analysis. *Biotechnology Letters*, 29(10), 1599–1603.
- Watanabe, Y., Kobayashi, T., Yamamoto, H., Hoshida, H., Akada, R., Inagaki, F., Ohsumi, Y., & Noda, N. N. (2012). Structure-based Analyses Reveal Distinct Binding Sites for Atg2 and Phosphoinositides in Atg18. *Journal of Biological Chemistry*, 287(38), 31681–31690.
- Weaver, L. H., Kwon, K., Beckett, D., & Matthews, B. W. (2001). Corepressor-induced organization and assembly of the biotin repressor: A model for allosteric activation of a transcriptional regulator. *Proceedings of the National Academy of Sciences*, 98(11), 6045–6050.
- Wen, X., & Klionsky, D. J. (2016). An overview of macroautophagy in yeast. *Journal of Molecular Biology*, 428(9), 1681–1699.
- Wickner, W., & Rizo, J. (2017). A cascade of multiple proteins and lipids catalyzes membrane fusion. *Molecular Biology of the Cell*, 28(6), 707–711.

6. Bibliography

- Worby, C. A., & Dixon, J. E. (2002). Sorting out the cellular functions of sorting nexins. *Nature Reviews Molecular Cell Biology*, 3(12), 919–931.
- Wu, Y., Takar, M., Cuentas-Condori, A. A., & Graham, T. R. (2016). Neo1 and phosphatidylethanolamine contribute to vacuole membrane fusion in *Saccharomyces cerevisiae*. *Cellular Logistics*, 6(3), e1228791.
- Xie, Z., Nair, U., & Klionsky, D. J. (2008). Atg8 Controls Phagophore Expansion during Autophagosome Formation. *Molecular Biology of the Cell*, 19(8), 3290–3298.
- Xu, C., & Min, J. (2011). Structure and function of WD40 domain proteins. *Protein and Cell*, 2(3), 202–214.
- Xu, Y., Fan, X., & Hu, Y. (2021). In vivo interactome profiling by enzyme-catalyzed proximity labeling. *Cell and Bioscience*, 11(1), 1–9.
- Yamamoto, H., Fujioka, Y., Suzuki, S. W., Noshiro, D., Suzuki, H., Kondo-Kakuta, C., Kimura, Y., Hirano, H., Ando, T., Noda, N. N., & Ohsumi, Y. (2016). The Intrinsically Disordered Protein Atg13 Mediates Supramolecular Assembly of Autophagy Initiation Complexes. *Developmental Cell*, 38(1), 86–99.
- Yamamoto, H., Kakuta, S., Watanabe, T. M., Kitamura, A., Sekito, T., Kondo-Kakuta, C., Ichikawa, R., Kinjo, M., & Ohsumi, Y. (2012). Atg9 vesicles are an important membrane source during early steps of autophagosome formation. *Journal of Cell Biology*, 198(2), 219–233.
- Yamasaki, A., & Noda, N. N. (2017). Structural Biology of the Cvt Pathway. *Journal of Molecular Biology*, 429(4), 531–542.
- Yen, W. L., & Klionsky, D. J. (2008). How to live long and prosper: Autophagy, mitochondria, and aging. *Physiology*, 23(5), 248–262.
- Yen, W. L., Legakis, J. E., Nair, U., & Klionsky, D. J. (2007). Atg27 Is Required for Autophagy-dependent Cycling of Atg9. *Molecular Biology of the Cell*, 18(2), 581–593.
- Yu, Z.-Q., Ni, T., Hong, B., Wang, H.-Y., Jiang, F.-J., Zou, S., Chen, Y., Zheng, X.-L., Klionsky, D. J., Liang, Y., & Xie, Z. (2012). Dual roles of Atg8–PE deconjugation by Atg4 in autophagy. *Autophagy*, 8(6), 883–892.
- Yuga, M., Gomi, K., Klionsky, D. J., & Shintani, T. (2011). Aspartyl Aminopeptidase Is Imported from the Cytoplasm to the Vacuole by Selective Autophagy in *Saccharomyces cerevisiae**. *Journal of Biological Chemistry*, 286(15), 13704–13713.
- Zabrocki, P., Van Hoof, C., Goris, J., Thevelein, J. M., Winderickx, J., & Wera, S. (2002). Protein phosphatase 2A on track for nutrient-induced signalling in yeast. *Molecular Microbiology*, 43(4), 835–842.
- Zavodszky, E., Seaman, M. N. J., Moreau, K., Jimenez-Sanchez, M., Breusegem, S. Y., Harbour, M. E., & Rubinsztein, D. C. (2014). Mutation in VPS35 associated with Parkinson's disease impairs WASH complex association and inhibits autophagy. *Nature Communications*, 5(May), 1–16.
- Zheng, J.-X., Li, Y., Ding, Y.-H., Liu, J.-J., Zhang, M.-J., Dong, M.-Q., Wang, H.-W., & Yu, L. (2017). Architecture of the ATG2B-WDR45 complex and an aromatic Y/HF motif crucial for complex formation. *Autophagy*, 13(11), 1870–1883.
- Zhou, F., Wu, Z., Zhao, M., Murtazina, R., Cai, J., Zhang, A., Li, R., Sun, D., Li, W., Zhao, L., Li, Q., Zhu, J., Cong, X., Zhou, Y., Xie, Z., Gyurkovska, V., Li, L., Huang, X., Xue, Y., ... Segev, N. (2019). Rab5-dependent autophagosome closure by ESCRT. *Journal of Cell Biology*, 218(6), 1908–1927.

6. Bibliography

- Zhou, F., Zou, S., Chen, Y., Lipatova, Z., Sun, D., Zhu, X., Li, R., Wu, Z., You, W., Cong, X., Zhou, Y., Xie, Z., Gyurkovska, V., Liu, Y., Li, Q., Li, W., Cheng, J., Liang, Y., & Segev, N. (2017). A Rab5 GTPase module is important for autophagosome. *PLoS Genetics*, *13*(9), 1–24.
- Zick, M., & Wickner, W. (2012). Phosphorylation of the effector complex HOPS by the vacuolar kinase Yck3p confers Rab nucleotide specificity for vacuole docking and fusion. *Molecular Biology of the Cell*, *23*(17), 3429–3437.
- Zieger, M., & Mayer, A. (2012). Yeast vacuoles fragment in an asymmetrical two-phase process with distinct protein requirements. *Molecular Biology of the Cell*, *23*(17), 3438–3449.
- Zimprich, A., Benet-Pagès, A., Struhal, W., Graf, E., Eck, S. H., Offman, M. N., Haubenberger, D., Spielberger, S., Schulte, E. C., Lichtner, P., Rossle, S. C., Klopp, N., Wolf, E., Seppi, K., Pirker, W., Presslauer, S., Mollenhauer, B., Katzenschlager, R., Foki, T., ... Strom, T. M. (2011). A mutation in VPS35, encoding a subunit of the retromer complex, causes late-onset parkinson disease. *American Journal of Human Genetics*, *89*(1), 168–175.

7. Supplement

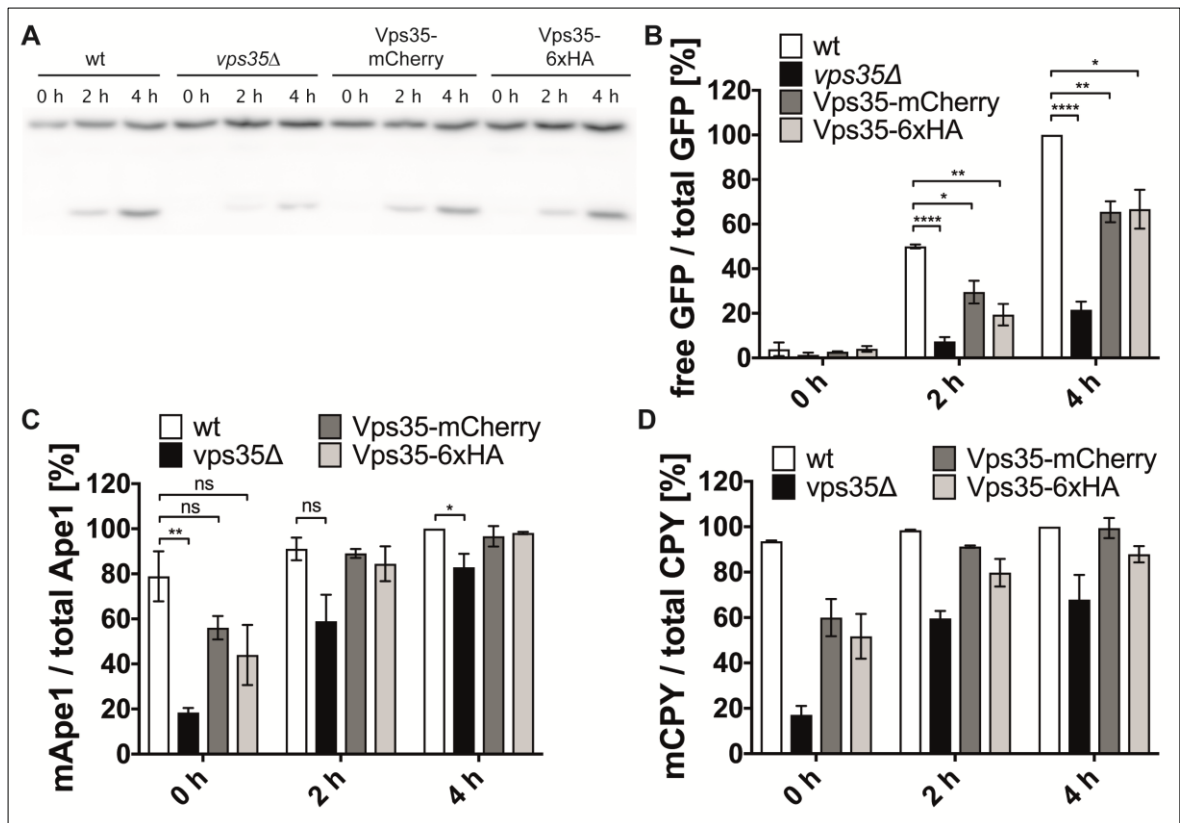


Figure 7-1: Functionality of tagged Vps35 in autophagy.

Vps35 was chromosomally tagged with either GFP, HA or mCherry. Functionality of the tagged protein was tested with autophagic activity assays GFP degradation and Ape1 maturation, function in protein sorting was analyzed with a CPY assay. Cells were grown in selection medium to an OD_{600} of 2-3 and transferred to SD-N medium. Samples were taken after 0h, 2h and 4h and alkaline lysed. **(A)** Wildtype, *vps35Δ* or chromosomally tagged Vps35-mCherry or Vps35-6xHA were expressed together with GFP-Atg8 with an endogenous promoter from plasmid. Western blots were decorated with antibodies against GFP. **(B)** Quantification of GFP-Atg8 degradation rate (free GFP divided by the total amount of GFP and GFP-Atg8) was measured in three independent experiments. 4h sample of wildtype was set to 100%. Statistical relevance was determined with one sample t-test and indicated with asterisks. **(C+D)** Wildtype, *vps35Δ* or chromosomally tagged Vps35-mCherry or Vps35-6xHA were grown and treated as described. Western blots were decorated with antibodies against either Ape1 (C) or CPY (D). Quantification for Ape1 and CPY maturation was done comparable to GFP assay (signal for mApe1/mCPY divided by total Ape1(CPY signal) for three and two independent experiments, respectively).

7. Supplement

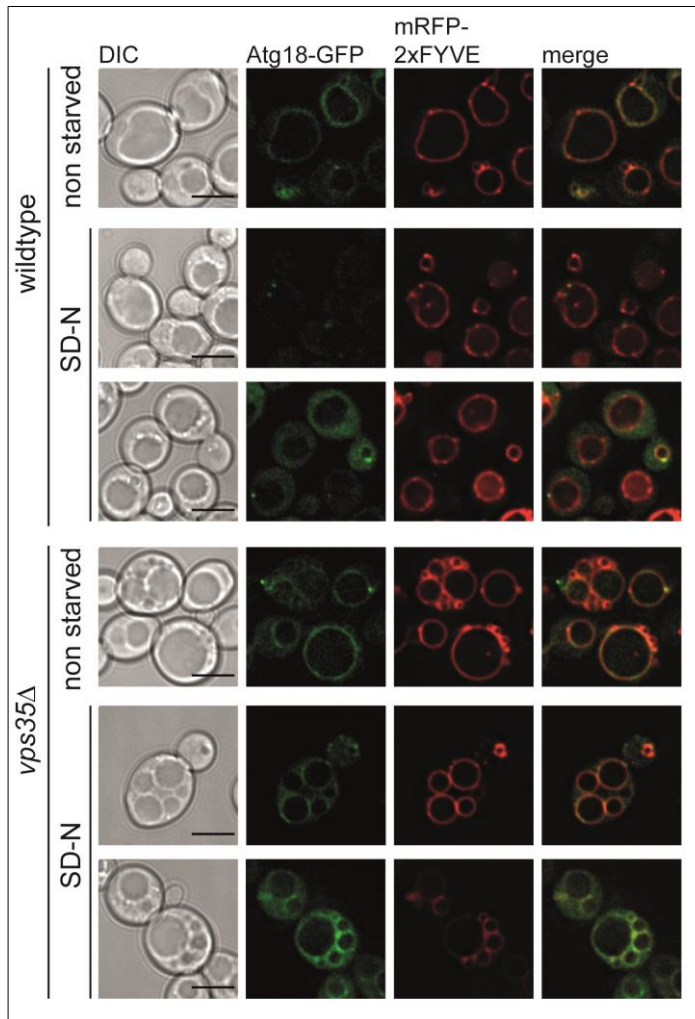


Figure 7-2: PtdIns3P at the vacuolar membrane is similar to wildtype and can also be found at the vesicle like structures.

A 2xFYVE construct conjugated with mRFP was used to analyze the distribution of PtdIns3P in the absence of Vps35. *Atg18Δ* and *atg18Δ vps35Δ* strains expressing ATG18-GFP with an endogenous promoter and mRFP-2xFYVE with a *TEF* promoter from plasmids were grown in selection medium to an OD₆₀₀ of 2-3 and transferred to SD-N medium. Cells were analyzed after 0h, 2h or 4h starvation. Scale bar is set to 5 μm.

Acknowledgement

First of all I want to thank my supervisor, Prof. Dr. Michael Thumm, for giving me the opportunity of working on this thesis. Thank you for your insights and helpful ideas in the last three and a half years!

I want to thank the members of my Thesis Advisory Committee, Prof. Dr. Blanche Schwappach-Pignataro and Dr. Hans-Dieter Schmitt, for your comments and ideas as well as the relaxed atmosphere during all two and a half TAC meetings.

I have to thank Dr. Oliver Valerius and Dr. Kerstin Schmitt (Institute for Microbiology and Genetics, Georg-August-University) for their help with the BioID assay: they shared their protocol for the experiment, performed the LC-MS analyses for me and explained in detail how to evaluate the raw data. My thanks to Olaf Bernhard (Institute for Cellular Biochemistry, UMG), who spent hours on processing the samples for the LC-MS.

Special thanks to our former PostDoc and my friend Lena, for almost four years of emotional and practical support. Thank you for reading my thesis after a whole day of work and still providing valuable feedback. The same for Matt, who generously gave his time to check this thesis for spelling and grammar mistakes and had to add hundreds of 'the's and 'a's.

My thanks to the whole AG Thumm, present members Florian the second and Matt as well as former members Florian the first, Steffi, Hussein, Lisa Ju (the first), Lisa Mi (the second), Peter (the one and only) and our former PostDoc Rosi. Liebe Petra, danke für deine Unterstützung und meinen Tauchschein!

Und nicht zuletzt vielen Dank an meine Familie, die immer für mich da war (sogar bei meinem Umzug zu den Eisbären in den hohen Norden).